Title
Energy Based Thermo-Elastoviscoplastic Damage-Self Healing Formulations for Bituminous Composites

Author
Hong, Seongwon

Publication Date
2014

UNIVERSITY OF CALIFORNIA

Los Angeles

Energy Based Thermo-Elastoviscoplastic Damage-Self Healing Formulations for Bituminous Composites

A dissertation submitted in partial satisfaction of the

requirements for the degree Doctor of Philosophy

in Civil Engineering

by

Seongwon Hong

2014

ABSTRACT OF THE DISSERTATION

Energy Based Thermo-Elastoviscoplastic Damage-Self Healing Formulations

for Bituminous Composites

by

Seongwon Hong

Doctor of Philosophy in Civil Engineering

University of California, Los Angeles, 2014

Professor Jiann-Wen Ju, Chair

New initial strain energy based thermo-elastoviscoplastic isotropic and two-parameter damage-self healing formulations for bituminous materials are proposed and employed for comparisons between model predictions and experimental measurements. First, a class of elastoviscoplastic constitutive isotropic damage-self healing model, based on a continuum thermodynamic framework, is developed within an *initial elastic strain energy* based formulation. An *Arrhenius-type temperature term* is proposed and uncoupled with Helmholtz free energy potential to account for the effect of temperature. In particular, the governing *incremental* damage and healing evolutions are *coupled* and characterized through the *net stress* concept in

conjunction with the *hypothesis of strain equivalence*. The viscoplastic flow is introduced by means of an additive split of the stress tensor. The (undamaged) energy norm of strain tensor is redefined as *equivalent strain* and employed for damage and healing criteria. A rate-dependent (viscous) damage model with a structure analogous to viscoplasticity of the Perzyna type is used for rate sensitivity of bituminous materials.

Computational algorithms based on the two-step *operator splitting* methodology are systematically proposed and implemented for numerical simulations. The elastic damage self-healing predictor and the viscoplastic corrector coupled with Arrhenius-type temperature term via the net stress concept in conjunction with the hypothesis of strain equivalence are considered as numerical implementation of the models. Experimental validation of the proposed formulations against monotonic constant-strain test under different temperatures and controlled-strain cyclic tension test is presented. Qualitative and quantitative agreement between experimental results and numerical simulations is observed. In particular, the softening behavior of the bituminous materials is well predicted for monotonic constant-strain rate-test and the viscous damage behavior can be reasonably captured by the proposed new damage models with the Arrhenius-type temperature term and step-by-step computational algorithms.

Secondly, new initial strain energy based thermo-elastoviscoplastic *two-parameter* damage-self healing formulations for bituminous composites are developed and employed for comparisons between computational simulations and experimental data. In general, the fourth-order form of isotropic damage tensor is composed of two independent parts: the *volumetric* and *deviatoric* parts. If the damage in volumetric part has the same magnitude as deviatoric part, the damage tensor can lead to a scalar damage model which implies that the

Poisson's ratio remains constant when degradation continues pointed out by Ju (1990). A class of elastoviscoplastic two-parameter constitutive damage-self healing model, based on a continuum thermodynamic framework, is proposed within an initial elastic strain energy based formulation. Helmholtz free energy potential is employed and uncoupled with an Arrhenius-type temperature term in order to account for the effect of temperature. In particular, the governing incremental damage and healing evolutions are coupled in volumetric and deviatoric parts and characterized through the net stress concept in conjunction with the hypothesis of strain equivalence. The (undamaged) energy norm of volumetric and deviatoric strain tensors as equivalent volumetric and deviatoric strain is redefined and used for two-parameter damage and healing criteria. A rate-dependent (viscous) volumetric and deviatoric damage model with a structure analogous to viscoplasticity of the Perzyna type is used for rate sensitivity of bituminous composites. Completely new computational algorithms are systematically developed based on the two-step *operator splitting* methodology. It is observed that numerical simulations by two-parameter model agree well with experimental results. In particular, the softening responses of the bituminous composites is well predicted for monotonic constant-strain rate test and the viscous damage behavior can be reasonably predicted by the proposed two-parameter damage models with the Arrhenius-type temperature term and step-by-step computational algorithms. It is noted that the two-parameter model can better predict the thermo-mechanical behavior of asphalt and is more *versatile* than the isotropic damage-self healing model.

The dissertation of Seongwon Hong is approved.

Scott J. Brandenberg

Jenn-Ming Yang

Jian Zhang

Jiann-Wen Ju, Committee Chair

University of California, Los Angeles

2014

DEDICATION

To My Father, Won Pyo Hong

Proud of civil engineering.

To My Mother, Jeong Kyo Kim

I love you forever. *RIP*.

To My Lovely Wife, Hyun Jung Ju

Your endless love and sacrifice gave me encouragement to finish my Ph.D. journey.

To My Lovely Daughter, Jiwon Hong

You are my new love.

TABLE OF CONTENTS

LIST OF FIGURES

LIST OF TABLES

ACKNOWLEDGEMENTS

First of all, the greatest appreciation and gratitude go to my academic advisor, Professor Jiann-Wen Woody Ju, for his countless professional guidance, continuous encouragement, significant support, invaluable advice, and goodwill throughout the duration of my graduate study at UCLA. In particular, in 2012 without Professor Ju's help, it is impossible that I can finish my doctoral research. Moreover, after joining Professor Ju's research group, I have learned not only how to do research but also how to treat students kindly. He is my real advisor and mentor in my life.

I would also like to express my deepest appreciation to Professor Scott J. Brandenberg who helped me transfer my Ph.D. program in 2012 and is now my new committee professor. I gratefully thank Professor Jenn-Ming Yang who introduced Professor Ju to me in 2012 and Professor Jian Zhang for serving on my Ph.D. dissertation committee.

I would like to express my sincere appreciation to Dr. Kuo-Yao (Matt) Yuan whose guidance and comments have always been invaluable for observing the problems and finding the solutions. Working and studying with him have made me a better academic researcher and practical engineer. Without him, this research would not have been completed. I would also like to thank my office mates, Dr. Yi Wu, Mr. Chia-So Chuang, and Mr. Chung-Wen Chuang.

My most sincere appreciation is left for my father, mother, wife (Hyun Jung), and daughter (Jiwon). My father's priceless advice and unconditional support have made me finish my Ph.D. study. I do not forget my mother's last word. My wife's endless love and sacrifice gave me encouragement needed to complete my Ph.D. journey. The birth of my daughter in 2013 gave me great pleasure and new encouragement for research. We have gone through all difficulties

together. Bright future is waiting for my family.

VITA

September 8, 1980	Born, Osaka, Japan
February, 2003	Bachelor of Engineering, Department of Civil Engineering
	Chung-Ang University, Seoul, Korea
June, 2009	Master of Science, Civil and Environmental Engineering
	Geomehanics, Stanford University, Stanford, USA
2010-2014	Graduate Student Researcher/ Teaching Assistant/
	Teaching Associate/ Teaching Fellow
	Department of Civil and Environmental Engineering
	Geotechnical Engineering/Structural Mechanics
	University of California, Los Angeles, USA

1. INTRODUCTION

1.1 Motivation

Bituminous composite materials, such as asphalt concrete pavement, are very complex systems with respect to their thermal sensitivity, loading-rate sensitivity, and healing properties during rest periods. These properties are affected by various factors, such as a variety of combinations of traffic loadings, i.e., type, time, and rate of loading and rest periods, and environmental conditions, i.e., aging, moisture, and temperature. Therefore, development of a realistic, mathematical, constitutive model of bituminous composites is a critical and challenging task that poses significant and complex problems for engineers. Over the past two decades, various rational, thermodynamics-based, constitutive models have been proposed and developed for metal and polymers. However, in spite of the contributions of these studies, a reliable constitutive model of the mechanical behavior of bituminous materials has not been clearly studied and developed to date. In addition, experimental observations in many different fields in the last few decades have clearly shown that some materials can be partially or even fully healed, recovered, or repaired automatically and autonomously, i.e. without any external intervention. In particular, during the unloading process and rest periods with above certain temperature level, microcracks, cavities, and voids in asphalt concrete gradually become smaller and eventually recover their original strength and stiffness. Consequently, the system can be rehabilitated and the integrity of the materials is repaired to a certain extent. A few studies that have been reported in the literature have shown that the damaged materials can fully recover their strength and stiffness so that they have the same properties as undamaged materials. Given our knowledge of the healing process in bituminous materials during unloading and rest periods, it is apparent that the healing effect must be considered when the loading is below a certain level. Therefore, there is a fundamental need for models that can provide a comprehensive assessment of the damage and healing of bituminous composites under complex and cyclic loading and different temperature conditions.

1.2 Objectives and Outline

The primary objective of this research is to develop initial strain energy based thermo-elastoviscoplastic isotropic and two-parameter damage-self healing models and their computational frameworks. The major tasks of this research are concluded as follows:

1. **Development of new initial elastic strain energy based thermo-elastoviscoplastic *isotropic* damage-self healing formulation for bituminous composites:** A class of elastoviscoplastic constitutive damage-self healing model, based on a continuum thermodynamic framework, is proposed within an *initial elastic strain energy* based formulation. An ***Arrhenius-type temperature term*** is uncoupled with Helmholtz free energy potential to account for the effect of temperature. In particular, the governing ***incremental*** damage and healing evolutions are ***coupled*** and characterized through the net stress concept in conjunction with the ***hypothesis of strain equivalence***. The viscoplastic flow is introduced by means of an additive split of the stress tensor. The (undamaged) energy norm of strain tensor is redefined and employed as *equivalent strain*. A rate-dependent (viscous) damage model with a structure analogous to viscoplasticity of the Perzyna type is used for rate sensitivity of bituminous materials. In net space, Drucker-Prager yield function and Perzyna

viscoplastic model are employed.

2. **Development of computational framework for new initial elastic strain energy based thermo-elastoviscoplastic isotropic damage-self healing model:** Computational algorithms based on the two-step ***operator splitting*** methodology are systematically developed and employed for numerical simulations. The elastic damage self-healing predictor and the viscoplastic corrector coupled with *Arrhenius-type temperature term* via the net stress concept in conjunction with the hypothesis of strain equivalence are entirely considered as numerical implementation of the models. Several numerical examples of one-dimensional problems are first presented to show the effect of temperature and rest periods for healing. Experimental validation of the proposed formulations against monotonic constant-strain test under different temperatures and controlled-strain cyclic tension test is presented. Qualitative and quantitative agreement between experimental results and numerical simulations is also observed. In particular, the softening behavior of the bituminous materials is well predicted for monotonic constant-strain rate-test and the viscous damage behavior can be reasonably captured by the proposed new damage models with the Arrhenius-type temperature term and step-by-step computational algorithms.

3. **Development of new initial elastic strain energy based thermo-elastoviscoplastic *two-parameter* damage-self healing formulation for bituminous composites:** A class of elastoviscoplastic ***two-parameter*** constitutive damage-self healing model, based on a continuum thermodynamic framework, is developed within an ***initial volumetric*** and ***deviatoric elastic strain energies*** based formulation. Helmholtz free energy potential is employed and uncoupled with an Arrhenius-type temperature term in order to account for the

effect of temperature. In particular, the governing ***incremental*** damage and healing evolutions are ***coupled*** in ***volumetric*** and ***deviatoric*** parts and characterized through the net stress concept in conjunction with the ***hypothesis of strain equivalence***. The (undamaged) energy norm of volumetric and deviatoric strain tensors as ***equivalent volumetric*** and ***deviatoric strain*** is redefined and employed for two-parameter damage and healing criteria. A rate-dependent (viscous) volumetric and deviatoric damage model with a structure analogous to viscoplasticity of the Perzyna type is used for rate sensitivity of bituminous composites.

4. **Development of computational framework for new initial elastic strain energy based thermo-elastoviscoplastic two-parameter damage-self healing model:** Novel computational algorithms based on the two-step ***operator splitting*** methodology are proposed and employed for numerical results. The elastic two-parameter damage self-healing predictor and the viscoplastic corrector are first coupled with Arrhenius-type temperature term via the net stress concept in conjunction with the hypothesis of strain equivalence and then systematically used for numerical implementation of the models. Four numerical examples of three-dimensional problems are first demonstrated for the effect of temperature and rest periods for healing phenomenon. Finally, experimental validation of the proposed model against monotonic constant-strain test under different temperatures and controlled-strain cyclic tension test is presented. It is observed that numerical simulations by two-parameter model agree well with experimental results. In particular, the softening responses of the bituminous composites is well predicted for monotonic constant-strain rate test and the viscous damage behavior can be reasonably predicted by the proposed two-parameter damage models with the Arrhenius-type temperature term and step-by-step computational

algorithms. It is note that the two-parameter model can better predict the thermo-mechanical behavior of asphalt and is more ***versatile*** than isotropic damage-self healing model.

The remainder of this paper is organized as follows: Chapter 2 includes the review of the general laws, theories, concepts, and healing phenomena. In Chapter 3, new initial strain energy based thermo-elastoviscoplastic isotropic damage-self healing models are presented. Chapter 4 summarizes the computational algorithmic frameworks based on the proposed damage-self healing model, as shown in Chapter 3. new initial strain energy based thermo-elastoviscoplastic two-parameter damage-self healing models are developed in Chapter 5. In Chapter 6, the algorithmic frameworks by using the proposed two-parameter damage-self healing models are used for predicting the temperature-dependent mechanical behavior of bituminous materials under complex loading conditions with different temperatures. The conclusions and future works of this research are summarized in Chapter 7.

2. LITERATURE REVIEW

This chapter summarizes the basic laws, theories, and concepts applicable to this research. The first section of the chapter describes the primary principles for constitutive modeling of materials based on the thermodynamic approach. The second section presents definitions of damage phenomena, the fundamental concept of effective stress, and the hypothesis of equivalent strain. In third section, general mechanical models of bituminous composites are reviewed. Different healing processes of materials such as asphalt, concrete, metallic materials, composites, and ceramics are presented in the fourth section.

2.1 General Principles

Figure 2.1 shows the overview of general principles in order to describe continuum mechanics based on thermodynamics laws. The first law of thermodynamics can be combined with balance of momentum and mechanical energy balance to present energy equation. The second law of thermodynamics is concerned with how the energy is transferred between systems. In continuum mechanics, another way of expressing the second law of thermodynamics is the Clausius-Duhem inequality. This inequality (or Clausius-Planck inequality) is a statement concerning the irreversibility of natural processes, when energy dissipates, and particularly useful in determining whether the constitutive relation of a material is thermodynamically allowable or not. The general principles are basic ingredients to model mechanical behavior of bituminous materials in this research [101].

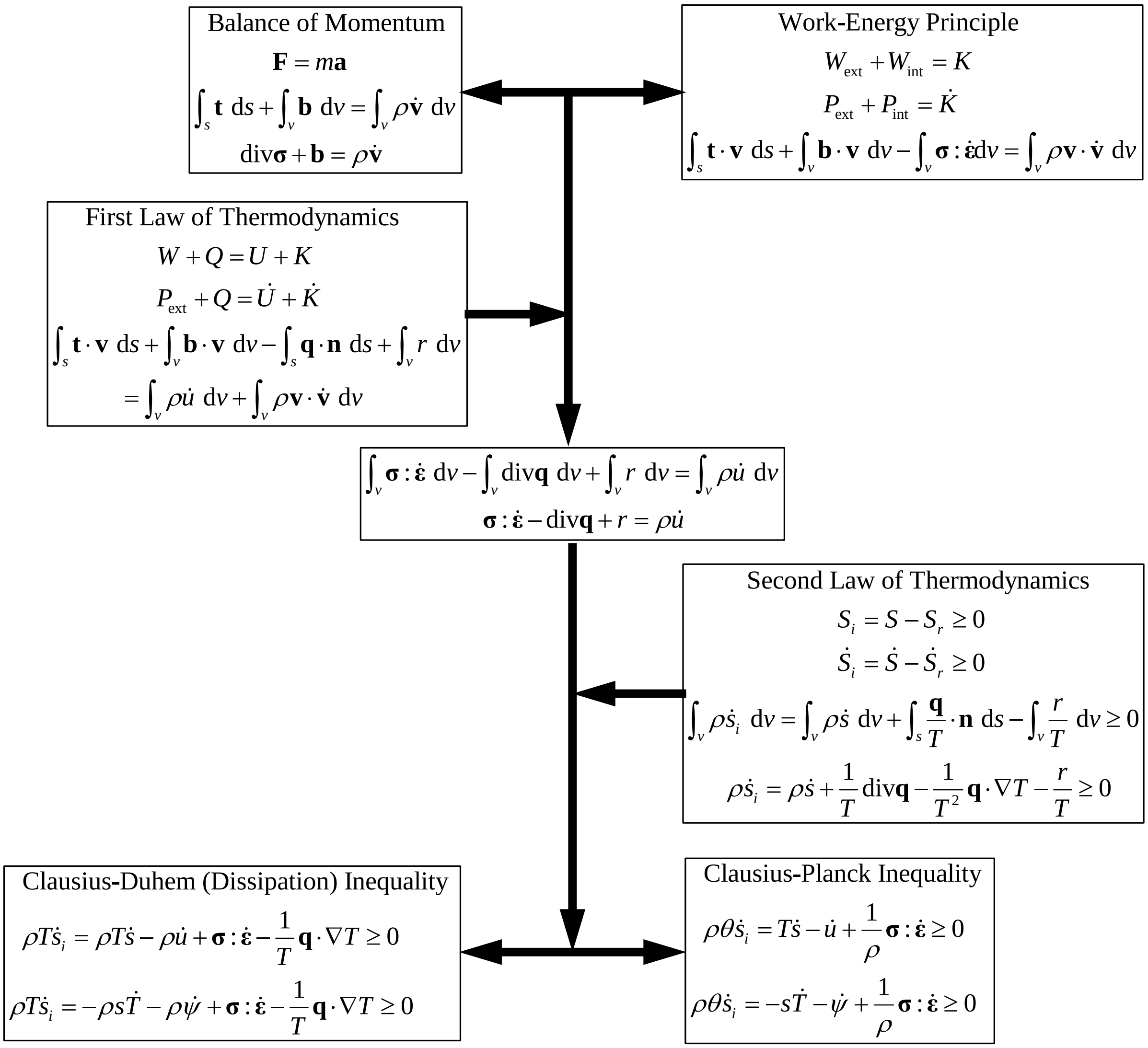

Figure 2.1 Overview of general principles

2.1.1 Balance of Momentum

Euler's Laws are an equivalent set of dynamics law appropriate for finite-sized collection of moving particles and can be used for the force and moment equilibrium in terms of integrals. Once an object is in motion, momentum is a measure of the tendency of an object to keep moving and then the product of the mass and velocity of an object, $\mathbf{p} = m\mathbf{v}$. The rate of change of momentum $\dot{\mathbf{p}}$ is as follows:

$$\frac{d\mathbf{p}}{dt} = m\frac{d\mathbf{v}}{dt} = m\mathbf{a} = \mathbf{F} \tag{2.1}$$

Eq. (2.1) can be generalized to the continuum mechanics and the total linear momentum of the mass of the material is

$$\mathbf{L}(t) = \int_v \rho(\mathbf{x},t)\,\mathbf{v}(\mathbf{x},t)dv \tag{2.2}$$

where $\rho(\mathbf{x},t)$ is spatial mass density and $\mathbf{v}(\mathbf{x},t)$ is spatial velocity description.

Let us consider the derivative of the total linear momentum of the mass of the material.

$$\dot{\mathbf{L}}(t) = \frac{d}{dt}\int_v \rho(\mathbf{x},t)\,\mathbf{v}(\mathbf{x},t)dv = \int_v \rho(\mathbf{x},t)\,\dot{\mathbf{v}}(\mathbf{x},t)dv = \mathbf{F}(t) \tag{2.3}$$

where $\mathbf{F}(t)$ is the resultant of the forces acting on the portion of material.

The total external resultant force acting on the body is the sum of two parts: the surface tractions acting on over surface element and body forces acting on volume elements.

$$\mathbf{F}(t) = \int_s \mathbf{t}ds + \int_v \mathbf{b}dv \tag{2.4}$$

Therefore, the balance of momentum can be expressed as follows:

$$\int_s \mathbf{t}ds + \int_v \mathbf{b}dv = \int_v \rho(\mathbf{x},t)\,\dot{\mathbf{v}}(\mathbf{x},t)dv \quad \text{or} \quad \mathrm{div}\boldsymbol{\sigma} + \mathbf{b} = \rho\dot{\mathbf{v}} \tag{2.5}$$

2.1.2 Work-Energy Principles (Mechanical Energy Balance)

Let us consider the balance of mechanical energy.

$$W_{\text{ext}} + W_{\text{int}} = K \tag{2.6}$$

where W_{ext} is the work by the external forces, W_{int} is the work by the internal forces, and K is kinetic energy.

The rate from of Eq. (2.6) is as follows:

$$P_{\text{ext}} + P_{\text{int}} = \dot{K} \tag{2.7}$$

where P_{ext} is the external power, P_{int} is internal power, and $\dot{K}$ is the rate form of kinetic energy.

Since Eq. (2.4) is the total external resultant force acting on the materials, the external power can be expressed as

$$P_{\text{ext}} = \int_s \mathbf{t} \cdot \mathbf{v} ds + \int_v \mathbf{b} \cdot \mathbf{v} dv \tag{2.8}$$

When the internal forces are conservative (no energy dissipation and all energy stored as internal energy), the power of the internal forces can be expressed in terms of a potential function or stress power as follows

$$P_{\text{int}} = \int_v \rho \frac{du}{dt} dv = -\int_v \boldsymbol{\sigma} : \dot{\boldsymbol{\varepsilon}} dv \tag{2.9}$$

The Kinetic energy and its rate from are as follows:

$$K = \int_v \frac{1}{2} \rho \mathbf{v} \cdot \mathbf{v} dv \tag{2.10}$$

$$\dot{K} = \int_v \rho \mathbf{v} \cdot \dot{\mathbf{v}} dv \tag{2.11}$$

The conservation of mechanical energy is now as follows:

$$\int_s \mathbf{t} \cdot \mathbf{v} \, \mathrm{d}s + \int_v \mathbf{b} \cdot \mathbf{v} \, \mathrm{d}v - \int_v \boldsymbol{\sigma} : \dot{\boldsymbol{\varepsilon}} \mathrm{d}v = \int_v \rho \mathbf{v} \cdot \dot{\mathbf{v}} \, \mathrm{d}v \tag{2.12}$$

The first and second terms in Eq. (2.12) are called the power of surface forces and body forces, respectively. Third term is the power of internal forces and last term is the rate of change of kinetic energy. From the balance of mechanical energy, it is concluded that some of the power exerted by the external forces can transform the kinetic energy and/or internal energy statues.

2.1.3 Laws of Thermodynamics

The classical thermodynamics has been extended to the thermo-mechanics of a continuum since the 1960s [15][17][18][27]. The state variables are enabled to vary throughout a material body and the processes are allowed to be irreversible and move far from thermal and mechanical equilibrium. Therefore, thermodynamics can provide significant restrictions on the form of constitutive equations and these restrictions are useful in the treatment of switch conditions such as the loading-unloading conditions in plasticity. However, a constitutive relation cannot be derived from thermodynamics; only its general admissible form can be checked. In this chapter, the two laws of thermodynamics and its approaches generally accepted in the community of the solid mechanics are reviewed.

- First Law of Thermodynamics

The first law of thermodynamics is a version of conservation of energy and its rate from is expressed as

$$P_{\text{ext}} + Q = \dot{U} + \dot{K} \tag{2.13}$$

where Q is the rate at which heat is supplied and $\dot{U}$ is the rate of change of the internal energy.

The total heat supply to ta finite volume of material as an integral over the volume ca be written as

$$Q = -\int_v \mathrm{div}\mathbf{q}\ \mathrm{d}v + \int_v r\ \mathrm{d}v \tag{2.14}$$

where $\mathbf{q}$ is the heat flux and r is the heat source.

Plugging Eqs. (2.8), (2.11), and (2.14) into Eq. (2.13) leads to

$$\int_v \boldsymbol{\sigma} : \dot{\boldsymbol{\varepsilon}}\ \mathrm{d}v - \int_v \mathrm{div}\mathbf{q}\ \mathrm{d}v + \int_v r\ \mathrm{d}v = \int_v \rho \dot{u}\ \mathrm{d}v \tag{2.15}$$

where $\dot{u}$ is the rate of the specific internal energy per unit mass.

Since this equation holds for any partial volume within the material body, one has the local form of the first law

$$\boldsymbol{\sigma} : \dot{\boldsymbol{\varepsilon}} - \mathrm{div}\mathbf{q} + r = \rho \dot{u} \tag{2.16}$$

- Second Law of Thermodynamics

  The second law of thermodynamics states that the entropy of isolated system never decreases because isolated systems always evolve toward thermodynamic equilibrium: the maximum entropy state.

  The entropy and the entropy supply are defined as the scalar form:

$$S = \int_v \rho s dv \tag{2.17}$$

$$S_r = -\int_s s_q \cdot \mathbf{n} ds + \int_v s^r dv \tag{2.18}$$

where s is the specific entropy or entropy density, s_q is the entropy flux through the element surface, and s^r is the entropy supply due to sources within the element. Eq. (2.18) can be expressed as

$$S_r = -\int_s s_q \cdot \mathbf{n} ds + \int_v s^r dv = -\int_s \frac{\mathbf{q}}{T} \cdot \mathbf{n} ds + \int_v \frac{r}{T} dv \tag{2.19}$$

where T is the non-negative scalar absolute temperature.

The entropy production is now defined and is a non-negative quantity.

$$S_i = S - S_r \geq 0 \tag{2.20}$$

2.1.4 Clausisus-Duhem and Clausius-Planck Inequality

From the definition of the entropy production, the Clausius-Duhem inequality is derived

$$\int_v \rho \dot{s}_i \, \mathrm{d}v = \int_v \rho \dot{s} \, \mathrm{d}v + \int_s \frac{\mathbf{q}}{T} \cdot \mathbf{n} \, \mathrm{d}s - \int_v \frac{r}{T} \, \mathrm{d}v \geq 0 \tag{2.21}$$

where $\dot{s}_i$ is a specific entropy production.

By applying the Gauss-Green theorem, the local form of the Clausius-Duhem inequality is obtained

$$\rho \dot{s}_i = \rho \dot{s} + \frac{1}{T} \mathrm{div}\mathbf{q} - \frac{1}{T^2} \mathbf{q} \cdot \nabla T - \frac{r}{T} \geq 0 \tag{2.22}$$

This is the continuum statement of the second law of thermodynamics.

By using Eqs.(2.16) and (2.22), the dissipation inequality is derived as:

$$\rho T \dot{s}_i = \rho T \dot{s} - \rho \dot{u} + \boldsymbol{\sigma} : \dot{\boldsymbol{\varepsilon}} - \frac{1}{T} \mathbf{q} \cdot \nabla T \geq 0 \tag{2.23}$$

The dissipation inequality can be expressed in terms of a specific free energy:

$$\rho T \dot{s}_i = -\rho s \dot{T} - \rho \dot{\psi} + \boldsymbol{\sigma} : \dot{\boldsymbol{\varepsilon}} - \frac{1}{T} \mathbf{q} \cdot \nabla T \geq 0 \tag{2.24}$$

In many applications, the thermal dissipation is very much smaller than the mechanical dissipation so that it is reasonable to assume that the thermal dissipation rate can be ignored. The

Clausius-Duhem becomes Clausius-Plank inequality which takes the form for any admissible process.

$$\rho\theta\dot{s}_i = T\dot{s} - \dot{u} + \frac{1}{\rho}\boldsymbol{\sigma}:\dot{\boldsymbol{\varepsilon}} \geq 0 \tag{2.25}$$

$$\rho\theta\dot{s}_i = -s\dot{T} - \dot{\psi} + \frac{1}{\rho}\boldsymbol{\sigma}:\dot{\boldsymbol{\varepsilon}} \geq 0 \tag{2.26}$$

2.2 Continuum Damage Mechanics

Models based on continuum damage mechanics (CDM) assume that the degradation of materials is macroscopically homogeneous and that such degradation is clearly explained by the mechanics of continuous media and the thermodynamics of irreversible processes. Thus such models do not take into account the complicated microstructures of the materials that have been used and continue to be used extensively for all types of construction materials such as alloys, concrete, metals, rocks, soils, steels, and various types of woods. Palmgreen (1924), Miner (1945), and Robinson (1952) conceived the concept of the progressive deterioration related to a variable prior to crack propagation and final failure. However, Kachanov (1958) was considered as the pioneer who introduced a field variable called 'phenomenological continuity parameter' which is related to the density of the defects in order to describe the degradation of the material before the initiation of macro-cracks. Lemaitre (1992) used Kachanov's variable for fatigue problems, and Leckie and Hayhurst (1974), Hult (1974), and Lemaitre and Chaboche (1975) used it to solve issues associated with creep and creep-fatigue interactions. Rabotnov (1969) introduced the concept of effective stress within the framework of CDM which represents average material deterioration based on the various types of damage at the micro-level, such as nucleation and growth of voids, cavities, microcracks, and other microscopic defects.

In the 1980s, the thermodynamics-based framework of damage mechanics was actively studied and developed [27][34][35][88][89]. In addition to thermodynamics basis, Wu (1985) and Krajcinovic and Fanella (1986) developed the framework of damage mechanics based on micromechanics. CDM has now reached a stage that enables practical engineering applications in the modeling of elastic damage [19][20][34][43][44][57][77], damage in an elasto-viscoplastic models [29][85][86], ductile fracture based on the anisotropic damage mechanism [15][19][54][87], ductile plastic damage [13][14][20][23][24][34][35][36][56][58][59][88][89][93], brittle and creep fracture using anisotropic damage models [49][51][72][73], damage in composite materials [37][38][52][92][97], and the damage-viscoelastic-viscoplastic model [91]. Moreover, the concept has been used in many other applications [57][58].

2.2.1 Definition of Continuum Damage Mechanics [60]

Material damage has been defined as a progressive, physical process by which materials break, and the study of the mechanics of such damage is based on internal variables and the mechanisms involved in the deterioration under the loading condition. Damage of materials can generally be classified in terms of scale. At the microscale level of the representative volume element, damage is induced by the accumulation of micro-stresses in the neighborhood of interfaces and/or defects, resulting in the breaking of bonds. At the mesoscale level, damage results from the growth and the coalescence of microcracks and/or microvoids that initiate one crack. At the macroscale level, the cracks that have been formed expand and grow.

Micromechanical damage models are required for modeling microstructural change and individual microcracks, and phenomenological continuum damage models are required to model the microcracks are required in the first stage at the microscale level. The second stage, i.e., the mesoscale level, is usually studied by using the damage variables related to the mechanics of continuous media that have been defined for this level. The third stage, i.e., at the macroscale level is studied by fracture mechanics with the variables defined at this level. The consideration of a crack at the macroscopic level in the framework of fracture mechanics deduces a defect that substantially larger than the microscopic heterogeneities (grains, subgrains, other defects and microcracks, etc.) It is assumed that the main macroscopic crack is propagated through several grains to show a sufficient macroscopic homogeneity in size, geometry and direction, leading to possible treatment using the concepts of fracture mechanics. Chaboche's (1981) schematic illustration of these concepts is shown in Figure 2.2 and Figure 2.3.

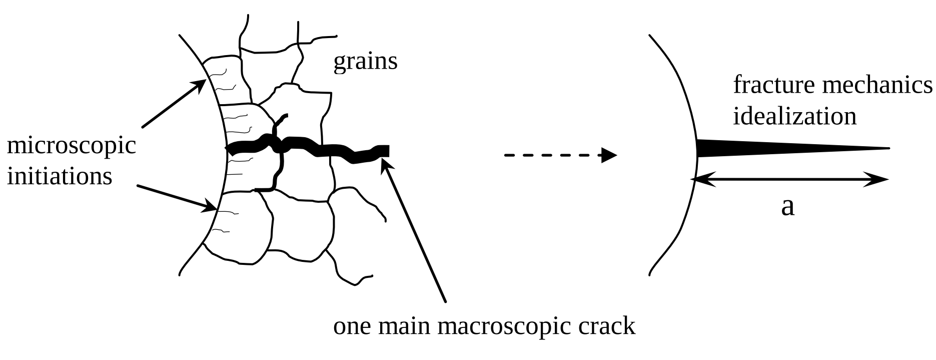

Figure 2.2 Schematics of the fatigue crack growth (Chaboche, 1981)

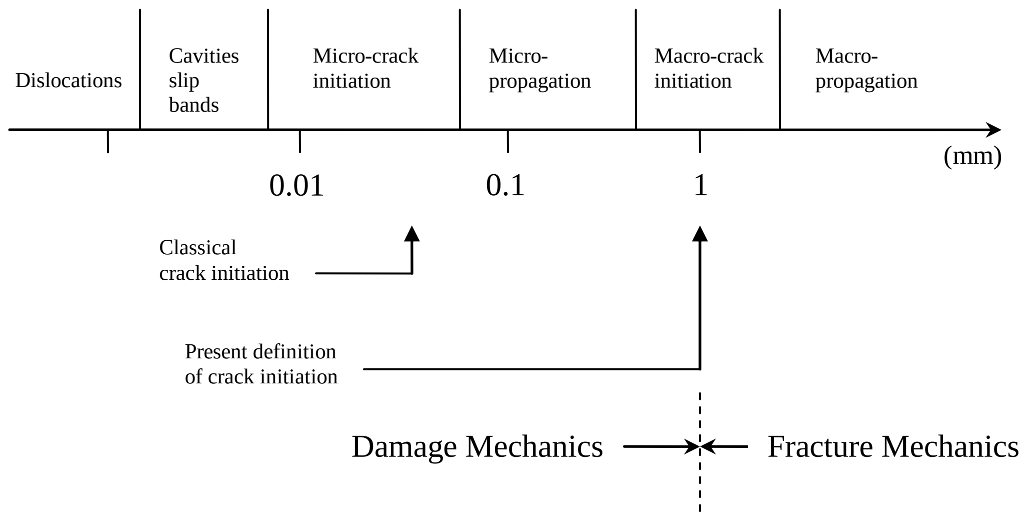

Figure 2.3 Illustration of a macroscopic crack initiation concept (Chaboche, 1981)

In continuum mechanics, quantities defined at a mathematical point have been dealt with, and they represent averages on a certain volume from the physical perspective. The representative volume element (RVE) is small enough to avoid smoothing of high gradients, but it is large enough to represent an average of the microprocesses. For the purposes of experiments and numerical analysis, various orders of magnitude of the RVE for different materials have been used, e.g., metals and ceramics $(0.1\,mm)^3$, polymers and most composites $(1\,mm)^3$, wood $(10\,mm)^3$, concrete $(100\,mm)^3$ [60].

2.2.2 Concept of Effective Strain and Hypothesis of Stress Equivalence

A principle must be postulated at the level of macro-scale to avoid a micromechanical analysis for each type of defect and mechanism of damage. From the method of local state in thermodynamics, it is assumed that the thermo-mechanical state at a point can be completely defined by the time values of a set of continuous state variables which depend upon the point considered. This postulate introduced by Lemaitre [56] imposes that the constitutive equations for the strain of a micro-volume element are not modified by a neighboring micro-volume element containing a microcrack. Extrapolating to the macro-scale, it means that the strain constitutive equations written for the damaged surface are not modified by the damage or that the true stress loading on the material is the effective stress $\bar{\sigma}$ instead of σ.

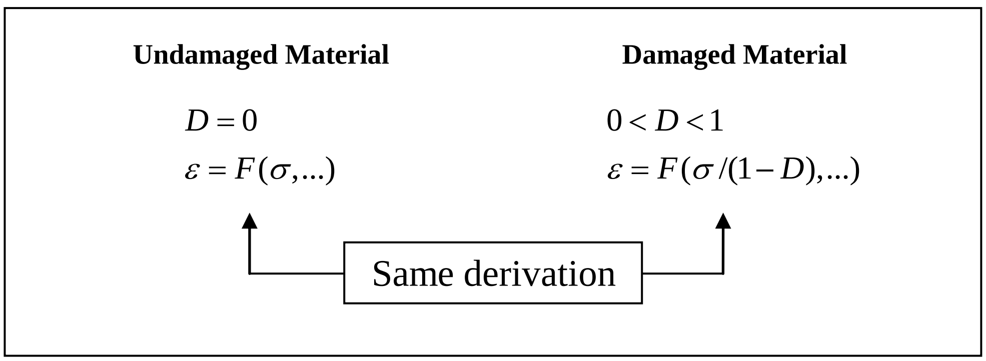

Figure 2.4 Schematic illustration of the derivation for undamaged and damaged materials (Lemaitre, 1992)

Lemaitre [56] states the following principle results:

"Any strain constitutive equation for a damaged material may be derived in the same way as for a virgin material except that the usual stress is replaced by the effective stress". A schematic representation of this principle illustrated in Figure 2.4.

Physically, degradation of the material properties is the result of the initiation, growth and coalescence of microcracks or microvoids. Within the context of continuum mechanics, one may model this process by introducing an internal damage variable which can be a scalar or a tensorial quantity. $\underset{\sim}{\mathrm{M}}=(\underset{\sim}{\mathrm{I}}-\underset{\sim}{\mathrm{D}})$, a fourth-order tensor, characterizes the state of damage and transforms the homogenized stress tensor $\underset{\sim}{\sigma}$ into the effective stress tensor $\underset{\sim}{\bar{\sigma}}$ (or vice versa). Accordingly, it can be written as

$$\underset{\sim}{\bar{\sigma}} \equiv \underset{\sim}{\mathrm{M}}^{-1} : \underset{\sim}{\sigma} \tag{2.27}$$

For the isotropic damage case, the mechanical behavior of microcracks or microvoids is independent of their orientation and depends only on a scalar damage variable, d . Accordingly, $\underset{\sim}{\mathrm{M}}$ will simply reduce to $(1\text{-}d)\underset{\sim}{\mathrm{I}}$ where $\underset{\sim}{\mathrm{I}}$ is the rank four identity tensor, and Eq. (2.27) collapses to

$$\underset{\sim}{\bar{\sigma}}(t) = \frac{\underset{\sim}{\sigma}(t)}{1-d(t)} \tag{2.28}$$

where $\underset{\sim}{\sigma}(t)$ is the Cauchy stress tensor, and $\underset{\sim}{\bar{\sigma}}(t)$ denotes the effective stress tensor, both at time t. The coefficient $1-d(t)$ dividing the stress tensor in Eq.(2.28) results in a reduction factor associated with the amount of damage in the material first introduced by Kachanov [42]. The value $d=0$ corresponds to the undamaged state whereas other value of d corresponds to a damaged state. The damage parameter d may be interpreted physically as the ratio of damaged surface area over total (nominal) surface area at a local material point.

Lemaitre’s hypothesis of strain equivalence [56] states:

“The strain associated with a damaged state under the applied stress is equivalent to the strain associated with its undamaged state under the effective stress”

We can refer to Figure 2.5 for a schematic illustration of this hypothesis [88].

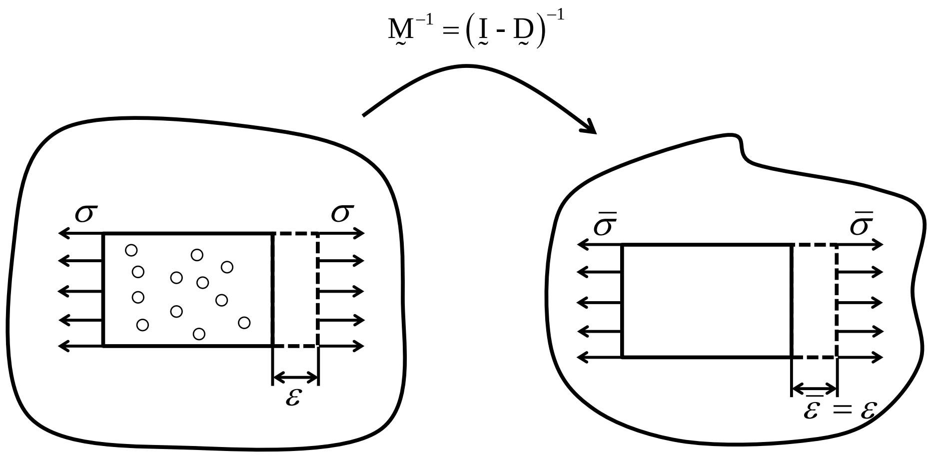

Physical Space **Effective Space**

Figure 2.5 Schematic illustration of the hypothesis of strain equivalence (Simo and Ju, 1987)

2.3 Mechanical Modeling of Asphalt Concretes

In order to establish the constitutive modeling of bituminous materials to describe the linear and nonlinear behavior, theory of viscoplasticity with yield function must be used and incorporated with continuum damage mechanics. In general, the Drucker-Prager yield function and Perzyna viscoplastic model are the basis for development of asphalt concrete materials because the experiment results for bituminous materials show the dependence upon the hydrostatic stress components and viscous-behavior. Therefore, these two models are briefly reviewed in this chapter.

2.3.1 The Drucker-Prager Yield Criterion

The Drucker-Prager criterion [11] as loading function can be written in the form

$$f\left(\boldsymbol{\sigma},\varepsilon_{vp}\right)=\|\mathbf{s}\|-\left(A\left(\varepsilon_{vp}\right)-Bp\right) \tag{2.29}$$

where $\|\ \|$ is operation of tensor norm, $\mathbf{s}$ is the deviatoric stress tensor satisfying the condition $\mathrm{tr}(\mathbf{s})=0$, 'tr' is the trace operator, $p=\mathrm{tr}(\boldsymbol{\sigma})/3$ is the mean normal stress, and A and B are material constants. Lemaitre and Chaboche (1990) and Tan et al. (1994) show that B in Drucker-Prager model is almost constant as the material permanently deforms while A evolves with the permanent deformation. The evolution form of A is a function of equivalent viscoplastic strain given by

$$A\left(\varepsilon_{vp}\right)=A_0+A_1\left(1-\exp\left(-A_2\varepsilon_{vp}\right)\right) \tag{2.30}$$

where ε_{vp} is the equivalent viscoplastic strain.

Chen and Han (1987) showed that the loading function, $F(\boldsymbol{\sigma})$, can be expressed in terms of power form

$$F(\boldsymbol{\sigma})=C\sigma_e^n \tag{2.31}$$

where $F(\boldsymbol{\sigma})=\|\mathbf{s}\|+Bp$ and σ_e is equivalent stress

For the uniaxial test ($\boldsymbol{\sigma}_1=\boldsymbol{\sigma}_e$ and $\boldsymbol{\sigma}_2=\boldsymbol{\sigma}_3=0$), we have

$$F(\boldsymbol{\sigma})=\|\mathbf{s}\|+Bp=\sqrt{\frac{2}{3}}\sigma_e+\frac{B}{3}\sigma_e=C\sigma_e^n \tag{2.32}$$

Therefore,

$$n=1,\quad C=\sqrt{\frac{2}{3}}+\frac{B}{3},\quad \sigma_e=\frac{\|\mathbf{s}\|+Bp}{\sqrt{\frac{2}{3}}+\frac{B}{3}} \tag{2.33}$$

The equivalent viscoplastic strain increment in terms of the plastic work per unit volume is as follows

$$dW_{vp} = \sigma_e d\varepsilon_{vp} = \frac{\sqrt{d\varepsilon_{ij}^{vp} d\varepsilon_{ij}^{vp}}\, nF}{\sqrt{\partial F/\partial \sigma_{mn}\, \partial F/\partial \sigma_{mn}}} \tag{2.34}$$

where $\left(\partial F/\partial \sigma_{mn}\right)\left(\partial F/\partial \sigma_{mn}\right) = B^2 + 1$ and $n = 1$.

$$d\varepsilon_{vp} = \frac{\sqrt{2/3} + B/3}{\sqrt{B^2 + 1}} \sqrt{d\varepsilon_{ij}^{vp} d\varepsilon_{ij}^{vp}} \tag{2.35}$$

2.3.2 Perzyna Type Viscoplasticity

Experimental measurements for the bituminous materials indicate that the yield surface is not the same as the viscoplastic potential surface because the associative flow rule overestimates the behavior of dilation for asphalt composites [76] [79][99]. It is assumed that the flow function equals to nonlinear loading function, i.e. $g(f) = f^m$ and the non-associative flow rule yields shown in Figure 2.6. (see the Appendix)

$$\dot{\boldsymbol{\varepsilon}}^{vp} = \dot{\gamma} \frac{\partial g_p}{\partial \boldsymbol{\sigma}} = \frac{< g\left(f\right) >}{\eta} \frac{\partial g_p}{\partial \boldsymbol{\sigma}} = \frac{< f^m >}{\eta} \left(\mathbf{n} + \frac{D}{3}\mathbf{1}\right) \tag{2.36}$$

where $g_p\left(\boldsymbol{\sigma}\right) = \left\|\mathbf{s}\right\| - \left(C - Dp\right)$ is the viscoplastic potential function.

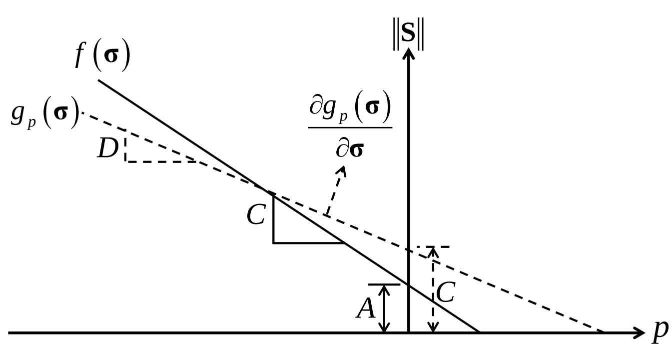

Figure 2.6 Demonstration of yield surface and viscoplastic potential function

2.3.3 Viscoplastic Consistency Condition and Elastoviscoplastic Tangent Moduli

For consistent (algorithmic) tangent moduli, the conventional Drucker-Prager model and the Perzyna type viscoplasticity are chosen and employed in this chapter.

The symmetric stress tensor is denoted by $\boldsymbol{\sigma}$ and its additive decomposition into volumetric and deviatoric parts gives

$$\boldsymbol{\sigma} = p\mathbf{1} + \mathbf{s} \tag{2.37}$$

where $\mathbf{1}$ is the second-order identity tensor.

For isotropic linearly elastic material, the elastic constitutive equations are

$$p = K\varepsilon_v \tag{2.38}$$

$$\mathbf{s} = 2G\mathbf{e} \tag{2.39}$$

where K and G are the elastic bulk and shear moduli, respectively. $\varepsilon_v = \mathrm{tr}(\boldsymbol{\varepsilon})$ is the volumetric strain and $\mathbf{e}$ is the deviatoric strain tensor satisfying the condition $\mathrm{tr}(\mathbf{e}) = 0$ This gives

$$\boldsymbol{\sigma} = K\varepsilon_v\mathbf{1} + 2G\mathbf{e} = \mathbf{C}^0 : \boldsymbol{\varepsilon}^e = \mathbf{C}^0 : \left(\boldsymbol{\varepsilon} - \boldsymbol{\varepsilon}^{vp}\right) \tag{2.40}$$

where $\mathbf{C}^0 = K\mathbf{1}\otimes\mathbf{1} + 2G\left(\mathbf{I} - \frac{1}{3}\mathbf{1}\otimes\mathbf{1}\right)$ is the rank-four tensor of elastic moduli. Therefore, the rate constitutive equation is defined as (see the Appendix)

$$\dot{\boldsymbol{\sigma}} = \mathbf{C}^0 : \left(\dot{\boldsymbol{\varepsilon}} - \dot{\boldsymbol{\varepsilon}}^{vp}\right) = \mathbf{C}^0 : \dot{\boldsymbol{\varepsilon}} - \dot{\gamma}\left(2G\mathbf{n} + KD\mathbf{1}\right) \tag{2.41}$$

For loading $\dot{\gamma} \geq 0$ and $f = 0$, $\dot{\gamma}$ is determined by viscoplastic consistency condition $\dot{f} = 0$. (see the Appendix)

$$\dot{\gamma} = \frac{\left(2G\mathbf{n} + KB\mathbf{1}\right) : \boldsymbol{\varepsilon}}{\left[2G + KBD + A'\left(\varepsilon_{vp}\right)E\right]} = \frac{\left(2G\mathbf{n} + KB\mathbf{1}\right) : \boldsymbol{\varepsilon}}{F} \tag{2.42}$$

where $E = \dfrac{\sqrt{2/3} + B/3}{\sqrt{B^2 + 1}}$ and $F = \left[2G + KBD + A'\left(\varepsilon_{vp}\right)E\right]$

Substitution of Eq. (2.42) into Eq. (2.41) yields $\dot{\boldsymbol{\sigma}} = \mathbf{C}^{evp} : \dot{\boldsymbol{\varepsilon}}$ where $\mathbf{C}^{evp}$ is the elastoviscoplastic tangent moduli given by: (see the Appendix)

$$\mathbf{C}^{evp} = 2G\mathbf{I} + \left(K - \frac{2G}{3} - \frac{K^2 BD}{F}\right)\mathbf{1}\otimes\mathbf{1} - \frac{2GKB}{F}\mathbf{1}\otimes\mathbf{n} - \frac{2GKD}{F}\mathbf{n}\otimes\mathbf{1} - \frac{\left(2G\right)^2}{F}\mathbf{n}\otimes\mathbf{n} \tag{2.43}$$

By applying backward Euler algorithm and local Newton iteration, the viscoplastic consistency parameter can be derived and the following viscoplastic consistency parameter is derived when the flow function equals to linear loading function, i.e. $g(f) = f$. (see the Appendix)

$$\hat{\gamma}_{n+1} = \frac{\dfrac{f_{n+1}^{trial}}{2G}}{\left(1 + \dfrac{\tau}{\Delta t} + \dfrac{KBD}{2G}\right)} \tag{2.44}$$

The exact (consistent) tangent operator is defined by the rank-four tensor

$$\mathbf{C}_{n+1}^{evp} = \left.\frac{\partial\boldsymbol{\sigma}}{\partial\boldsymbol{\varepsilon}}\right|_{n+1} \tag{2.45}$$

With the aid of backward Euler algorithms Eq. (2.42) and Eq. (2.45), we obtain the following expression for $\mathbf{C}_{n+1}^{ep}$ (see the Appendix)

$$\mathbf{C}_{CONS\ n+1}^{evp} = \mathbf{C}^0 - \frac{\partial\hat{\gamma}_{n+1}}{\partial\boldsymbol{\varepsilon}_{n+1}} \otimes KD\mathbf{1} - 2G\left(\frac{\partial\hat{\gamma}_{n+1}}{\partial\boldsymbol{\varepsilon}_{n+1}} \otimes \mathbf{n}_{n+1} + \hat{\gamma}_{n+1}\frac{\partial\mathbf{n}_{n+1}}{\partial\boldsymbol{\varepsilon}_{n+1}}\right) \tag{2.46}$$

By computing the term of $\partial\hat{\gamma}_{n+1}/\partial\boldsymbol{\varepsilon}_{n+1}$ and $\partial\mathbf{n}_{n+1}/\partial\boldsymbol{\varepsilon}_{n+1}$, we obtain the final expression of the consistency tangent moduli. (see the Appendix)

$$\mathbf{C}^{evp}_{CONS\ n+1} = \left(2G - \theta_{n+1}\right)\mathbf{I} + \left(K - \frac{2G}{3} - \frac{K^2 BD}{F} + \frac{\theta_{n+1}}{3}\right)\mathbf{1}\otimes\mathbf{1} - \frac{2GKB}{F}\mathbf{1}\otimes\mathbf{n}_{n+1} - \frac{2GKD}{F}\mathbf{n}_{n+1}\otimes\mathbf{1} - \left(\frac{\left(2G\right)^2}{F} - \theta_{n+1}\right)\mathbf{n}_{n+1}\otimes\mathbf{n}_{n+1} \tag{2.47}$$

$$\mathbf{C}^{evp}_{CONS\ n+1} = \mathbf{C}^{evp} - \frac{\left(2G\right)^2 \hat{\gamma}_{n+1}}{\left\|\mathbf{s}^{tr}_{n+1}\right\|}\left(\mathbf{I} - \frac{1}{3}\mathbf{1}\otimes\mathbf{1} - \mathbf{n}_{n+1}\otimes\mathbf{n}_{n+1}\right) \tag{2.48}$$

where $\theta_{n+1} = \dfrac{\left(2G\right)^2 \hat{\gamma}_{n+1}}{\left\|\mathbf{s}^{tr}_{n+1}\right\|}$

$\mathbf{C}^{evp}$ is the material tangent response, whereas $\mathbf{C}^{evp}_{CONS\ n+1}$ represent the material tangent response for numerical algorithm as well as the material tangent response. As $\hat{\gamma}_{n+1} \to 0$ $\mathbf{C}^{evp}_{CONS\ n+1}$ becomes $\mathbf{C}^{evp}$. If non-associative flow rule is employed, $\mathbf{C}^{evp}_{CONS\ n+1}$ becomes a non-symmetric operator. Radial return algorithm is summarized in BOX 2.2 and BOX 2.1.

BOX 2.1 Radial return algorithm

1. Update strain tensor.

$$\boldsymbol{\varepsilon}_{n+1}=\boldsymbol{\varepsilon}_n+\Delta\boldsymbol{\varepsilon}_{n+1}$$

$$\mathbf{e}_{n+1}=\boldsymbol{\varepsilon}_{n+1}-\frac{1}{3}\operatorname{tr}\left(\boldsymbol{\varepsilon}_{n+1}\right)\mathbf{1}$$

2. Compute *trial elastic* stress.

$$\boldsymbol{\sigma}_{n+1}^{trial}=\boldsymbol{\sigma}_n+\mathbf{C}\;:\Delta\boldsymbol{\varepsilon}_{n+1}$$

$$p_{n+1}^{trial}=\frac{1}{3}\operatorname{tr}\left(\boldsymbol{\sigma}_{n+1}^{trial}\right)$$

$$\mathbf{s}_{n+1}^{trial}=2G\;\left(\mathbf{e}_{n+1}-\mathbf{e}_n^{vp}\right)$$

3. Check yield condition

$$f_{n+1}^{trial}=\left\|\mathbf{s}_{n+1}^{trial}\right\|-\left(A\left(\varepsilon_{vp,n}\right)-Bp_{n+1}^{trial}\right)$$

IF $f_{n+1}^{trial}\leq 0$ THEN:

$$\mathbf{e}_{n+1}^{vp}=\mathbf{e}_n^{vp}\qquad p_{n+1}=p_{n+1}^{trial}$$

$$\mathbf{s}_{n+1}=\mathbf{s}_{n+1}^{trial}\qquad \boldsymbol{\sigma}_{n+1}^{net}=\boldsymbol{\sigma}_{n+1}^{trial}$$

ENDIF.

4. Compute $\mathbf{n}_{n+1}$ and $\hat{\gamma}_{n+1}$ from BOX 2.2

$$\mathbf{n}_{n+1}=\frac{\mathbf{s}_{n+1}^{trial}}{\left\|\mathbf{s}_{n+1}^{trial}\right\|}$$

5. Update viscoplastic strain and net stress

$$\varepsilon_{vp,n+1}=\varepsilon_{vp,n}+\frac{\sqrt{2/3}+B/3}{\sqrt{B^2+1}}\hat{\gamma}_{n+1}$$

$$A\left(\varepsilon_{vp,n+1}\right)=A_0+A_1\left(1-\exp\left(-A_2\varepsilon_{vp,n+1}\right)\right)$$

$$\mathbf{e}_{n+1}^{vp}=\mathbf{e}_n^{vp}+\hat{\gamma}_{n+1}\mathbf{n}_{n+1}\qquad p_{n+1}=p_{n+1}^{trial}-\hat{\gamma}_{n+1}KB$$

$$\mathbf{s}_{n+1}=\mathbf{s}_{n+1}^{trial}-\hat{\gamma}_{n+1}2G\mathbf{n}_{n+1}\qquad \boldsymbol{\sigma}_{n+1}=p_{n+1}\mathbf{1}+\mathbf{s}_{n+1}$$

6. Compute consistent elastoviscoplastic tangent moduli

$$\mathbf{C}_{n+1}^{evp}=\left(2G-\theta_{n+1}\right)\mathbf{I}+\left(K-\frac{2G}{3}-\frac{K^2BD}{F}+\frac{\theta_{n+1}}{3}\right)\mathbf{1}\otimes\mathbf{1}-\frac{2GKB}{F}\mathbf{1}\otimes\mathbf{n}_{n+1}$$
$$-\frac{2GKD}{F}\mathbf{n}_{n+1}\otimes\mathbf{1}-\left(\frac{\left(2G\right)^2}{F}-\theta_{n+1}\right)\mathbf{n}_{n+1}\otimes\mathbf{n}_{n+1}$$

$$\theta=\frac{\left(2G\right)^2\hat{\gamma}_{n+1}}{\left\|\mathrm{s}_{n+1}^{tr}\right\|}$$

BOX 2.2 Consistency condition and determination of $\hat{\gamma}_{n+1}$

1. Initialize:

$\hat{\gamma}_{n+1}=0$

2. Iterate:

DO UNTIL: $\left|h\left(\hat{\gamma}_{n+1}\right)\right| < TOL$

$k \leftarrow k+1$

$$h\left(\hat{\gamma}_{n+1}^{k}\right)=\left\langle f_{n+1}^{trial}\right\rangle-\hat{\gamma}_{n+1}^{k}\left(2G+KBD\right)-\left(\frac{\hat{\gamma}_{n+1}^{k}\eta}{\Delta t}\right)^{\frac{1}{m}}$$

$$Dh\left(\hat{\gamma}_{n+1}^{k}\right)=-\left(2G+KBD\right)-\frac{1}{m}\left(\frac{\eta}{\Delta t}\right)^{\frac{1}{m}}\left(\hat{\gamma}_{n+1}^{k}\right)^{\frac{1}{m}-1}$$

$$\hat{\gamma}_{n+1}^{k+1}=\hat{\gamma}_{n+1}^{k}-\frac{h\left(\hat{\gamma}_{n+1}^{k}\right)}{Dh\left(\hat{\gamma}_{n+1}^{k}\right)}$$

2.4 Healing Phenomenon of Engineering Materials

During the past two decades, experimental data in many different areas have clearly demonstrated that some engineering materials can be partially or even fully healed, recovered, or repaired automatically and autonomously, i.e., without any external triggering [8][9][28][30][31] [39][40][41][45][47][69][82][98][99]. In particular, during the loading or unloading processes with above certain temperature level, microcracks, microvoids, and cavities in polymers and bituminous materials slowly reduce in size and finally recover their undamaged strength and stiffness [1][21][22][48][55][65][95]. According to Wool and Oconnor (1981), this healing in polymers occurs due to (a) surface rearrangement, (b) surface approach, (c) wetting, (d), diffusion, and (e) randomization. Healing process can be defined as the antithesis to damage.

Consequently, the system can be rehabilitated and the integrity of the materials is repaired to a certain extent. A few reports in the literature have shown that the damaged materials can fully recover their original strength and stiffness, making them equivalent to undamaged materials [10][21][48][64]. In this chapter, the healing processes and mechanisms of engineering materials such as asphalt, concrete, metallic materials, composites, and ceramics, are reviewed.

(1) Asphalt

Complex irregular traffic causes the deterioration of asphalt concrete pavement and during the night the damaged asphalt concrete can be recovered partially and undergo automatic healing when there is less traffic loading. The main reason for the healing is the properties of bituminous materials, such as their viscosity. The extent of the healing of asphalt concrete was first measured by Kim et al. (1994) using the nonlinear viscoelastic correspondence principles; the impact resonance test method; and the stress-wave testing method.

It was concluded that, after exposure to higher temperatures, there is a detectable increment of moduli that results from the microcrack healing of asphalt concrete. A twenty-four-hour stress-wave test demonstrated that the elastic modulus of asphalt mixtures decreases as their temperature increases. An increase in elastic modulus was observed after the rest period due to microcrack healing in the asphalt concrete layers. Since the healing phenomenon was confirmed, several constitutive models have been proposed for the prediction of the damage growth and partial recovery of asphalt mixtures under the tensile uniaxial cyclic tests and the cyclic loading condition. [1][10][55][64][65][79]

(2) Concrete

Ordinary Portland cement (OPC), which is used in making concrete, is the most extensively used man-made building material worldwide, and vast quantities of it (~ 20 billion metric tons in 2010[68]) are being used to build infrastructure throughout the world. Although concrete structure can easily crack in tension, microcracks and microvoids due to the restraint of shrinkage deformations at early ages are the most unavoidable characteristics of OPC, and they are considered to be inherent, unavoidable features of this product. If these microcracks propagate and accumulate, they finally initiate large cracks than can cause damage and lead to the failure of the structure. In the 21st century, several techniques have proposed and developed to prevent such microcracks and microvoids at early ages, ultimately preventing damage due to the loading and age effect. Two methods, i.e., healing agents and microcapsule embedment techniques, have been used extensively in the concrete construction industry. The main agents for healing the concrete are epoxy resins, cyanoacrylates, and alkali-silica solutions [63][70][75]. It has been determined that the effectiveness of the healing is due to the capillary forces and the viscosity of the repair agents. There are various encapsulation materials, including a microencapsulated, enclosing repair agent embedded in the concrete mixture; a continuous glass supply pipe to provide a supply of repair agent in concrete; and cyanoacrylate enclosed in capillary tubes sealed with silicon [70].

(3) Metal and alloy

Metals are solid materials that have been used in many roles throughout human history. An alloy is a mixture of metals or a ‘solid solution’ that consists of two (or more) metals. Alloys are typically hard, opaque, and have very good electrical and thermal conductivity. If metals and alloys are improperly designed and inappropriately used, failures can occur rapidly, including fatigue, creep, damage, and fracture.

Even if a material is appropriately designed, microcracks and microvoids in the materials can propagate under certain loading conditions and accumulated microcrakcs and microvoids can cause the materials to deteriorate and eventually fail. Designers are focused on increasing the reliability of structural materials, and one of the best solutions would be identifying self-healing materials. A common theme in the area of self-healing metals is the manipulation and control of the microstructure of the material. Self-healing metals are usually categorized as liquid-assisted healing and solid-state healing materials. The design of liquid-assisted self-healing metals has centered on metal-matrix composites reinforced with shape memory alloy wires in which the matrix partially liquefies at an elevated temperature [25][26][45][46][66][67]. The microstructure is designed to maintain structural stability during healing by only allowing the liquid available at the surface of the crack to participate in damage remediation. The metals in the second category rely on the solid-state self-healing mechanism to exploit the strong driving force for solute diffusion to high-energy surfaces such as cracks or voids.

(4) Composites

Composites (or composite materials) are made from the combination of two or more constituent materials to form new materials with enhanced properties [5]. Typical engineered composites can be broadly classified into four categories: (1) building composite materials, such as cements, concrete, and asphalt; (2) reinforced plastics, such as fiber-reinforced polymers; (3) metal composites; and (4) ceramic composites. In this section, fiber-reinforced polymers are reviewed. The self-healing of glass fiber-reinforced epoxy laminates has been proposed using the interalaminar dispersion of the healing agent and a ruthenimum catalyst [6]. A microencapsulated healing agent such as dicyclopentadiene (DCPD) is embedded and dispersed throughout structural composites. A catalyst is also encapsulated and dispersed in a similar manner. The processes of automatic healing are as follows: (1) a crack propagates in the matrix when damage occurs; (2) the propagating crack breaks the microcapsules, releasing the healing agent into the plane of the crack through capillary action; and (3) the healing agent contacts the catalyst, triggering polymerization and resulting in crack closure, as shown in Figure 2.7. A continuum damage and healing model has been developed for predicting the effect of damage and self-healing as a function of loading history; this model includes generalized continuum damage mechanics combined with healing by a phenomenological thermodynamic approach [7].

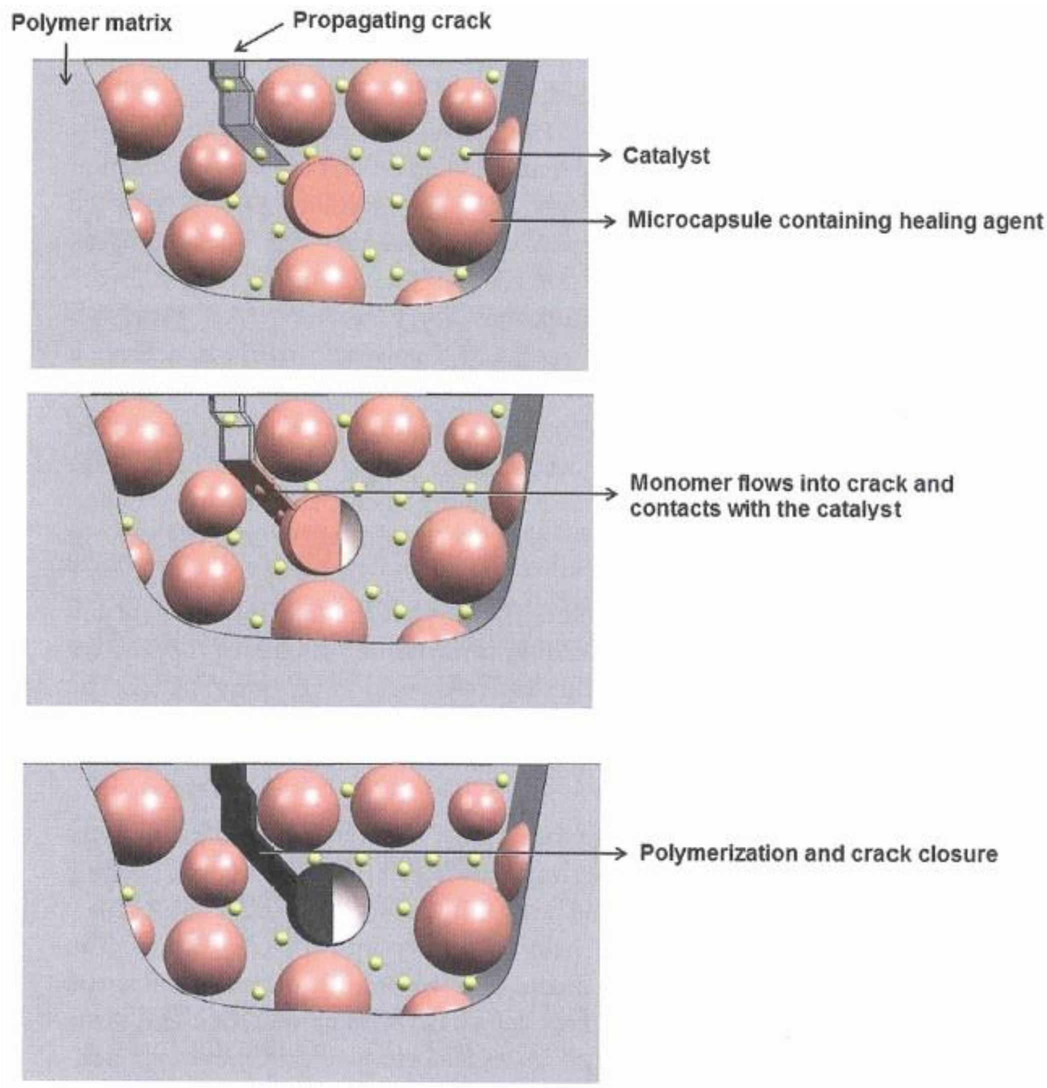

Figure 2.7 Schematic representation of composite materials with embedded microcapsules (White et al., 2001).

(5) Ceramics

In the case of structural ceramics, the most severe damage results from surface cracks, which may be introduced by impacts, fatigue, thermal shock, and corrosion during their service time. Over the past three decades, ceramics have become the key structural materials for high temperature application due to their enhanced quality and good process ability. Structural ceramics, because of their chemical stability, also are used in the corrosion environments. Therefore, the self-healing of surface cracks in structural ceramics materials is an important issue to ensure their structural integrity. In general, healing the surface cracks of structural ceramic materials is best performed in the following conditions: (1) healing must be triggered by cracking; (2) healing must occur at high temperature in the corrosive atmosphere; and (3) the strength of the healed zone must be superior to that of the base material. Figure 2.8 shows the schematic of the crack healing in the ceramics that contain SiC particles and that was heated at a high temperature in the presence of air. Cracking allows the SiC particles that are located on the walls of the crack to react with oxygen, resulting healing and significant increase in the strength of the materials [2][3][4][12][74].

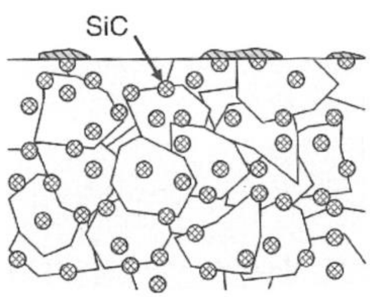

(a) Before cracking

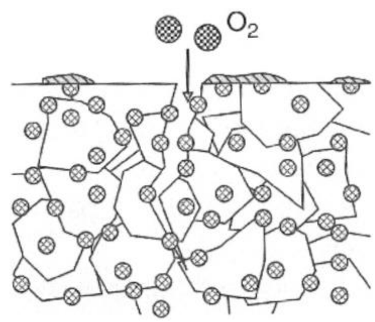

(b) After cracking

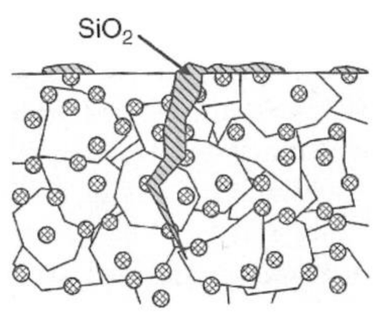

After healing

Figure 2.8 Schematic illustration of crack-healing mechanism (Nakao et al, 2005)

2.5 Appendix

Summary of general mathematic rule is as follows:

$$\mathbf{1}:\mathbf{1}=3/\ \ \mathbf{n}:\mathbf{1}=0/\ \ \mathbf{C}^0:\mathbf{1}=3K\mathbf{1}/\ \ \mathbf{C}^0:\mathbf{n}=2G\mathbf{n}$$

For isotopic linearly elastic material, the elastic constitutive equations are

$$\boldsymbol{\sigma}\ =p\ \mathbf{1}+\mathbf{s}\ =Ktr(\boldsymbol{\varepsilon})+2G\mathbf{e}=\mathbf{C}^0:\boldsymbol{\varepsilon}^e$$

where $p\ =\frac{tr(\boldsymbol{\sigma}\ )}{3}=Ktr(\boldsymbol{\varepsilon})$, $\mathbf{s}\ =2G\mathbf{e}$, K is the elastic bulk moduli and G is shear moduli, $\mathbf{C}^0=K\mathbf{1}\otimes\mathbf{1}+2G\left(\mathbf{I}-\frac{1}{3}\mathbf{1}\otimes\mathbf{1}\right)$ is the rank-four tensor of elastic moduli.

For Perzyna type viscoplasticity, the derivation of flow function is

$$\frac{\partial g_p}{\partial\boldsymbol{\sigma}}=\frac{\partial\|\mathbf{s}\|-(C-Dp)}{\partial\boldsymbol{\sigma}}=\frac{\partial\|\mathbf{s}\|}{\partial\boldsymbol{\sigma}}+\frac{D\partial p}{\partial\boldsymbol{\sigma}}=\mathbf{n}+\frac{D}{3}\mathbf{1}$$

$$\frac{\partial\|\mathbf{s}\|}{\partial\boldsymbol{\sigma}}=\frac{\partial\sqrt{\mathbf{s}:\mathbf{s}}}{\partial\boldsymbol{\sigma}}=\frac{\partial(\mathbf{s}:\mathbf{s})^{1/2}}{\partial\boldsymbol{\sigma}}=\frac{1}{2}(\mathbf{s}:\mathbf{s})^{-1/2}\mathbf{s}:\frac{\partial\mathbf{s}}{\partial\boldsymbol{\sigma}}\times 2=\frac{\mathbf{s}}{\|\mathbf{s}\|}:\frac{\partial\mathbf{s}}{\partial\boldsymbol{\sigma}}=\mathbf{n}:\frac{\partial\mathbf{s}}{\partial\boldsymbol{\sigma}}=\mathbf{n}:\left(\mathbf{I}-\frac{1}{3}\mathbf{1}\otimes\mathbf{1}\right)=\mathbf{n}$$

$$\frac{\partial\mathbf{s}}{\partial\boldsymbol{\sigma}}=\frac{\partial\boldsymbol{\sigma}}{\partial\boldsymbol{\sigma}}-\frac{\partial p}{\partial\boldsymbol{\sigma}}\otimes\mathbf{1}=\mathbf{I}-\frac{1}{3}\mathbf{1}\otimes\mathbf{1}$$

$$\frac{\partial p}{\partial\boldsymbol{\sigma}}=\frac{1}{3}\frac{\partial\sigma_{kk}}{\partial\sigma_{pq}}=\frac{1}{3}\delta_{pq}=\frac{1}{3}\mathbf{1}$$

The derivation of the rate constitutive equation is as follows:

$$\dot{\boldsymbol{\sigma}} = \mathbf{C}^0 : \dot{\boldsymbol{\varepsilon}}^e = \mathbf{C}^0 : \left(\dot{\boldsymbol{\varepsilon}} - \dot{\boldsymbol{\varepsilon}}^{vp}\right) = \mathbf{C}^0 : \left(\dot{\boldsymbol{\varepsilon}} - \dot{\gamma}\left(\mathbf{n} + \frac{D}{3}\mathbf{1}\right)\right) = \mathbf{C}^0 : \dot{\boldsymbol{\varepsilon}} - \left(\mathbf{C}^0 : \dot{\gamma}\left(\mathbf{n} + \frac{D}{3}\mathbf{1}\right)\right)$$
$$= \mathbf{C}^0 : \dot{\boldsymbol{\varepsilon}} - \dot{\gamma}\left(2G\mathbf{n} + KD\mathbf{1}\right)$$

From viscoplastic consistency condition, viscoplastic consistency parameter can be calculated:

$$\dot{f} = \frac{\partial f}{\partial \boldsymbol{\sigma}} : \dot{\boldsymbol{\sigma}} + \frac{\partial f}{\partial \varepsilon_{vp}} \dot{\varepsilon}_{vp} = \left(\mathbf{n} + \frac{B}{3}\mathbf{1}\right) : \left\{\mathbf{C}^0 : \dot{\boldsymbol{\varepsilon}} - \dot{\gamma}\left(2G\mathbf{n} + KD\mathbf{1}\right)\right\} - A'\left(\varepsilon_{vp}\right)E\dot{\gamma}$$
$$= \mathbf{n} : \mathbf{C}^0 : \dot{\boldsymbol{\varepsilon}} - \mathbf{n} : \dot{\gamma}\left(2G\mathbf{n} + KD\mathbf{1}\right) + \frac{B}{3}\mathbf{1} : \mathbf{C}^0 : \dot{\boldsymbol{\varepsilon}} - \frac{B}{3}\mathbf{1} : \dot{\gamma}\left(2G\mathbf{n} + KD\mathbf{1}\right) - A'\left(\varepsilon_{vp}\right)E\dot{\gamma}$$
$$= 2G\mathbf{n} : \dot{\boldsymbol{\varepsilon}} - 2G\dot{\gamma} + KB\mathbf{1} : \dot{\boldsymbol{\varepsilon}} - KBD\dot{\gamma} - A'\left(\varepsilon_{vp}\right)E\dot{\gamma} = 0$$

$$\rightarrow \left(2G\mathbf{n} + KB\mathbf{1}\right) : \dot{\boldsymbol{\varepsilon}} = \left\{2G + KBD + A'\left(\varepsilon_{vp}\right)E\right\}\dot{\gamma}$$

$$\rightarrow \dot{\gamma} = \frac{\left(2G\mathbf{n} + KB\mathbf{1}\right) : \boldsymbol{\varepsilon}}{\left[2G + KBD + A'\left(\varepsilon_{vp}\right)E\right]} = \frac{\left(2G\mathbf{n} + KB\mathbf{1}\right) : \boldsymbol{\varepsilon}}{F}$$

where $E = \dfrac{\sqrt{2/3} + B/3}{\sqrt{B^2 + 1}}$ and $F = \left[2G + KBD + A'\left(\varepsilon_{vp}\right)E\right]$

The derivation of the elastoviscoplastic tangent moduli is as follows:

$$\dot{\boldsymbol{\sigma}} = \mathbf{C}^0 : \dot{\boldsymbol{\varepsilon}} - \dot{\gamma}\left(2G\mathbf{n} + KD\mathbf{1}\right) = \mathbf{C}^0 : \dot{\boldsymbol{\varepsilon}} - \frac{\left(2G\mathbf{n} + KB\mathbf{1}\right) : \boldsymbol{\varepsilon}}{F} \otimes \left(2G\mathbf{n} + KD\mathbf{1}\right)$$
$$= \left[\mathbf{C}^0 - \frac{1}{F}\left(2G\mathbf{n} + KB\mathbf{1}\right) \otimes \left(2G\mathbf{n} + KD\mathbf{1}\right)\right] : \dot{\boldsymbol{\varepsilon}} = \mathbf{C}^{evp} : \dot{\boldsymbol{\varepsilon}}$$

$$\mathbf{C}^{evp} = \left[\mathbf{C}^0 - \frac{1}{F}\left(2G\mathbf{n} + KB\mathbf{1}\right)\otimes\left(2G\mathbf{n} + KD\mathbf{1}\right) \right]$$
$$= 2G\mathbf{I} + \left(K - \frac{2G}{3} \right)\mathbf{1}\otimes\mathbf{1} - \frac{1}{F}\left[\left(2G\right)^2 \mathbf{n}\otimes\mathbf{n} + 2GKD\mathbf{n}\otimes\mathbf{1} + 2GKB\mathbf{1}\otimes\mathbf{n} + K^2BD\mathbf{1}\otimes\mathbf{1} \right]$$
$$= 2G\mathbf{I} + \left(K - \frac{2G}{3} - \frac{K^2BD}{F} \right)\mathbf{1}\otimes\mathbf{1} - \frac{2GKB}{F}\mathbf{1}\otimes\mathbf{n} - \frac{2GKD}{F}\mathbf{n}\otimes\mathbf{1} - \frac{\left(2G\right)^2}{F}\mathbf{n}\otimes\mathbf{n}$$

$$\left(2G\mathbf{n} + KB\mathbf{1}\right)\otimes\left(2G\mathbf{n} + KD\mathbf{1}\right) = \left(2G\right)^2 \mathbf{n}\otimes\mathbf{n} + 2GKD\mathbf{n}\otimes\mathbf{1} + 2GKB\mathbf{1}\otimes\mathbf{n} + K^2BD\mathbf{1}\otimes\mathbf{1}$$

$$\mathbf{C}^0 = 2G\mathbf{I} + \left(K - \frac{2G}{3} \right)\mathbf{1}\otimes\mathbf{1}$$

Computational viscoplastic consistency parameter can be derived from the following procedure:

$$p_{n+1} = p_{n+1}^{trial} - \hat{\gamma}_{n+1}KD$$

$$\mathbf{s}_{n+1} = \mathbf{s}_{n+1}^{trial} - \hat{\gamma}_{n+1}2G\mathbf{n}_{n+1}$$

$$\mathbf{s}_{n+1} = \mathbf{s}_{n+1}^{trial} - 2G\frac{< f_{n+1} >}{\eta}\Delta t\mathbf{n}_{n+1}$$

$$\Rightarrow \left\|\mathbf{s}_{n+1}\right\| = \left\|\mathbf{s}_{n+1}^{trial}\right\| - 2G\frac{< f_{n+1} >}{\eta}\Delta t$$

$$\Rightarrow \frac{< f_{n+1} >}{\eta}\Delta t = \frac{1}{2G}\left(\left\|\mathbf{s}_{n+1}^{trial}\right\| - \left\|\mathbf{s}_{n+1}\right\| \right) = \frac{1}{2G}\left(\left\|\mathbf{s}_{n+1}^{trial}\right\| - < f_{n+1} > - \left(A - Bp_{n+1}\right) \right)$$
$$= \frac{1}{2G}\left(\left\|\mathbf{s}_{n+1}^{trial}\right\| - \left(A - Bp_{n+1}\right) \right) - \frac{1}{2G} < f_{n+1} >$$
$$= \frac{1}{2G}\left(\left\|\mathbf{s}_{n+1}^{trial}\right\| - \left(A - B(p_{n+1}^{trial} - \frac{< f_{n+1} >}{\eta}\Delta tKD \right) \right) - \frac{1}{2G} < f_{n+1} >$$

$$\Rightarrow\left(1+\frac{1}{2G}\frac{\eta}{\Delta t}+\frac{KBD}{2G}\right)\frac{<f_{n+1}>}{\eta}\Delta t=\frac{1}{2G}\left(\left\|\mathbf{s}_{n+1}^{trial}\right\|-\left(A-Bp_{n+1}^{trial}\right)\right)$$

$$\Rightarrow\frac{<f_{n+1}>}{\eta}\Delta t=\frac{\frac{1}{2G}\left(\left\|\mathbf{s}_{n+1}^{trial}\right\|-\left(A-Bp_{n+1}^{trial}\right)\right)}{\left(1+\frac{1}{2G}\frac{\eta}{\Delta t}+\frac{KBD}{2G}\right)}=\frac{\frac{f_{n+1}^{trial}}{2G}}{\left(1+\frac{\tau}{\Delta t}+\frac{KBD}{2G}\right)}=\hat{\gamma}_{n+1}$$

Derivation of consistent viscoplastic tangent moduli is as follows:

$$\begin{aligned}\boldsymbol{\sigma}_{n+1}&=p_{n+1}\mathbf{1}+\mathbf{s}_{n+1}=\left(p_{n+1}^{tr}-\hat{\gamma}_{n+1}KD\right)\mathbf{1}+2G\left(\mathbf{e}_{n+1}-\mathbf{e}_{n+1}^{vp}\right)\\&=Ktr\left(\boldsymbol{\varepsilon}_{n+1}\right)\mathbf{1}-\hat{\gamma}_{n+1}KD\mathbf{1}+2G\left(\mathbf{e}_{n+1}-\mathbf{e}_{n}^{vp}-\hat{\gamma}_{n+1}\mathbf{n}_{n+1}\right)\\&=\mathbf{C}^0:\boldsymbol{\varepsilon}_{n+1}^{e}=\mathbf{C}^0:\left(\boldsymbol{\varepsilon}_{n+1}-\boldsymbol{\varepsilon}_{n+1}^{vp}\right)\end{aligned}$$

$$\begin{aligned}d\boldsymbol{\sigma}_{n+1}&=\mathbf{C}^0:d\boldsymbol{\varepsilon}_{n+1}-d\hat{\gamma}_{n+1}KD\mathbf{1}-2G\left(d\hat{\gamma}_{n+1}\mathbf{n}_{n+1}+\hat{\gamma}_{n+1}d\mathbf{n}_{n+1}\right)\\&=\left[\mathbf{C}^0-\frac{d\hat{\gamma}_{n+1}}{d\boldsymbol{\varepsilon}_{n+1}}\otimes KD\mathbf{1}-2G\left(\frac{d\hat{\gamma}_{n+1}}{d\boldsymbol{\varepsilon}_{n+1}}\otimes\mathbf{n}_{n+1}+\hat{\gamma}_{n+1}\frac{d\mathbf{n}_{n+1}}{d\boldsymbol{\varepsilon}_{n+1}}\right)\right]:d\boldsymbol{\varepsilon}_{n+1}\end{aligned}$$

$$\begin{aligned}\mathbf{C}_{CONS\ n+1}^{evp}&=\mathbf{C}^0-\frac{d\hat{\gamma}_{n+1}}{d\boldsymbol{\varepsilon}_{n+1}}\otimes KD\mathbf{1}-2G\left(\frac{d\hat{\gamma}_{n+1}}{d\boldsymbol{\varepsilon}_{n+1}}\otimes\mathbf{n}_{n+1}+\hat{\gamma}_{n+1}\frac{d\mathbf{n}_{n+1}}{d\boldsymbol{\varepsilon}_{n+1}}\right)\\&=2G\mathbf{I}+\left(K-\frac{2G}{3}\right)\mathbf{1}\otimes\mathbf{1}-\frac{2GKD}{F}\mathbf{n}_{n+1}\otimes\mathbf{1}-\frac{K^2BD}{F}\mathbf{1}\otimes\mathbf{1}-\frac{(2G)^2}{F}\mathbf{n}_{n+1}\otimes\mathbf{n}_{n+1}\\&\quad-\frac{2GKB}{F}\mathbf{1}\otimes\mathbf{n}_{n+1}-\frac{(2G)^2\hat{\gamma}_{n+1}}{\left\|\mathbf{s}_{n+1}^{tr}\right\|}\left(\mathbf{I}-\frac{1}{3}\mathbf{1}\otimes\mathbf{1}-\mathbf{n}_{n+1}\otimes\mathbf{n}_{n+1}\right)\\&=\left(2G-\theta_{n+1}\right)\mathbf{I}+\left(K-\frac{2G}{3}-\frac{K^2BD}{F}+\frac{\theta_{n+1}}{3}\right)\mathbf{1}\otimes\mathbf{1}-\frac{2GKB}{F}\mathbf{1}\otimes\mathbf{n}_{n+1}\\&\quad-\frac{2GKD}{F}\mathbf{n}_{n+1}\otimes\mathbf{1}-\left(\frac{(2G)^2}{F}-\theta_{n+1}\right)\mathbf{n}_{n+1}\otimes\mathbf{n}_{n+1}\\&=\mathbf{C}^{evp}-\frac{(2G)^2\hat{\gamma}_{n+1}}{\left\|\mathbf{s}_{n+1}^{tr}\right\|}\left(\mathbf{I}-\frac{1}{3}\mathbf{1}\otimes\mathbf{1}-\mathbf{n}_{n+1}\otimes\mathbf{n}_{n+1}\right)\end{aligned}$$

$$\frac{d\mathbf{n}_{n+1}}{d\boldsymbol{\varepsilon}_{n+1}} = \frac{2G}{\left\|\mathbf{s}_{n+1}^{tr}\right\|}\left(\mathbf{I} - \frac{1}{3}\mathbf{1}\otimes\mathbf{1} - \mathbf{n}_{n+1}\otimes\mathbf{n}_{n+1}\right)$$

$$\frac{d\mathbf{n}}{d\boldsymbol{\varepsilon}} = \frac{\frac{d\mathbf{s}^{tr}}{d\boldsymbol{\varepsilon}}\left\|\mathbf{s}^{tr}\right\| - \mathbf{s}^{tr}\otimes\frac{d\left\|\mathbf{s}^{tr}\right\|}{d\boldsymbol{\varepsilon}}}{\left\|\mathbf{s}^{tr}\right\|^{2}} = \frac{2G}{\left\|\mathbf{s}^{tr}\right\|}\left(\mathbf{I} - \frac{1}{3}\mathbf{1}\otimes\mathbf{1}\right) - \frac{\mathbf{n}}{\left\|\mathbf{s}^{tr}\right\|}\otimes 2G\mathbf{n}$$

$$= \frac{2G}{\left\|\mathbf{s}^{tr}\right\|}\left(\mathbf{I} - \frac{1}{3}\mathbf{1}\otimes\mathbf{1} - \mathbf{n}\otimes\mathbf{n}\right)$$

$$\frac{d\mathbf{s}^{tr}}{d\boldsymbol{\varepsilon}} = \frac{d\boldsymbol{\sigma}^{tr}}{d\boldsymbol{\varepsilon}} - \frac{dp^{tr}}{\partial\boldsymbol{\varepsilon}}\otimes\mathbf{1} = 2G\left(\mathbf{I} - \frac{1}{3}\mathbf{1}\otimes\mathbf{1}\right)$$

$$\frac{\partial\left\|\mathbf{s}^{tr}\right\|}{\partial\boldsymbol{\varepsilon}} = \frac{\partial\sqrt{\mathbf{s}^{tr}:\mathbf{s}^{tr}}}{\partial\boldsymbol{\varepsilon}} = \frac{\partial\left(\mathbf{s}^{tr}:\mathbf{s}^{tr}\right)^{1/2}}{\partial\boldsymbol{\varepsilon}} = \frac{1}{2}\left(\mathbf{s}^{tr}:\mathbf{s}^{tr}\right)^{-1/2}\mathbf{s}^{tr}:\frac{\partial\mathbf{s}^{tr}}{\partial\boldsymbol{\varepsilon}}\times 2 = \frac{\mathbf{s}^{tr}}{\left\|\mathbf{s}^{tr}\right\|}:\frac{\partial\mathbf{s}^{tr}}{\partial\boldsymbol{\varepsilon}} = \mathbf{n}:\frac{\partial\mathbf{s}^{tr}}{\partial\boldsymbol{\varepsilon}}$$

$$= \mathbf{n}:2G\left(\mathbf{I} - \frac{1}{3}\mathbf{1}\otimes\mathbf{1}\right) = 2G\mathbf{n}$$

$$\frac{d\hat{\gamma}_{n+1}}{d\boldsymbol{\varepsilon}_{n+1}}\otimes KD\mathbf{1} = \frac{\left(2G\mathbf{n}_{n+1} + KB\mathbf{1}\right)}{F}\otimes KD\mathbf{1} = \frac{2GKD}{F}\mathbf{n}_{n+1}\otimes\mathbf{1} + \frac{K^{2}BD}{F}\mathbf{1}\otimes\mathbf{1}$$

$$\frac{d\hat{\gamma}_{n+1}}{d\boldsymbol{\varepsilon}_{n+1}} = \frac{\left(2G\mathbf{n}_{n+1} + KB\mathbf{1}\right)}{F}$$

$$\frac{\partial p^{tr}}{\partial\boldsymbol{\varepsilon}} = K\frac{\partial tr\left(\boldsymbol{\varepsilon}^{tr}\right)}{\partial\boldsymbol{\varepsilon}} = K\mathbf{1} \quad \left(\because \frac{\partial\varepsilon_{ii}}{\partial\varepsilon_{mn}} = \delta_{im}\delta_{in} = \delta_{mn} = \mathbf{1}\right)$$

$$2G\frac{d\hat{\gamma}_{n+1}}{d\boldsymbol{\varepsilon}_{n+1}}\otimes\mathbf{n}_{n+1} = 2G\frac{\left(2G\mathbf{n}_{n+1} + KB\mathbf{1}\right)}{F}\otimes\mathbf{n}_{n+1} = \frac{\left(2G\right)^{2}}{F}\mathbf{n}_{n+1}\otimes\mathbf{n}_{n+1} + \frac{2GKB}{F}\mathbf{1}\otimes\mathbf{n}_{n+1}$$

$$2G\hat{\gamma}_{n+1}\frac{d\mathbf{n}_{n+1}}{d\boldsymbol{\varepsilon}_{n+1}} = \frac{\left(2G\right)^{2}\hat{\gamma}_{n+1}}{\left\|\mathbf{s}_{n+1}^{tr}\right\|}\left(\mathbf{I} - \frac{1}{3}\mathbf{1}\otimes\mathbf{1} - \mathbf{n}_{n+1}\otimes\mathbf{n}_{n+1}\right)$$

The increment from of constitutive equation with additive strain split is as follows:

$$\boldsymbol{\varepsilon} = \boldsymbol{\varepsilon}^{e} + \boldsymbol{\varepsilon}^{vp} \rightarrow \dot{\boldsymbol{\varepsilon}} = \dot{\boldsymbol{\varepsilon}}^{e} + \dot{\boldsymbol{\varepsilon}}^{vp} \rightarrow \Delta\boldsymbol{\varepsilon} = \Delta\boldsymbol{\varepsilon}^{e} + \Delta\boldsymbol{\varepsilon}^{vp} \rightarrow \boldsymbol{\varepsilon}_{n+1}^{e} = \boldsymbol{\varepsilon}_{n}^{e} + \Delta\boldsymbol{\varepsilon} - \Delta\boldsymbol{\varepsilon}^{vp} = \boldsymbol{\varepsilon}_{n+1}^{e,trial} - \Delta\boldsymbol{\varepsilon}^{vp}$$

$$\mathbf{C}^{0} : \boldsymbol{\varepsilon}_{n+1}^{e} = \mathbf{C}^{0} : \boldsymbol{\varepsilon}_{n+1}^{e,trial} - \mathbf{C}^{0} : \Delta\boldsymbol{\varepsilon}^{vp} \rightarrow \boldsymbol{\sigma}_{n+1} = \boldsymbol{\sigma}_{n+1}^{trial} - \mathbf{C}^{0} : \Delta\boldsymbol{\varepsilon}^{vp} \rightarrow \boldsymbol{\sigma}_{n+1}^{trial} = \mathbf{C}^{0} : \boldsymbol{\varepsilon}_{n}^{e} + \mathbf{C}^{0} : \Delta\boldsymbol{\varepsilon}$$

$$\boldsymbol{\sigma}_{n+1} = \boldsymbol{\sigma}_{n+1}^{trial} - \mathbf{C}^{0} : \Delta\boldsymbol{\varepsilon}^{vp}$$

2.6 Reference

[1] Abu Al-Rub, R. K., Darabi, M.K., Little, D.N., and Masad, E.A. (2010). A Micro-Damage Healing Model that Improves Prediction of Fatigue Life in Asphalt Mixes, International Journal of Engineering Science, **48 (11)**: pp. 966-990

[2] Ando, K., Ikeda, T., Sato, S., Yao, F., and Kobayashi, Y. (1998). A preliminary study on crack healing behavior of Si3N4/SiC composite ceramics. *Fatigue & Fracture of Engineering Materials & Structures*, **21(1)**, 119-122.

[3] Ando, K., Chu, M. C., Tsuji, K., Hirasawa, T., Kobayashi, Y., and Sato, S. (2002). Crack healing behavior and high-temperature strength of mullite/SiC composite ceramics. *Journal of the European Ceramic Society*, **22(8)**, 1313-1319.

[4] Ando, K., Houjyou, K., Chu, M. C., Takeshita, S., Takahashi, K., Sakamoto, S., and Sato, S. (2002). "Crack-healing behavior of Si3N4/SiC ceramics under stress and fatigue strength at the temperature of healing (1000 degrees C)." *Journal of the European Ceramic Society*, **22(8)**, 1339-1346.

[5] Barbero, E.J. (1999). Introduction to Composite Materials Design. Taylor & Francis, Philadephia, PA.

[6] Barbero, E.J., and Ford, K.J. (2007). Characterization of Self-Healing Fiber-Reinforced

Polymer-Matrix Composites with Distributed Damage. *Journal of Advanced Materials* (SAMPE), **39(4)**: pp. 20-27

[7] Barbero, E.J., Greco, F., Lonetti, P. (2005). Continuum Damage-Healing Mechanics with Application to Self-Healing Composites. *International Journal of Damage Mechanics*, **14(1)**: pp. 51-81.

[8] Bhasin, A., Little, D.N., Bommavaram, R., and Vasconcelos, K. (2008). A Framework to Quantify the Effect of Healing in Bituminous Materials using Material Properties, *Road Materials and Pavement Design 9*: pp. 219-242.

[9] Brown, E. N., Sottos, N.R., and White, S.R. (2002). Fracture Testing of a Self-Healing Polymer Composite, *Experimental Mechanics*, **42**: pp. 372-379.

[10] Carpenter, S. H., and Shen, S. (2006). A Dissipated Energy Approach to Study HMA Healing in Fatigue, *85th Annual Meeting of the Transportation Research Board Washington D.C.*

[11] Chen, W.F., and Han, D.J. (1988). Plasticity for structural engineers, Springer-Verlag, NY

[12] Chu, M. C., Sato, S., Kobayashi, Y., and Ando, K. (1995). Damage Healing and Strengthening Behavior in Intelligent Mullite/Sic Ceramics. *Fatigue & Fracture of Engineering Materials & Structures*, 18(9), 1019-1029.

[13] Chow, C. L., and Wang, J. (1987a). An Anisotropic Theory of Continuum Damage Mechanics for Ductile Fracture, *Engineering Fracture Mechanics*, **27**: pp. 547-558.

[14] Chow, C. L., and Wang, J. (1987b). An Anisotropic Continuum Damage Theory and its Application to Ductile Crack Initiation. In: Wang, A.S.D. and Haritos, G.K. (eds), *Proceedings of ASME Winter Annual Meeting, 13-18 December, Boston, MA*: pp. 1-9.

[15] Chow, C. L., and Wang, J. (1988). Durctile Fracture Characterization with an Anisotropic Continuum Damage Theory, *Engineering Fracture Mechanics*, **30**: pp. 547-563.

[16] Chaboche, J. L. (1981). Continuous damage mechanics - a tool to describe phenomena before crack initiation. *Nuclear Engineering and Design*, 64(2), 233-247.

[17] Chaboche, J. L. (1988). Continuum damage mechanics .1. General concepts. *Journal of Applied Mechanics, ASME*, 55(1), 59-64.

[18] Chaboche, J. L. (1988). Continuum damage mechanics .2. Damage growth, crack initiation, and crack-growth. *Journal of Applied Mechanics*, *ASME*, 55(1), 65-72.

[19] Cordebois, J. P., and Sidoroff, F. (1979). Damage Induced Elastic Anisotropy. In: Boehler, J.P. (ed.), *Proceedings of EUROMECH Colloque on Mechanical Behavior of Anisotropic Solids*, **115**: 19-22 June, Villard-de Lans: pp. 761-774.

[20] Cordebois, J.P., and Sidoroff, F. (1982). Endommagement Anisotrope En Elasticite Et Plasticite, *Journal de Mecanique Theorique et Appliquee*, No. special: pp. 45-59.

[21] Daniel, J. S., and Kim, Y.R. (2001). Laboratory Evaluation of Fatigue Damage and Healing of Asphalt Mixtures, *Journal of Materials in Civil Engineering, ASCE*, **13** (6): pp. 434-440.

[22] Darabi, M. K., Abu Al-Rub, R.K., Masad, E.A., and Little, D.N. (2013). Constitutive Modeling of Fatigue Damage Response of Asphalt Concrete Materials with Consideration of Micro-Damage Healing, *International Journal of Solids and Structures,* **50**: pp. 2901-2913.

[23] Dragon, A. (1985). Plasticity and Ductile Fracture Damage: Study of Void Growth in Metals, *Engineering Fracture Mechanics*, **21**: pp. 875-885.

[24] Dragon, A., and Chihab, A. (1985). On Finite Damage: Ductile Fracture-Damage Evolution, *Mechanics of Materials*, **4**: pp. 95-106.

[25] Files, B.S. (1997). Design of a Biomimetic Self-Healing Super-alloy Composite, Dissertation, Northwestern University.

[26] Files, B., and Olson, G. (1997). Terminator 3: Biomimetic Self-Healing Alloy Composite, in SMST-97: *Proceedings of the Second International Conference on Shape Memory and Superelastic Technologies* (eds A. Pelton, D. Hodgson, S. Russell and T. Duerig), The International Organization on Shape Memory and Superelastic Technologies.

[27] Germain, P., Nguyen, Q. S., and Suquet, P. (1983). "Continuum thermodynamics." *Journal of Applied Mechanics, ASME,* 50(4B), 1010-1020.

[28] Ghosh, S. K. (2009). Self-healing Materials: Fundamentals, Design Strategies, and Applications, Weinheim: Wiley-VCH.

[29] Graham, M. A. (2009). Damaged viscoelastic-viscoplastic model for asphalt mixes, Civil Engineering. Texas A&M University, College Station, Texas.

[30] Guo, Y. F., and Guo, W.L., (2006). Self-Healing Properties of Flaws in Nanoscale Materials: Effects of Soft and Hard Molecular Dynamics Simulations and Boundaries Studied Using a Continuum Mechanical Model, *Physical Review B*, **73**: pp. 1-7.

[31] Herbst, O., and Luding, S. (2008). Modeling Particulate Self-Healing Materials and Application to Uni-Axial Compression, *International Journal of Fracture*, **154**: pp. 87-103.

[32] Hill, R., and Rice, J. R. (1973). "Elastic potentials and structure of inelastic constitutive laws." *Siam Journal on Applied Mathematics,* 25(3), 448-461.

[33] Hult, J. (1974). Creep in Continua and Structures, *Topics in Applied Continuum Mecahnics*, Springer, N.Y.: p. 137.

[34] Ju, J. W. (1989a). On Energy-Based Coupled Elastoplastic Damage Theories-Constitutive

Modeling and Computational Aspects, *International Journal of Solids and Structures*, **25**: pp. 803-833.

[35] Ju, J. W. (1989b). On Energy-Based Coupled Elastoplastic Damage Models at Finite Strains, *Journal of Engineering Mechanics, ASCE*, **115**: pp. 2507-2525.

[36] Ju, J. W. (1990). Isotropic and Anisotropic Damage Variables in Continuum Damage Mechanics, *Journal of Engineering Mechanics, ASCE*, **116**: pp. 2764-2770.

[37] Ju, J. W., Ko, Y.F., and Zhang, X.D. (2009). Multi-level Elastoplastic Damage Mechanics for Elliptical Fiber Reinforced Composites with Evolutionary Fiber Debonding, *International Journal of Damage Mechanics*, **18**: pp. 419-460.

[38] Ju, J. W., and Yanase, K. (2009). Micromechanical Elastoplastic Damage Mechanics for Elliptical Fiber Reinforced Composites with Progressive Partial Fiber Debonding, *International Journal of Damage Mechanics*, **18**: pp. 639-668.

[39] Ju, J. W., and Yuan, K.Y. (2012c). New Strain-Energy-Based Coupled Elastoplastic Two-Parameter Damage and Healing Models for Earth-Moving Processes, *International Journal of Damage Mechanics*, **21** (7): pp. 989-1019.

[40] Ju, J. W., Yuan, K.Y., and Kuo, W. (2012a). Novel Strain Energy Based Coupled Elastoplastic Damage and Healing Models for Geomaterials - Part I: Formulations, *International Journal of Damage Mechanics*, **21** (4): pp. 525-549.

[41] Ju, J. W., Yuan, K.Y. Kuo, W., and Chen, J.S. (2012b). Novel Strain Energy Based Coupled Elastoplastic Damage and Healing Models for Geomaterials - Part II: Computational Aspects, *International Journal of Damage Mechanics*, **21** (4): pp. 551-576.

[42] Kachanov, L.M. (1958). Rupture Time under Creep Conditions, *Izvestia Akademii Nauk*

SSSR, Otdelenie Tekhnicheskich Nauk, **8**: pp. 26-31.

[43] Kachanov, M. (1980). Continuum Model of Medium with Cracks, *Journal of the Engineering Mechanics Division, ASCE,* **106**: pp. 1039-1051.

[44] Kachanov, M. (1987). Elastic Solids with Many Cracks - A Simple Method of Analysis, *International Journal of Solids and Structures*, **23**: pp. 23-43.

[45] Kessler, M.R. (2007). Self-Healing: A New Paradigm in Materials Design, *Proceedings of the Institution of Mechanical Engineers Part G-Journal of Aerospace Engineering,* **221**: pp. 479-495.

[46] Kessler, M.R., Blaiszik, B.J., White, S.R., and Sottos, N.R. (2007). Recent Advances in Self-Healing Materials Systems, In Adaptive Structures: Engineering Applications (eds D. Wagg, I. Bond, P. Weaver, and M. Friswell), John Wiley & Sons, West Sussex: pp. 247-260.

[47] Kessler, M.R., and White, S.R. (2001). Self-Activated Healing of Delamination Damage in Woven Composites, *Composites Part a-Applied Science and Manufacturing*, **32**: pp. 683-699.

[48] Kim, Y.R., Whitmoyer, S.L., and Little, D.N. (1994). Healing in Asphalt Concrete Pavements: Is it Real?, *Transportation Research Board 1454*: pp. 89-96.

[49] Krajcinovic, D. (1983). Constitutive Equations for Damage Materials. *Journal of Applied Mechanics,* **50**: pp. 355-360.

[50] Krajcinovic, D. and Fanella, D. (1986). A Micromechanical Damage Model for Concrete, Engineering Fracture Mechanics, **25**: pp. 585-596.

[51] Krajcinovic, D., and Fonseka, G.U. (1981). The Continuous Damage Theory of Brittle Materials. Part 1: General-theory, *Journal of Applied Mechanics, ASME,* **48**: pp. 809-815.

[52] Ladeveze, P., and Lubineau, G. (2003). On a Damage Mesomodel for Laminates: Micromechanics Basis and Improvement, *Mechanics of Materials*, **35**: pp. 763-775.

[53] Leckie, J. L., and Hayhurst, D. (1974). Creep Rupture of Structure, *Proc. Royal Society, London*, **A340**: pp. 323-347.

[54] Lee, H., Peng, K., and Wang, J. (1985). An Anisotropic Damage Criterion for Deformation Instability and its Application to Forming Limit Analysis of Metal Plates, *Engineering Fracture Mechanics*, **21**: pp. 1031-1054.

[55] Lee, H. J., and Kim. Y.R. (1998). Viscoelastic Continuum Damage Model of Asphalt Concrete with Healing, *Journal of Engineering Mechanics, ASCE*, **124** (11): pp. 1224-1232.

[56] Lemaitre, J. (1971). Evaluation of Dissipation and Damage in Metals Submitted to Dynamic Loading, *Proceedings of the First International Conference*, Kyoto, Japan; Aug. 15-20: pp. 540-549.

[57] Lemaitre, J. (1984). How to Use Damage Mechanics, *Nuclear Engineering and Design*, **80**: pp. 233-245.

[58] Lemaitre, J. (1985). A Continuous Damage Mechanics Model for Ductile Fracture, *Journal of Engineering Materials and Technology*, **107**: pp. 83-89.

[59] Lemaitre, J. (1986). Plasticity and Damage Under Random Loading. In: Lamb, J.P. (ed.), *Proceedings of the 10th US National Congress of Applied Mechanics*, 16-20 June, Austin, TX: pp. 125-134.

[60] Lemaitre, J. (1992). A course on damage mechanics. *Springer-Verlag, Berlin.*

[61] Lemaitre, J., and Chaboche, J.L. (1975). A Nonlinear Model of Creep Fatigue Cumulation and Interaction, *Proc. IUTAM, Symposium on Mechanics of Viscoelastic Media and Bodies*:

pp. 291-301.

[62] Lemaitre, J., and Chaboche, J.L. (1990). Mechanics of solid materials. Cambridge University Press, Cambridge, UK

[63] Li, V.C., Lim Y.M., and Chan, YW (1998). Feasibility Study of A Passive Smart Self-Healing Cementitious Composite. *Composite Part B: Engineering* **29(B)**: pp. 819-827

[64] Little, D. N., and Bhasin, A. (2007). Exploring mechanisms of healing in asphalt mixtures and quantifying its impact. In: van der Zwaag, S. (ed.). *Self healing materials*. Springer, Dordrecht, The Netherlands.

[65] Lytton, R. L., Chen, C.W., and Little, D.N. (2001). Microdamage Healing in Asphalt and Asphalt Concrete, Volume IV: A Viscoelastic Continuum Damage Fatigue Model of Asphalt Concrete With Microdamage Healing, *FHWA-RD-98-144*

[66] Manuel, M.V. (2007). Design of a Biomimetic Self-Healing Alloy Composite, Northwestern University.

[67] Manuel, M.V. ,and Olson, G.B. (2007). Biomimetic Self-Healing Metals, in *Proceedings of the First International Conference on Self-Healing Materials*, Series in Materials Science, Vol. 100, Springer, Noordwijk aan Zee, pp. 18-20.

[68] Mehta, P.K., and Meryman, H., (2009). Tools for reducing carbon emissions due to cement consumption, Structure: pp.12-15

[69] Miao, S., Wang, M.L., and Schreyer, H.L. (1995). Constitutive Models for Healing of Materials with Application to Compaction of Crushed Rock-Salt, *Journal of Engineering Mechanics, ASCE*, 121: pp. 1122-1129.

[70] Mihashi, H., Kaneko, Y., Nishiwaki, T., and Otsuka, K. (2000). Fundamental Study on

Development of Intelligent Concrete Characterized by Self-Healing Capability for Strength, *Transactions of the Japan Concrete Institute*, 22: pp. 441-450.

[71] Miner, M. A. (1945). Cumulative Damage in Fatigue, *Journal of Applied Mechanics, ASME*, **67**: A159-A164.

[72] Murakami, S. (1983). Notion of Continuum Damage Mechanics and its Application to Anisotropic Cree Damage Theory, *Journal of Engineering Materials and Technology*, **105**: pp. 99-105.

[73] Murakami, S., and Ohno, N. (1981). A Continuum Theory of Creep and Creep Damage, *Proc. IUTAM, Symposium on Creep in Structures*: pp. 422-444.

[74] Nakao, W., Takahashi, K., and Ando, K. (2005). Self-Healing of Surface Cracks in Structural Ceramics, Self-Healing Materials: Fundamentals, Design Strategies, and Applications, pp. 183-218.

[75] Nishiwaki, T., Mihashi, H., Jang, B-K, and Miura, K. (2006). Development of Self-Healing System for Concrete with Selective Heating around Crack. *Journal of Advanced Concrete Technology*, **4(2)**: pp. 267-275.

[76] Oda, M., and Nakayama, H. (1989). Yield function for soil with anisotropic fabric, *Journal of Engineering Mechanics, ASCE* **15**(1): pp. 89-105.

[77] Ortiz, M. (1985). A Constitutive Theory for the Inelastic Behavior of Concrete, *Mechanics of Materials Science and Engineering*, **4**: pp. 67-93.

[78] Palmgreen, A. (1924). The Service Life of Ball Bearings, *Zeitschrift des Vereines Deutscher Ingenieure*, **68** (14): pp. 339-341.

[79] Perzyna, P. (1966). Fundamental Problems in Viscoplasticity, *Advances in Applied*

Mechanics, **9** (2): pp. 244-368.

[80] Pronk, A.C. (2011). Partial Healing in Fatigue Tests on Asphalt Specimens, *Road Materials and Pavement Design*, 2(4): pp. 433-445.

[81] Rabotnov, Y. N. (1969). Creep Rupture. In: Hetenyi, M. and Vincenti, W.G. (eds), *Proceedings of the 12th International Congress of Applied Mechanics*, Stanford, Springer-Verlag, Berlin.

[82] Reinhardt, H. W., and Jooss, M., (2003). Permeability and Self-Healing of Cracked Concrete as a Function of Temperature and Crack Width, *Cement and Concrete Research*, **33**: pp. 981-985.

[83] Rice, J. R. (1971). "Inelastic constitutive relations for solids - an internal-variable theory and its application to metal plasticity." *Journal of the Mechanics and Physics of Solids*, 19(6), 433-455.

[84] Robinson, E. L. (1952). Effect of Temperature Variations on the Long Time Strength of Steel, *Transaction ASME*, 74: pp. 777-780.

[85] Saadeh, S., and Masad, E. (2010). On the Relationship of Microstructure Properties of Asphalt Mixtures to Their Constitutive Behavior, *International Journal of Materials and Structural Integrity*, **4**: pp. 186-214.

[86] Saadeh, S., Masad, E., and Little, D. (2007). Characterization of Hot Mix Asphalt Using Anisotropic Damage Viscoelastic-Viscoplastic Model and Repeated Loading, *Journal of Materials in Civil Engineering, ASCE*, **19**: pp. 912-924.

[87] Sidoroff, F. (1981). Description of Anisotropic Damage Application to Elasticity, *IUTAM Colloqium on Physical Nonlinearities in Structural Analysis*: pp. 237-244.

[88] Simo, J. C., and Ju, J.W. (1987a). Strain-Based and Stress-Based Continuum Damage Models, Part I: Formulation, *International Journal of Solids and Structures*, **23**: pp. 821-840.

[89] Simo, J. C., and Ju, J.W. (1987b). Strain-Based and Stress-Based Continuum Damage Models, Part II: Computational Aspects, *International Journal of Solids and Structures*, **23**: pp. 841-869.

[90] Tan, S. A., Low, B. H., and Fwa, T. F. (1994). Behavior of asphalt concrete mixtures in triaxial compression. *Journal of Testing and Evaluation*, **22(3)**, 195-203.

[91] Uzan, J. (2005). Viscoelastic-viscoplastic model with damage for asphalt concrete, *Journal of Materials in Civil Engineering, ASCE*, 17: pp. 528-534.

[92] Violeau, D., Ladeveze, P., and Lubineau, G. (2009). Micromodel-Based Simulations for Laminated Composites, *Composite Science and Technology*, **69**: pp. 1367-1371.

[93] Voyiadjis, G.Z., and Kattan, P.I. (2006). *Advances in Damage Mechanics: Metals and Metal Matrix Composites with an Introduction to Fabric Tensors*, 2nd edition, Elsevier Ltd., Amsterdam, ISBN 978-0-08-044688-2.

[94] White, S.R., Sottos, N.R., Geubelle, P.H., Moore, J.S., Kessler, M.R., Sriram, S.R., Brown, E.N., and Viswanathan, S., (2001). Autonomic Healing of Polymer Composites, *Nature*, **409**: pp. 794-797

[95] Wool, R. P., and Oconnor, K.M. (1981). A Theory of Crack Healing in Polymers, *Journal of Applied Physics*, **52**: pp. 5953-5963.

[96] Wu, C.H. (1985). Tension-Compression Test of a Concrete Specimen via a Structure Damage Theory. In: Stubbs, N. and Krajcinovic, D. (eds), Damage Mechanics and

Continuum Modelling, New York, Elsevier Science, pp. 1-12.

[97] Yanase, K., and Ju, J.W. (2011). Effective Elastic Moduli of Spherical Particle Reinforced Composites Containing Imperfect Interfaces, *International Journal of Damage Mechanics of Materials* with DOI: 10.1177/1056789510397076.

[98] Yuan, K. Y., and Ju, J.W. (2013). New Strain Energy–Based Coupled Elastoplastic Damage-Healing Formulations Accounting for Effect of Matric Suction during Earth-Moving Processes, *Journal of Engineering Mechanics, ASCE*, **139** (2): pp. 188-199.

[99] Yuan, K. Y., Ju, J.W., Yuan, W., Yang, J.M. (2014). Numerical Predictions of Mechanical Behavior of Innovative Pothole Patching Materials Featuring High Toughness, Low-Viscosity Nano-Molecular Resins, *Acta Mechanica*, **225** (4), pp. 1141-1151.

[100] Zeinkiewicz, O., Huphenson, C., and Lewis, R. (1975). Associated and non-associated visco-plasticity in soils mechanics, *Journal of Geotechnique* **25**(5): pp. 671-689.

[101] http://homepages.engineering.auckland.ac.nz/~pkel015/SolidMechanicsBooks/index.html

3. NEW INITIAL STRAIN ENERGY BASED THERMO-ELASTOVISCOPLASTIC ISOTPRIC DAMAGE-SELF HEALING MODEL FOR BITUMINOUS COMPOSITES – PART I: FORMULATIONS

3.1 Introduction

New ***initial elastic energy*** based thermo-elastoviscoplastic ***isotropic*** damage-self healing formulations, based on continuum thermodynamics framework, are developed in the next section. In order to account for the healing effect, the concept of net space is defined because the effective space only considers the damage. In addition, an ***Arrhenius-type temperature term*** is proposed and uncoupled with Helmholtz free energy potential to account for the effect of temperature. The viscoplastic flow is introduced by means of an additive split of the stress tensor. In particular, the governing damage and self-healing evolutions are ***coupled*** in an incremental form with definition of damage and healing area and characterized through the ***net stress*** concept in conjunction with the hypothesis of strain equivalence in this chapter.

3.2 A Coupled Isotropic Formulation

A basic concept underlining the initial (undamaged) elastic strain energy based isotropic damage-healing model shown in this chapter is the hypothesis that incremental damage and self-healing histories in asphalt mixtures are directly linked to the history of total strains with temperature. The notion of net healed stress along with the hypothesis of strain equivalence follows from the assumed form of free energy. In order to consider the effect of the temperature, the Arrhenius-type temperature term is chosen uncoupled for simplicity. The proposed isotropic damage, isotropic healing, and the combined (net) damage-healing variables are mainly focused in this chapter.

3.2.1 Definition of Net (Combined) Variables of the Isotropic Damage and Healing

Let us define d as the damage variable and R as the healing variable, respectively, below with the damaged area A^d, the healed area A^R, and the unhealed A^{uR} presented in Figure 3.1.

$$d = A^d / A \tag{3.1}$$

$$R = A^R / A^d \tag{3.2}$$

Due to the assumption that only undamaged and healed area can sustain the loading in continuum damage mechanics and the applied forces are equal in physical space and net space as shown in Eq. (3.3), we define d^{net} as a scalar variable to describe the net (combined) effect of damage-healing

$$\mathbf{F} = \boldsymbol{\sigma} A = \boldsymbol{\sigma}^{net} A^{net} \tag{3.3}$$

$$d^{net} = d\left(1 - R\right) \tag{3.4}$$

Because of the assumption that applied forces in net space and effective space are identical presented in Eq.(3.5), the following relationship between stresses in net space and effective space can be obtained and expressed in Eq.(3.6).

$$\mathbf{F} = \boldsymbol{\sigma}^{net} A^{net} = \bar{\boldsymbol{\sigma}} \bar{A} \tag{3.5}$$

$$\bar{\boldsymbol{\sigma}} = \frac{\left(1 - d^{net}\right)}{\left(1 - d\right)} \boldsymbol{\sigma}^{net} \tag{3.6}$$

Eq.(3.6) presents that the effective stress and the net stress are equal to each other only if either damage variable or healing variable is zero. Otherwise, the effective stress is always greater than the net stress since damage net variable is smaller than the damage variable due to the healing effect.

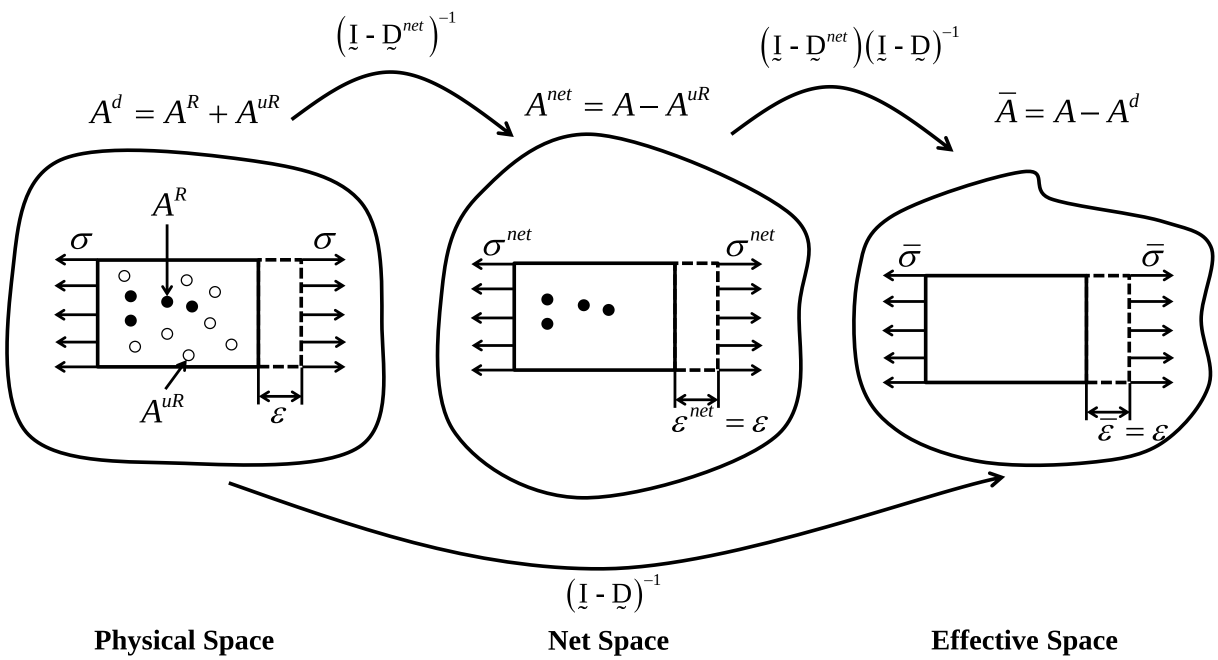

Figure 3.1 Schematic illustration of the physical, net, and effective spaces

3.2.2 Net Stress Concept and Hypothesis of Strain Equivalence

Physically, degradation of the material properties is the result of the initiation, growth and coalescence of microcracks or microvoids. Conversely, if the induced microdamage is gradually healed and subsequently its strength and stiffness are partially or fully recovered, it is called healing phenomenon. Within the context of continuum mechanics, one may model these processes by introducing an internal damage-healing variable which can be a scalar or a tensorial quantity. We denote by $\mathbf{M}^{net} = (\mathbf{I} - \mathbf{D}^{net})$ a fourth-order tensor which characterizes the state of damage net and transforms the homogenized stress tensor $\boldsymbol{\sigma}$ into the net stress tensor $\boldsymbol{\sigma}^{net}$ (or vice versa). Accordingly, it can be written as

$$\boldsymbol{\sigma}^{net} = \vartheta(T)^{-1}\left(\mathbf{M}^{net}\right)^{-1} : \boldsymbol{\sigma} \tag{3.7}$$

where $\vartheta(T)$ is the Arrhenius-type temperature term and defined as follows

$$\vartheta(T) = \exp\left\{-\boldsymbol{\delta}\left(1 - \frac{T}{T_0}\right)\right\} \tag{3.8}$$

where $\boldsymbol{\delta}$ is a material constant and T_0 is the reference temperature (°C).

For the isotropic damage and healing case, the mechanical behavior of micro damage and healing is independent of their orientation and depends only on a scalar variable $d^{net} = d(1-R)$ and $\mathbf{M}^{net}$ will simply reduce to $\left(1\text{-}d^{net}\right)\mathbf{I}$, where $\mathbf{I}$ is the rank four identity tensor. Eq.(3.7) then collapses to

$$\boldsymbol{\sigma}^{net}(t) = \frac{\boldsymbol{\sigma}(t)}{1 - d^{net}(t)} \tag{3.9}$$

where $d^{net}(\mathrm{t}) \in \left[0, d_{\mathrm{c}}^{net}\right]$ for $t \in \mathbb{R}_+$ is the net damage-healing variable , $\boldsymbol{\sigma}(t)$ is the Cauchy stress tensor, and $\boldsymbol{\sigma}^{net}(t)$ is the net stress tensor. Here, $d_{\mathrm{c}}^{net} \in (0,1]$ is a constant. The coefficient, $1-d^{net}\left(t\right)$, in the denominator of Eq. (3.9) is a reduction factor associated with combined effect of damage and healing in the materials. The value $d^{net}=0$ corresponds to the undamaged state or fully healing state whereas a value $d^{net}\in\left(0,d_c^{net}\right)$ represents a damaged state. The value $d^{net}=d_c^{net}$ defines complete local rupture. The net damage-healing variable may be interpreted physically as a ratio of difference between damaged and healed surface area to total surface area at a local material point. In addition, Lemaitre's hypothesis of strain equivalence [5] states:

"The strain associated with a damaged state under the applied stress is equivalent to the strain associated with its undamaged state under the effective stress"

However, this definition does not take into account healing effect. Therefore, we introduce the following hypothesis of strain equivalence by extending from the effective stress space to the net stress space:

"The strain associated with a damaged and healed state under the applied stress is equivalent to the strain ε^{net} associated with its damaged and healed state under the net stress". See Figure 3.2 for a schematic illustration.

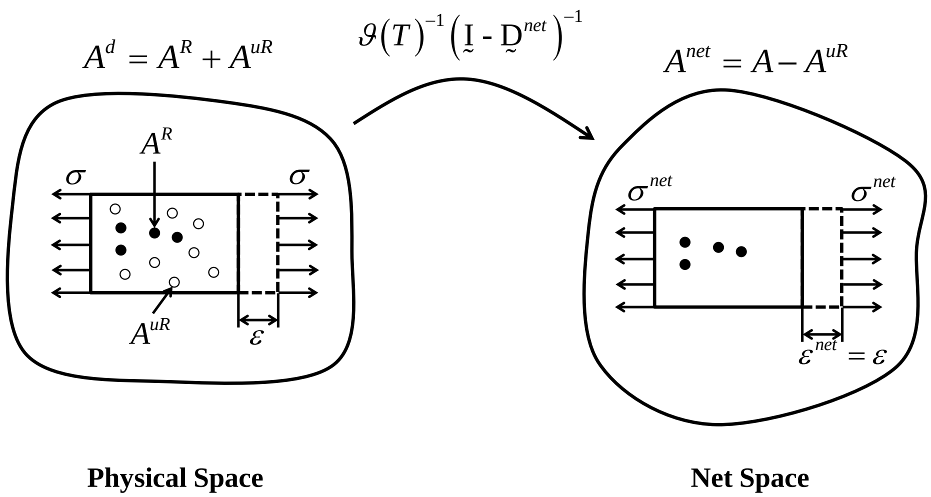

Figure 3.2 Schematic illustration of the hypothesis of strain

3.2.3 The Additive Stress Split

Within the present strain space framework, the viscoplastic flow is introduced by means of an additive split of the stress tensor into initial elastic and inelastic parts. By following the same concept within the net space owing to the healing phenomenon, one can yield

$$\boldsymbol{\sigma}^{net} = \frac{\partial \Psi^0(\boldsymbol{\varepsilon})}{\partial \boldsymbol{\varepsilon}} - \boldsymbol{\sigma}^{vp,net} \tag{3.10}$$

where $\boldsymbol{\sigma}^{net}$ is the net stress, $\boldsymbol{\varepsilon}$ is the total strain, $\Psi^0(\boldsymbol{\varepsilon})$ is the initial elastic strain energy function of the undamaged material, and $\boldsymbol{\sigma}^{vp,net}$ denotes the net viscoplastic relaxation stress. For linear elasticity, we write

$$\Psi^0(\boldsymbol{\varepsilon}) = \frac{1}{2}\boldsymbol{\varepsilon} : \mathbf{C}^0 : \boldsymbol{\varepsilon} \tag{3.11}$$

where $\mathbf{C}^0$ denotes the linear elasticity tensor. Eq. (3.10) then can be rewritten as the following

$$\boldsymbol{\sigma}^{net} = \mathbf{C}^0 : \boldsymbol{\varepsilon} - \boldsymbol{\sigma}^{vp,net} \tag{3.12}$$

3.2.4 The Thermodynamic Basis

In order to introduce the *net effect* of the damage-healing, viscoplastic flow processes and temperature effect, a free energy potential in the following form is proposed:

$$\Psi\left(\boldsymbol{\varepsilon}, \boldsymbol{\sigma}^{vp}, \mathbf{q}, d^{net}, T\right) \equiv \left\{\left(1 - d^{net}\right)\Psi^0\left(\boldsymbol{\varepsilon}\right) - \boldsymbol{\varepsilon} : \boldsymbol{\sigma}^{vp} + \Xi\left(\mathbf{q}, \boldsymbol{\sigma}^{vp}\right)\right\}\vartheta\left(T\right) \tag{3.13}$$

where $\boldsymbol{\varepsilon}$ denotes the total strain tensor, $\boldsymbol{\sigma}^{vp}$ is the viscoplastic relaxation stress tensor, $\mathbf{q}$ is a suitable set of internal (viscoplastic) variables. d^{net} will be further discussed in the subsequent section. $\Psi^0\left(\boldsymbol{\varepsilon}\right)$ is the initial elastic strain energy function of the undamaged material, and $\Xi\left(\mathbf{q}, \boldsymbol{\sigma}^{vp}\right)$ is the viscoplastic potential function.

In many applications, the thermal dissipation is very much smaller than the mechanical dissipation so that it is reasonable to assume that the thermal dissipation rate can be ignored. The Clausius-Duhem becomes Clausius-Plank inequality which takes the form for any admissible process in this research

$$-s\dot{T} - \dot{\Psi} + \boldsymbol{\sigma} : \dot{\boldsymbol{\varepsilon}} \geq 0 \tag{3.14}$$

By taking the time derivative of Eq.(3.13), substituting it into Eq. (3.14), and making use of standard arguments [2] along with the additional assumption that the net effect of damage-healing and viscoplastic unloading are elastic processes, we can obtain the stress-strain constitutive law

$$\boldsymbol{\sigma} = \frac{\partial \Psi(\boldsymbol{\varepsilon})}{\partial \boldsymbol{\varepsilon}} \vartheta(T) = \left\{ \left(1 - d^{net}\right) \frac{\partial \Psi^0(\boldsymbol{\varepsilon})}{\partial \boldsymbol{\varepsilon}} - \boldsymbol{\sigma}^{vp} \right\} \vartheta(T) = \left(1 - d^{net}\right) \boldsymbol{\sigma}^{net} \vartheta(T) \tag{3.15}$$

, the dissipative inequalities

$$\left\{ -\frac{\partial \Xi}{\partial \mathbf{q}} \cdot \ \dot{\mathbf{q}} - \left(\frac{\partial \Xi}{\partial \boldsymbol{\sigma}^p} - \boldsymbol{\varepsilon} \right) : \dot{\boldsymbol{\sigma}}^{vp} \right\} \vartheta(T) \geq 0 \tag{3.16}$$

$$\left\{ \Psi^0(\boldsymbol{\varepsilon}) \ \dot{d}^{net} - \frac{\partial \Xi}{\partial \mathbf{q}} \cdot \ \dot{\mathbf{q}} - \left(\frac{\partial \Xi}{\partial \boldsymbol{\sigma}^{vp}} - \boldsymbol{\varepsilon} \right) : \dot{\boldsymbol{\sigma}}^{vp} \right\} \vartheta(T) \geq 0 \tag{3.17}$$

and the entropy

$$s = -\frac{\partial \vartheta(T)}{\partial T} \Psi\left(\boldsymbol{\varepsilon}, \boldsymbol{\sigma}^{vp}, \mathbf{q}, d^{net}\right) \tag{3.18}$$

It follows from Eq.(3.15) that within the present strain space formulation, the stress tensor is split into elastic-damage-healing and the viscoplastic relaxation parts. From Eqs.(3.16) and (3.17), we observe that the dissipative energy by viscoplasticity itself is positive; if damage-healing effect is involved, the sum of damage-healing and viscoplasticity effect is also positive. It is also noted from Eqs.(3.15), (3.16), and (3.17) that the present framework is capable of accommodating general (nonlinear) elastic response and general viscoplastic response.

The potential $\Xi\left(\mathbf{q}, \boldsymbol{\sigma}^{vp}\right)$ is linked to viscoplastic dissipation. Its role is such that inequality (3.17) is satisfied for arbitrary processes. Note that we have assumed that $\Xi(\mathbf{q}, \boldsymbol{\sigma}^{vp})$ is independent of d^{net}. From Eq.(3.13), it then follows that

$$-Y \equiv -\frac{\partial \Psi\left(\boldsymbol{\varepsilon}, \boldsymbol{\sigma}^p, \mathbf{q}, d^{net}, T\right)}{\partial d^{net}} = \Psi^0(\boldsymbol{\varepsilon}) \vartheta(T) \tag{3.19}$$

Hence, the initial (undamaged) elastic strain energy $\Psi^0(\boldsymbol{\varepsilon})$ with Arrhenius-type temperature term $\vartheta(T)$ is the thermodynamic force Y conjugate to the net damage-healing variable d^{net}.

3.2.5 Characterization of Initial-Elastic Strain-Energy Based Isotropic Damage

The progressive degradation of mechanical properties of asphalt concrete due to damage by means of a simple isotropic damage mechanism is first characterized. To this end, we propose to define the notion of equivalent strain ξ as the (undamaged) energy norm of the strain tensor.

$$\xi \equiv \sqrt{\Psi^0(\boldsymbol{\varepsilon})\vartheta(T)} = \sqrt{\left\{\frac{1}{2}\boldsymbol{\varepsilon} : \mathbf{C}^0 : \boldsymbol{\varepsilon}\right\} \exp\left\{-\boldsymbol{\delta}\left(1-\frac{T}{T_0}\right)\right\}} \tag{3.20}$$

where $\boldsymbol{\delta}$ is a material constant and T_0 is the reference temperature (°C).

We now characterize the state of damage in asphalt mixtures by means of a damage criterion $\phi^d(\xi_t, g_t) \leq 0$, formulated in strain space, with the following functional form:

$$\phi^d(\xi_t, g_t) \equiv \xi_t - g_t \leq 0 \qquad t \in \mathbb{R}_+ \tag{3.21}$$

where the subscript t refers to a value at current time $t \in \mathbb{R}_+$, and g_t is the damage threshold at the current time t. It is noted that the numerical value of g_t would be lowered due to the incremental healing (if any) from the previous time step. Let g_0 denote the initial damage threshold before any loading is applied; we then have $g_t \geq g_0$. Here, g_0 is considered as a characteristic material property. The condition (3.21) states that damage in asphalt is initiated when the energy norm of the strain tensor ξ_t exceeds the initial damage threshold g_0. For the isotropic damage case, we define the evolution of the damage variable d_t and the damage threshold g_t, respectively, by the rate equations:

$$\dot{d}_t = \dot{\mu} H(\xi_t, d_t) \tag{3.22}$$

$$\dot{g} = \dot{\mu} \tag{3.23}$$

where $\dot{\mu} \geq 0$ is a damage consistency parameter that defines the damage loading/unloading conditions according to the Kuhn-Tucker relations

$$\dot{\mu} \geq 0, \qquad \phi^d(\xi_t, g_t) \leq 0, \qquad \dot{\mu}\ \phi^d(\xi_t, g_t) = 0 \tag{3.24}$$

The conditions (3.24) are standard for problems involving unilateral constraint. If $\phi^d(\xi_t, g_t) < 0$, the damage criterion is not satisfied and by conditions (3.24), $\dot{\mu} = 0$; hence, the damage rule (3.22) implies that $\dot{d} = 0$ and no further damage takes place. If, on the other hand, $\dot{\mu} > 0$; that is, further damage ("loading") is taking place, then conditions (3.24) implies that $\phi^d(\xi_t, g_t) = 0$. In this event, the value of $\dot{\mu}$ is determined by the damage consistency condition; i.e.,

$$\phi^d(\xi_t, g_t) = \dot{\phi}^d(\xi_t, g_t) = 0 \Rightarrow \dot{\mu} = \dot{\xi} \tag{3.25}$$

and g_t is defined by the expression presented in Eq.(3.26)

$$g_t = \max\left(g_0, \max_{s \in (-\infty, t)} \boldsymbol{\xi}_s\right) - g_{h,(t-1)} \tag{3.26}$$

where $g_{h(t-1)}$ defines the reduced value for the current damage threshold due to the incremental healing (if any) from the previous time step.

If $H(\xi_t, d_t)$ in condition (3.22) is independent of $\dot{d}_t$, the above formulation may be rephrased as follows. let $G : \mathbb{R} \to \mathbb{R}_+$ be such that $H(\xi_t) \equiv \partial G(\xi_t) / \partial \xi_t$. We shall assume that

$G(\cdot)$ is a monotonic function. A damage criterion entirely equivalent to condition (3.21) is given by $\bar{\phi}^d(\xi_t, g_t) \equiv G(\xi_t) - G(g_t) \le 0$. The flow rule and loading/unloading conditions then become

$$\dot{d}_t = \dot{\mu} \frac{\partial \bar{\phi}^d(\xi_t, g_t)}{\partial \xi_t}, \qquad g_t = \dot{\mu} \tag{3.27}$$

$$\dot{\mu} \ge 0, \qquad \bar{\phi}^d(\xi_t, g_t) \le 0, \qquad \dot{\mu}\bar{\phi}^d(\xi_t, g_t) = 0 \tag{3.28}$$

Conditions (3.27) and (3.28) are simply the Kuhn-Tucker optimality conditions of a principle of maximum damage dissipation.

Existing experimental results of bituminous materials suggest that the amount of microcracks or microcavities at a particular strain level exhibits *rate sensitivity* to the applied rate of loading in a (high strain rate) dynamic environment. A simple phenomenological characterization of this effect may be obtained by means of a *viscous regularization* of the rate-independent strain-based damage model introduced previously. Formally, the structure of this regularization is entirely analogous to the classical viscoplastic regularization of the Perzyna type [8][9]. The resulting rate-sensitive damage model (a) requires only one additional material parameter, i.e. the *damage fluidity coefficient* (μ); (b) as μ approaches zero exhibits instantaneous elastic response, whereas μ approaches infinity reduces to the rate-independent damage characterization; and (c) predicts decrease in nonlinearity of the stress-strain curves as the strain rate is increased. In other words, microcrack or microcavity growth is retarded at low strain rates.

Rate equations governing visco-damage behavior are obtained from their rate-independent counterpart by replacing consistency parameter $\dot{\mu}$ by $\mu g\left(\phi^d\right)$. Here μ is the damage fluidity coefficient (a material constant). The scalar function $g\left(\phi^d\right)$ represents the viscous damage flow function and ϕ^d is defined in Eq.(3.21). Accordingly, we have

$$\dot{d}_t = \mu\left\langle g\left(\phi^d\right)\right\rangle H\left(\xi_t, d_t\right) \tag{3.29}$$

$$\dot{g}_t = \mu\left\langle g\left(\phi^d\right)\right\rangle \tag{3.30}$$

where $\langle\cdot\rangle$ denotes the McAuley bracket (ramp function). For simplicity, in what follows we shall assume linear viscous damage, i.e. $g\left(\phi^d\right) = \phi^d$. Hence, Eqs.(3.29) and (3.30) reduce to

$$\dot{d}_t = \mu\left\langle \phi^d\left(\xi_t, g_t\right)\right\rangle H\left(\xi_t, d_t\right) \tag{3.31}$$

$$\dot{g}_t = \mu\left\langle \phi^d\left(\xi_t, g_t\right)\right\rangle \equiv \mu\left\langle \xi_t - g_t\right\rangle \tag{3.32}$$

The inviscid damage characterization and the instantaneous elasticity response can then be obtained as special cases of the rate-dependent damage formulation. These special cases and the related algorithmic treatments of visco-damage are addressed in details in Chapter 4.

3.2.6 Characterization of Initial-Elastic Strain-Energy Based Isotropic Healing

Similar to the characterization of damage in the previous section, we characterize the progressive recovery of mechanical properties of asphalt due to healing by means of a simple isotropic healing mechanism. However, there are required conditions to evolve healing in asphalt concrete; (a) the microcracks and microvoids are close to each other when there is healing, (b) healing cannot occur during the damage process (microdamage either propagate or heal at the same time), and (c) healing rate is zero when damage is evolving ($\dot{d} \geq 0$).

We use the same notion of equivalent strain energy ξ as the energy norm of the strain tensor. We also characterize the state of healing in asphalt mixtures by using a healing criterion $\phi^h(\xi_t, r_t) \leq 0$, formulated in the strain space, with the following functional form:

$$\phi^h(\xi_t, r_t) \equiv r_t - \xi_t \leq 0 \qquad t \in \mathbb{R}_+ \tag{3.33}$$

Here, r_t is the healing threshold at the current time t. We note that r_t will be lowered in value due to the incremental damage (if any) from the previous time step. If r_0 denotes the initial healing threshold before any healing occurs, we must have $r_t \geq r_0$. It is noted that r_0 is also considered as a characteristic material property. Condition (3.33) then states that healing in the material is initiated when the energy norm of the strain tensor ξ_t is smaller than the initial healing threshold r_0. For the isotropic healing case, we define the evolution of the healing variable R and the healing threshold r_t, respectively, by the rate equations

$$\dot{R}_t = \dot{\zeta} Z(\xi_t, R_t) \tag{3.34}$$

$$\dot{r} = \dot{\zeta} \tag{3.35}$$

where $\dot{\zeta} \geq 0$ is a healing consistency parameter that defines healing loading/unloading conditions according to the Kuhn-Tucker relations

$$\dot{\zeta} \geq 0, \qquad \phi^h(\xi_t, r_t) \leq 0, \qquad \dot{\zeta}\ \phi^h(\xi_t, r_t) = 0 \tag{3.36}$$

Conditions (3.36) are also standard for problems involving unilateral constraint. If $\phi^h(\xi_t, r_t) < 0$, the healing criterion is not satisfied and by conditions (3.36), $\dot{\zeta} = 0$; hence, the healing rule (3.34) implies that $\dot{R} = 0$ and no further healing takes place. If, on the other hand, $\dot{\zeta} > 0$; that is, further healing is taking place, then conditions (3.36) implies that $\phi^h(\xi_t, r_t) \le 0$. In this event, the value of $\dot{\zeta}$ is determined by the healing consistency condition; i.e.

$$\phi^h(\xi_t, r_t) = \dot{\phi}^h(\xi_t, r_t) = 0 \Rightarrow \dot{\zeta} = \dot{\xi} \tag{3.37}$$

and r_t is given by the expression

$$r_t = \min\left(r_0, \min_{s\in(-\infty,t)} \xi_s\right) + r_{d,(t-1)} \tag{3.38}$$

where $r_{d,(t-1)}$ is the value for the current healing threshold to be numerically increased due to the incremental damage (if any) from the previous time step.

If $Z(\xi_t, R_t)$ in condition (3.34) is independent of $\dot{R}_t$, the above formulation may be rephrased as follows. Let $G^*: \mathbb{R} \to \mathbb{R}_+$ be such that $Z(\xi_t) \equiv -\partial G^*(\xi_t)/\partial \xi_t$. We shall assume that $G^*(\cdot)$ is a monotonic function. A healing criterion entirely equivalent to conditions (3.33) is given by $\bar{\phi}^h(\xi_t, r_t) \equiv G^*(r_t) - G^*(\xi_t) \le 0$. The flow rule and loading/unloading conditions then become

$$\dot{R}_t = \dot{\zeta}\frac{\partial \bar{\phi}^h(\xi_t, r_t)}{\partial \xi_t}, \qquad r_t = \dot{\zeta} \tag{3.39}$$

$$\dot{\zeta} \ge 0, \qquad \bar{\phi}^h(\xi_t, r_t) \le 0, \qquad \dot{\zeta}\bar{\phi}^h(\xi_t, r_t) = 0 \tag{3.40}$$

3.2.7 Net (Combined) Effect of the Isotropic Damage and Healing

Taking the time derivative of Eq.(3.1) would lead to

$$\dot{d} = \dot{A}^d / A \tag{3.41}$$

As the derivations are based on linearization of the residual functions associated with the implicit backward Euler algorithms, the above equation can be expressed in the following incremental form for the updated damage variable:

$$d_{n+1} = d_n + \Delta d_{n+1} \tag{3.42}$$

In order to calculate the incremental form of healing variable, the same procedure can be applied under the condition of no damage evaluation because healing does not occur during the damage process or vice versa. However, during the damage process updated healing variable can be reduced by a ratio of damage variables since both the healed area, A^h, and the damaged area, $A^d = A^h + A^{uR}$, are changed. Therefore the updated healing variable would be as follows:

$$R_{n+1} = R_n + \Delta R_{n+1} \quad \left(\Delta d_{n+1} = 0\right) \tag{3.43}$$

$$R_{n+1} = \frac{d_{n+1}}{2d_{n+1} - d_n} R_n \quad \left(\Delta d_{n+1} > 0\right) \tag{3.44}$$

Taking the time derivative of (3.4) would yield

$$\begin{aligned} d_{n+1}^{net} &= d_n^{net} + \Delta d_{n+1}^{net} \\ \Delta d_{n+1}^{net} &= \Delta d_{n+1} - \Delta R_{n+1} d_n^{net} \end{aligned} \tag{3.45}$$

Let us consider, for conceptual illustration, a system with four springs as shown in Figure 3.3 and perform a series of cyclic conceptual tension- rest period (Four steps: T1-R1-T2-R2) tests on this hypothetical system

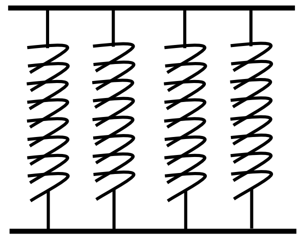

Figure 3.3 A system with four springs

We assume that these springs will be broken under tension and healed during rest periods. At the first step, tension T1 is applied on the system and two out of four springs are assumed to be broken. The damage variable of the system is therefore 2/4 = 0.5 as shown in Figure 3.4 (a). Next, the system is left for the rest period R1 and one spring is assumed to be healed as shown in Figure 3.4 (b). Since one of the broken springs is assumed healed, the healing variable of the system is 1/2 = 0.5 and the net damage-healing variable of the system is therefore 1/4 = 0.25. At the third step, tension T2 is applied and this time, three springs are assumed to be broken. The net damage-healing variable of the system is thus 3/4 = 0.75. Finally, during the rest period R2 all broken springs are completely recovered. The healing variable of the system at this stage is therefore 3/3 = 1 and the net damage -healing variable of the system is therefore 0. The computations of d^{net} by Eq. (3.45) at each time step for the system as shown in are listed in Table 3.1.

The characterizations of damage and healing, as discussed in the previous sections, can be considered as the *predictor formula* in our damage-healing algorithms. Once the associated damage or healing variables are computed at time step n+1 (damage and healing will not occur at the same step), net damage-healing variable at time step (n+1) is finally calculated. More details on algorithms about the coupling of damage and healing are provided in details in Chapter 4.

Table 3.1 Computation of d^{net} at different time step

Step	Δd_{n+1}	d_{n+1}	ΔR_{n+1}	R_{n+1}	Δd_{n+1}^{net}	d_{n+1}^{net}
1	$\frac{2}{4}$	$\frac{2}{4}$	0	0	$\frac{2}{4}$	$\frac{2}{4}$
2	0	$\frac{2}{4}$	$\frac{1}{2}$	$\frac{1}{2}$	$-\frac{1}{4}$	$\frac{1}{4}$
3	$\frac{2}{4}$	$\frac{4}{4}$	0	$\frac{1}{3}$	$\frac{2}{4}$	$\frac{3}{4}$
4	0	$\frac{4}{4}$	1	$\frac{4}{3}$	$-\frac{3}{4}$	0

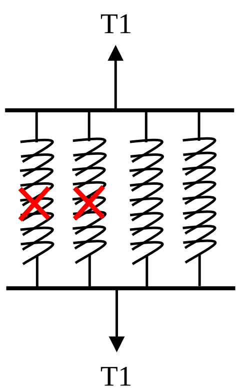

(a) System at step 1

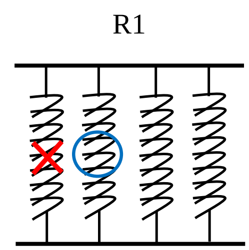

(b) System at step 2

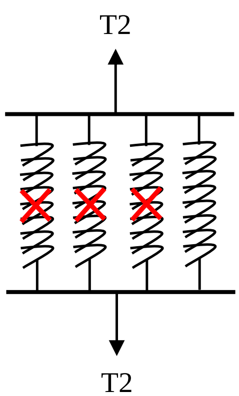

(c) System at step 3

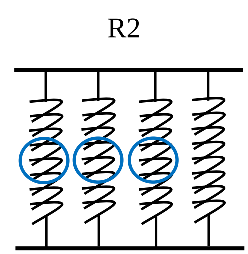

(d) System at step 4

Figure 3.4 The associated damage and healing variables of four-spring system at each step

3.3 Characterization of Net Viscoplastic Response and Consistent Tangent Moduli

In accordance with the notion of net stress, the characterization of the viscoplastic response should be formulated in the net stress space in terms of net stresses $\boldsymbol{\sigma}^{net}$ and $\boldsymbol{\sigma}^{vp,net}$. Therefore, for the classical situation in which the yield function is postulated in the stress space, we replace the homogenized Cauchy stress tensor $\boldsymbol{\sigma}$ by the net stress tensor $\boldsymbol{\sigma}^{net}$, so that the elastic-damage-healing domain is characterized by $f\left(\boldsymbol{\sigma}^{net},\mathbf{q}\right)\le 0$. Here, $\mathbf{q}$ represents the internal viscoplastic variables and the evolution of which is defined below. With the assumption of a non-associative flow rule, rate-dependent plastic response is characterized in the strain space by the flowing constitutive equations [3][4][8][9].

$$\dot{\boldsymbol{\sigma}}^{vp,net} = \dot{\gamma}\,\frac{\partial g_p}{\partial \boldsymbol{\varepsilon}}\left(\frac{\partial \Psi^0(\boldsymbol{\varepsilon})}{\partial \boldsymbol{\varepsilon}} - \boldsymbol{\sigma}^{vp,net},\mathbf{q}\right) \qquad (non-associative\ flow\ rule) \tag{3.46}$$

$$\dot{\mathbf{q}} = \dot{\gamma}\mathbf{h}\left(\frac{\partial \Psi^0(\boldsymbol{\varepsilon})}{\partial \boldsymbol{\varepsilon}} - \boldsymbol{\sigma}^{vp,net},\mathbf{q}\right) \qquad (viscoplastic\ hardening\ law) \tag{3.47}$$

$$f\left(\frac{\partial \Psi^0(\boldsymbol{\varepsilon})}{\partial \boldsymbol{\varepsilon}} - \boldsymbol{\sigma}^{vp,net},\mathbf{q}\right) \le 0 \qquad (loading\ condition) \tag{3.48}$$

$$\dot{\gamma} = \frac{1}{\eta}\left\langle g\left(f\left(\frac{\partial \Psi^0(\boldsymbol{\varepsilon})}{\partial \boldsymbol{\varepsilon}} - \sigma^{vp,net},\mathbf{q}\right)\right)\right\rangle \qquad (viscoplastic\ consistency\ parameter) \tag{3.49}$$

where g_p is the viscoplastic potential function, $\dot{\boldsymbol{\sigma}}^{vp,net}$ denotes the viscoplastic relaxation net stress rate tensor, γ denotes the viscoplastic consistency parameter, $\mathbf{h}$ signifies the hardening law, $\eta \in \left(0,\infty\right)$ is the so-called fluidity parameter, and $g(f)$ is a flow function, i.e. $g\left(f\right) = f^m$. $<\ >$ is *McAuley bracket*. As $\eta \to 0$ (no viscosity), one expects to recover the rate-independent formulation, i.e. $\dfrac{\langle (g(f)) \rangle}{\eta} \rightarrow \dot{\gamma}$ (finite). One argues that, as $\eta \rightarrow \infty$ (huge viscosity), states are instantaneous elasticity, i.e. $\dfrac{\langle (g(f)) \rangle}{\eta} \rightarrow 0$ (no viscoplastic strain). Eqs. (3.46) ~ (3.49) provide a characterization of viscoplasticity in the strain space. The loading/unloading conditions may be expressed in a compact form by requiring that

$$f\left(\frac{\partial \Psi^0(\boldsymbol{\varepsilon})}{\partial \boldsymbol{\varepsilon}} - \boldsymbol{\sigma}^{vp,net}, \mathbf{q}\right) \leq 0, \quad \dot{\gamma} \geq 0, \quad \dot{\gamma} f\left(\frac{\partial \Psi^0(\boldsymbol{\varepsilon})}{\partial \boldsymbol{\varepsilon}} - \boldsymbol{\sigma}^{vp,net}, \mathbf{q}\right) = 0 \tag{3.50}$$

Note that if $f < 0$, then $\dot{\gamma} = 0$ and the process is elastic damage. On the other hand, for loading $\dot{\gamma} \geq 0$ and $f = 0$. In the latter, $\dot{\gamma}$ is determined by requiring that $\dot{f} = 0$, which is considered viscoplastic consistency condition.

Making use of the notation $\boldsymbol{\sigma}^{net} = \partial \Psi^0(\boldsymbol{\varepsilon}) / \partial \boldsymbol{\varepsilon} - \boldsymbol{\sigma}^{vp,net}$ during loading, one arrives at

$$\frac{\partial f}{\partial \boldsymbol{\sigma}^{net}} : \dot{\boldsymbol{\sigma}}^{net} + \frac{\partial f}{\partial \mathbf{q}} \cdot \dot{\mathbf{q}} = 0 \tag{3.51}$$

where $\partial f / \partial \boldsymbol{\sigma}^{net}$ signifies the partial derivative of $f\left(\partial \Psi^0(\boldsymbol{\varepsilon}) / \partial \boldsymbol{\varepsilon} - \boldsymbol{\sigma}^{vp,net}, \mathbf{q}\right)$ with respect to the first argument. From Eq. (3.15), one can obtain

$$\dot{\boldsymbol{\sigma}}^{net} = \frac{\partial^2 \Psi^0(\boldsymbol{\varepsilon})}{\partial \boldsymbol{\varepsilon}^2} : \dot{\boldsymbol{\varepsilon}} - \dot{\boldsymbol{\sigma}}^{vp,net} = \frac{\partial^2 \Psi^0(\boldsymbol{\varepsilon})}{\partial \boldsymbol{\varepsilon}^2} : \left(\dot{\boldsymbol{\varepsilon}} - \dot{\gamma} \frac{\partial g_p}{\partial \boldsymbol{\sigma}^{net}}\right) \tag{3.52}$$

where the non-associative flow rule (3.46) has been applied. Thus, $\dot{\gamma}$ is determined from Eqs. (3.50) and (3.51) and the viscoplastic hardening law (3.47) as

$$\dot{\gamma}=\frac{\dfrac{\partial f}{\partial \boldsymbol{\sigma}^{net}}:\dfrac{\partial^2 \Psi^0(\boldsymbol{\varepsilon})}{\partial \boldsymbol{\varepsilon}^2}:\dot{\boldsymbol{\varepsilon}}}{\dfrac{\partial f}{\partial \boldsymbol{\sigma}^{net}}:\dfrac{\partial^2 \Psi^0(\boldsymbol{\varepsilon})}{\partial \boldsymbol{\varepsilon}^2}:\dfrac{\partial g_p}{\partial \boldsymbol{\sigma}^{net}}-\dfrac{\partial f}{\partial \mathbf{q}}\cdot \mathbf{h}} \tag{3.53}$$

Substituting Eq. (3.53) into Eq. (3.52) yields $\dot{\boldsymbol{\sigma}}^{net}=\mathbf{C}^{evp,net}:\dot{\boldsymbol{\varepsilon}}$, where $\mathbf{C}^{evp,net}$ is the net elastoviscoplastic tangent moduli given by

$$\mathbf{C}^{evp,net}=\frac{\partial^2 \Psi^0(\boldsymbol{\varepsilon})}{\partial \boldsymbol{\varepsilon}^2}-\frac{\dfrac{\partial f}{\partial \boldsymbol{\sigma}^{net}}:\dfrac{\partial^2 \Psi^0(\boldsymbol{\varepsilon})}{\partial \boldsymbol{\varepsilon}^2}\otimes\dfrac{\partial g_p}{\partial \boldsymbol{\sigma}^{net}}:\dfrac{\partial^2 \Psi^0(\boldsymbol{\varepsilon})}{\partial \boldsymbol{\varepsilon}^2}}{\dfrac{\partial f}{\partial \boldsymbol{\sigma}^{net}}:\dfrac{\partial^2 \Psi^0(\boldsymbol{\varepsilon})}{\partial \boldsymbol{\varepsilon}^2}:\dfrac{\partial g_p}{\partial \boldsymbol{\sigma}^{net}}-\dfrac{\partial f}{\partial \mathbf{q}}\cdot \mathbf{h}} \tag{3.54}$$

It is observe from Eq. (3.54) that $\mathbf{C}^{evp,net}$ is a non-symmetric tensor. If associative flow rule is selected $\partial f / \partial \boldsymbol{\sigma}^{net}=\partial g_p / \partial \boldsymbol{\sigma}^{net}$, $\mathbf{C}^{evp,net}$ becomes the major symmetry of the constitutive operator.

3.4 Model Example: Derivation of Consistent Tangent Moduli for Bituminous Materials in Net Space

For consistent (algorithmic) tangent moduli, the Perzyna [7] is employed in this work. In particular, the conventional Drucker-Prager model is chosen as a model problem for demonstration because the experiment results for bituminous materials show the dependence upon the hydrostatic stress components.

The Drucker-Prager criterion as loading function can be written in the form in the net space

$$f\left(\boldsymbol{\sigma}^{net},\varepsilon_{vp}\right)=\left\|\mathbf{s}^{net}\right\|-\left(A\left(\varepsilon_{vp}\right)-Bp^{net}\right) \tag{3.55}$$

where $\| \ \|$ is operation of tensor norm, $\mathbf{s}^{net}$ is the deviatoric net stress tensor satisfying the condition $\mathrm{tr}\left(\mathbf{s}^{net}\right)=0$, 'tr' is the trace operator, ε_{vp} is the equivalent viscoplastic strain, $p^{net}=\mathrm{tr}\left(\boldsymbol{\sigma}^{net}\right)/3$ is the mean normal net stress, and A and B are material constants. Lemaitre and Chaboche (1990) and Tan et al. (1994) show that B in the Drucker-Prager model is almost a constant as the material permanently deforms while A evolves with the permanent deformation. The evolution form of A is a function of equivalent viscoplastic strain given by

$$A\left(\varepsilon_{vp}\right)=A_0+A_1\left(1-\exp\left(-A_2\varepsilon_{vp}\right)\right) \tag{3.56}$$

where ε_{vp} is the equivalent viscoplastic strain given by [1]

$$d\varepsilon_{vp}=\frac{\sqrt{2/3}+B/3}{\sqrt{B^2+1}}\sqrt{d\varepsilon_{ij}^{vp}d\varepsilon_{ij}^{vp}} \tag{3.57}$$

For Perzyna-type viscoplasticity, it is assumed that the flow function equals to nonlinear loading function, i.e. $g(f)=f^m$ and the non-associative flow rule yields

$$\dot{\boldsymbol{\varepsilon}}^{vp}=\dot{\gamma}\frac{\partial g_p}{\partial\boldsymbol{\sigma}}=\frac{<g\left(f\right)>}{\eta}\frac{\partial g_p}{\partial\boldsymbol{\sigma}}=\frac{<f^m>}{\eta}\left(\mathbf{n}^{net}+\frac{D}{3}\mathbf{1}\right) \tag{3.58}$$

where $\mathbf{n}^{net}$ is the unit normal vector of $\mathbf{s}^{net}$ defined as $\frac{\mathbf{s}^{net}}{\left\|\mathbf{s}^{net}\right\|}$ and $g_p\left(\boldsymbol{\sigma}^{net}\right)=\left\|\mathbf{s}^{net}\right\|-\left(C-Dp^{net}\right)$ is the viscoplastic potential function. Experimental measurements for the bituminous materials indicate that the yield surface is not the same as the viscoplastic potential surface because the associative flow rule overestimates the behavior of dilation for asphalt composites [6][10].

The symmetric net stress tensor is denoted by $\boldsymbol{\sigma}^{net}$ and its additive decomposition into volumetric and deviatoric parts gives

$$\boldsymbol{\sigma}^{net} = p^{net}\mathbf{1} + \mathbf{s}^{net} \tag{3.59}$$

where $\mathbf{1}$ is the second-order identity tensor.

For isotropic linearly elastic material, the elastic constitutive equations are

$$p^{net} = K\varepsilon_v \tag{3.60}$$

$$\mathbf{s}^{net} = 2G\mathbf{e} \tag{3.61}$$

where K and G are the elastic bulk and shear moduli, respectively. $\varepsilon_v = \mathrm{tr}(\boldsymbol{\varepsilon})$ is the volumetric strain and $\mathbf{e}$ is the deviatoric strain tensor satisfying the condition $\mathrm{tr}(\mathbf{e}) = 0$ This gives

$$\boldsymbol{\sigma}^{net} = K\varepsilon_v\mathbf{1} + 2G\mathbf{e} = \mathbf{C}^0 : \boldsymbol{\varepsilon}^e = \mathbf{C}^0 : \left(\boldsymbol{\varepsilon} - \boldsymbol{\varepsilon}^{vp}\right) \tag{3.62}$$

where $\mathbf{C}^0 = K\mathbf{1}\otimes\mathbf{1} + 2G\left(\mathbf{I} - \frac{1}{3}\mathbf{1}\otimes\mathbf{1}\right)$ is the rank-four tensor of elastic moduli. Therefore, the rate constitutive equation is defined as

$$\dot{\boldsymbol{\sigma}}^{net} = \mathbf{C}^0 : \left(\dot{\boldsymbol{\varepsilon}} - \dot{\boldsymbol{\varepsilon}}^{vp}\right) = \mathbf{C}^0 : \dot{\boldsymbol{\varepsilon}} - \dot{\gamma}\left(2G\mathbf{n} + KD\mathbf{1}\right) \tag{3.63}$$

For loading $\dot{\gamma} \geq 0$ and $f = 0$, $\dot{\gamma}$ is determined by viscoplastic consistency condition $\dot{f} = 0$.

$$\dot{\gamma} = \frac{\left(2G\mathbf{n}^{net} + KB\mathbf{1}\right) : \boldsymbol{\varepsilon}}{\left[2G + KBD + A'\left(\varepsilon_{vp}\right)E\right]} = \frac{\left(2G\mathbf{n}^{net} + KB\mathbf{1}\right) : \boldsymbol{\varepsilon}}{F} \tag{3.64}$$

where $E = \frac{\sqrt{2/3} + B/3}{\sqrt{B^2 + 1}}$ and $F = \left[2G + KBD + A'\left(\varepsilon_{vp}\right)E\right]$

Substitution of Eq. (3.64) into Eq. (3.63) yields $\dot{\boldsymbol{\sigma}}^{net} = \mathbf{C}^{evp,net} : \dot{\boldsymbol{\varepsilon}}$ where $\mathbf{C}^{evp,net}$ is the net elastoviscoplastic tangent moduli given by:

$$\begin{aligned} \mathbf{C}^{evp,net} = 2G\mathbf{I} + \left(K - \frac{2G}{3} - \frac{K^2 BD}{F} \right) \mathbf{1} \otimes \mathbf{1} - \frac{2GKB}{F} \mathbf{1} \otimes \mathbf{n}^{net} \\ - \frac{2GKD}{F} \mathbf{n}^{net} \otimes \mathbf{1} - \frac{(2G)^2}{F} \mathbf{n}^{net} \otimes \mathbf{n}^{net} \end{aligned} \tag{3.65}$$

By applying backward Euler algorithm and local Newton iteration, the viscoplastic consistency parameter can be derived (detailed derivation is demonstrated in Chapter 4) and the following viscoplastic consistency parameter is derived when the flow function equals to linear loading function, i.e. $g(f) = f$.

$$\hat{\gamma}_{n+1}^{net} = \frac{\dfrac{f_{n+1}^{trial,net}}{2G}}{\left(1 + \dfrac{\tau}{\Delta t} + \dfrac{KBD}{2G} \right)} \tag{3.66}$$

The exact (consistent) tangent operator is defined by the rank-four tensor

$$\mathbf{C}_{n+1}^{evp,net} = \left. \frac{\partial \boldsymbol{\sigma}^{net}}{\partial \boldsymbol{\varepsilon}} \right|_{n+1} \tag{3.67}$$

With the aid of backward Euler algorithms Eq.(3.64) and Eq.(3.67), we obtain the following expression for $\mathbf{C}_{n+1}^{ep,net}$

$$\mathbf{C}_{CONS\ n+1}^{evp,net} = \mathbf{C}^0 - \frac{\partial \hat{\gamma}_{n+1}^{net}}{\partial \boldsymbol{\varepsilon}_{n+1}} \otimes KD\mathbf{1} - 2G \left(\frac{\partial \hat{\gamma}_{n+1}^{net}}{\partial \boldsymbol{\varepsilon}_{n+1}} \otimes \mathbf{n}_{n+1}^{net} + \hat{\gamma}_{n+1}^{net} \frac{\partial \mathbf{n}_{n+1}^{net}}{\partial \boldsymbol{\varepsilon}_{n+1}} \right) \tag{3.68}$$

By computing the term of $\partial \hat{\gamma}_{n+1}^{net} / \partial \boldsymbol{\varepsilon}_{n+1}$ and $\partial \mathbf{n}_{n+1}^{net} / \partial \boldsymbol{\varepsilon}_{n+1}$, we obtain the final expression of the consistency tangent moduli in the net space

$$\mathbf{C}^{evp,net}_{CONS\ n+1} = \mathbf{C}^{evp,net} - \frac{(2G)^2 \hat{\gamma}^{net}_{n+1}}{\left\|\mathbf{s}^{tr}_{n+1}\right\|}\left(\mathbf{I} - \frac{1}{3}\mathbf{1}\otimes\mathbf{1} - \mathbf{n}_{n+1}\otimes\mathbf{n}_{n+1}\right)$$

$$= (2G - \theta_{n+1})\mathbf{I} + \left(K - \frac{2G}{3} - \frac{K^2 BD}{F} + \frac{\theta_{n+1}}{3}\right)\mathbf{1}\otimes\mathbf{1} - \frac{2GKB}{F}\mathbf{1}\otimes\mathbf{n}^{net}_{n+1} \quad (3.69)$$

$$- \frac{2GKD}{F}\mathbf{n}^{net}_{n+1}\otimes\mathbf{1} - \left(\frac{(2G)^2}{F} - \theta_{n+1}\right)\mathbf{n}^{net}_{n+1}\otimes\mathbf{n}^{net}_{n+1}$$

$$\theta_{n+1} = \frac{(2G)^2 \hat{\gamma}^{net}_{n+1}}{\left\|\mathbf{s}^{tr}_{n+1}\right\|} \quad (3.70)$$

$\mathbf{C}^{evp,net}$ is the material tangent response, whereas $\mathbf{C}^{evp,net}_{CONS\ n+1}$ represent the material tangent response for numerical algorithm as well as the material tangent response. As $\hat{\gamma}^{net}_{n+1} \to 0$ $\mathbf{C}^{evp,net}_{CONS\ n+1}$ becomes $\mathbf{C}^{evp,net}$. Since non-associative flow rule is employed, $\mathbf{C}^{evp,net}_{CONS\ n+1}$ is a non-symmetric operator.

3.5 Reference

[1] Chen, W.F., and Han, D.J. (1988). Plasticity for structural engineers, Springer-Verlag, NY

[2] Coleman, B.D. and Gurtin, M.E. (1967). Thermodynamics with Internal State Variables, *Journal of Chemical Physics*, **47**: 597613.

[3] Ju, J. W., Yuan, K.Y., and Kuo, W. (2012a). Novel Strain Energy Based Coupled Elastoplastic Damage and Healing Models for Geomaterials - Part I: Formulations, *International Journal of Damage Mechanics*, **21** (4): pp. 525-549.

[4] Ju, J. W., Yuan, K.Y. Kuo, W., and Chen, J.S. (2012b). Novel Strain Energy Based Coupled Elastoplastic Damage and Healing Models for Geomaterials - Part II: Computational

Aspects, *International Journal of Damage Mechanics*, **21** (4): pp. 551-576.

[5] Lemaitre, J. (1971). Evaluation of Dissipation and Damage in Metals Submitted to Dynamic Loading, *Proceedings of the First International Conference*, Kyoto, Japan; Aug. 15-20: pp. 540-549.

[6] Oda, M., and Nakayama, H. (1989). Yield function for soil with anisotropic fabric, *Journal of Engineering Mechanics, ASCE* **15**(1): pp. 89-105.

[7] Perzyna, P. (1966). Fundamental Problems in Viscoplasticity, *Advances in Applied Mechanics*, **9** (2): pp. 244-368.

[8] Simo, J. C., and Ju, J.W. (1987a). Strain-Based and Stress-Based Continuum Damage Models, Part I: Formulation, *International Journal of Solids and Structures*, **23**: pp. 821-840.

[9] Simo, J. C., and Ju, J.W. (1987b). Strain-Based and Stress-Based Continuum Damage Models, Part II: Computational Aspects, *International Journal of Solids and Structures*, **23**: pp. 841-869.

[10] Zeinkiewicz, O., Huphenson, C., and Lewis, R. (1975). Associated and non-associated visco-plasticity in soils mechanics, *Journal of Geotechnique* **25**(5): pp. 671-689.

4. NEW INITIAL STRAIN ENERGY BASED THERMO-ELASTOVISCOPLASTIC ISOTPRIC DAMAGE-SELF HEALING MODEL FOR BITUMINOUS COMPOSITES – PART II: COMPUTATIONAL ASPECTS

4.1 Introduction

First, the two-step ***operator splitting*** methodology is systematically proposed and employed for the proposed thermo-elastoviscoplastic isotropic damage-self healing in Chapter 3. In particular, the resulting procedure takes the form of an ***elastic damage-self healing predictor*** and ***net viscoplastic return mapping corrector*** scheme. Secondly, a series of one-dimensional numerically driven simulations by different loading processes (loading-unloading-reloading and one cyclic loading) are given to illustrate the variables calculated by the model such as stress-strain curve, damage variable, and healing variable. Finally, experimental validations are presented to demonstrate the applicability of proposed damage-self healing models and algorithms in this chapter.

4.2 Computational Algorithms

4.2.1 Two-Step Operator Splitting Methodology

In Chapter 3, new strain energy based isotropic damage-self healing models are developed with the concept of net stress space and damage-self healing process [2][3][4][9][10]. This section presents the computational features of the proposed formulations by using the operator splitting methodology. Eqs. (3.22) ~ (3.25), (3.34) ~ (3.36), and (3.46) ~ (3.50) in Chapter 3 are referred.

$$
\begin{aligned}
&\dot{\varepsilon} = \nabla^{s}\dot{\mathrm{u}}(t) \\
&\begin{cases}
\dot{d}_t = \dot{\mu}\, H(\xi_t, d_t) \\
\dot{g} = \dot{\mu} \\
\dot{\mu} \geq 0, \qquad \phi^{d}(\xi_t, g_t) \leq 0, \qquad \dot{\mu}\,\phi^{d}(\xi_t, g_t) = 0
\end{cases} \\
&\begin{cases}
\dot{R}_t = \dot{\zeta}\, Z(\xi_t, R_t) \\
\dot{r} = \dot{\zeta} \\
\dot{\zeta} \geq 0, \qquad \phi^{h}(\xi_t, r_t) \leq 0, \qquad \dot{\zeta}\,\phi^{h}(\xi_t, r_t) = 0
\end{cases} \\
&\dot{d}^{net} = \dot{d} - \dot{R}\, d^{net} \\
&\dot{\boldsymbol{\sigma}}^{net} = \frac{d}{dt}\left[\frac{\partial \Psi^{0}(\boldsymbol{\varepsilon})}{\partial \boldsymbol{\varepsilon}}\right] - \dot{\boldsymbol{\sigma}}^{vp,net} \\
&\begin{cases}
\dot{\boldsymbol{\sigma}}^{vp,net} = \gamma \dfrac{\partial g_p}{\partial \boldsymbol{\varepsilon}}\left(\dfrac{\partial \Psi^{0}(\boldsymbol{\varepsilon})}{\partial \boldsymbol{\varepsilon}} - \boldsymbol{\sigma}^{vp,net}, \mathbf{q}\right) & (\textit{non-associative flow rule}) \\
\dot{\mathbf{q}} = \dot{\lambda}\, \mathbf{h}\left(\dfrac{\partial \Psi^{0}(\boldsymbol{\varepsilon})}{\partial \boldsymbol{\varepsilon}} - \boldsymbol{\sigma}^{vp,net}, \mathbf{q}\right) & (\textit{viscoplastic hardening law}) \\
f\left(\dfrac{\partial \Psi^{0}(\boldsymbol{\varepsilon})}{\partial \boldsymbol{\varepsilon}} - \boldsymbol{\sigma}^{vp,net}, \mathbf{q}\right) \leq 0 & (\textit{loading condition})
\end{cases}
\end{aligned}
\tag{4.1}
$$

From an algorithmic viewpoint, the problem of integrating the evolution Eq.(4.1) reduces to updating the basic variables $\left\{\boldsymbol{\sigma}, d^{net}, \boldsymbol{\sigma}^{vp,net}, \mathbf{q}\right\}$ in a manner consistent with the proposed damage-self healing models. It is essential to realize that the history of strains $t \rightarrow \boldsymbol{\varepsilon} \equiv \nabla^{s}\mathbf{u}(t)$ is assumed to be prescribed; i.e., a strain-drive computational algorithms.

Equations of evolution are to be solved incrementally over a sequence of given time steps $[t_n, t_{n+1}] \subset \mathscr{R}_+$, $n = 0,1,2...$. Therefore, the initial conditions for the governing evolution equations are

$$\left\{\boldsymbol{\sigma}, d^{net}, \boldsymbol{\sigma}^{vp,net}, \mathbf{q}\right\}\Big|_{t=t_n} = \left\{\boldsymbol{\sigma}_n, d_n^{net}, \boldsymbol{\sigma}_n^{vp,net}, \mathbf{q}_n\right\} \tag{4.2}$$

In accordance with the notion of operator splitting, we consider the following innovative, additive decomposition of the original problem of evolutions in Eq. (4.1) into the elastic-damage-healing part and the plastic part as follows:

$$\begin{aligned}
&\textbf{1. Elastic - damage - self healing part:}\\
&\dot{\boldsymbol{\varepsilon}} = \nabla^{s}\dot{\mathbf{u}}(t)\\
&\dot{d} = \begin{cases} H(\boldsymbol{\xi})\,\dot{\xi}, & iff \quad \phi_t^d = \dot{\phi}_t^d = 0 \\ 0, & otherwise \end{cases}\\
&\dot{g} = \begin{cases} \dot{\xi}, & iff \quad \phi_t^d = \dot{\phi}_t^d = 0 \\ 0, & otherwise \end{cases}\\
&\dot{R} = \begin{cases} Z(\boldsymbol{\xi})\,\dot{\xi}, & iff \quad \phi_t^h = \dot{\phi}_t^h = 0 \\ 0, & otherwise \end{cases}\\
&\dot{r} = \begin{cases} \dot{\xi}, & iff \quad \phi_t^h = \dot{\phi}_t^h = 0 \\ 0, & otherwise \end{cases}\\
&\dot{d}^{net} = \dot{d} - \dot{R}\, d^{net}\\
&\dot{\boldsymbol{\sigma}}^{net} = \frac{d}{dt}\left[\frac{\partial \Psi^0(\boldsymbol{\varepsilon})}{\partial \boldsymbol{\varepsilon}}\right]\\
&\dot{\boldsymbol{\sigma}}^{vp,net} = 0\\
&\dot{\mathbf{q}} = 0
\end{aligned} \tag{4.3}$$

$$
\begin{aligned}
&\textbf{2. Viscoplastic part:}\\
&\dot{\boldsymbol{\varepsilon}} = 0\\
&\dot{d}^{net} = 0\\
&\dot{\boldsymbol{\sigma}}^{net} = -\dot{\boldsymbol{\sigma}}^{vp,net}\\
&\dot{\boldsymbol{\sigma}}^{vp,net} = \gamma \frac{\partial g_p}{\partial \boldsymbol{\varepsilon}}\left(\frac{\partial \Psi^0(\boldsymbol{\varepsilon})}{\partial \boldsymbol{\varepsilon}} - \boldsymbol{\sigma}^{vp,net}, \mathbf{q}\right)\\
&\dot{\mathbf{q}} \;\; = \gamma\, \mathbf{h}\left(\frac{\partial \Psi^0(\boldsymbol{\varepsilon})}{\partial \boldsymbol{\varepsilon}} - \boldsymbol{\sigma}^{vp,net}, \mathbf{q}\right)
\end{aligned}
\tag{4.4}
$$

It is noted that Eqs. (4.3) and (4.4) do indeed add up to Eq. (4.1), in agreement with the notion of operator split. In the following, we propose two new computational algorithms. The first one is consistent with problem (4.3) (the elastic damage-self healing predictor) while the second one is consistent with problem (4.4) (the net viscoplastic return mapping corrector). In turn, the product algorithm obtained by successive application of these two algorithms is consistent with the original problem (4.1).

4.2.2 The Elastic Damage-Self Healing Predictor

A novel computational algorithm consistent with problem (4.1), referred to as the *elastoviscoplastic-damage-healing predictor* in this paper, is shown in the following step-by-step numerical strain-driven procedure.

Step 1: Strain update: Given the incremental displacement field $\mathbf{u}_{n+1}$, the strain tensor is updated as:

$$\boldsymbol{\varepsilon}_{n+1} = \boldsymbol{\varepsilon}_n + \nabla^{\mathbf{s}} \mathbf{u}_{n+1} \tag{4.5}$$

Step 2: Compute the initial (undamaged) elastic strain energy ξ_{n+1} coupled with Arrhenius-type temperature term

$$\boldsymbol{\xi}_{n+1} \equiv \sqrt{\Psi^0\left(\boldsymbol{\varepsilon}_{n+1}\right)\vartheta(T_{n+1})} = \sqrt{\left\{\frac{1}{2}\boldsymbol{\varepsilon}_{n+1} : \mathbf{C}^0 : \boldsymbol{\varepsilon}_{n+1}\right\}\exp\left\{-\boldsymbol{\delta}\left(1-\frac{T_{n+1}}{T_0}\right)\right\}} \tag{4.6}$$

Step 3: Update the current damage threshold g_{n+1} for a damage criterion based on ξ_{n+1} and time increment.

If the incremental healing at the previous time step is larger than zero, compute the $g_{h,(n)}$ by using a nonlinear saturation type of functional evaluation $g_{h,(n)} = Q\left(1-e^{-bn}\right)$ and $\Delta g_{h,(n)} = b\left(Q - g_{h,(n-1)}\right)\Delta n$

$$g_{n+1} = \max\left(g_0, \max_{s\in(-\infty,n+1)} \xi_s\right) - g_{h,(n)} \tag{4.7}$$

Step 4: Compute the scalar damage predictor d_{n+1} based on ξ_{n+1}.

If $\boldsymbol{\xi}_{n+1}$ at the current time step is less than the current damage threshold g_{n+1}, no further damage occurs; set $\Delta d_{n+1} = 0$. However, if ξ_{n+1} is larger than the current damage threshold g_{n+1}, compute the scalar damage predictor Δd_{n+1} by using a nonlinear saturation type of damage functional evaluation. Conceptually, if initial defects, damage, or interfacial debonding between aggregate and matrix (such as microvoids or microcracks) can be observed and quantified by nondestructive evaluation (such as by computed tomography), then the ***initial damage*** d_0 can be characterized and quantified accordingly. Otherwise, the initial damage d_0 is typically set as zero.

$$d_{n+1} = d_n + \Delta d_{n+1} \tag{4.8}$$

Step 5: Compute the *incremental* isotropic damage predictor tensor $\Delta\mathbf{D}_{n+1}$ and the damage tensor $\mathbf{D}_{n+1}$

$$\Delta\mathbf{D}_{n+1} = \Delta d_{n+1}\,\mathbf{I} \tag{4.9}$$

$$\mathbf{D}_{n+1} = \mathbf{D}_n + \Delta\mathbf{D}_{n+1} \tag{4.10}$$

Step 6: Update the current healing threshold r_{n+1} for a healing criterion based on ξ_{n+1}.

If the incremental damage at the previous time step is larger than zero, compute the $r_{d,(n)}$ by using a nonlinear saturation type of functional evaluation. Otherwise, $r_{d,(n)}$ is zero.

$$r_{n+1} = \min\left(r_0, \min_{s\in(-\infty,n+1)} \boldsymbol{\xi}_s\right) + r_{d,(n)} \tag{4.11}$$

Step 7: Compute the scalar healing predictor R_{n+1} based on ξ_{n+1}.

If ξ_{n+1} at the current time step is larger than the current healing threshold r_{n+1}, no further healing occurs; set $\Delta R_{n+1} = 0$. However, if ξ_{n+1} is less than the current healing threshold r_{n+1}, compute the scalar damage predictor ΔR_{n+1} by using a nonlinear saturation type of healing functional evaluation.

$$R_{n+1} = R_n + \Delta R_{n+1} \quad \left(\Delta d_{n+1} = 0\right) \tag{4.12}$$

$$R_{n+1} = \frac{d_{n+1}}{2d_{n+1} - d_n} R_n \quad \left(\Delta d_{n+1} > 0\right) \tag{4.13}$$

Step 8: Compute the *incremental* isotropic healing predictor tensor $\Delta\mathbf{R}_{n+1}$

$$\Delta\mathbf{R}_{n+1} = \Delta R_{n+1}\ \mathbf{I} \tag{4.14}$$

Step 9: Update the isotropic net (combined) damage-self healing tensor $\mathbf{D}_{n+1}^{net}$ based on the *incremental* isotropic net (combined) damage-self healing tensor $\Delta\mathbf{D}_{n+1}^{net}$

$$\Delta\mathbf{D}_{n+1}^{net} = \Delta\mathbf{D}_{n+1} - \mathbf{D}_{n}^{net}\Delta\mathbf{R}_{n+1} \tag{4.15}$$

$$\mathbf{D}_{n+1}^{net} = \mathbf{D}_{n}^{net} + \Delta\mathbf{D}_{n+1}^{net} \tag{4.16}$$

By substitution of the total strain tensor $\boldsymbol{\varepsilon}_{n+1}$ into the potential for the stress tensor, we obtain the trial (predictor) stress:

$$\begin{aligned} \boldsymbol{\sigma}_{n+1}^{0} &= \frac{\partial \Psi^{0}}{\partial \boldsymbol{\varepsilon}}\left(\boldsymbol{\varepsilon}_{n+1}\right) \\ \boldsymbol{\sigma}_{n+1}^{trial,net} &= \boldsymbol{\sigma}_{n+1}^{0} - \boldsymbol{\sigma}_{n}^{vp,net} \\ \mathbf{q}_{n+1}^{trial} &= \mathbf{q}_{n} \end{aligned} \tag{4.17}$$

4.2.3 The Net Viscoplastic Return Mapping Corrector

To develop an algorithm consistent with the viscoplastic part of the operator split, we first check the loading/unloading conditions.

Step 10: Check for net *yielding*:

The algorithmic counterpart of the Kuhn-Tucker conditions is implemented in terms of the elastic-damage-self healing trial stress; cf. Simo and Ju (1987b). One simply checks:

$$f(\boldsymbol{\sigma}_{n+1}^{trial,net}, \mathbf{q}_{n+1}^{trial}) \begin{cases} \leq 0, & \text{elastic - damage - healing} \Rightarrow \text{predictor = final state} \\ > 0, & \text{viscoplastic} \Rightarrow \text{return mapping} \end{cases} \tag{4.18}$$

Step 11: Net viscoplastic return mapping *corrector*:

In the case of net viscoplastic loading, the predictor stresses and internal variables are "returned back" to the net yield surface along the algorithmic counterpart of the flow generated by Eq. (4.4). The framework of the radial return algorithm is employed in this work.

Step 12: Update the homogenized (nominal) stress $\boldsymbol{\sigma}_{n+1}$:

$$\boldsymbol{\sigma}_{n+1} = \left[\left\{ \mathbf{I} - \mathbf{D}_{n+1}^{net} \right\} : \boldsymbol{\sigma}_{n+1}^{net} \right] \vartheta\left(T_{n+1}\right) \tag{4.19}$$

4.3 Applications and Validations

First of all, a one-dimensional driver problem based on the developed damage-self healing mechanism is conducted by the Matlab codes. Two models are demonstrated: (1) thermo-***elastic*** damage-self healing model and (2) thermo-***elastoviscoplastic*** damage-self healing model. Secondly, to validate the damage-self healing models, experimental data obtained by Texas A&M University (TAMU) and the North Carolina State University (NCSU) for asphalt mixtures are compared with numerical prediction by the proposed thermo-elastoviscoplastic isotropic damage-healing models.

4.3.1 One-Dimensional Driver Problem

Based on the proposed thermo damage-healing mechanism, the history of homogenized stress, net stress, damage and healing thresholds, and damage net variables can be calculated and obtained under a specified cycle of strain control. Two cases are studied and presented using the (1) *thermo-elastic damage* model and (2) *thermo-elastoviscoplastic damage-self healing* model by adjusting temperature condition, the yield stresses, the initial damage thresholds, and the initial healing thresholds in the Matlab codes. The corresponding numerical results are presented and discussed in the following.

Case I: Thermo-elastic damage-self healing model

In this case, there are four different scenarios: (1) general loading-unloading-reloading (LUR), (2) cyclic loading (one cycle), (3) temperature effect for LUR, and (4) rest period effect for LUR. The initial damage threshold and the healing threshold are set as 0.08 and 0, respectively. Elastic behavior is only considered so that the yield stress is set as infinity. Figure 4.1(a) shows that the decrease in stress is observed due to the evolution of damage after strain energy norm is greater than the initial damage threshold, 0.08. However, there is no stress reduction and the same shape and magnitude of stress in net space presented in Figure 4.1(b) because of *no damage* and *thermo effect* included. In Figure 4.1 (c), strain goes back to origin under the unloading situation and 300 steps later the reloading starts. The slope of the stress-strain curve after 300 steps is greater than that before 300 steps since self-healing lasts for 300 steps. Figure 4.1(d) represents the evolution of the damage net variable and this process is now reversible because microcracks and/or other microscopic defeats can be recovered during the rest period. Similarly, healing variable is able to decrease in value because damaged area increases during reloading. On the contrary to damage net and healing variables, process of damage is assumed to be irreversible and the damage is a monotonically increasing function of strain energy norm as shown in Figure 4.1(e). Comparing 10 ℃ (the dashed line) and 20 ℃ (the solid line), the stress for 10 ℃ is higher than that for 20 ℃ because viscosity of asphalt mixtures exposed to higher temperature is higher than lower one. In other words, bituminous materials exposed to 10 ℃ carry the higher load than 20 ℃. For damage net and damage variables in Figure 4.1(d) and (e), the variable for 10 ℃ is higher since its strain energy norm is higher. In contrast, the healing variable for 10 ℃ is lower than that for 20 ℃ since a detectable increase in moduli after exposure to the higher temperature is observed due to viscosity of asphalt mixtures [5].

Figure 4.2 demonstrates one cycle loading case. For simplicity, the behavior of material in tension and compression is assumed to be the same. The initial damage threshold and the healing threshold are set as 0.08 and 0.005, respectively. The same fashion of homogenized stress as general LUR in tension is shown in Figure 4.2(a), but different homogenized stress history in compression is recorded due to accumulated damage net variable when compressive stress starts. Therefore, the maximum compressive stress is smaller than the maximum tensile stress. In Figure 4.2(b), no damage and temperature effects are observed in net space. Since the yield stress is set as infinity, stress-strain curve always passes through the origin. Figure 4.2(d) represents the damage net variable and this variable decreases when the homogenized compressive stress reaches zero and strain energy norm is below certain point.

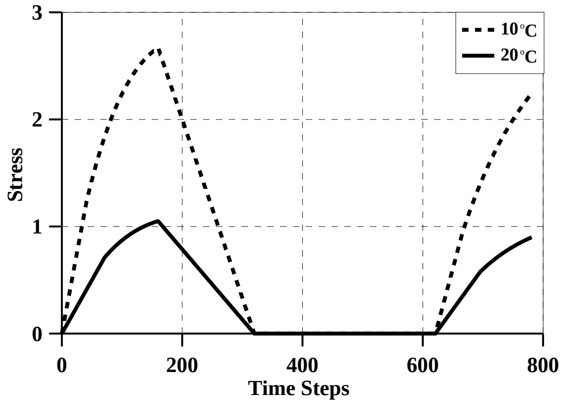

(a) Homogenized Stress

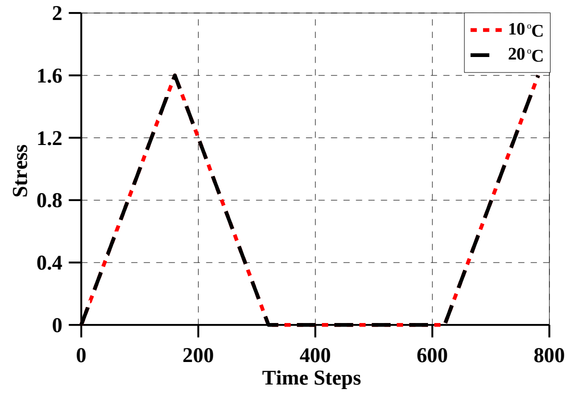

(b) Net Stress

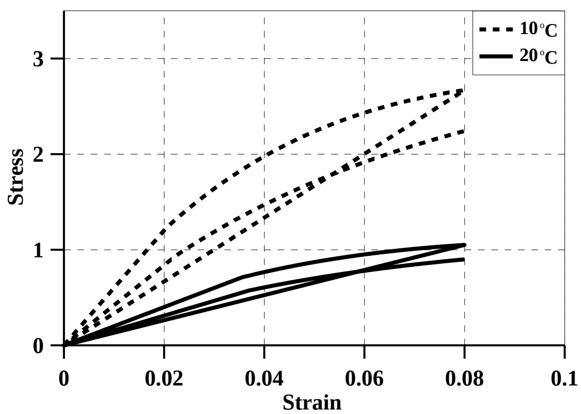

(c) Stress-Strain

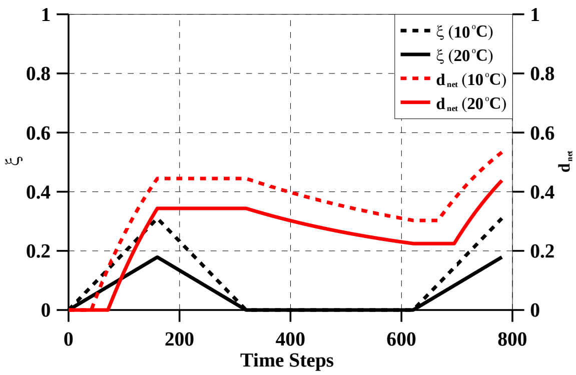

(d) Damage Net Variable

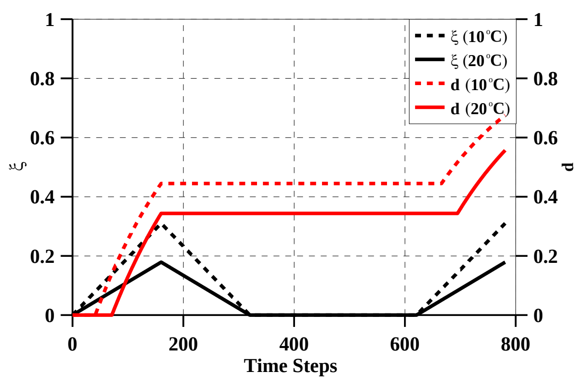

(e) Damage Variable

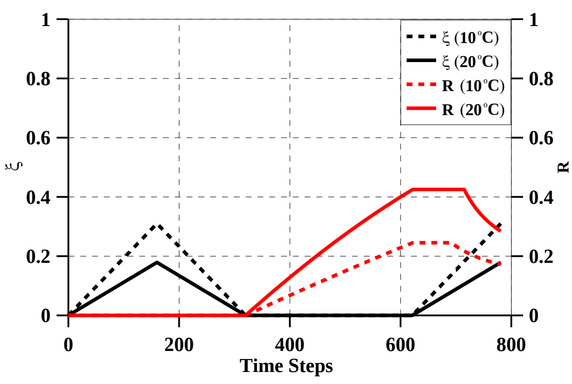

(f) Healing Variable

Figure 4.1 Corresponding results of one-dimensional driver problems by thermo-elastic damage and healing model (10 ℃ and 20 ℃)

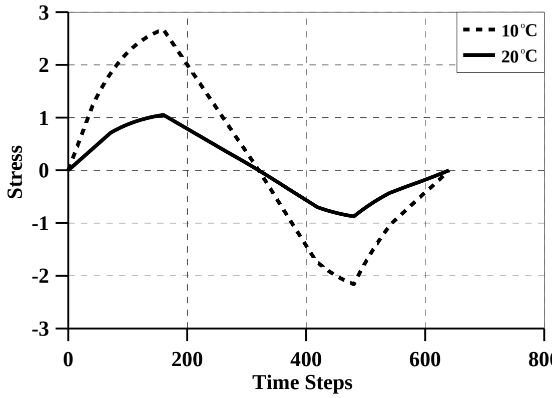

(a) Homogenized Stress

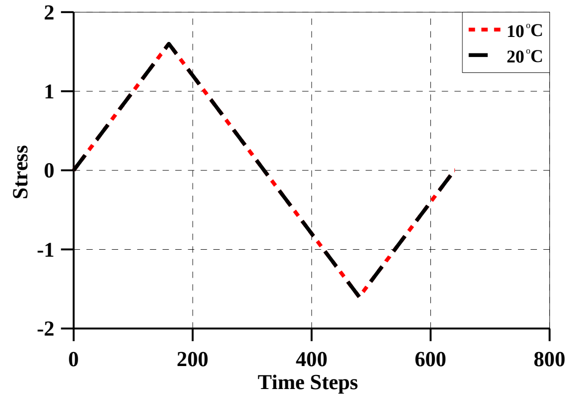

(b) Net Stress

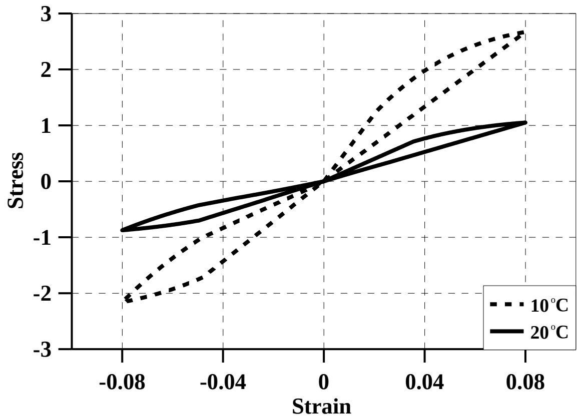

(c) Stress-Strain

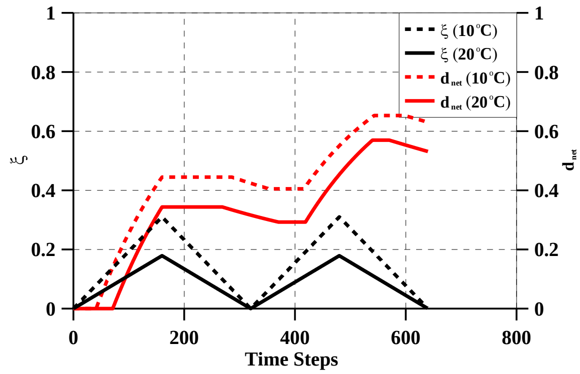

(d) Damage Net Variable

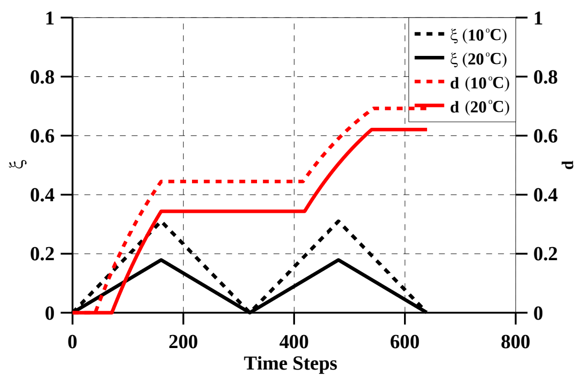

(e) Damage Variable

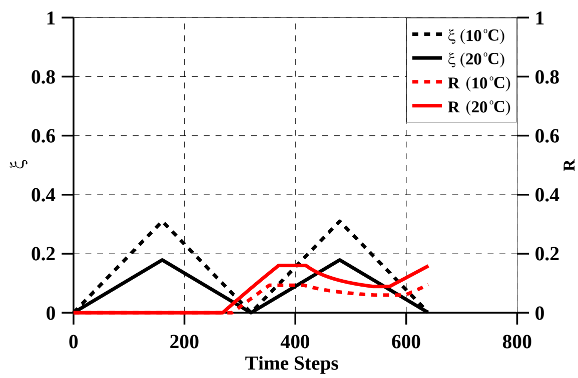

(f) Healing Variable

Figure 4.2 Corresponding results of one-dimensional driver problems by thermo-elastic damage and healing model (10 ℃ and 20 ℃)

According to Kim et al. (1994), healing is a function of both temperature and rest periods. Figure 4.3 and Figure 4.4 are demonstrated to illustrate these two effects. The initial damage threshold and the healing threshold are set as 0.08 and 0 again. In Figure 4.3, the temperature is set the same, 20 ℃, until the end of unloading. Then, one case keeps the same temperature (20 ℃) for 300 time steps (from point A to B), and the other case increase the temperature to 30 ℃. Reloading starts after 300 steps (point B). The solid line and the dashed line represent the response at 20 ℃ and 30 ℃, respectively. In homogenized stress history in Figure 4.3 (a), the maximum stress at 30 ℃ is clearly larger than that at 20 ℃ because more healing is accumulated during the rest period due to higher temperature. In Figure 4.3(b), the slope of stress-strain curve after exposure to higher temperature is definitely higher than one exposed to lower temperature. The smaller damage net variable is observed at 30 ℃ because it has more healing. There is not much difference for damage variable between two temperatures since the damage occurs during loading and unloading process. Figure 4.4 shows the healing effect due to the rest period under controlled temperature. In Figure 4.4(a), the difference of maximum stress between 100 steps and 300 steps is not clear because of time gap. It is also no difference in net space as presented in Figure 4.4(b). In case of homogenized stress-strain curve shown in Figure 4.4(c), the slope for 300 time steps is higher than one for 100 steps in the beginning of reloading and the homogenized stress for 300 steps of the rest period is entirely larger than one for 100 time steps.

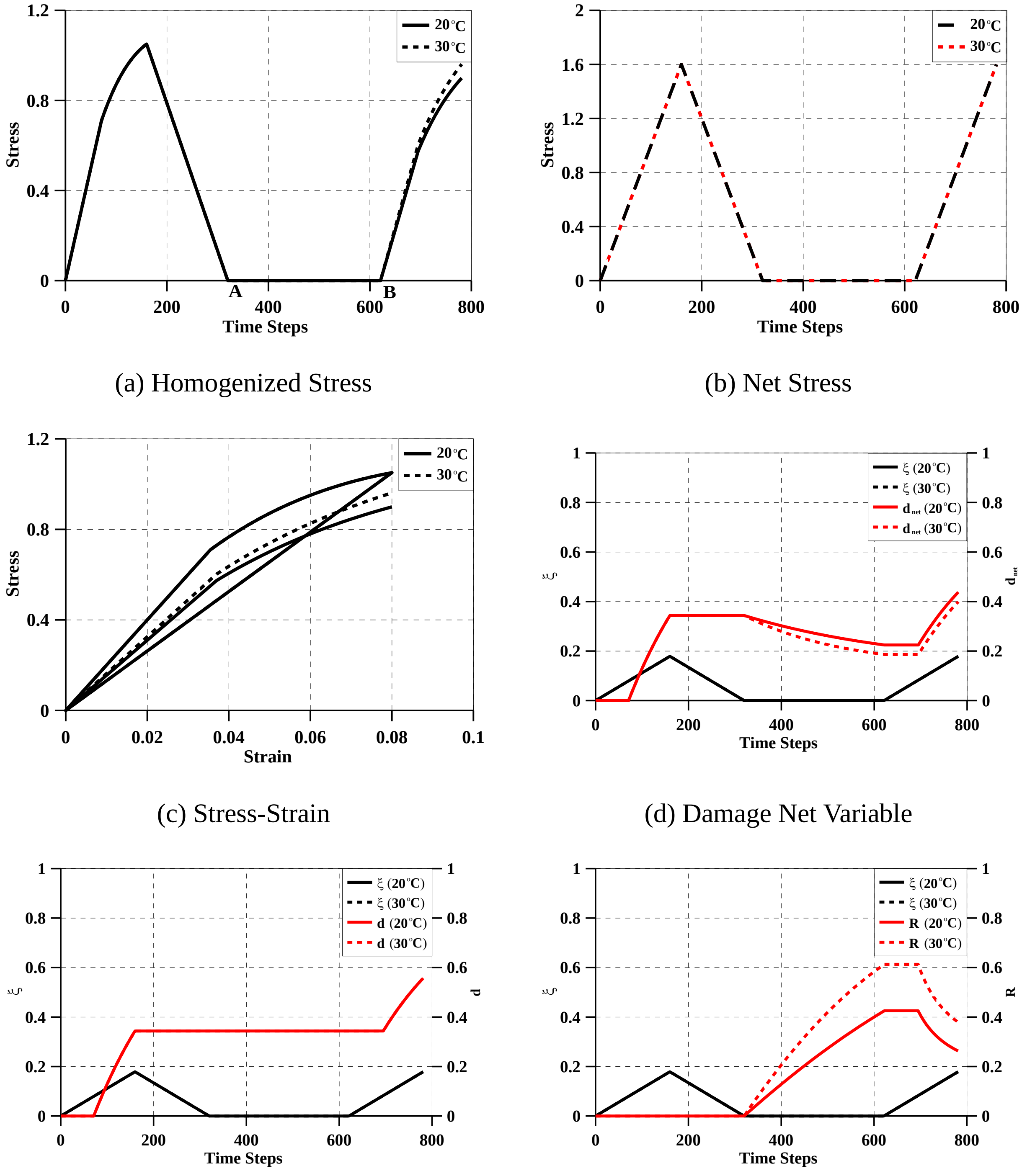

(a) Homogenized Stress (b) Net Stress

(c) Stress-Strain (d) Damage Net Variable

(e) Damage Variable (f) Healing Variable

Figure 4.3 Corresponding results of one-dimensional driver problems by thermo-elastic damage and healing model (20 ℃ and 30 ℃ for healing period)

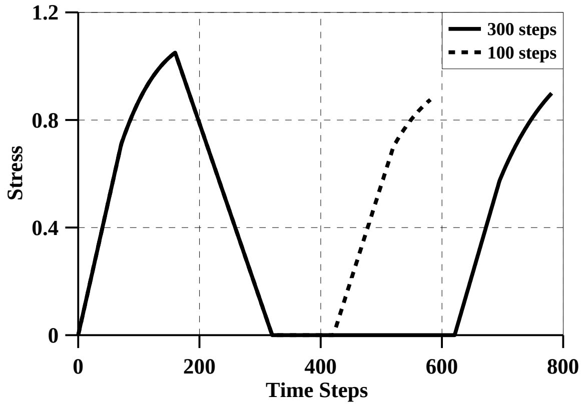

(a) Homogenized Stress

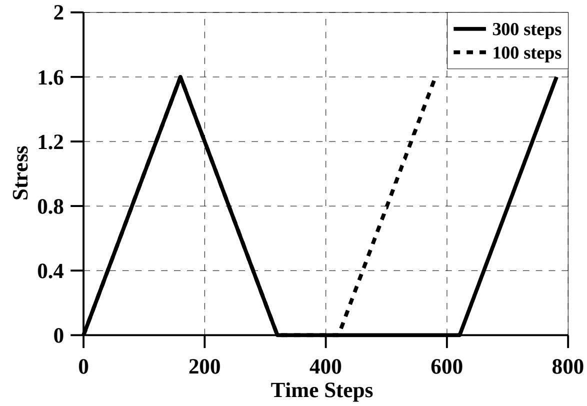

(b) Net Stress

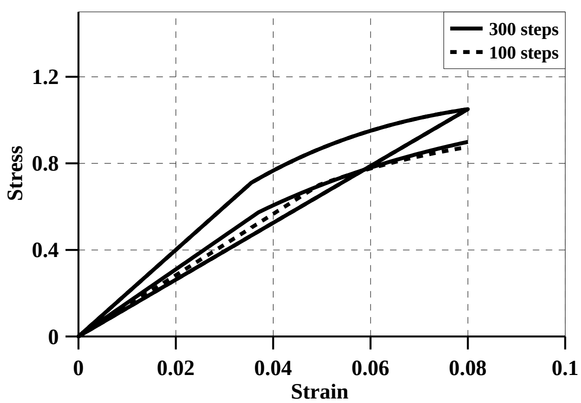

(c) Stress-Strain

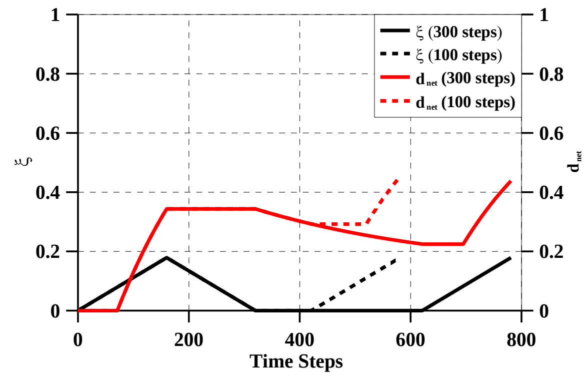

(d) Damage Net Variable

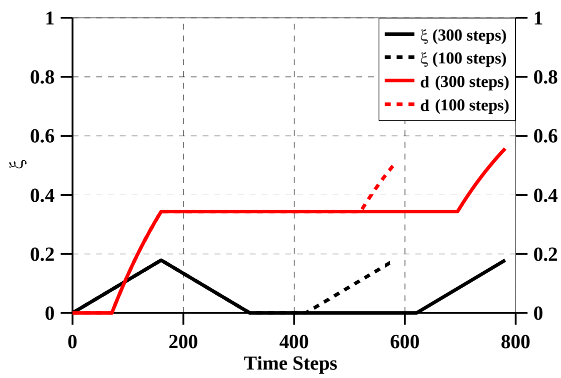

(e) Damage Variable

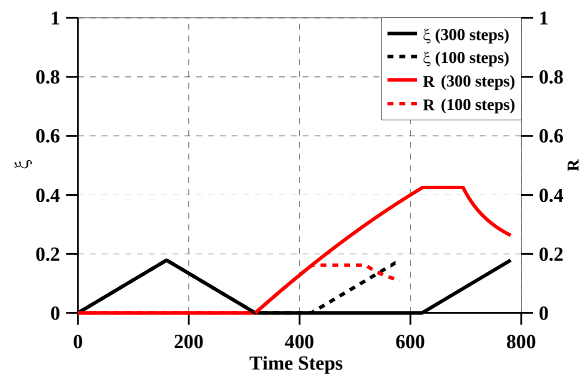

(f) Healing Variable

Figure 4.4 Corresponding results of one-dimensional driver problems by thermo-elastic damage and healing model (100 steps and 300 steps for healing period)

Case II: Thermo-elastoviscoplastic damage-self healing model

Similar to Case I, four different scenarios are demonstrated: (1) general LUR, (2) cyclic loading (one cycle), (3) temperature effect for LUR, and (4) rest period effect for LUR. For the general simulation case, the initial damage threshold and the healing threshold are set as 0.08 and 0.1, respectively, and the yield stress is assumed to be 1. Figure 4.5(a) indicates that the stress softening response is presented due to damage and viscoplastic deformation in physical space, whereas the stress decreases with time because of only viscoplastic deformation considered in net space in Figure 4.5(b). For the stress-strain curve in Figure 4.5(c), the softening is clearly observed due to the combination of viscoplastic strain and damage variable. Since healing occurs during the rest period, the elastic Young's modulus for reloading is greater than that for unloading. The fashion of damage net, damage, and healing variables is the same as the thermo-elastic damage-self healing model because damage and healing process is completely independent on viscoplastic deformation process.

Figure 4.6 demonstrates one cycle loading under two different temperature conditions. The initial damage threshold and the yield stress are the same as LUR case, while the healing threshold is assumed to be 0.03. Moreover, it is assumed that the model is isotropic hardening and the damage due to both compressive and tensile loading are the same for this simple demonstration. Decrease in homogenized stress in Figure 4.6(a) is caused by both viscoplastic deformation and damage, while the reduction in net stress shown in Figure 4.6(b) is due to only viscoplastic strain. The softening response is clearly observed in Figure 4.6(c) because of viscoplastic strain and damage variable. Since damage and healing processes are definitely independent, they are separately evolved. In other words, no healing evolves when damage occurs. Vice versa, healing evolves only if no damage occurs. Moreover, healing is able to decrease in value when damage occurs again under the reloading because healing is reversible process. Therefore, the damage net variable can be reduced by amount of healing shown in Figure 4.6(f).

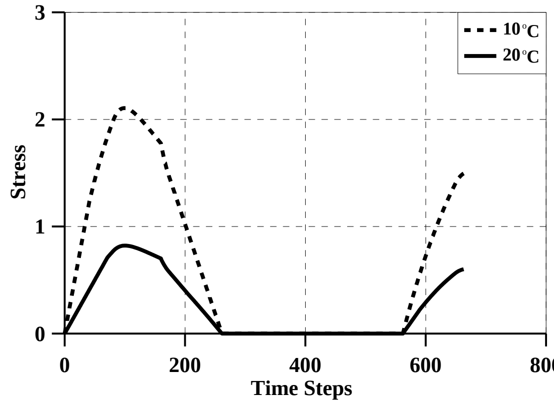

(a) Homogenized Stress

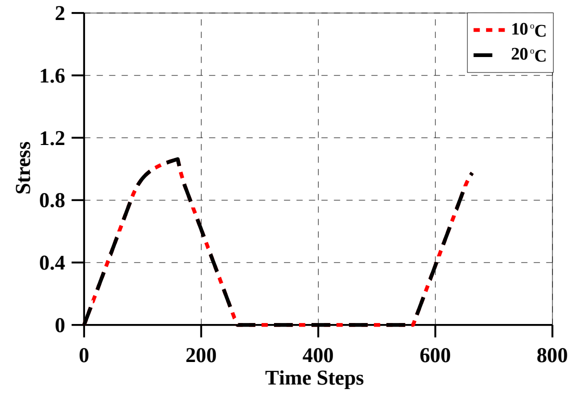

(b) Net Stress

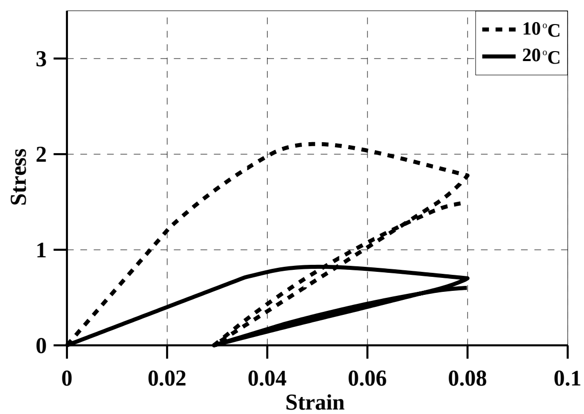

(c) Stress-Strain

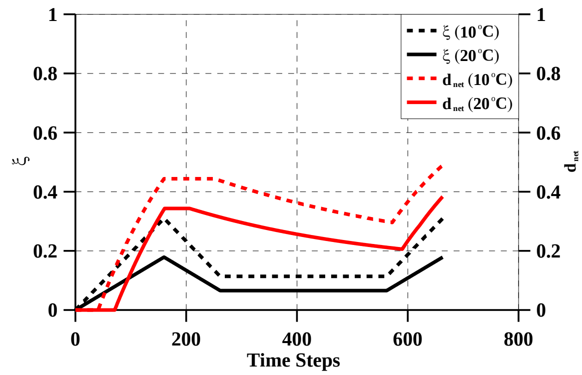

(d) Damage Net Variable

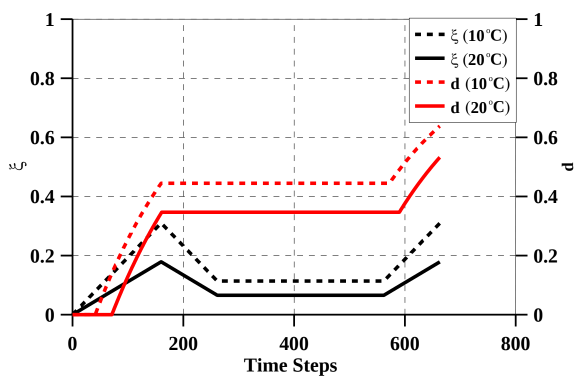

(e) Damage Variable

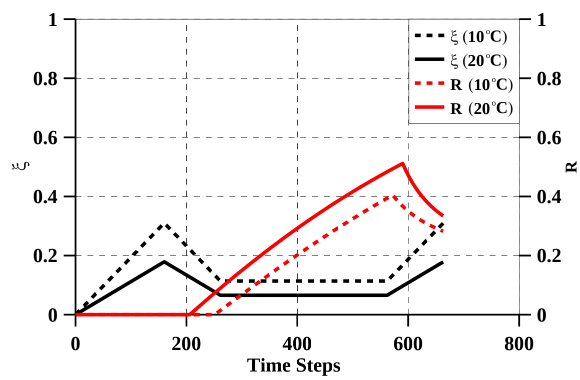

(f) Healing Variable

Figure 4.5 Corresponding results of one-dimensional driver problems by thermo-elastoviscoplastic damage and healing model (10 ℃ and 20 ℃)

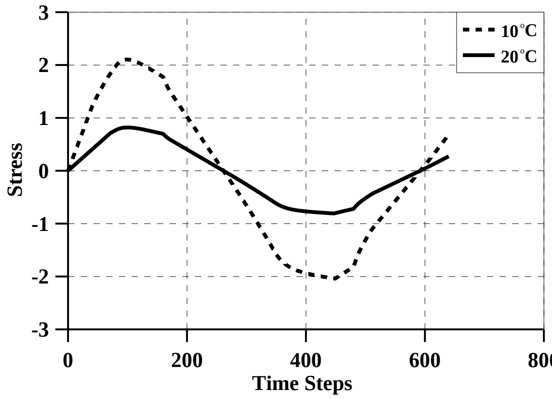

(a) Homogenized Stress

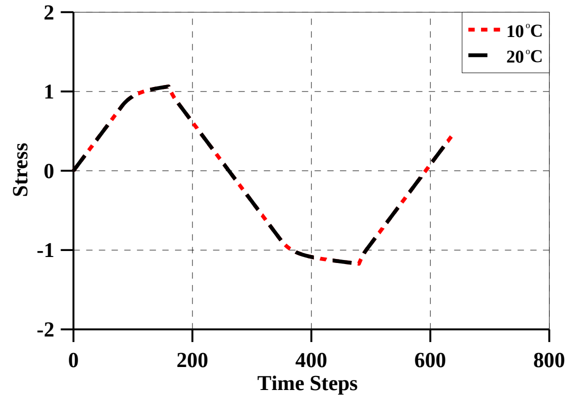

(b) Net Stress

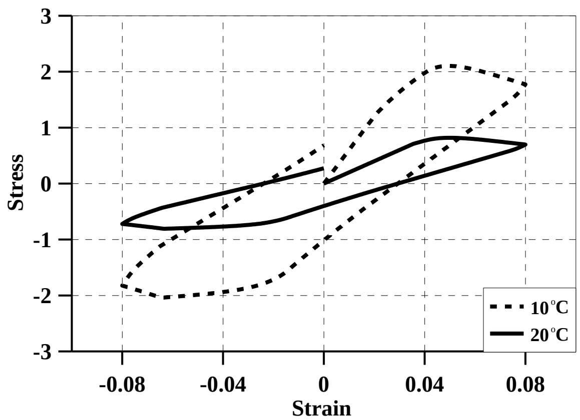

(c) Stress-Strain

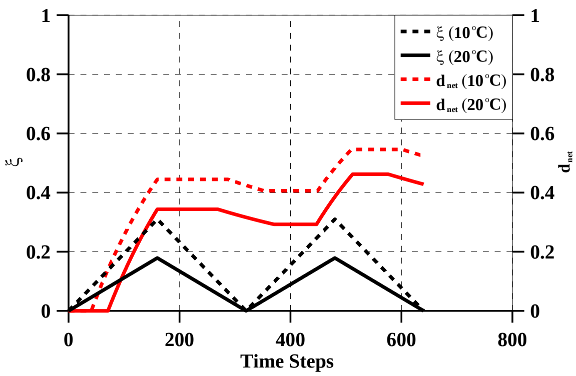

(d) Damage Net Variable

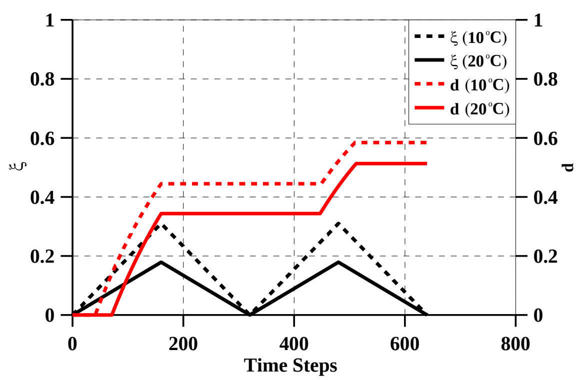

(e) Damage Variable

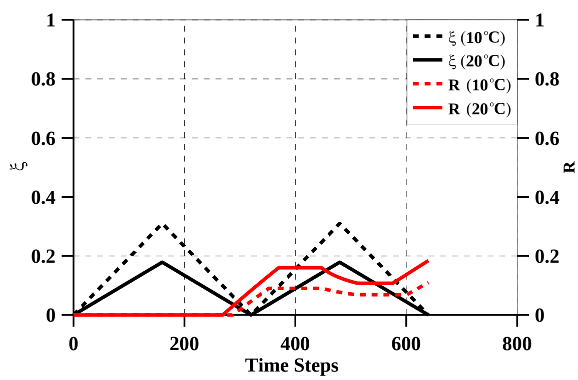

(f) Healing Variable

Figure 4.6 Corresponding results of one-dimensional driver problems by thermo-elastoviscoplastic damage and healing model (10 ℃ and 20 ℃)

Figure 4.7 and Figure 4.8 provide healing effect due to either temperature or the rest period. It is assumed that the initial damage threshold and the healing threshold are 0.08 and 0.1, respectively, and the yield stress is 1. In Figure 4.7, increase in temperature for the rest period (point A to B) causes more healing. As a result, the homogenized stress at 30 ℃ is higher than that at 20 ℃ after reloading is completed in presented Figure 4.7(a). In contrast to the homogenized stress history, the net stresses are the same in Figure 4.7(b) because temperature effect, damage, and healing are not considered in net space. In Figure 4.7(c), the Elastic Young's modulus at 30 ℃ is greater than that at 20 ℃ after reloading is finished since the bituminous material exposed to 30 ℃ is partially recovered. Damage occurs only when loading is applied so that the damage variables for both cases are the same shown in Figure 4.7(e) because the temperature for reloading is the same. However, the amount of healing is different due to temperature difference for the rest period as presented in Figure 4.7(f). Therefore, the damage net at 30 ℃ after completion of the rest period is smaller than that at 20 ℃. The homogenized stress for 100 steps is slightly small than that for 300 steps shown in Figure 4.8(a), whereas the net stresses are the same for 100 steps and 300 steps. In Figure 4.8(c), it is observed that the Young's modulus after 100 steps is slightly small than 300 steps. For damage variable in Figure 4.8(e), the final damage variable after 100 steps is definitely smaller than that after 300 steps because more healing makes the damage threshold lower and then more damage can occur. However, when the damage and the healing are combined to make damage net variable, it becomes very close to each other as presented in Figure 4.8(d). This is the main reason the Young's modulus after 300 steps is slightly higher than that after 100 steps.

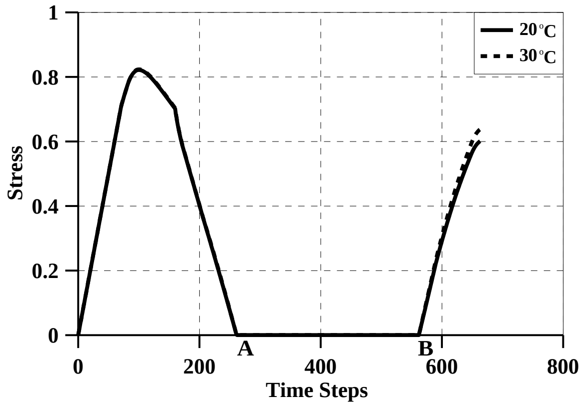

(a) Homogenized Stress

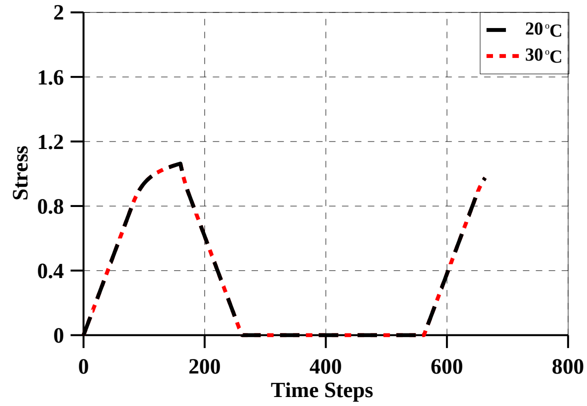

(b) Net Stress

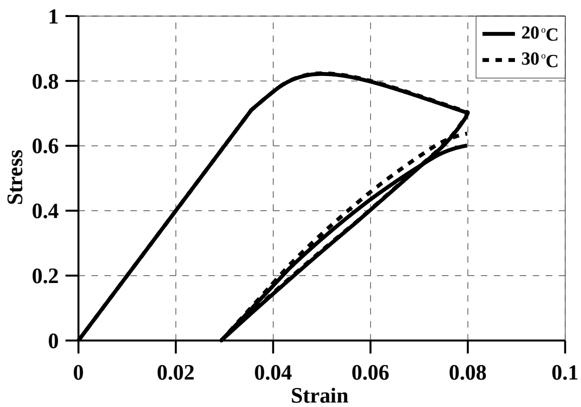

(c) Stress-Strain

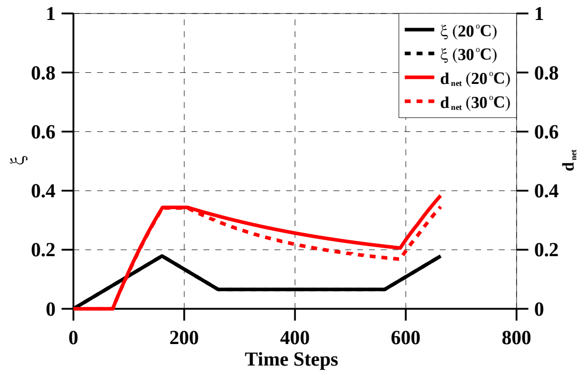

(d) Damage Net Variable

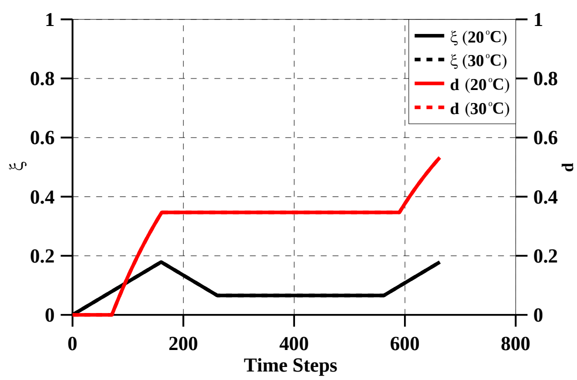

(e) Damage Variable

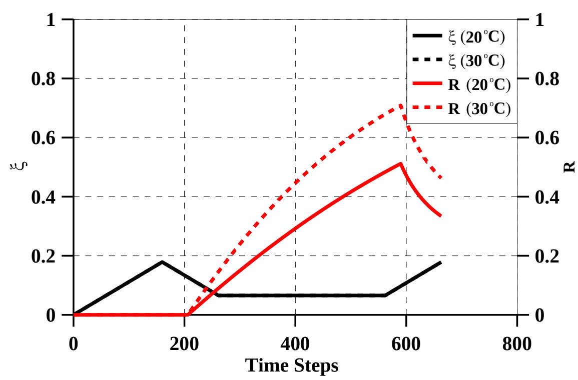

(f) Healing Variable

Figure 4.7 Corresponding results of one-dimensional driver problems by thermo-elastoviscoplastic damage and healing model (20 ℃ and 30 ℃ for healing period)

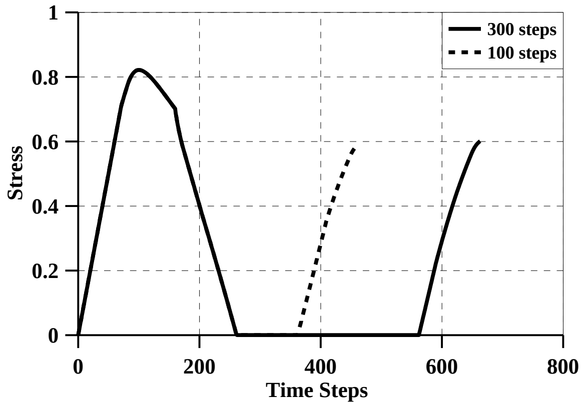

(a) Homogenized Stress

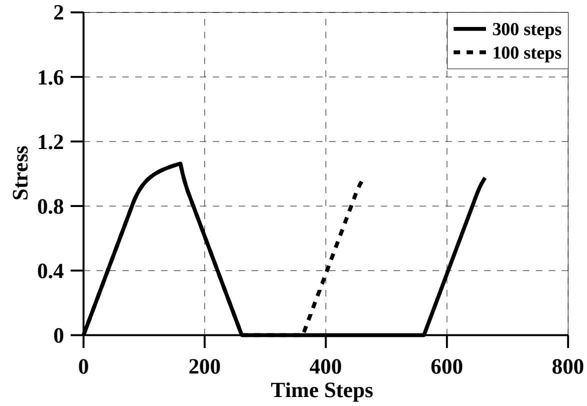

(b) Net Stress

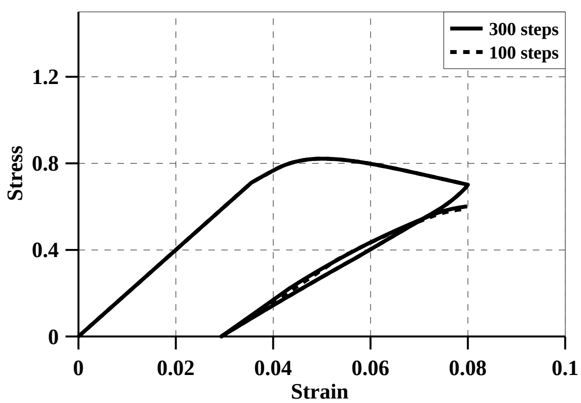

(c) Stress-Strain

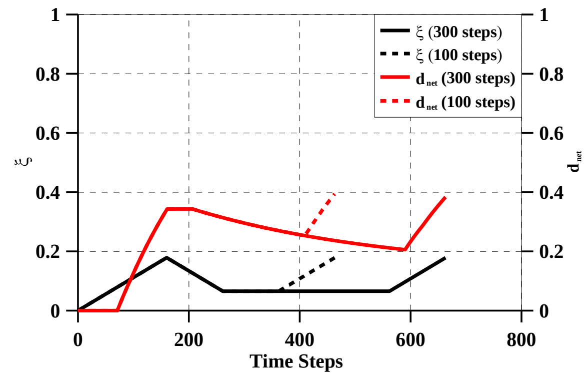

(d) Damage Net Variable

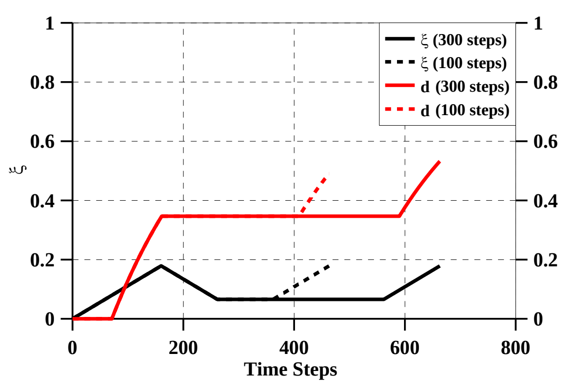

(e) Damage Variable

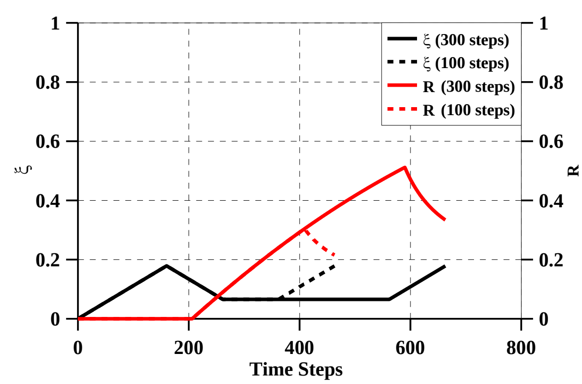

(f) Healing Variable

Figure 4.8 Corresponding results of one-dimensional driver problems by thermo-elastoviscoplastic damage and healing model (100 steps and 300 steps for healing period)

4.3.2 Comparison between Experimental Results and Model Prediction

The initial energy-based thermo-elastoviscoplastic isotropic damage-self healing mechanism and computational framework developed in Chapter 3 and previous section is employed in this section for predicting fundamental characteristics of the behavior of bituminous composites within experimental error. In view of the wide scattering in available experimental data for asphalt mixtures and the present imperfection of experimental techniques, a precise quantitative evaluation of the predicting capabilities of a given constitutive model with this damage-self healing model may not seem to be guaranteed. However, a comprehensive qualitative production of the main features of asphalt material behavior should play a central role in material modeling.

A two-invariant Drucker-Prager yield criterion with Perzyna viscoplasticity model is chosen and employed because it is hydrostatic stress dependent and a viscoplastic material. In addition, experimental measurements for the bituminous materials indicate that the yield surface is not the same as the viscoplastic potential surface because the associative flow rule overestimates the behavior of dilation for asphalt composites [8][12]. Therefore, non-associative flow rule is employed in the model. Lemaitre and Chaboche (1990) and Tan et al. (1994) shows that material constant A in Drucker-Pracker yield evolves the permanent deformation while B is almost a constant as the materials permanently deforms. Moreover, equivalent viscoplastic strain is used for the hardening law. Based on these reasons, radial return algorithm [2] is summarized in BOX 4.2 and BOX 4.2.

BOX 4.1 Radial return algorithm in net space

1. Update strain tensor.

$$\boldsymbol{\varepsilon}_{n+1}=\boldsymbol{\varepsilon}_n+\Delta\boldsymbol{\varepsilon}_{n+1}$$

$$\mathbf{e}_{n+1}=\boldsymbol{\varepsilon}_{n+1}-\frac{1}{3}\operatorname{tr}\left(\boldsymbol{\varepsilon}_{n+1}\right)\mathbf{1}$$

2. Compute *trial elastic* stress.

$$\boldsymbol{\sigma}_{n+1}^{trial,net}=\boldsymbol{\sigma}_n^{net}+\mathbf{C}\ :\Delta\boldsymbol{\varepsilon}_{n+1}$$

$$p_{n+1}^{trial,net}=\frac{1}{3}\operatorname{tr}\left(\boldsymbol{\sigma}_{n+1}^{trial,net}\right)$$

$$\mathbf{s}_{n+1}^{trial,net}=2G\ \left(\mathbf{e}_{n+1}-\mathbf{e}_n^{vp}\right)$$

3. Check yield condition

$$f_{n+1}^{trial,net}=\left\|\mathbf{s}_{n+1}^{trial,net}\right\|-\left(A\left(\varepsilon_{vp,n}\right)-Bp_{n+1}^{trial,net}\right)$$

IF $f_{n+1}^{trial,net}\leq 0$ THEN:

$$\mathbf{e}_{n+1}^{vp}=\mathbf{e}_n^{vp} \qquad p_{n+1}^{net}=p_{n+1}^{trial,net}$$

$$\mathbf{s}_{n+1}^{net}=\mathbf{s}_{n+1}^{trial,net} \qquad \boldsymbol{\sigma}_{n+1}^{net}=\boldsymbol{\sigma}_{n+1}^{trial,net}$$

ENDIF.

4. Compute $\mathbf{n}_{n+1}^{net}$ and $\hat{\gamma}_{n+1}^{net}$ from BOX 4.2

$$\mathbf{n}_{n+1}^{net}=\frac{\mathbf{s}_{n+1}^{trial,net}}{\left\|\mathbf{s}_{n+1}^{trial,net}\right\|}$$

5. Update viscoplastic strain and net stress

$$\varepsilon_{vp,n+1}=\varepsilon_{vp,n}+\frac{\sqrt{2/3}+B/3}{\sqrt{B^2+1}}\hat{\gamma}_{n+1}^{net}$$

$$A\left(\varepsilon_{vp,n+1}\right)=A_0+A_1\left(1-\exp\left(-A_2\varepsilon_{vp,n+1}\right)\right)$$

$$\mathbf{e}_{n+1}^{vp}=\mathbf{e}_n^{vp}+\hat{\gamma}_{n+1}^{net}\mathbf{n}_{n+1}^{net} \qquad p_{n+1}^{net}=p_{n+1}^{trial,net}-\hat{\gamma}_{n+1}^{net}KB$$

$$\mathbf{s}_{n+1}^{net}=\mathbf{s}_{n+1}^{trial,net}-\hat{\gamma}_{n+1}^{net}2G\mathbf{n}_{n+1}^{net} \qquad \boldsymbol{\sigma}_{n+1}^{net}=p_{n+1}^{net}\mathbf{1}+\mathbf{s}_{n+1}^{net}$$

6. Compute consistent elastoviscoplastic tangent moduli

$$\mathbf{C}_{n+1}^{evp,net}=\left(2G-\theta_{n+1}\right)\mathbf{I}+\left(K-\frac{2G}{3}-\frac{K^2BD}{F}+\frac{\theta_{n+1}}{3}\right)\mathbf{1}\otimes\mathbf{1}-\frac{2GKB}{F}\mathbf{1}\otimes\mathbf{n}_{n+1}$$
$$-\frac{2GKD}{F}\mathbf{n}_{n+1}\otimes\mathbf{1}-\left(\frac{\left(2G\right)^2}{F}-\theta_{n+1}\right)\mathbf{n}_{n+1}\otimes\mathbf{n}_{n+1}$$

$$\theta_{n+1}=\frac{\left(2G\right)^2\hat{\gamma}_{n+1}^{net}}{\left\|\mathrm{s}_{n+1}^{tr}\right\|}$$

BOX 4.2 Consistency condition and determination of $\hat{\gamma}_{n+1}^{net}$

1. Initialize:

$$\hat{\gamma}_{n+1}^{net}=0$$

2. Iterate:

DO UNTIL: $\left|h\left(\hat{\gamma}_{n+1}^{net}\right)\right| < TOL$

$k \leftarrow k+1$

$$h\left(\hat{\gamma}_{n+1}^{k,net}\right) = \left\langle f_{n+1}^{trial} \right\rangle - \hat{\gamma}_{n+1}^{k,net}\left(2G + KBD\right) - \left(\frac{\hat{\gamma}_{n+1}^{k,net}\eta}{\Delta t}\right)^{\frac{1}{m}}$$

$$Dh\left(\hat{\gamma}_{n+1}^{k,net}\right) = -\left(2G + KBD\right) - \frac{1}{m}\left(\frac{\eta}{\Delta t}\right)^{\frac{1}{m}}\left(\hat{\gamma}_{n+1}^{k,net}\right)^{\frac{1}{m}-1}$$

$$\hat{\gamma}_{n+1}^{k+1,net} = \hat{\gamma}_{n+1}^{k,net} - \frac{h\left(\hat{\gamma}_{n+1}^{k,net}\right)}{Dh\left(\hat{\gamma}_{n+1}^{k,net}\right)}$$

To validate the proposed damage-self healing model, the experimental data are taken from the well-documented experimental program preformed at the Texas A&M University (TAMU) and the North Carolina State University (NCSU) [1][6]. Due to the limitation of available experimental data, the thermo-elastoviscoplastic damage model against the monotonic uniaxial compression tests with different strain rates at different temperatures is first chosen and the elastoviscoplastic damage-self healing model against the cyclic strain loading control test at constant temperature for two different asphalt materials is shown for the verification in this section. The proposed thermo-elastoviscoplastic damage-self healing model is equivalent to the thermo-elastoviscoplastic damage model when the damage is considered only for monotonic uniaxial tests. As a result, the net space is equal to the effective space and damage net variable is the same as damage variable. In the case of the second example, the proposed model becomes the elastoviscoplastic damage-self healing model since the experiment was conducted under the only one constant temperature. By comparing these two cases, the proposed models demonstrate capability in predicting the temperature-dependent mechanical behavior of bituminous composites.

TAMU asphalt concrete data

The experimental data for the following example are retrieved from the literature paper [1] on monotonic uniaxial compression tests of Hot Mix Asphalt. 10 mm Dense Bitumen Macadam which is a continuously graded mixture with asphalt binder content of 5.5% and Granite aggregates and an asphalt binder with a penetration grade of 70/100 were used for tests. The size of cylindrical specimen is 100 mm in diameter and 100 mm in height compacted by the gyrator compactor. The tests were conducted at three different temperatures, 10 ℃, 20 ℃, and 40 ℃. The three different strain rates were used from 0.005 s^{-1} to 0.00005 s^{-1} for 10 ℃ and 20 ℃, while for 40 ℃ only two strain rates, 0.005 s^{-1} and 0.0005 s^{-1}, were tested. The experimental data for 20 ℃ were considered as reference material properties. The optimal material parameters of the bituminous composites for simulations are obtained from the experimental data by fitting and summarized in Table 4.1.

Table 4.1 The associated bituminous material properties at 20 ℃ in simulations

	$\dot{\varepsilon} = 0.005\ s^{-1}$	$\dot{\varepsilon} = 0.0005\ s^{-1}$	$\dot{\varepsilon} = 0.00005\ s^{-1}$
Young's modulus	290,000 (kPa)	130,000 (kPa)	70,000 (kPa)
Poisson's ratio	0.35		
Viscosity	244 (kPa/sec)		
Lame constants	250,617 (kPa)	112.345 (kPa)	60,493 (kPa)
Shear modulus	107,407 (kPa)	48,148 (kPa)	25,925 (kPa)
Initial damage threshold	2.0		
A_0	20 (kPa)		

Figure 4.9 shows the experimental and numerical results at two or three strain rates under different temperature conditions. The stress in y-axis in Figure 4.9(a), (c), and (e) is the stress in axial direction. Good qualitative and quantitative agreements between the proposed thermo-elastoviscoplastic damage model and the experimental data are clearly observed. In particular, softening responses are well captured as presented in Figure 4.9(a), (c), and (e). The damage net variable is equivalent to the damage variable because the monotonic uniaxial compression experimental results were employed for comparisons between model prediction and simulation. Therefore, the thermo-elastoviscoplastic damage-self healing model was employed so that the damage net variable was used for the plots as shown in Figure 4.9(b), (d), and (f). Figure 4.9(b) describes that accumulated damage increases as strain increase and the maximum damage is approximately 0.9 when the strain reaches 12%. For $\dot{\varepsilon} = 0.0005\ \mathrm{s}^{-1}$ case, the damage net variables are slight higher than 0.8 while in case of $\dot{\varepsilon} = 0.00005\ \mathrm{s}^{-1}$ the damage net variables are clearly lower than 0.8. In view of temperature, the damage net for high temperature at the same strain rate is the lowest variable because the bituminous materials become more viscous and it lowers the damage level. Moreover, the damage starting point for lower temperature is close to zero strain level. In other words, the asphalt concretes are more susceptible to damage at low temperature because they lose viscous material properties and become brittle. Figure 4.9(c) and (d) show that the proposed model is able to capture the experimental data. However, there is a small gap between the model and the experimental data. Authors may expect the reasons of this small gap because the volumetric and deviatoric damage is different to each other [4]. The damage net variables for different strain rate, 0.0005 s^{-1} to 0.00005 s^{-1}, are plotted in Figure 4.9(d) and (f), respectively. Their patterns are the exact same as the strain rate of 0.005 s^{-1}. The damage net variables are replotted at the same temperature in Figure 4.10 to demonstrate viscous damage effect. The damage net increases with increasing strain rate. In other words, the fast loading causes more damage on bituminous materials.

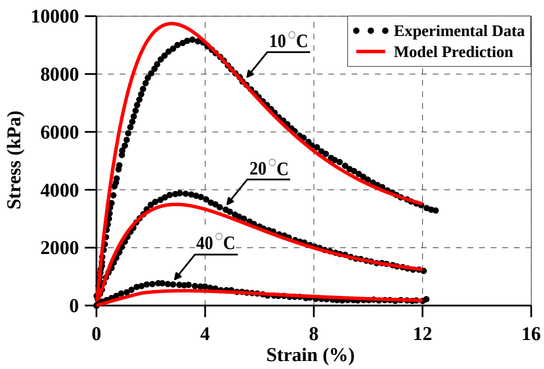

(a) Stress-Strain ($\dot{\varepsilon} = 0.005\ \mathrm{s}^{-1}$)

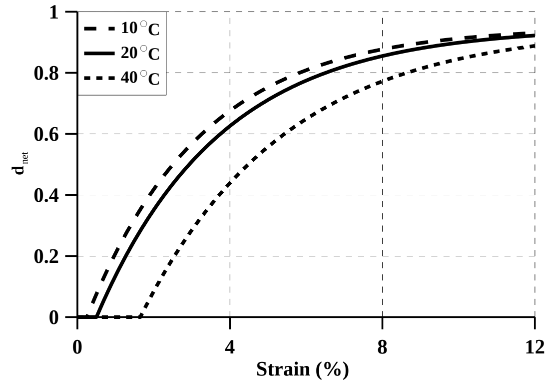

(b) Damage Net Variable($\dot{\varepsilon} = 0.005\ \mathrm{s}^{-1}$)

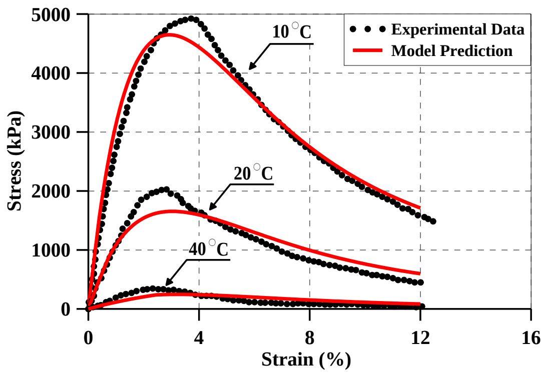

(c) Stress-Strain($\dot{\varepsilon} = 0.0005\ \mathrm{s}^{-1}$)

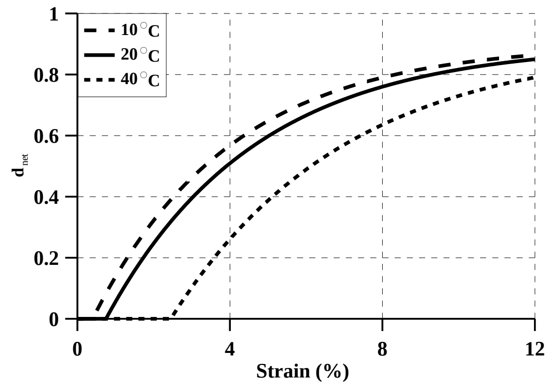

(d) Damage Net Variable($\dot{\varepsilon} = 0.0005\ \mathrm{s}^{-1}$)

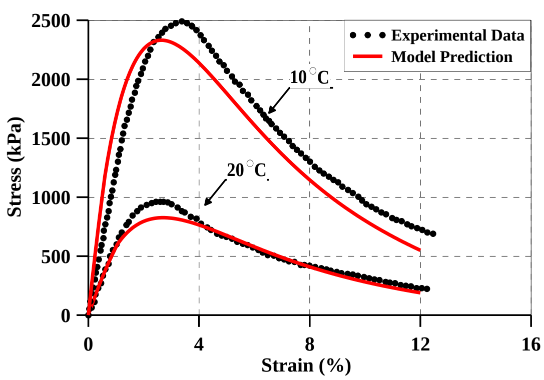

(e) Stress-Strain($\dot{\varepsilon} = 0.00005\ \mathrm{s}^{-1}$)

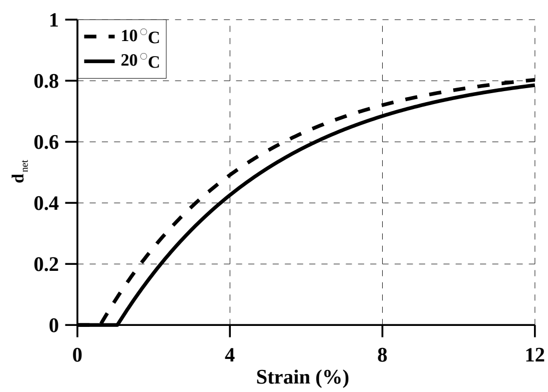

(f) Damage Net Variable($\dot{\varepsilon} = 0.00005\ \mathrm{s}^{-1}$)

Figure 4.9 Comparison between experimental data and model prediction for the uniaxial constant strain rate test in compression ($\dot{\varepsilon} = 0.005 \sim 0.00005\ \mathrm{s}^{-1}$)

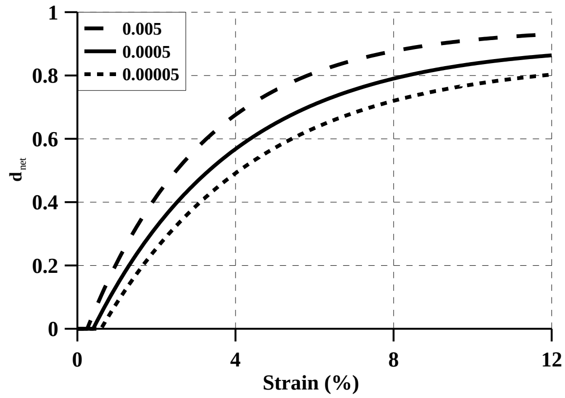

(a) 10 ℃

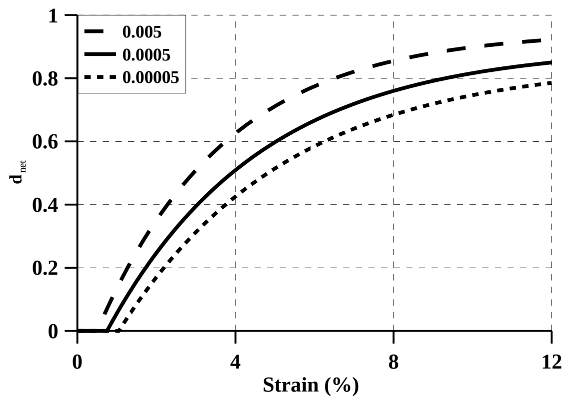

(b) 20 ℃

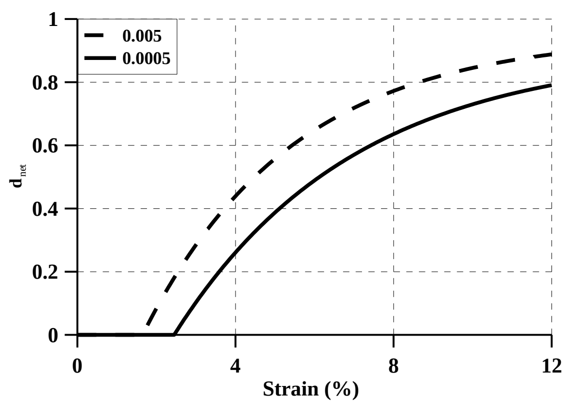

(c) 40 ℃

Figure 4.10 Comparison for damage net variables at constant temperature

NCSU asphalt mixture data

The experimental data for the following example are taken from Lee's dissertation [6] on controlled-strain cyclic tension tests of two different asphalt concretes, AAD and AAM. AAD has a tendency for age hardening and cracking and AAM is described as a good performer with a low temperature susceptibility and potential for a low temperature cracking. The size of cylindrical specimen was 10.2 cm in diameter and 25 cm in height. The strain amplitudes of controlled-strain cyclic tests were 0.0009 and 0.001 for AAD and AAM mixtures, respectively, and the frequency of the test was set as 1 Hz. Due to the limitation of experimental tension data at different temperatures, the model and experimental results for the cyclic strain controlled in tension are compared at only one constant temperature, 25 ℃. Although healing theoretically occurs during unloading of the first cycle, it is close to zero because the amount of accumulated damage is small. As the number of cycles grows, the increase in accumulated damage result in increase in damaged healing threshold and increase in the amount of healing. Therefore, more healing can be observed as the number of cycles increases. The optimal material parameters of AAD and AAM for simulations are also obtained from the experimental data by fitting and summarized in Table 4.2 The associated asphalt material properties at 25 ℃ in simulations.

Table 4.2 The associated asphalt material properties at 25 ℃ in simulations

	AAD	AAM
Young's modulus	1,300,000 (kPa)	1,200,000 (kPa)
Poisson's ratio	0.3	
Viscosity	244 (kPa/sec)	
Lame constants	750,000 (kPa)	692,307(kPa)
Shear modulus	500,000 (kPa)	461,538 (kPa)
Initial damage threshold	0.15	
Initial healing threshold	0.13	
A_0	20 (kPa)	

Figure 4.11 clearly shows that the proposed elastoviscoplastic damage-self healing model can capture the results of the controlled-strain cyclic loading tests for AAD and AAM. Since a two-invariant Drucker-Prager yield criterion with Perzyna viscoplasticity model is employed, the stress-strain curve moves down as increasing cycles. As a result, stress-strain loops for 287th cycle for AAD and 1188 cycle for AAM move down from the first cycle loop for each type of asphalt concrete. As shown in Figure 4.11(c), the 287th cyclic experimental data are close to the simulated results (red solid line) when the damage-self healing model is employed. However, if damage is only considered, damage variable is higher than damage net and the stiffness of the material is reduced (blue solid line). Figure 4.11(d) demonstrates that the numerical result (blue solid line) when the damage model is chosen does not predict the experimental data for 1188th cyclic loading due to too much damage. The history of damage net for AAD and AAM is plotted in Figure 4.11(e) and (f). The shape of these damage net variables seem to be similar to the damage variable as shown in Figure 4.10(b), (d), and (f). However, enlarging damage net variable shown in Figure 4.12, the damage net variable increases with increasing damage variable and decreases when healing occurs. Since the damage net is combination of damage

variable and healing variable, there are many possibilities for the same damage net variables so that only damage net variable is plotted in Figure 4.11 and Figure 4.12. When the energy norm due to cyclic loading exceeds healed damage threshold (point A) in Figure 4.13(a), damage and damage net variables increase until the end of reloading (B). The unloading reign is between points B and D and the healing occurs at point C in Figure 4.13(a) and damage net variable decreases when the energy norm is smaller than damaged healing threshold. At point D as presented in Figure 4.13(a), the reloading starts again and damage and damage net is constant until it reaches healed damage threshold at point E as shown Figure 4.13(a). Comparison between AAD and AAM in Figure 4.13(b) shows that damage net variable is clearly dependent on material properties.

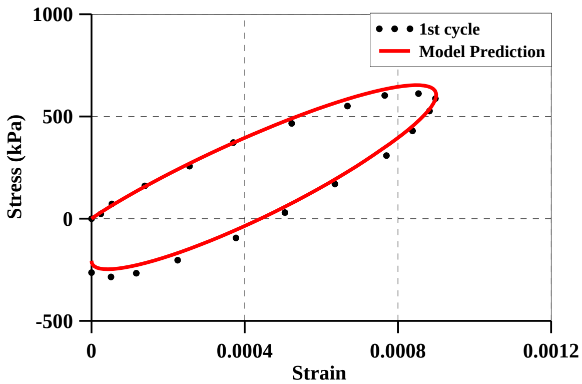

(a) 1st Cycle (AAD)

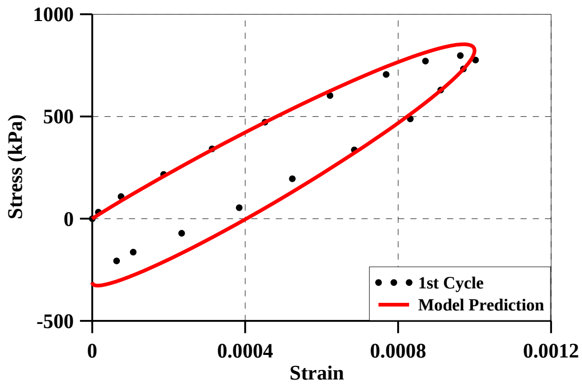

(b) 1st Cycle (AAM)

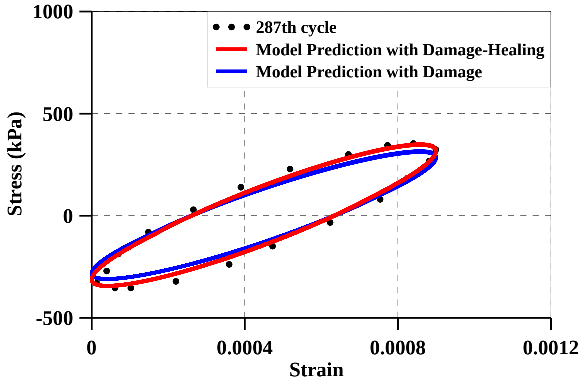

(c) 287th Cycle (AAD)

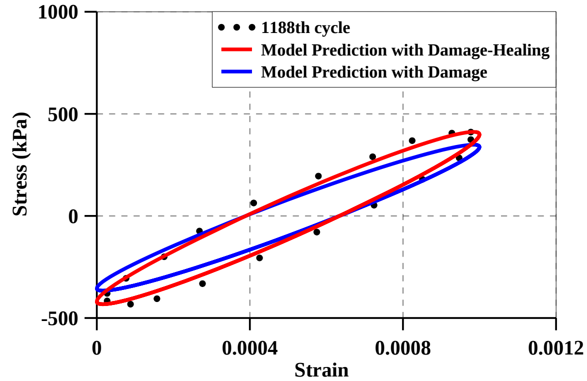

(d) 1188th Cycle (AAM)

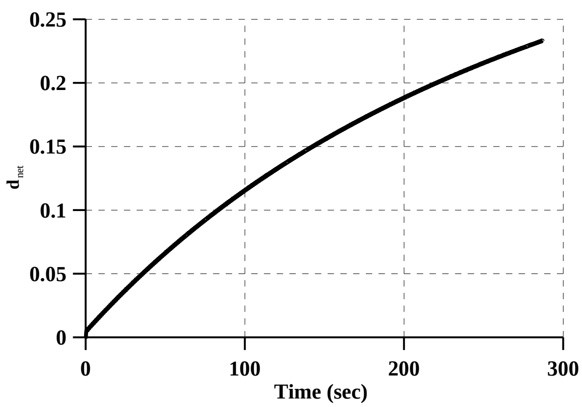

(e) Damage Net Variable (AAD)

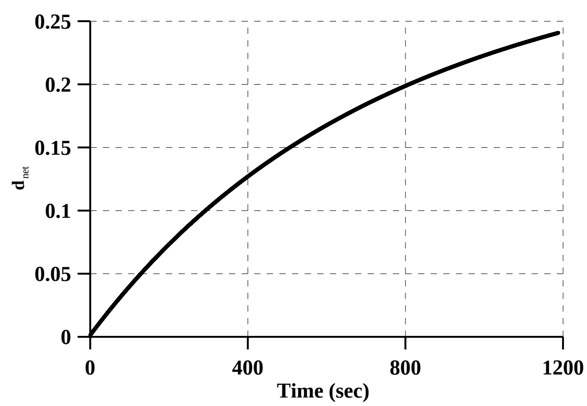

(f) Damage Net Variable (AAM)

Figure 4.11 Comparison between experimental data and model prediction for the cyclic loading in tension

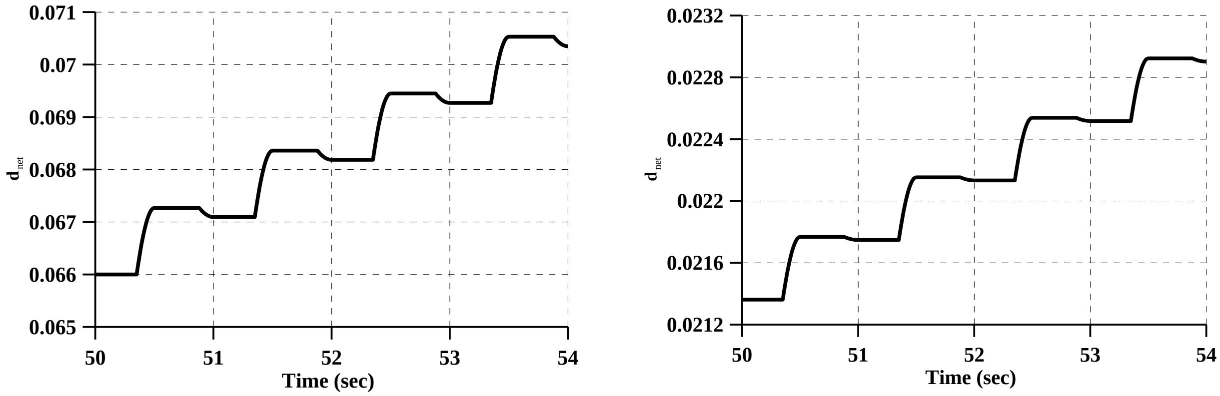

(a) Damage Net Variable (AAD)

(b) Damage Net Variable (AAM)

Figure 4.12 Enlarged damage net variables

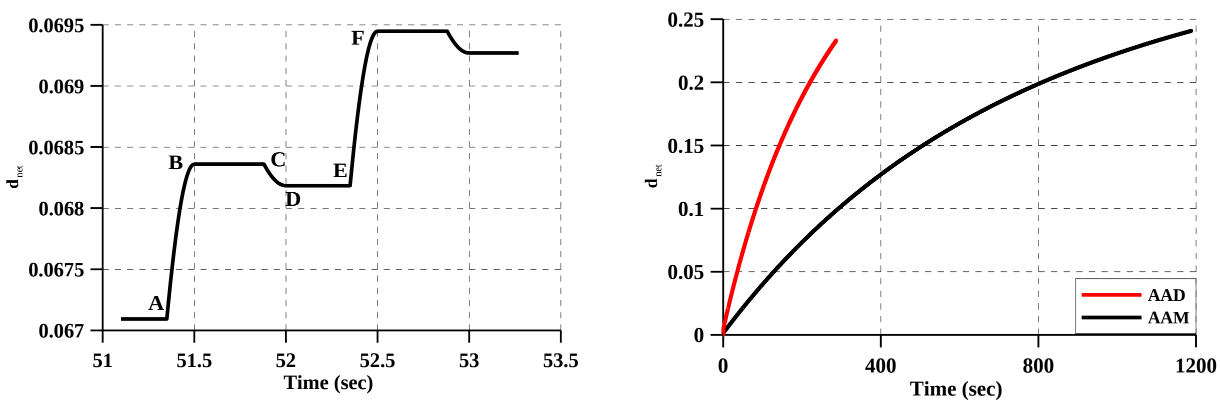

(a) Loading Cycle (AAD)

(b) Damage Net Variable

Figure 4.13 Loading cycle for AAD and comparison of damage net variables between AAD and AAM

4.4 Reference

[1] Darabi, M. K., Abu Al-Rub, R.K., Masad, E.A., and Little, D.N. (2011). "Thermodynamic-based model for coupling temperature-dependent viscoelastic,

viscoplastic, and viscodamage constitutive behavior of asphalt mixtures." Int. J. Numer. Anal. Meth. Geomech. DOI: 10.1002/nag.1030

[2] Ju, J. W. (1989). On Energy-Based Coupled Elastoplastic Damage Theories-Constitutive Modeling and Computational Aspects, *International Journal of Solids and Structures*, **25**: pp. 803-833.

[3] Ju, J. W., Yuan, K.Y. Kuo, W., Chen, J.S. (2012b). Novel Strain Energy Based Coupled Elastoplastic Damage and Healing Models for Geomaterials - Part II: Computational Aspects, *International Journal of Damage Mechanics*, **21** (4): pp. 551-576.

[4] Ju, J. W., Yuan, K.Y., and Kuo, W. (2012a). Novel Strain Energy Based Coupled Elastoplastic Damage and Healing Models for Geomaterials - Part I: Formulations, *International Journal of Damage Mechanics*, **21** (4): pp. 525-549.

[5] Kim, Y. R., Whitmoyer, S.L., and Little, D.N. (1994). Healing in Asphalt Concrete Pavements: Is it Real?, *Transportation Research Board 1454*: pp. 89-96.

[6] Lee, H. J. (1996). Uniaxial Constitutive Modleing of Asphalt Concrete Using Viscoelasticity and Continuum Damage Theory, Department of Civil Engineering, North Carolina State University, Ph.D. Dissertation.

[7] Lemaitre, J. and Chaboche, J.-L. (1990). Mechanics of solid materials. Cambridge University Press, Cambridge, UK

[8] Oda, M., and Nakayama, H. (1989). Yield function for soil with anisotropic fabric, *Journal of Engineering Mechanics, ASCE*, **15**(1), 89-105.

[9] Simo, J. C., and Ju, J.W. (1987a). Strain-Based and Stress-Based Continuum Damage Models, Part I: Formulation, *International Journal of Solids and Structures*, **23**: pp.

821-840.

[10] Simo, J. C., and Ju, J.W. (1987b). Strain-Based and Stress-Based Continuum Damage Models, Part II: Computational Aspects, *International Journal of Solids and Structures*, **23**: pp. 841-869.

[11] Tan, S. A., Low, B.H., and Fwa, T.F. (1994). Behavior of asphalt concrete mixtures in triaxial compression, *Journal of Testing and Evaluation*, **22**: pp. 195-203.

[12] Zeinkiewicz, O., Humpheson, C., and Lewis, R. (1975). Associated and non-associated visco-plasticity in soils mechanics, *Journal of Geotechnique*, **25**(2): pp. 671-689.

5. NEW INITIAL STRAIN ENERGY BASED THERMO-ELASTOVISCOPLASTIC TWO-PARAMERTER DAMAGE-SELF HEALING MODEL FOR BITUMINOUS COMPOSITES – PART I: FORMULATIONS

5.1 Introduction

First, new ***initial elastic energy*** based thermo-elastoviscoplastic ***two-parameter*** damage-self healing formulations, based on continuum thermodynamics framework, are developed in this chapter. In particular, the governing ***volumetric*** and ***deviatoric*** damage and self-healing evolutions are coupled in an incremental form with definition of volumetric and deviatoric damage and healing area and characterized through the net stress concept in conjunction with the hypothesis of strain equivalence. Then, a conceptual example with two linearly independent springs which are in vertical and horizontal direction is conceptually illustrated for the proposed two-parameter model.

5.2 A Coupled Isotropic Formulation

A basic idea underlining the initial (undamaged) elastic strain energy based two-parameter damage-self healing formulations presented in this section is the hypothesis that incremental two parameter damage and self-healing histories in bituminous composite are directly linked to the history of total strains with Arrhenius-type temperature term. The notion of net healed stress along with the hypothesis of strain equivalence follows from the assumed form of free energy. The Arrhenius-type temperature term is chosen uncoupled for simplicity in order to consider the effect of the temperature for bituminous materials. The proposed volumetric and deviatoric damage, healing, and their combined (net) damage-healing variables are mainly focused in this chapter.

5.2.1 Definition of Net (Combined) Variables of the Volumetric Damage and Healing

We conceptually assume that area A can be decomposed into two parts: the volumetric area A_v and the deviatoric area A_d. Moreover, it is assumed that the overlapping area does not exist and they is linearly independent.

$$A_v \cap A_d = \varnothing \tag{5.1}$$

Let us define d_v as the volumetric damage variable and R_v as the volumetric healing variable, respectively, in the following with the volumetric damaged area A_v^d, the volumetric healed area A_v^R, and the volumetric unhealed A_v^{uR}.

$$d_v = A_v^d / A_v \tag{5.2}$$

$$R_v = A_v^R / A_v^d \tag{5.3}$$

Due to the assumption that only volumetric undamaged and healed area can sustain the volumetric loading in continuum damage mechanics presented in Figure 5.1, we define d_v^{net} as a scalar variable to describe the net (combined) effect of volumetric damage-healing

$$\boldsymbol{\sigma}_v A_v = \boldsymbol{\sigma}_v^{net} A_v^{net} \tag{5.4}$$

$$d_v^{net} = d_v \left(1 - R_v\right) \tag{5.5}$$

5.2.2 Definition of Net (Combined) Variables of the Deviatoric Damage and Healing

Let us define d_d as the deviatoric damage variable and R_d as the deviatoric healing variable, respectively, below with the deviatoric damaged area A_d^d, the deviatoric healed area A_d^R, and the deviatoric unhealed A_d^{uR}.

$$d_d = A_d^d / A_d \tag{5.6}$$

$$R_d = A_d^R / A_d^d \tag{5.7}$$

Due to the assumption that only deviatoric undamaged and healed area can sustain the deviatoric loading in continuum damage mechanics presented in Figure 5.1, we define d_d^{net} as a scalar variable to describe the net (combined) effect of deviatoric damage-healing

$$\boldsymbol{\sigma}_d A_d = \boldsymbol{\sigma}_d^{net} A_d^{net} \tag{5.8}$$

$$d_d^{net} = d_d \left(1 - R_d\right) \tag{5.9}$$

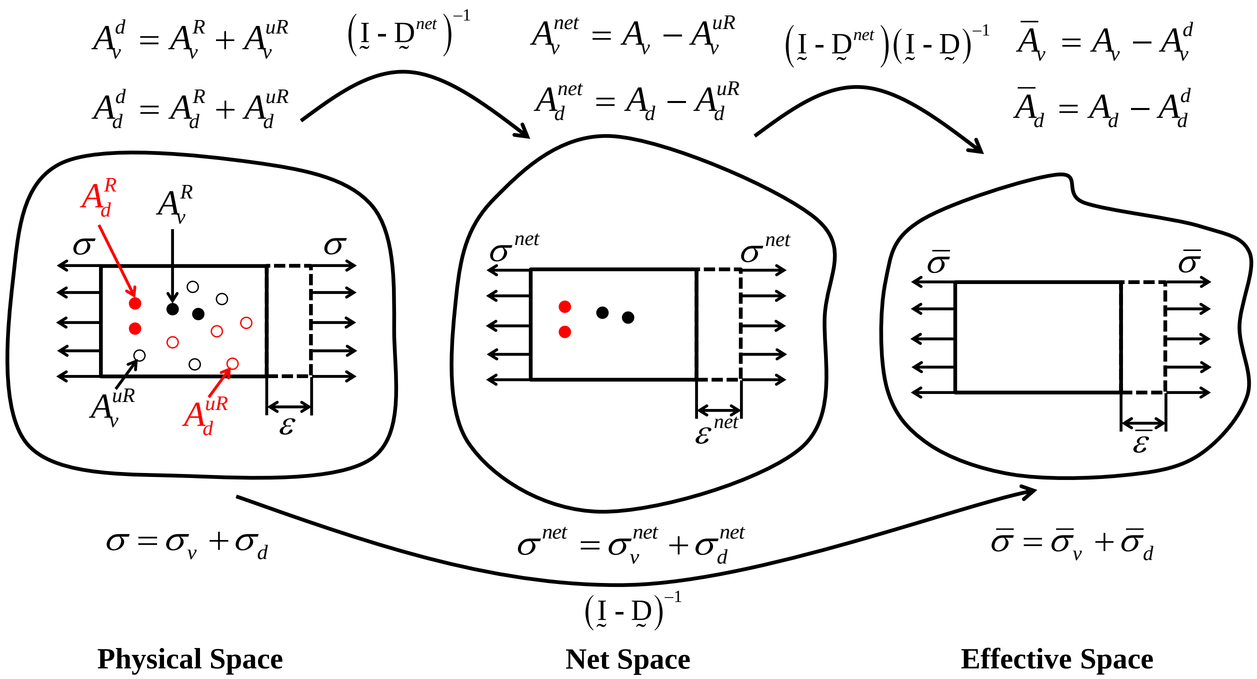

Figure 5.1 Schematic illustration of the physical, net, and effective spaces

5.2.3 Net Stress Concept and Hypothesis of Strain Equivalence

The initiation, growth, and coalescence of microcracks and microvoids result in physical and mechanical deterioration of the material properties. On the contrary to this degradation, if the damage is gradually and subsequently recovered due to the effect of temperature and compactions and its strength and stiffness are partially or fully healed, this is called healing. Within the continuum mechanics, one can model these processes by introducing the internal damage-healing variables which can be a tensorial quantity with two variables. We denote by $\mathbf{M}^{net} = (\mathbf{I} - \mathbf{D}^{net})$ a fourth-order tensor which characterizes the state of damage net and transforms the homogenized stress tensor $\boldsymbol{\sigma}$ into the net stress tensor $\boldsymbol{\sigma}^{net}$ (or vice versa). Accordingly,

$$\boldsymbol{\sigma}^{net} = \vartheta(T)^{-1}\left(\mathbf{M}^{net}\right)^{-1} : \boldsymbol{\sigma} \tag{5.10}$$

where $\vartheta(T)$ is the Arrhenius-type temperature term and defined as follows

$$\vartheta(T) = \exp\left\{-\boldsymbol{\delta}\left(1-\frac{T}{T_0}\right)\right\} \tag{5.11}$$

wherein which $\boldsymbol{\delta}$ is a material constant and T_0 is the reference temperature (℃).

For the isotropic two-parameter damage and healing case, the mechanical behavior of microdamage and healing is independent of their orientation and depends only on two scalar variables $d_v^{net} = d_v(1-R_v)$ and $d_d^{net} = d_d(1-R_d)$ and Eq.(5.10) then collapses to (see the Appendix)

$$\begin{aligned}\boldsymbol{\sigma}(t) &= \left[(\mathbf{I}-\mathbf{D}^{net}) : \boldsymbol{\sigma}^{net}(t)\right]\vartheta(T) \\ &= \left[\left(1-d_v^{net}(t)\right)\boldsymbol{\sigma}_v^{net}(t) + \left(1-d_d^{net}(t)\right)\boldsymbol{\sigma}_d^{net}(t)\right]\vartheta(T)\end{aligned} \tag{5.12}$$

$$\mathbf{D}^{net} = \frac{1}{3}d_v^{net}\mathbf{1}\otimes\mathbf{1} + d_d^{net}\left(\mathbf{I}-\frac{1}{3}\mathbf{1}\otimes\mathbf{1}\right) \tag{5.13}$$

where $d_v^{net}(t) \in \left[0, d_{v,c}^{net}\right]$ for $t \in \mathbb{R}_+$ is the volumetric net damage-healing variable, $d_d^{net}(t) \in \left[0, d_{d,c}^{net}\right]$ for $t \in \mathbb{R}_+$ is the deviatoric net damage-healing variable, $\boldsymbol{\sigma}(t)$ is the Cauchy stress tensor, and $\boldsymbol{\sigma}^{net}(t)$ is the net stress tensor. Here, $d_{v,c}^{net} \in (0,1]$ and $d_{d,c}^{net} \in (0,1]$ are a constant. The coefficients, $1-d_v^{net}(t)$ and $1-d_d^{net}(t)$, in Eq. (5.12) are a reduction factor associated with combined effect of damage and healing in the materials. The value $d_v^{net} = 0$ corresponds to the volumetric undamaged state or fully volumetric healing state whereas a value $d_v^{net} \in \left(0, d_{v,c}^{net}\right)$ represents a volumetric damaged state. The value $d_v^{net} = d_{v,c}^{net}$ defines complete local volumetric rupture. The value $d_d^{net} = 0$ corresponds to the deviatoric undamaged state or fully deviatoric healing state whereas a value $d_d^{net} \in \left(0, d_{d,c}^{net}\right)$ represents a deviatoric damaged state. The value $d_d^{net} = d_{d,c}^{net}$ defines complete local volumetric rupture. We assume that it is complete local rupture when either the volumetric damage net variable d_v^{net} or the deviatoric damage net variable d_d^{net} is equal to either $d_{v,c}^{net}$ or $d_{d,c}^{net}$, respectively. The volumetric net damage-healing variable may be interpreted physically as a ratio of difference between volumetric damaged and healed surface area to total volumetric surface area at a local material point. Similar to volumetric net damage-healing variable, the deviatoric net damage-healing variable have the same concept because they are orthogonal.

We introduced the following hypothesis of strain equivalence by extending from the effective stress space to the net stress space [2]:

"The strain associated with a damaged and healed state under the applied stress is equivalent to the strain ε^{net} associated with its damaged and healed state under the net stress". See Figure 5.2 for a schematic illustration.

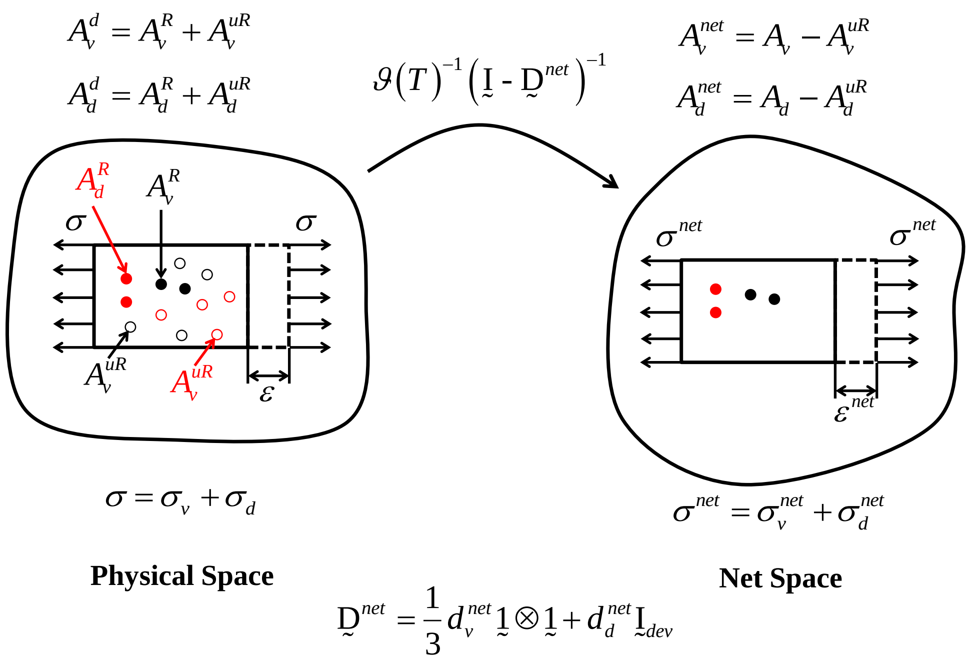

Figure 5.2 Schematic illustration of the *hypothesis of strain* with Arrhenius-type temperature term

5.2.4 The Thermodynamic Basis

In order to introduce the *net effect* of the two parameter damage-healing, viscoplastic flow processes and temperature effect, a free energy potential in the following form is proposed: (see the Appendix)

$$\begin{aligned} &\Psi\left(\boldsymbol{\varepsilon}_{\mathbf{v}}, \mathbf{e}, \boldsymbol{\sigma}^{vp}, \mathbf{q}, d_v^{net}, d_d^{net}, T\right) \\ &\equiv \left\{(1-d_v^{net})\Psi_v^0(\boldsymbol{\varepsilon}_{\mathbf{v}}) + (1-d_d^{net})\Psi_d^0(\mathbf{e}) - \frac{1}{2}\boldsymbol{\varepsilon} : \boldsymbol{\sigma}^{vp} + \Xi\left(\mathbf{q}, \boldsymbol{\sigma}^{vp}\right)\right\}\vartheta\left(T\right) \end{aligned} \tag{5.14}$$

where $\boldsymbol{\varepsilon}_v \equiv \frac{1}{3}\boldsymbol{\varepsilon}_{kk}\, \underset{\sim}{\mathbf{1}}$ denotes the volumetric strain tensor, $\mathbf{e}$ is the deviatoric strain tensor, $\boldsymbol{\sigma}^{vp}$ is the viscoplastic relaxation stress tensor, $\mathbf{q}$ is a suitable set of internal (viscoplastic) variables. Here, d_v^{net} signifies the scalar variable of net (combined) effect of volumetric damage and healing, which depends on the volumetric damage variable d_v, the incremental volumetric damage variable Δd_v, the volumetric healing R_v, and the incremental volumetric healing variable ΔR_v, all between 0 and 1 in numerical values. Similarly, d_d^{net} is the scalar variable of *net* (combined) effect of deviatoric damage and healing, which depends on the deviatoric damage variable d_d, the incremental deviatoric damage variable Δd_d, the volumetric healing R_v, and the incremental deviatoric healing variable ΔR_d, all between 0 and 1 in numerical values. Moreover, $\Psi_v^0(\boldsymbol{\varepsilon}_v)$ defines the initial-elastic volumetric stored energy function of the undamaged material, $\Psi_d^0(\mathbf{e})$ is the initial-elastic deviatoric stored energy function of the undamaged material, and $\Xi(\mathbf{q}, \boldsymbol{\sigma}^{vp})$ is the viscoplastic potential function. For the linear elasticity case, we have $\Psi_v^0(\boldsymbol{\varepsilon}_v) = \frac{1}{2}\boldsymbol{\varepsilon}_v : (K \underset{\sim}{\mathbf{1}} \otimes \underset{\sim}{\mathbf{1}}) : \boldsymbol{\varepsilon}_v = \frac{1}{2} K (\boldsymbol{\varepsilon}_{kk})^2$, where K denotes the bulk modulus and $\Psi_d^0(\mathbf{e}) = G\ \mathbf{e} : \mathbf{e}$, where G represents the shear modulus.

In many applications, the thermal dissipation is very much smaller than the mechanical dissipation so that it is reasonable to assume that the thermal dissipation rate can be ignored. The Clausius-Duhem becomes Clausius-Plank inequality which takes the form for any admissible process in this chapter

$$-s\dot{T} - \dot{\Psi} + \boldsymbol{\sigma} : \dot{\boldsymbol{\varepsilon}} \geq 0 \tag{5.15}$$

By taking the time derivative of Eq.(5.14), substituting it into Eq. (5.15), and making use of standard arguments [1] along with the additional assumption that the net effect of damage-healing and viscoplastic unloading are elastic processes, we can obtain the stress-strain constitutive law

$$\begin{aligned}\boldsymbol{\sigma} &= \left\{ \left(1-d_v^{net}\right) \frac{\partial \Psi_v^0\left(\boldsymbol{\varepsilon}_{\mathbf{v}}\right)}{\partial \boldsymbol{\varepsilon}_{\mathbf{v}}} + \left(1-d_d^{net}\right) \frac{\partial \Psi_d^0\left(\mathbf{e}\right)}{\partial \mathbf{e}} - \boldsymbol{\sigma}^{vp} \right\} \vartheta\left(T\right) \\ &= \left\{ \left(1-d_v^{net}\right) \boldsymbol{\sigma}_v^{net} + \left(1-d_d^{net}\right) \boldsymbol{\sigma}_d^{net} \right\} \vartheta\left(T\right)\end{aligned} \tag{5.16}$$

, the dissipative inequalities

$$\left\{ -\frac{\partial \Xi}{\partial \mathbf{q}} \cdot \dot{\mathbf{q}} - \left(\frac{\partial \Xi}{\partial \sigma^{vp}} - \frac{1}{2} \varepsilon \right) : \dot{\sigma}^{vp} \right\} \vartheta\left(T\right) \geq 0 \tag{5.17}$$

$$\left\{ \Psi_v^0\left(\boldsymbol{\varepsilon}_{\mathbf{v}}\right) \dot{d}_v^{net} + \Psi_d^0\left(\mathbf{e}\right) \dot{d}_d^{net} - \frac{\partial \Xi}{\partial \mathbf{q}} \cdot \dot{\mathbf{q}} - \left(\frac{\partial \Xi}{\partial \boldsymbol{\sigma}^{vp}} - \frac{1}{2} \boldsymbol{\varepsilon} \right) : \dot{\boldsymbol{\sigma}}^{vp} \right\} \vartheta\left(T\right) \geq 0 \tag{5.18}$$

and the entropy

$$s = -\frac{\partial \vartheta\left(T\right)}{\partial T} \Psi\left(\boldsymbol{\varepsilon}_{\mathbf{v}}, \mathbf{e}, \boldsymbol{\sigma}^{vp}, \mathbf{q}, d_v^{net}, d_d^{net}\right) \tag{5.19}$$

It follows from Eq.(5.16) that within the present strain space formulation, the stress tensor is split into elastic-damage-healing and the viscoplastic relaxation parts. From Eqs.(5.17) and (5.18), we observe that the dissipative energy by viscoplasticity itself is positive; if damage-healing effect is involved, the sum of damage-healing and viscoplasticity effect is also positive. It is also noted from Eqs. (5.17), (5.18), and (5.19) that the present framework is capable of accommodating general (nonlinear) elastic response and general viscoplastic response.

The potential $\Xi\left(\mathbf{q}, \boldsymbol{\sigma}^{vp}\right)$ is linked to viscoplastic dissipation. Its role is such that inequality (5.18) is satisfied for arbitrary processes. Note that we have assumed that $\Xi(\mathbf{q}, \boldsymbol{\sigma}^{vp})$ is independent of d_v^{net} and d_d^{net}. From Eq.(5.14), it then follows that

$$-Y_v \equiv -\frac{\partial \Psi\left(\boldsymbol{\varepsilon}_v, \mathbf{e}, \boldsymbol{\sigma}^{vp}, \mathbf{q}, d_v^{net}, d_d^{net}, T\right)}{\partial d_v^{net}} = \Psi_v^0\left(\boldsymbol{\varepsilon}_v\right)\vartheta\left(T\right) \tag{5.20}$$

$$-Y_d \equiv -\frac{\partial \Psi\left(\boldsymbol{\varepsilon}_v, \mathbf{e}, \boldsymbol{\sigma}^{vp}, \mathbf{q}, d_v^{net}, d_d^{net}, T\right)}{\partial d_d^{net}} = \Psi_d^0\left(\mathbf{e}\right)\vartheta\left(T\right) \tag{5.21}$$

Hence, the initial (undamaged) *volumetric* elastic strain energy $\Psi_v^0\left(\boldsymbol{\varepsilon}_v\right)$ is the thermodynamic force Y_v conjugate to the net volumetric damage-healing variable d_v^{net}; the initial (undamaged) *deviatoric* elastic strain energy $\Psi_d^0\left(\mathbf{e}\right)$ is the thermodynamic force Y_d conjugate to the net deviatoric damage-healing variable d_d^{net}. Attention is then focused on the volumetric and deviatoric damage, the volumetric and deviatoric healing, and their interactions.

5.2.5 Characterization of Initial-Elastic Strain-Energy Based Volumetric Damage

The progressive degradation of mechanical properties of asphalt concrete due to damage by means of a simple isotropic damage mechanism is first characterized. To this end, we propose to define the notion of equivalent volumetric strain ξ_v as the (undamaged) energy norm of the volumetric strain tensor.

$$\xi_v \equiv \sqrt{\Psi^0\left(\boldsymbol{\varepsilon}_v\right)\vartheta(T)} = \sqrt{\left\{\frac{1}{2}K\left(\varepsilon_{kk}\right)^2\right\}\exp\left\{-\boldsymbol{\delta}\left(1-\frac{T}{T_0}\right)\right\}} \tag{5.22}$$

where $\varepsilon_{kk} = \varepsilon_{11} + \varepsilon_{22} + \varepsilon_{33}$

We now characterize the state of volumetric damage in asphalt composites by means of a damage criterion $\phi_v^d\left(\xi_{v,t}, g_{v,t}\right) \leq 0$, formulated in the strain space, with the following functional form:

$$\phi_v^d\left(\xi_{v,t}, g_{v,t}\right) \equiv \xi_{v,t} - g_{v,t} \le 0 \qquad t \in \mathbb{R}_+ \tag{5.23}$$

where the subscript t refers to a value at current time $t \in \mathbb{R}_+$, and $g_{v,t}$ is the volumetric damage threshold at the current time t. It is noted that the numerical value of $g_{v,t}$ would be lowered due to the incremental volumetric healing (if any) from the previous time step. Let $g_{v,0}$ denote the initial volumetric damage threshold before any loading is applied; we then have $g_{v,t} \ge g_{v,0}$. Here, $g_{v,0}$ is considered as a characteristic material property. The condition (5.23) states that volumetric damage in bituminous materials is initiated when the volumetric energy norm of the strain tensor $\xi_{v,t}$ exceeds the initial volumetric damage threshold $g_{v,0}$. For the volumetric damage case, we define the evolution of the volumetric damage variable $d_{v,t}$ and the volumetric damage threshold $g_{v,t}$, respectively, by the rate equations:

$$\dot{d}_{v,t} = \dot{\mu}_v H_v\left(\xi_{v,t}, d_{v,t}\right) \tag{5.24}$$

$$\dot{g}_v = \dot{\mu}_v \tag{5.25}$$

where $\dot{\mu}_v \ge 0$ is a volumetric damage consistency parameter that defines the volumetric damage loading/unloading conditions according to the Kuhn-Tucker relations

$$\dot{\mu}_v \ge 0, \qquad \phi_v^d\left(\xi_{v,t}, g_{v,t}\right) \le 0, \qquad \dot{\mu}_v \; \phi_v^d\left(\xi_{v,t}, g_{v,t}\right) = 0 \tag{5.26}$$

The conditions (5.26) are standard for problems involving unilateral constraint. If $\phi_v^d\left(\xi_{v,t}, g_{v,t}\right) < 0$, the damage criterion is not satisfied and by conditions (5.26), $\dot{\mu}_v = 0$; hence, the volumetric damage rule (5.24) implies that $\dot{d}_v = 0$ and no further volumetric damage takes place. If, on the other hand, $\dot{\mu}_v > 0$; that is, further volumetric damage ("loading") is taking place, then conditions (5.26) implies that $\phi_v^d\left(\xi_{v,t}, g_{v,t}\right) = 0$. In this event, the value of $\dot{\mu}_v$ is determined by the volumetric damage consistency condition; i.e.,

$$\phi_v^d\left(\xi_{v,t}, g_{v,t}\right) = \dot{\phi}_v^d\left(\xi_{v,t}, g_{v,t}\right) = 0 \Rightarrow \dot{\mu}_v = \dot{\xi}_v \tag{5.27}$$

and $g_{v,t}$ is defined by the expression presented in Eq. (5.28)

$$g_{v,t} = \max\left(g_{v,0}, \max_{s\in(-\infty,t)} \boldsymbol{\xi}_{v,s}\right) - g_{vh,(t-1)} \tag{5.28}$$

where $g_{vh,(t-1)}$ defines the reduced value for the current volumetric damage threshold due to the incremental volumetric healing (if any) from the previous time step.

If $H_v\left(\xi_{v,t}, d_{v,t}\right)$ in condition (5.24) is independent of $\dot{d}_{v,t}$, the above formulation may be rephrased as follows. let $G_v : \mathbb{R} \to \mathbb{R}_+$ be such that $H_v\left(\xi_{v,t}\right) \equiv \partial G_v\left(\xi_{v,t}\right) / \partial \xi_{v,t}$. We shall assume that $G_v\left(\cdot\right)$ is a monotonic function. A damage criterion entirely equivalent to condition (5.23) is given by $\bar{\phi}_v^d\left(\xi_{v,t}, g_{v,t}\right) \equiv G_v\left(\xi_{v,t}\right) - G_v\left(g_{v,t}\right) \le 0$. The flow rule and loading/unloading conditions then become

$$\dot{d}_{v,t} = \dot{\mu}\frac{\partial\bar{\phi}_v^d\left(\xi_{v,t}, g_{v,t}\right)}{\partial \xi_{v,t}}, \qquad g_{v,t} = \dot{\mu}_v \tag{5.29}$$

$$\dot{\mu}_v \ge 0, \qquad \bar{\phi}_v^d\left(\xi_{v,t}, g_{v,t}\right) \le 0, \qquad \dot{\mu}_v \bar{\phi}_v^d\left(\xi_{v,t}, g_{v,t}\right) = 0 \tag{5.30}$$

Conditions (5.29) and (5.30) are simply the Kuhn-Tucker optimality conditions of a principle of maximum volumetric damage dissipation.

Existing experimental data of asphalt materials present that the amount of microcracks or microcavities at a particular strain level demonstrates *rate sensitivity* to the applied rate of loading in a (high strain rate) dynamic environment. A simple phenomenological characterization of this effect may be obtained by means of a *viscous regularization* of the rate-independent strain-based damage model introduced previously. Formally, the structure of this regularization is entirely analogous to the classical viscoplastic regularization of the Perzyna type [2][3]. The resulting rate-sensitive damage model (a) requires only one additional material parameter, i.e. the *volumetric damage fluidity coefficient* (μ_v); (b) as μ_v approaches zero exhibits instantaneous elastic response, whereas μ_v approaches infinity reduces to the rate-independent volumetric damage characterization; and (c) predicts decrease in nonlinearity of the stress-strain curves as the strain rate is increased. In other words, microcrack or microcavity growth is retarded at low strain rates.

Rate equations governing visco-damage behavior are obtained from their rate-independent counterpart by replacing consistency parameter $\dot{\mu}_v$ by $\mu_v g\left(\phi_v^d\right)$. Here μ_v is the volumetric damage fluidity coefficient (a material constant). The scalar function $g\left(\phi_v^d\right)$ represents the viscous volumetric damage flow function and ϕ_v^d is defined in Eq. (5.23). Accordingly, we have

$$\dot{d}_{v,t} = \mu_v \left\langle g\left(\phi_v^d\right)\right\rangle H_v\left(\xi_{v,t}, d_{v,t}\right) \tag{5.31}$$

$$\dot{g}_{v,t} = \mu_v \left\langle g\left(\phi_v^d\right)\right\rangle \tag{5.32}$$

where $\langle\cdot\rangle$ denotes the McAuley bracket (ramp function). For simplicity, in what follows we shall assume linear viscous damage, i.e. $g\left(\phi_v^d\right) = \phi_v^d$. Hence, Eqs.(5.31) and (5.32) reduce to

$$\dot{d}_{v,t} = \mu_v \left\langle \phi_v^d \left(\xi_{v,t}, g_{v,t} \right) \right\rangle H_v \left(\xi_{v,t}, d_{v,t} \right) \tag{5.33}$$

$$\dot{g}_{v,t} = \mu_v \left\langle \phi_v^d \left(\xi_{v,t}, g_{v,t} \right) \right\rangle \equiv \mu_v \left\langle \xi_{v,t} - g_{v,t} \right\rangle \tag{5.34}$$

The inviscid volumetric damage characterization and the instantaneous elasticity response can then be obtained as special cases of the rate-dependent damage formulation. These special cases and the related algorithmic treatments of visco-damage are addressed in details in Chapter 6.

5.2.6 Characterization of Initial-Elastic Strain-Energy Based Deviatoric Damage

Similarly, we ascribe the notion of equivalent deviatoric strain ξ_d as the (undamaged) energy norm of the deviatoric strain tensor. Motivated by Eq. (5.21), we define:

$$\xi_d \equiv \sqrt{\Psi^0(\mathbf{e})\vartheta(T)} = \sqrt{\left\{ \frac{1}{2} G(\mathbf{e} : \mathbf{e}) \right\} \exp\left\{ -\delta \left(1 - \frac{T}{T_0} \right) \right\}} \tag{5.35}$$

where $\mathbf{e} = \boldsymbol{\varepsilon} - \frac{1}{3} \boldsymbol{\varepsilon}_{kk} \mathbf{1}$

Likewise, we characterize the state of deviatoric damage in asphalt composites by means of a deviatoric damage criterion $\phi_d^d \left(\xi_{d,t}, g_{d,t} \right) \le 0$, formulated in strain space, with the following functional form:

$$\phi_d^d \left(\xi_{d,t}, g_{d,t} \right) \equiv \xi_{d,t} - g_{d,t} \le 0 \qquad t \in \mathbb{R}_+ \tag{5.36}$$

where the subscript t refers to a value at current time $t \in \mathbb{R}_+$, and $g_{d,t}$ is the deviatoric damage threshold at the current time t. It is noted that the numerical value of $g_{d,t}$ would be lowered due to the incremental deviatoric healing (if any) from the previous time step. Let $g_{d,0}$ denote the initial deviatoric damage threshold before any loading is applied; we then have $g_{d,t} \geq g_{d,0}$. Here, $g_{d,0}$ is considered as a characteristic material property. The condition (5.36) states that deviatoric damage in asphalt materials is initiated when the deviatoric energy norm of the strain tensor $\xi_{d,t}$ exceeds the initial deviatoric damage threshold $g_{d,0}$. For the deviatoric damage case, we define the evolution of the deviatoric damage variable $d_{d,t}$ and the deviatoric damage threshold $g_{d,t}$, respectively, by the rate equations:

$$\dot{d}_{d,t} = \dot{\mu}_d H_d \left(\xi_{d,t}, d_{d,t}\right) \tag{5.37}$$

$$\dot{g}_d = \dot{\mu}_d \tag{5.38}$$

where $\dot{\mu}_d \geq 0$ is a deviatoric damage consistency parameter that defines the deviatoric damage loading/unloading conditions according to the Kuhn-Tucker relations

$$\dot{\mu}_d \geq 0, \qquad \phi_d^d \left(\xi_{d,t}, g_{d,t}\right) \leq 0, \qquad \dot{\mu}_d \;\; \phi_d^d \left(\xi_{d,t}, g_{d,t}\right) = 0 \tag{5.39}$$

The conditions (5.39) are standard for problems involving unilateral constraint. If $\phi_d^d \left(\xi_{d,t}, g_{d,t}\right) < 0$, the deviatoric damage criterion is not satisfied and by conditions (5.39), $\dot{\mu}_d = 0$; hence, the deviatoric damage rule (5.37) implies that $\dot{d}_d = 0$ and no further deviatoric damage takes place. If, on the other hand, $\dot{\mu}_d > 0$; that is, further deviatoric damage ("loading") is taking place, then conditions (5.39) implies that $\phi_d^d \left(\xi_{d,t}, g_{d,t}\right) = 0$. In this event, the value of $\dot{\mu}_d$ is determined by the deviatoric damage consistency condition; i.e.,

$$\phi_d^d\left(\xi_{d,t}, g_{d,t}\right) = \dot{\phi}_d^d\left(\xi_{d,t}, g_{d,t}\right) = 0 \Rightarrow \dot{\mu}_d = \dot{\xi}_d \tag{5.40}$$

and $g_{d,t}$ is defined by the expression presented in Eq. (5.28)

$$g_{d,t} = \max\left(g_{d,0}, \max_{s\in(-\infty,t)} \boldsymbol{\xi}_{d,s}\right) - g_{dh,(t-1)} \tag{5.41}$$

where $g_{dh,(t-1)}$ defines the reduced value for the current deviatoric damage threshold due to the incremental deviatoric healing (if any) from the previous time step.

If $H_d\left(\xi_{d,t}, d_{d,t}\right)$ in condition (5.37) is independent of $\dot{d}_{d,t}$, the above formulation may be rephrased as follows. let $G_d : \mathbb{R} \to \mathbb{R}_+$ be such that $H_d\left(\xi_{d,t}\right) \equiv \partial G_d\left(\xi_{d,t}\right) / \partial \xi_{d,t}$. We shall assume that $G_d\left(\cdot\right)$ is a monotonic function. A damage criterion entirely equivalent to condition (5.23) is given by $\bar{\phi}_d^d\left(\xi_{d,t}, g_{d,t}\right) \equiv G_d\left(\xi_{d,t}\right) - G_d\left(g_{d,t}\right) \le 0$. The flow rule and loading/unloading conditions then become

$$\dot{d}_{d,t} = \dot{\mu} \frac{\partial \bar{\phi}_d^d\left(\xi_{d,t}, g_{d,t}\right)}{\partial \xi_{d,t}}, \qquad g_{d,t} = \dot{\mu}_d \tag{5.42}$$

$$\dot{\mu}_d \ge 0, \qquad \bar{\phi}_d^d\left(\xi_{d,t}, g_{d,t}\right) \le 0, \qquad \dot{\mu}_d \bar{\phi}_d^d\left(\xi_{d,t}, g_{d,t}\right) = 0 \tag{5.43}$$

Conditions (5.42) and (5.43) are simply the Kuhn-Tucker optimality conditions of a principle of maximum deviatoric damage dissipation.

Analogous to the rate-dependent volumetric damage model, the resulting rate-sensitive deviatoric damage model (a) requires only one additional material parameter, i.e. the *deviatoric damage fluidity coefficient* (μ_d); (b) as μ_d approaches zero exhibits instantaneous elastic response, whereas μ_d approaches infinity reduces to the rate-independent deviatoric damage characterization; and (c) predicts decrease in nonlinearity of the stress-strain curves as the strain rate is increased. In other words, microcrack or microcavity growth is retarded at low strain rates. Rate equations governing visco-damage behavior are obtained from their rate-independent counterpart by replacing consistency parameter $\dot{\mu}_d$ by $\mu_d g\left(\phi_d^d\right)$. Here μ_d is the deviatoric damage fluidity coefficient (a material constant). The scalar function $g\left(\phi_v^d\right)$ represents the viscous deviatoric damage flow function and ϕ_d^d is defined in Eq.(5.36). Accordingly, we have

$$\dot{d}_{d,t} = \mu_d \left\langle g\left(\phi_d^d\right)\right\rangle H_d\left(\xi_{d,t}, d_{d,t}\right) \tag{5.44}$$

$$\dot{g}_{d,t} = \mu_d \left\langle g\left(\phi_d^d\right)\right\rangle \tag{5.45}$$

where $\langle\cdot\rangle$ denotes the McAuley bracket (ramp function). For simplicity, in what follows we shall assume linear viscous damage, i.e. $g\left(\phi^d\right) = \phi^d$. Hence, Eqs.(5.44) and (5.45) reduce to

$$\dot{d}_{d,t} = \mu\left\langle \phi_d^d\left(\xi_{d,t}, g_{d,t}\right)\right\rangle H_d\left(\xi_{d,t}, d_{d,t}\right) \tag{5.46}$$

$$\dot{g}_{d,t} = \mu_d \left\langle \phi_d^d\left(\xi_{d,t}, g_{d,t}\right)\right\rangle \equiv \mu_d \left\langle \xi_{d,t} - g_{d,t}\right\rangle \tag{5.47}$$

The inviscid deviatoric damage characterization and the instantaneous elasticity response can then be obtained as special cases of the rate-dependent deviatoric damage formulation. These special cases and the related algorithmic treatments of visco-damage are addressed in details in Chapter 6.

5.2.7 Characterization of Initial-Elastic Strain-Energy Based Volumetric Healing

Similar to the characterization of volumetric and deviatoric damage in the previous section, we characterize the progressive recovery of mechanical properties of asphalt due to healing by means of a simple two-parameter healing mechanism.

We define the same notion of equivalent volumetric strain ξ_v as the (undamaged) energy norm of the volumetric strain tensor. We also characterize the state of volumetric healing in bituminous composite by using a volumetric healing criterion $\phi_v^h\left(\xi_{v,t}, r_{v,t}\right) \le 0$, formulated in the strain space, with the following functional form:

$$\phi_v^h\left(\xi_{v,t}, r_{v,t}\right) \equiv r_{v,t} - \xi_{v,t} \le 0 \qquad t \in \mathbb{R}_+ \tag{5.48}$$

Here, $r_{v,t}$ is the volumetric healing threshold at the current time t. We note that $r_{v,t}$ will be lowered in value due to the incremental volumetric damage (if any) from the previous time step. If $r_{v,0}$ denotes the initial volumetric healing threshold before any volumetric healing occurs, we must have $r_{v,t} \ge r_{v,0}$. It is noted that $r_{v,0}$ is also considered as a characteristic material property. Condition (5.48) then states that healing in the material is initiated when the energy norm of the volumetric strain tensor $\xi_{v,t}$ is smaller than the initial volumetric healing threshold $r_{v,0}$. We define the evolution of the volumetric healing variable R_v and the volumetric healing threshold $r_{v,t}$, respectively, by the rate equations

$$\dot{R}_{v,t} = \dot{\zeta}_v Z_v\left(\xi_{v,t}, R_{v,t}\right) \tag{5.49}$$

$$\dot{r}_v = \dot{\zeta}_v \tag{5.50}$$

where $\dot{\zeta}_v \ge 0$ is a volumetric healing consistency parameter that defines volumetric healing loading/unloading conditions according to the Kuhn-Tucker relations

$$\dot{\zeta}_v \geq 0, \qquad \phi_v^h\left(\xi_{v,t}, r_{v,t}\right) \leq 0, \qquad \dot{\zeta}_v \;\; \phi_v^h\left(\xi_{v,t}, r_{v,t}\right) = 0 \tag{5.51}$$

Conditions (5.51) are also standard for problems involving unilateral constraint. If $\phi_v^h\left(\xi_{v,t}, r_{v,t}\right) < 0$, the volumetric healing criterion is not satisfied and by conditions (5.51), $\dot{\zeta}_v = 0$; hence, the healing rule (5.49) implies that $\dot{R}_v = 0$ and no further volumetric healing takes place. If, on the other hand, $\dot{\zeta}_v > 0$; that is, further volumetric healing is taking place, then conditions (5.51) implies that $\phi_v^h\left(\xi_{v,t}, r_{v,t}\right) \leq 0$. In this event, the value of $\dot{\zeta}_v$ is determined by the volumetric healing consistency condition; i.e.

$$\phi_v^h\left(\xi_{v,t}, r_{v,t}\right) = \dot{\phi}_v^h\left(\xi_{v,t}, r_{v,t}\right) = 0 \Rightarrow \dot{\zeta}_v \; = \; \dot{\xi}_v \tag{5.52}$$

and $r_{v,t}$ is given by the expression

$$r_{v,t} = \min\left(r_{v,0}, \min_{s \in (-\infty, t)} \xi_{v,s}\right) + r_{vd,(t-1)} \tag{5.53}$$

where $r_{vd,(t-1)}$ is the value for the current volumetric healing threshold to be numerically increased due to the incremental volumetric damage (if any) from the previous time step.

If $Z_v\left(\xi_{v,t}, R_{v,t}\right)$ in condition (5.49) is independent of $\dot{R}_{v,t}$, the above formulation may be rephrased as follows. Let $G^*: \mathbb{R} \rightarrow \mathbb{R}_+$ be such that $Z_v\left(\xi_{v,t}\right) \equiv -\partial G_v^*\left(\xi_{v,t}\right) / \partial \xi_{v,t}$. We shall assume that $G_v^*\left(\cdot\right)$ is a monotonic function. A volumetric healing criterion entirely equivalent to conditions (5.48) is given by $\bar{\phi}_v^h\left(\xi_{v,t}, r_{v,t}\right) \equiv G_v^*\left(r_{v,t}\right) - G_v^*\left(\xi_{v,t}\right) \leq 0$. The flow rule and loading/unloading conditions then become

$$\dot{R}_{v,t} = \dot{\zeta}_v \frac{\partial \bar{\phi}_v^h\left(\xi_{v,t}, r_{v,t}\right)}{\partial \xi_{v,t}}, \qquad r_{v,t} = \dot{\zeta}_v \tag{5.54}$$

$$\dot{\zeta}_v \geq 0, \qquad \bar{\phi}_v^h\left(\xi_{v,t}, r_{v,t}\right) \leq 0, \qquad \dot{\zeta}_v \bar{\phi}_v^h\left(\xi_{v,t}, r_{v,t}\right) = 0 \tag{5.55}$$

5.2.8 Characterization of Initial-Elastic Strain-Energy Based Deviatoric Healing

We ascribe the same notion of equivalent deviatoric strain energy ξ_d as the energy norm of the deviatoric strain tensor. We also characterize the state of deviatoric healing in asphalt mixtures by using a deviatoric healing criterion $\phi_d^h\left(\xi_{d,t}, r_{d,t}\right) \leq 0$, formulated in the strain space, with the following functional form:

$$\phi_d^h\left(\xi_{d,t}, r_{d,t}\right) \equiv r_{d,t} - \xi_{d,t} \leq 0 \qquad t \in \mathbb{R}_+ \tag{5.56}$$

Here, $r_{d,t}$ is the deviatoric healing threshold at the current time t. We note that $r_{d,t}$ will be lowered in value due to the incremental deviatoric damage (if any) from the previous time step. If $r_{d,0}$ denotes the initial deviatoric healing threshold before any healing occurs, we must have $r_{v,t} \geq r_{v,0}$. It is noted that $r_{v,0}$ is also considered as a characteristic material property. Condition (5.56) then states that deviatoric healing in the material is initiated when the energy norm of the deviatoric strain tensor $\xi_{v,t}$ is smaller than the initial deviatoric healing threshold $r_{d,0}$. We define the evolution of the deviatoric healing variable R_d and the deviatoric healing threshold $r_{d,t}$, respectively, by the rate equations

$$\dot{R}_{d,t} = \dot{\zeta}_d Z_d\left(\xi_{d,t}, R_{d,t}\right) \tag{5.57}$$

$$\dot{r}_d = \dot{\zeta}_d \tag{5.58}$$

where $\dot{\zeta}_d \geq 0$ is a deviatoric healing consistency parameter that defines deviatoric healing loading/unloading conditions according to the Kuhn-Tucker relations

$$\dot{\zeta}_d \geq 0, \qquad \phi_d^h\left(\xi_{d,t}, r_{d,t}\right) \leq 0, \qquad \dot{\zeta}_d \ \phi_d^h\left(\xi_{d,t}, r_{d,t}\right) = 0 \tag{5.59}$$

Conditions (5.59) are also standard for problems involving unilateral constraint. If $\phi_d^h\left(\xi_{d,t}, r_{d,t}\right) < 0$, the deviatoric healing criterion is not satisfied and by conditions(5.59), $\dot{\zeta}_d = 0$; hence, the deviatoric healing rule (5.57) implies that $\dot{R}_d = 0$ and no further deviatoric healing takes place. If, on the other hand, $\dot{\zeta}_d > 0$; that is, further deviatoric healing is taking place, then conditions (5.59) implies that $\phi_d^h\left(\xi_{d,t}, r_{d,t}\right) \leq 0$. In this event, the value of $\dot{\zeta}_d$ is determined by the deviatoric healing consistency condition; i.e.

$$\phi_d^h\left(\xi_{d,t}, r_{d,t}\right) = \dot{\phi}_d^h\left(\xi_{d,t}, r_{d,t}\right) = 0 \Rightarrow \dot{\zeta}_d = \dot{\xi}_d \tag{5.60}$$

and $r_{d,t}$ is given by the expression

$$r_{d,t} = \min\left(r_{d,0}, \min_{s\in(-\infty,t)} \xi_{d,s}\right) + r_{dd,(t-1)} \tag{5.61}$$

where $r_{dd,(t-1)}$ is the value for the current deviatoric healing threshold to be numerically increased due to the incremental damage (if any) from the previous time step.

If $Z_d\left(\xi_{d,t}, R_{d,t}\right)$ in condition (5.57) is independent of $\dot{R}_{d,t}$, the above formulation may be rephrased as follows. Let $G_d^*: \mathbb{R} \to \mathbb{R}_+$ be such that $Z_d\left(\xi_{d,t}\right) \equiv -\partial G_d^*\left(\xi_{d,t}\right) / \partial \xi_{d,t}$. We shall assume that $G_d^*\left(\cdot\right)$ is a monotonic function. A deviatoric healing criterion entirely equivalent to conditions (5.56) is given by $\bar{\phi}_d^h\left(\xi_{d,t}, r_{d,t}\right) \equiv G_d^*\left(r_{d,t}\right) - G_d^*\left(\xi_{d,t}\right) \le 0$. The flow rule and loading/unloading conditions then become

$$\dot{R}_{d,t} = \dot{\zeta}_d \frac{\partial \bar{\phi}_d^h\left(\xi_{d,t}, r_{d,t}\right)}{\partial \xi_{d,t}}, \qquad r_{d,t} = \dot{\zeta}_d \tag{5.62}$$

$$\dot{\zeta}_d \ge 0, \qquad \bar{\phi}_d^h\left(\xi_{d,t}, r_{d,t}\right) \le 0, \qquad \dot{\zeta}_d \bar{\phi}_d^h\left(\xi_{d,t}, r_{d,t}\right) = 0 \tag{5.63}$$

5.2.9 Net (Combined) Effect of the Volumetric Damage and Healing

Taking the time derivative of Eq.(5.2) would lead to

$$\dot{d}_v = \dot{A}_v^d / A_v \tag{5.64}$$

As the derivations are based on linearization of the residual functions associated with the implicit backward Euler algorithms, the above equation can be expressed in the following incremental form for the updated volumetric damage variable:

$$d_{v,n+1} = d_{v,n} + \Delta d_{v,n+1} \tag{5.65}$$

In order to calculate the incremental form of volumetric healing variable, the same procedure can be applied under the condition of no volumetric damage evaluation because volumetric healing does not occur during the volumetric damage process or vice versa. However, during the volumetric damage process updated volumetric healing variable can be reduced by a ratio of volumetric damage variables since both the volumetric healed area, A_v^h, and the volumetric damaged area, $A_v^d = A_v^h + A_v^{uR}$, are changed. Therefore the updated volumetric healing variable would be as follows:

$$R_{v,n+1} = R_{v,n} + \Delta R_{v,n+1} \quad \left(\Delta d_{v,n+1} = 0\right) \tag{5.66}$$

$$R_{v,n+1} = \frac{d_{v,n+1}}{2d_{v,n+1} - d_{v,n}} R_{v,n} \quad \left(\Delta d_{v,n+1} > 0\right) \tag{5.67}$$

Taking the time derivative of (5.5) would yield

$$\begin{gathered} d^{net}_{v,n+1} = d^{net}_{v,n} + \Delta d^{net}_{v,n+1} \\ \Delta d^{net}_{v,n+1} = \Delta d_{v,n+1} - \Delta R_{v,n+1} d^{net}_{v,n} \end{gathered} \tag{5.68}$$

5.2.10 Net (Combined) Effect of the Deviatoric Damage and Healing

Taking the time derivative of Eq.(5.7) would lead to

$$\dot{d}_d = \dot{A}^d_d \big/ A_d \tag{5.69}$$

As the derivations are based on linearization of the residual functions associated with the implicit backward Euler algorithms, the above equation can be expressed in the following incremental form for the updated deviatoric damage variable:

$$d_{v,n+1} = d_{v,n} + \Delta d_{v,n+1} \tag{5.70}$$

In order to calculate the incremental form of deviatoric healing variable, the same procedure can be applied under the condition of no deviatoric damage evaluation because deviatoric healing does not occur during the deviatoric damage process or vice versa. However, during the deviatoric damage process updated deviatoric healing variable can be reduced by a ratio of deviatoric damage variables since both the deviatoric healed area, A^h_d, and the deviatoric damaged area, $A_d^d = A_d^h + A_d^{uR}$, are changed. Therefore the updated deviatoric healing variable would be as follows:

$$R_{d,n+1} = R_{d,n} + \Delta R_{d,n+1} \qquad \left(\Delta d_{d,n+1} = 0\right) \tag{5.71}$$

$$R_{d,n+1} = \frac{d_{d,n+1}}{2d_{d,n+1} - d_{d,n}} R_{d,n} \qquad \left(\Delta d_{d,n+1} > 0\right) \tag{5.72}$$

Taking the time derivative of (5.9) would yield

$$\begin{aligned} d_{d,n+1}^{net} &= d_{d,n}^{net} + \Delta d_{d,n+1}^{net} \\ \Delta d_{d,n+1}^{net} &= \Delta d_{d,n+1} - \Delta R_{d,n+1} d_{d,n}^{net} \end{aligned} \tag{5.73}$$

With known $d_{v,n+1}^{net}$ and $d_{d,n+1}^{net}$, the updated fourth-rank damage net tensor can be obtained by Eq. (5.13).

5.3 A Conceptual Example

Let us consider, for conceptual illustration, a system with eight springs as shown in Figure 5.3 and perform a series of cyclic conceptual tension-rest periods (Four steps: T1-R1-T2-R2) tests on this hypothetical system.

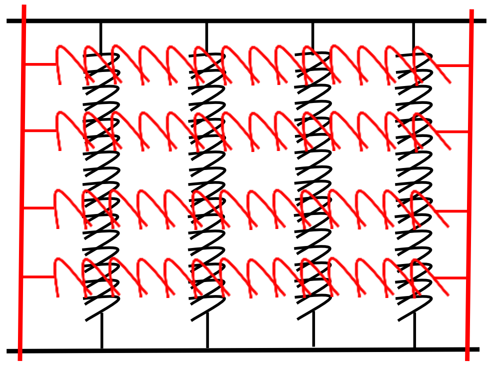

Figure 5.3 A system with eight springs

This conceptual illustration does not directly imply that volumetric part is in y-direction and deviatoric part is in x-direction because volumetric and deviatoric parts are only orthogonal in hyperspace. However, vertical and horizontal springs are linearly independent so that they do not influence to each other and they are good for the conceptual illustration. Therefore, we use the vertical and horizontal springs to represent volumetric and deviatoric systems, respectively, and we assume that the vertical and horizontal springs will be broken under vertical and horizontal tensions, respectively. Moreover, it is assumed that both damaged springs can be healed during rest periods in similar manner. At the first step, vertical and horizontal tensions T1 are applied on the system and four out of eight springs are assumed to be broken. The volumetric and deviatoric damage variables of the system are therefore 2/4 = 0.5 as shown in Figure 5.4(a). Next, the system is left for the rest period R1 in step 2 and total two springs are assumed to be healed as shown in Figure 5.4(b). Since one of the broken springs is assumed healed, the volumetric and deviatoric healing variables of the system are 1/2 = 0.5 and the net volumetric and deviatoric damage-healing variables of the system are therefore 1/4 = 0.25. At the third step, vertical and horizontal tensions T2 are applied and this time, three springs of vertical springs are assumed to be broken. It is assumed that only two of horizontal springs are broken due to horizontal tension. Thus, the net volumetric damage-healing variable of the system is 3/4 = 0.75 and the net deviatoric damage-healing variable is 0.5. Finally, during the rest period R2 all broken springs are completely recovered. The volumetric and deviatoric healing variables of the system at this stage are therefore 3/3 = 1 and the net volumetric and deviatoric damage-healing variables of the system are therefore all 0. The computations of d_v^{net} and d_d^{net} by Eq. (5.68) at each time step for the system as shown in are listed in Table 5.1 and Table 5.2. The characterizations of volumetric and deviatoric damage and healing, as discussed in the previous sections, can be considered as the *predictor formula* in our volumetric and deviatoric damage-healing algorithms. Once the associated volumetric and deviatoric damage or healing variables are computed at time step n+1 (volumetric and deviatoric damage and healing will not occur at the same step), net volumetric and deviatoric damage-healing variables at time step (n+1) are finally calculated. More details on algorithms about the coupling of damage and healing are provided in details in Chapter 6.

Table 5.1 Computation of d_v^{net} at different time step

Step	$\Delta d_{v,n+1}$	$d_{v,n+1}$	$\Delta R_{v,n+1}$	$R_{v,n+1}$	$\Delta d^{net}_{v,n+1}$	$d^{net}_{v,n+1}$
1	$\frac{2}{4}$	$\frac{2}{4}$	0	0	$\frac{2}{4}$	$\frac{2}{4}$
2	0	$\frac{2}{4}$	$\frac{1}{2}$	$\frac{1}{2}$	$-\frac{1}{4}$	$\frac{1}{4}$
3	$\frac{2}{4}$	$\frac{4}{4}$	0	$\frac{1}{3}$	$\frac{2}{4}$	$\frac{3}{4}$
4	0	$\frac{4}{4}$	$\frac{3}{3}$	$\frac{4}{3}$	$-\frac{3}{4}$	0

Table 5.2 Computation of d_d^{net} at different time step

Step	$\Delta d_{d,n+1}$	$d_{d,n+1}$	$\Delta R_{d,n+1}$	$R_{d,n+1}$	$\Delta d_{d,n+1}^{net}$	$d_{d,n+1}^{net}$
1	$\frac{2}{4}$	$\frac{2}{4}$	0	0	$\frac{2}{4}$	$\frac{2}{4}$
2	0	$\frac{2}{4}$	$\frac{1}{2}$	$\frac{1}{2}$	$-\frac{1}{4}$	$\frac{1}{4}$
3	$\frac{1}{4}$	$\frac{3}{4}$	0	$\frac{3}{8}$	$\frac{1}{4}$	$\frac{2}{4}$
4	0	$\frac{3}{4}$	$\frac{2}{2}$	$\frac{11}{8}$	$-\frac{2}{4}$	0

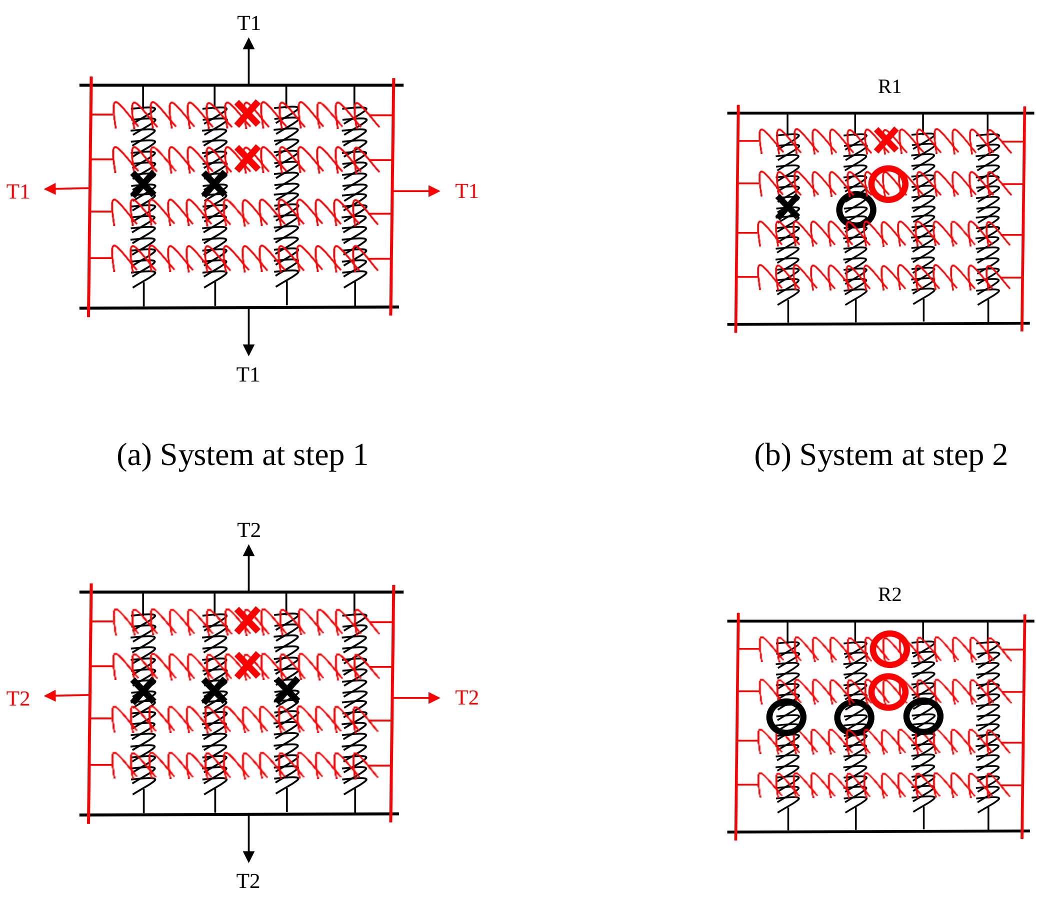

(a) System at step 1

(b) System at step 2

(c) System at step 3

(d) System at step 4

Figure 5.4 The associated damage and healing variables of four-spring system at each step

5.4 Appendix

Proposed definition of physical stress tensor without Arrhenius-type temperature term in Eq. (5.12) leads to

$$
\begin{aligned}
&\left(\mathbf{I}-\mathbf{D}^{net}\right):\boldsymbol{\sigma}^{net}\\
&=\left(\mathbf{I}-\mathbf{D}^{net}\right):\left(p^{net}\mathbf{1}+\mathbf{s}^{net}\right)=\left(p^{net}\mathbf{1}+\mathbf{s}^{net}\right)-\mathbf{D}^{net}:\left(p^{net}\mathbf{1}+\mathbf{s}^{net}\right)\\
&=\left(p^{net}\mathbf{1}+\mathbf{s}^{net}\right)-\left(\frac{1}{3}d_v^{net}\mathbf{1}\otimes\mathbf{1}+d_d^{net}\left(\mathbf{I}-\frac{1}{3}\mathbf{1}\otimes\mathbf{1}\right)\right):\left(p^{net}\mathbf{1}+\mathbf{s}^{net}\right)\\
&=\left(p^{net}\mathbf{1}+\mathbf{s}^{net}\right)-\left(d_v^{net}p^{net}\mathbf{1}+d_d^{net}p^{net}\cancel{\left(\mathbf{1}-\frac{1}{3}3\mathbf{1}\right)}+d_d^{net}\mathbf{s}^{net}\right)\\
&=\left(1-d_v^{net}\right)p^{net}\mathbf{1}+\left(1-d_d^{net}\right)\mathbf{s}^{net}\\
&=\left(1-d_v^{net}\right)\boldsymbol{\sigma}_v^{net}+\left(1-d_d^{net}\right)\boldsymbol{\sigma}_d^{net}
\end{aligned}
$$

where $\mathbf{D}^{net}=\frac{1}{3}d_v^{net}\mathbf{1}\otimes\mathbf{1}+d_d^{net}\left(\mathbf{I}-\frac{1}{3}\mathbf{1}\otimes\mathbf{1}\right)$ and $\boldsymbol{\sigma}^{net}=\boldsymbol{\sigma}_v^{net}+\boldsymbol{\sigma}_d^{net}=p^{net}\mathbf{1}+\mathbf{s}^{net}$

Proposed free energy potential for two-parameter formulation (Eq. (5.14))

$$
\begin{aligned}
&\Psi\left(\boldsymbol{\varepsilon}_\mathbf{v},\mathbf{e},\boldsymbol{\sigma}^{vp},\mathbf{q},d_v^{net},d_d^{net},T\right)\\
&\equiv\left\{(1-d_v^{net})\Psi_v^0(\boldsymbol{\varepsilon}_\mathbf{v})+(1-d_d^{net})\Psi_d^0(\mathbf{e})-\frac{1}{2}\boldsymbol{\varepsilon}:\boldsymbol{\sigma}^{vp}+\Xi\left(\mathbf{q},\boldsymbol{\sigma}^{vp}\right)\right\}\vartheta(T)
\end{aligned}
$$

Take derivative of $\Psi\left(\boldsymbol{\varepsilon}_\mathbf{v},\mathbf{e},\boldsymbol{\sigma}^{vp},\mathbf{q},d_v^{net},d_d^{net},T\right)$, we can obtain

$$
\begin{aligned}
\dot{\Psi} &= \left\{ \begin{array}{l} -\dot{d}_v^{net}\Psi_v^0(\boldsymbol{\varepsilon}_\mathbf{v}) + (1-d_v^{net})\dot{\Psi}_v^0(\boldsymbol{\varepsilon}_\mathbf{v}) - \dot{d}_d^{net}\Psi_d^0(\mathbf{e}) + (1-d_d^{net})\dot{\Psi}_d^0(\mathbf{e}) \\ -\frac{1}{2}\dot{\boldsymbol{\varepsilon}} : \boldsymbol{\sigma}^{vp} - \frac{1}{2}\boldsymbol{\varepsilon} : \dot{\boldsymbol{\sigma}}^{vp} + \dot{\Xi}(\mathbf{q}, \boldsymbol{\sigma}^{vp}) \end{array} \right\} \vartheta(T) \\
&\quad + \dot{\vartheta}(T)\Psi\left(\boldsymbol{\varepsilon}_\mathbf{v}, \mathbf{e}, \boldsymbol{\sigma}^p, \mathbf{q}, d_v^{net}, d_d^{net}\right) \\
&= \left\{ \begin{array}{l} -\dot{d}_v^{net}\Psi_v^0(\boldsymbol{\varepsilon}_\mathbf{v}) + (1-d_v^{net})\frac{\partial \Psi_v^0(\boldsymbol{\varepsilon}_\mathbf{v})}{\partial \boldsymbol{\varepsilon}_\mathbf{v}} : \dot{\boldsymbol{\varepsilon}}_\mathbf{v} - \dot{d}_d^{net}\Psi_d^0(\mathbf{e}) + (1-d_d^{net})\frac{\partial \Psi_d^0(\mathbf{e})}{\partial \mathbf{e}} : \dot{\mathbf{e}} \\ -\frac{1}{2}(\dot{\boldsymbol{\varepsilon}}_\mathbf{v} + \dot{\mathbf{e}}) : \boldsymbol{\sigma}^{vp} - \frac{1}{2}\boldsymbol{\varepsilon} : \dot{\boldsymbol{\sigma}}^{vp} + \frac{\partial \Xi(\mathbf{q}, \boldsymbol{\sigma}^{vp})}{\partial \mathbf{q}} \cdot \dot{\mathbf{q}} + \frac{\partial \Xi(\mathbf{q}, \boldsymbol{\sigma}^{vp})}{\partial \boldsymbol{\sigma}^{vp}} : \dot{\boldsymbol{\sigma}}^{vp} \end{array} \right\} \vartheta(T) \\
&\quad + \frac{\partial \vartheta(T)}{T}\dot{T}\ \Psi\left(\boldsymbol{\varepsilon}_\mathbf{v}, \mathbf{e}, \boldsymbol{\sigma}^p, \mathbf{q}, d_v^{net}, d_d^{net}\right)
\end{aligned}
$$

Plug in $\dot{\Psi}$ into the following Clausius-Plank inequality $-s\dot{T} - \dot{\Psi} + \boldsymbol{\sigma} : \dot{\boldsymbol{\varepsilon}} \geq 0$

We can have

$$
\left\{ \dot{d}_v^{net}\Psi_v^0(\boldsymbol{\varepsilon}_\mathbf{v}) + \dot{d}_d^{net}\Psi_d^0(\mathbf{e}) - \frac{\partial \Xi(\mathbf{q}, \boldsymbol{\sigma}^{vp})}{\partial \mathbf{q}} \cdot \dot{\mathbf{q}} - \left(\frac{\partial \Xi(\mathbf{q}, \boldsymbol{\sigma}^{vp})}{\partial \boldsymbol{\sigma}^{vp}} - \frac{1}{2}\boldsymbol{\varepsilon} \right) : \dot{\boldsymbol{\sigma}}^{vp} \right\} \vartheta(T) \geq 0
$$

$$
\boldsymbol{\sigma}_v = \left\{ (1-d_v^{net})\frac{\partial \Psi_v^0(\boldsymbol{\varepsilon}_\mathbf{v})}{\partial \boldsymbol{\varepsilon}_\mathbf{v}} - \frac{1}{2}\boldsymbol{\sigma}^{vp} \right\} \vartheta(T)
$$

$$
\boldsymbol{\sigma}_d = \left\{ (1-d_d^{net})\frac{\partial \Psi_d^0(\mathbf{e})}{\partial \mathbf{e}} - \frac{1}{2}\boldsymbol{\sigma}^{vp} \right\} \vartheta(T)
$$

$$
\boldsymbol{\sigma} = \boldsymbol{\sigma}_v + \boldsymbol{\sigma}_d = \left\{ (1-d_v^{net})\frac{\partial \Psi_v^0(\boldsymbol{\varepsilon}_\mathbf{v})}{\partial \boldsymbol{\varepsilon}_\mathbf{v}} + (1-d_d^{net})\frac{\partial \Psi_d^0(\mathbf{e})}{\partial \mathbf{e}} - \boldsymbol{\sigma}^{vp} \right\} \vartheta(T)
$$

5.5 Reference

[1] Coleman, B.D. and Gurtin, M.E. (1967). Thermodynamics with Internal State Variables, *Journal of Chemical Physics*, **47**: 597613.

[2] Hong, S., Yuan, K.Y., and Ju, J.W. (2014). Innovative Strain Energy Based Thermo-Elastoviscoplastic Damage-Self Healing Models for Bituminous Composites - Part

I: Formulations, *International Journal of Damage Mechanics*, (submitted).

[3] Simo, J. C., and Ju, J.W. (1987). Strain-Based and Stress-Based Continuum Damage Models, Part I: Formulation, *International Journal of Solids and Structures*, **23**: pp. 821-840.

6. NEW INITIAL STRAIN ENERGY BASED THERMO-ELASTOVISCOPLASTIC TWO-PARAMERTER DAMAGE-SELF HEALING MODEL FOR BITUMINOUS COMPOSITES – PART II: COMPUTATIONAL ASPECTS

6.1 Introduction

The two-step ***operator splitting*** methodology is systematically developed and used for the proposed thermo-elastoviscoplastic two-parameter damage-self healing model in Chapter 5. In particular, the resulting procedure takes the form of an ***elastic volumetric and deviatoric damage-self healing predictor*** and ***net viscoplastic return mapping corrector*** scheme. In sequence, a series of three-dimensional numerically driven simulations by different loading processes (loading-unloading-reloading and one cyclic loading) are given for the illustration of the variables calculated by the model such as stress-strain curve, volumetric and deviatoric damage variables, and two-parameter healing variables. Finally, experimental validations are presented for the demonstration of the applicability of proposed two-parameter damage-self healing models and algorithms.

6.2 Computational Algorithms

6.2.1 Two-Step Operator Splitting Methodology

New strain energy based two-parameter damage-self healing models have been proposed with the concept of net stress space and damage-self healing process [2][2][5][6][10][11]. In this section, the computational algorithms of the proposed formulations by using the two-step operator splitting methodology are presented in detail. Eqs. (5.24)~(5.27), (5.37)~(5.40), (5.49)~(5.52), and (5.57)~(5.60) in Chapter 5 and (3.46)~(3.50) in Chapter 3 are referred. More precisely, the attention is placed on the following local two-parameter elastoviscoplastic damage-self healing rate constitutive equations:

$$
\begin{aligned}
&\dot{\varepsilon} = \nabla^{s}\dot{\mathrm{u}}(t) \\
&\begin{cases} \dot{d}_{v,t} = \dot{\mu}_v \; H_v(\xi_{v,t}, d_{v,t}) \\ \dot{g}_v = \dot{\mu}_v \\ \dot{\mu}_v \geq 0, \qquad \phi_v^d(\xi_{v,t}, g_{v,t}) \leq 0, \qquad \dot{\mu}_v \; \phi_v^d(\xi_{v,t}, g_{v,t})=0 \end{cases} \\
&\begin{cases} \dot{d}_{d,t} = \dot{\mu}_d \; H_d(\xi_{d,t}, d_{d,t}) \\ \dot{g}_d = \dot{\mu}_d \\ \dot{\mu}_d \geq 0, \qquad \phi_d^d(\xi_{d,t}, g_{d,t}) \leq 0, \qquad \dot{\mu}_d \; \phi_d^d(\xi_{d,t}, g_{d,t})=0 \end{cases} \\
&\begin{cases} \dot{R}_{v,t} = \dot{\zeta}_v \; Z_v(\xi_{v,t}, R_{v,t}) \\ \dot{r}_v = \dot{\zeta}_v \\ \dot{\zeta}_v \geq 0, \qquad \phi_v^h(\xi_{v,t}, r_{v,t}) \leq 0, \qquad \dot{\zeta}_v \; \phi_v^h(\xi_{v,t}, r_{v,t})=0 \end{cases} \\
&\begin{cases} \dot{R}_{d,t} = \dot{\zeta}_d \; Z_d(\xi_{d,t}, R_{d,t}) \\ \dot{r}_d = \dot{\zeta}_d \\ \dot{\zeta}_d \geq 0, \qquad \phi_d^h(\xi_{d,t}, r_{d,t}) \leq 0, \qquad \dot{\zeta}_d \; \phi_d^h(\xi_{d,t}, r_{d,t})=0 \end{cases} \\
&\dot{d}_v^{net} = \dot{d}_v - \dot{R}_v \; d_v^{net} \qquad \dot{d}_d^{net} = \dot{d}_d - \dot{R}_d \; d_d^{net} \\
&\dot{\mathbf{D}}^{net} = \frac{1}{3}\dot{\mathrm{d}}_v^{net}\mathbf{1}\otimes\mathbf{1} + \dot{\mathrm{d}}_d^{net}\left(\mathbf{I} - \frac{1}{3}\mathbf{1}\otimes\mathbf{1}\right)
\end{aligned}
\tag{6.1}
$$

$$
\begin{aligned}
&\dot{\boldsymbol{\sigma}}^{net} = \frac{d}{dt}\left[\frac{\partial \Psi^0(\boldsymbol{\varepsilon})}{\partial \boldsymbol{\varepsilon}}\right] - \dot{\boldsymbol{\sigma}}^{vp,net} \\
&\begin{cases}
\dot{\boldsymbol{\sigma}}^{vp,net} = \gamma \dfrac{\partial g_p}{\partial \varepsilon}\left(\dfrac{\partial \Psi^0(\boldsymbol{\varepsilon})}{\partial \boldsymbol{\varepsilon}} - \boldsymbol{\sigma}^{vp,net}, \mathbf{q}\right) & (\textit{non-associative flow rule}) \\
\dot{\mathbf{q}} = \dot{\lambda}\, \mathbf{h}\left(\dfrac{\partial \Psi^0(\boldsymbol{\varepsilon})}{\partial \boldsymbol{\varepsilon}} - \boldsymbol{\sigma}^{vp,net}, \mathbf{q}\right) & (\textit{viscoplastic hardening law}) \\
f\left(\dfrac{\partial \Psi^0(\boldsymbol{\varepsilon})}{\partial \boldsymbol{\varepsilon}} - \boldsymbol{\sigma}^{vp,net}, \mathbf{q}\right) \le 0 & (\textit{loading condition})
\end{cases}
\end{aligned}
\tag{6.2}
$$

From an algorithmic viewpoint, the problem of integrating the evolution Eqs.(6.1) and (6.2) reduces to updating the basic variables $\left\{\boldsymbol{\sigma}, d_v^{net}, d_d^{net}, \boldsymbol{\sigma}^{vp,net}, \mathbf{q}\right\}$ in a manner consistent with the proposed damage-self healing models. It is essential to realize that the history of strains $t \to \boldsymbol{\varepsilon} \equiv \nabla^s \mathbf{u}(t)$ is assumed to be prescribed; i.e., a strain-drive computational algorithms.

Equations of evolution are to be solved incrementally over a sequence of given time steps $[t_n, t_{n+1}] \subset \mathcal{R}_+,\ n = 0,1,2...$. Therefore, the initial conditions for the governing evolution equations are

$$
\left\{\boldsymbol{\sigma}, d_v^{net}, d_d^{net}, \boldsymbol{\sigma}^{vp,net}, \mathbf{q}\right\}\Big|_{t=t_n} = \left\{\boldsymbol{\sigma}_n, d_{v,n}^{net}\ d_{d,n}^{net}, \boldsymbol{\sigma}_n^{vp,net}, \mathbf{q}_n\right\} \tag{6.3}
$$

In accordance with the notion of operator splitting, we consider the following innovative, additive decomposition of the original problem of evolutions in Eq. (6.1) into the elastic-damage-healing part and the plastic part as follows:

It is noted that Eqs. (6.4) and (6.5) do indeed add up to Eqs. (6.1) and (6.2), in agreement with the notion of operator split. In the following, we propose two new computational algorithms. The first one is consistent with problem (6.4) (the elastic two-parameter damage-self healing predictor) while the second one is consistent with problem (6.5) (the net viscoplastic return mapping corrector). In turn, the product algorithm obtained by successive application of these two algorithms is consistent with the original problems (6.1) and (6.2).

$$
\begin{aligned}
&\textbf{1. Elastic two-parameter damage-self healing part:}\\
&\dot{\boldsymbol{\varepsilon}} = \nabla^{s}\dot{\mathbf{u}}(t)\\
&\dot{d}_v = \begin{cases} H_v(\xi_v)\,\dot{\xi}_v\,, & iff \quad \phi^d_{v,t} = \dot{\phi}^d_{v,t} = 0 \\ 0\,, & otherwise \end{cases} \quad ; \quad \dot{d}_d = \begin{cases} H_d(\xi_d)\,\dot{\xi}_d\,, & iff \quad \phi^d_{d,t} = \dot{\phi}^d_{d,t} = 0 \\ 0\,, & otherwise \end{cases}\\
&\dot{g}_v = \begin{cases} \dot{\xi}_v\,, & iff \quad \phi^d_{v,t} = \dot{\phi}^d_{v,t} = 0 \\ 0\,, & otherwise \end{cases} \quad ; \quad \dot{g}_d = \begin{cases} \dot{\xi}_d\,, & iff \quad \phi^d_{d,t} = \dot{\phi}^d_{d,t} = 0 \\ 0\,, & otherwise \end{cases}\\
&\dot{R}_v = \begin{cases} Z_v(\xi_v)\,\dot{\xi}_v\,, & iff \quad \phi^h_{v,t} = \dot{\phi}^h_{v,t} = 0 \\ 0\,, & otherwise \end{cases} \quad ; \quad \dot{R}_d = \begin{cases} Z_d(\xi_d)\,\dot{\xi}_d\,, & iff \quad \phi^h_{d,t} = \dot{\phi}^h_{d,t} = 0 \\ 0\,, & otherwise \end{cases}\\
&\dot{r}_v = \begin{cases} \dot{\xi}_v\,, & iff \quad \phi^h_{v,t} = \dot{\phi}^h_{v,t} = 0 \\ 0\,, & otherwise \end{cases} \quad ; \quad \dot{r}_d = \begin{cases} \dot{\xi}_d\,, & iff \quad \phi^h_{d,t} = \dot{\phi}^h_{d,t} = 0 \\ 0\,, & otherwise \end{cases} \qquad (6.4)\\
&\dot{d}^{net}_v = \dot{d}_v - \dot{R}_v\, d^{net}_v \quad ; \quad \dot{d}^{net}_d = \dot{d}_d - \dot{R}_d\, d^{net}_d\\
&\dot{\mathbf{D}}^{net} = \frac{1}{3}\dot{d}^{net}_v \mathbf{1}\otimes\mathbf{1} + \dot{d}^{net}_d\left(\mathbf{I} - \frac{1}{3}\mathbf{1}\otimes\mathbf{1}\right)\\
&\dot{\boldsymbol{\sigma}}^{net} = \frac{d}{dt}\left[\frac{\partial \Psi^0(\boldsymbol{\varepsilon})}{\partial \boldsymbol{\varepsilon}}\right]\\
&\dot{\boldsymbol{\sigma}}^{vp,net} = 0\\
&\dot{\mathbf{q}} = 0
\end{aligned}
$$

2. Viscoplastic part :

$$
\begin{aligned}
&\dot{\boldsymbol{\varepsilon}} = 0 \\
&\dot{d}_v^{net} = 0 \\
&\dot{d}_d^{net} = 0 \\
&\dot{\boldsymbol{\sigma}}^{net} = -\dot{\boldsymbol{\sigma}}^{vp,net} \\
&\dot{\boldsymbol{\sigma}}^{vp,net} = \gamma \frac{\partial g_p}{\partial \boldsymbol{\varepsilon}}\left(\frac{\partial \Psi^0(\boldsymbol{\varepsilon})}{\partial \boldsymbol{\varepsilon}} - \boldsymbol{\sigma}^{vp,net}, \mathbf{q}\right) \\
&\dot{\mathbf{q}} = \gamma\, \mathbf{h}\left(\frac{\partial \Psi^0(\boldsymbol{\varepsilon})}{\partial \boldsymbol{\varepsilon}} - \boldsymbol{\sigma}^{vp,net}, \mathbf{q}\right)
\end{aligned}
\tag{6.5}
$$

6.2.2 The Elastic Two-Parameter Damage-Self Healing Predictor

A novel computational algorithm consistent with problems (6.1) and (6.2), referred to as the *elastic two-parameter damage-self healing predictor* in this chapter, is shown in the following step-by-step numerical strain-driven procedure.

Step 1: Strain update: Given the incremental displacement field $\mathbf{u}_{n+1}$, the strain tensor is updated as:

$$\boldsymbol{\varepsilon}_{n+1} = \boldsymbol{\varepsilon}_n + \nabla^{\mathbf{s}}\mathbf{u}_{n+1} \tag{6.6}$$

Step 2: Compute the initial (undamaged) elastic volumetric and deviatoric strain energies, $\xi_{v,n+1}$ and $\xi_{d,n+1}$,coupled with Arrhenius-type temperature term

$$\boldsymbol{\xi}_{v,n+1} \equiv \sqrt{\Psi_v^0\left(\boldsymbol{\varepsilon}_{v,n+1}\right)\vartheta(T)} = \sqrt{\left\{\frac{1}{2}K\left(\varepsilon_{kk,n+1}\right)^2\right\}\exp\left\{-\boldsymbol{\delta}\left(1-\frac{T}{T_0}\right)\right\}} \tag{6.7}$$

$$\xi_{d,n+1} \equiv \sqrt{\Psi_d^0\left(\mathbf{e}_{n+1}\right)\vartheta(T)} = \sqrt{\left\{\frac{1}{2}G\left(\mathbf{e}_{n+1} : \mathbf{e}_{n+1}\right)\right\}\exp\left\{-\boldsymbol{\delta}\left(1-\frac{T}{T_0}\right)\right\}} \tag{6.8}$$

where $\boldsymbol{\varepsilon}_{v,n+1} = \varepsilon_{kk,n+1} = \varepsilon_{11,n+1} + \varepsilon_{22,n+1} + \varepsilon_{33,n+1}$ and $\mathbf{e}_{n+1} = \boldsymbol{\varepsilon}_{n+1} - \frac{1}{3}\boldsymbol{\varepsilon}_{kk,n+1}\mathbf{1}$

Step 3: Update the current volumetric and deviatoric damage thresholds, $g_{v,n+1}$ and $g_{d,n+1}$, for a volumetric and deviatoric damage criteria based on $\xi_{v,n+1}$ and $\xi_{d,n+1}$ and time increment, respectively.

If the incremental volumetric healing at the previous time step is larger than zero, compute the $g_{vh,(n)}$ by using a nonlinear saturation type functional evaluation $g_{vh,(n)} = Q\left(1-e^{-bn}\right)$ and $\Delta g_{vh,(n)} = b\left(Q - g_{vh,(n-1)}\right)n$. Moreover, determine the $g_{dh,(n)}$ by using a nonlinear saturation type of functional evaluation $g_{dh,(n)} = Q\left(1-e^{-bn}\right)$ and $\Delta g_{dh,(n)} = b\left(Q - g_{dh,(n-1)}\right)\Delta n$ if the incremental deviatoric healing at the previous time step is greater than zero.

$$g_{v,n+1} = \max\left(g_{v,0}, \max_{s\in(-\infty,n+1)} \xi_{v,s}\right) - g_{vh,(n)} \tag{6.9}$$

$$g_{d,n+1} = \max\left(g_{d,0}, \max_{s\in(-\infty,n+1)} \xi_{d,s}\right) - g_{dh,(n)} \tag{6.10}$$

Step 4: Compute the two-scalar damage predictor $d_{v,n+1}$ and $d_{d,n+1}$ based on $\xi_{v,n+1}$ and $\xi_{d,n+1}$, respectively.

If $\xi_{v,n+1}$ at the current time step is less than the current volumetric damage threshold $g_{v,n+1}$, no further volumetric damage occurs; set $\Delta d_{v,n+1} = 0$. However, if $\xi_{v,n+1}$ is larger than the current volumetric damage threshold $g_{v,n+1}$, compute the volumetric damage predictor $\Delta d_{v,n+1}$ by using a nonlinear saturation type of damage functional evaluation. Similar to the volumetric part, if $\xi_{d,n+1}$ at the current time step is less than the current deviatoric damage threshold $g_{d,n+1}$, no further deviatoric damage occurs; set $\Delta d_{d,n+1} = 0$. However, if $\xi_{d,n+1}$ is larger than the current deviatoric damage threshold $g_{d,n+1}$, compute the deviatoric damage predictor $\Delta d_{d,n+1}$ by using a nonlinear saturation type of damage functional evaluation. Conceptually, if initial defects, damage, or interfacial debonding between aggregate and matrix (such as microvoids or microcracks) can be observed by nondestructive evaluation (such as by computed tomography), then the ***initial volumetric and deviatoric damage*** d_{v0} and d_{d0} can be characterized and quantified accordingly. Otherwise, the initial volumetric and deviatoric damage d_{v0} and d_{d0} are set as zero, respectively.

$$d_{v,n+1} = d_{v,n} + \Delta d_{v,n+1} \tag{6.11}$$

$$d_{d,n+1} = d_{d,n} + \Delta d_{d,n+1} \tag{6.12}$$

Step 5: Update the current volumetric and deviatoric healing threshold, $r_{v,n+1}$ and $r_{d,n+1}$, for a healing criterion based on $\xi_{v,n+1}$ and $\xi_{d,n+1}$.

If the incremental volumetric damage at the previous time step is larger than zero, compute the $r_{vd,(n)}$ by using a nonlinear saturation type of functional evaluation. Otherwise, $r_{vd,(n)}$ is zero. Similarly, compute the $r_{dd,(n)}$ by using a nonlinear saturation type functional evaluation if the incremental deviatoric damage at the previous time step is larger than zero. Otherwise, $r_{dd,(n)}$ is zero.

$$r_{v,n+1} = \min\left(r_{v,0}, \min_{s\in(-\infty,n+1)} \xi_{v,s}\right) + r_{vd,(n)} \tag{6.13}$$

$$r_{d,n+1} = \min\left(r_{d,0}, \min_{s\in(-\infty,n+1)} \xi_{d,s}\right) + r_{dd,(n)} \tag{6.14}$$

Step 6: Compute the two-parameter healing predictors, $R_{v,n+1}$ and $R_{d,n+1}$, based on $\xi_{v,n+1}$ and $\xi_{d,n+1}$.

If $\xi_{v,n+1}$ at the current time step is larger than the current volumetric healing threshold $r_{v,n+1}$, no further healing occurs; set $\Delta R_{v,n+1} = 0$. However, if $\xi_{v,n+1}$ is less than the current volumetric healing threshold $r_{v,n+1}$, compute the volumetric healing predictor $\Delta R_{v,n+1}$ by using a nonlinear saturation type of healing functional evaluation. Analogous to the volumetric part, if $\xi_{d,n+1}$ at the current time step is larger than the current deviatoric healing threshold $r_{d,n+1}$, no further healing occurs; set $\Delta R_{d,n+1} = 0$. However, if $\xi_{d,n+1}$ is less than the current deviatoric healing threshold $r_{d,n+1}$, compute the deviatoric healing predictor $\Delta R_{d,n+1}$ by using a nonlinear saturation type of healing functional evaluation.

$$R_{v,n+1} = R_{v,n} + \Delta R_{v,n+1} \quad \left(\Delta d_{v,n+1} = 0\right) \tag{6.15}$$

$$R_{v,n+1} = \frac{d_{v,n+1}}{2d_{v,n+1} - d_{v,n}} R_{v,n} \quad \left(\Delta d_{v,n+1} > 0\right) \tag{6.16}$$

$$R_{d,n+1} = R_{d,n} + \Delta R_{d,n+1} \quad \left(\Delta d_{d,n+1} = 0\right) \tag{6.17}$$

$$R_{d,n+1} = \frac{d_{d,n+1}}{2d_{d,n+1} - d_{d,n}} R_{d,n} \qquad \left(\Delta d_{d,n+1} > 0\right) \tag{6.18}$$

Step 7: Compute the *incremental* two-parameter damage net predictors $\Delta d^{net}_{v,n+1}$ and $\Delta d^{net}_{d,n+1}$

$$\Delta d^{net}_{v,n+1} = \Delta d_{v,n+1} - \Delta R_{v,n+1} d^{net}_{v,n} \tag{6.19}$$

$$\Delta d^{net}_{d,n+1} = \Delta d_{d,n+1} - \Delta R_{d,n+1} d^{net}_{d,n} \tag{6.20}$$

Step 8: Update the *incremental* two-parameter damage predictor tensor $\Delta\mathbf{D}_{v,n+1}$ and $\Delta\mathbf{D}_{d,n+1}$ and the damage tensor $\mathbf{D}_{n+1}$

$$\Delta\mathbf{D}^{net}_{n+1} = \frac{1}{3}\Delta d^{net}_{v,n+1}\mathbf{1}\otimes\mathbf{1} + \Delta d^{net}_{d,n+1}\left(\mathbf{I} - \frac{1}{3}\mathbf{1}\otimes\mathbf{1}\right) \tag{6.21}$$

$$\mathbf{D}^{net}_{n+1} = \mathbf{D}^{net}_{n} + \Delta\mathbf{D}^{net}_{n+1} \tag{6.22}$$

By substituting of the total strain tensor $\boldsymbol{\varepsilon}_{n+1}$ into the potential for the stress tensor, we obtain

$$\begin{aligned} \boldsymbol{\sigma}^{0}_{n+1} &= \frac{\partial \Psi^{0}}{\partial \boldsymbol{\varepsilon}}\left(\boldsymbol{\varepsilon}_{n+1}\right) \\ \boldsymbol{\sigma}^{trial,net}_{n+1} &= \boldsymbol{\sigma}^{0}_{n+1} - \boldsymbol{\sigma}^{vp,net}_{n} \\ \mathbf{q}^{trial}_{n+1} &= \mathbf{q}_{n} \end{aligned} \tag{6.23}$$

6.2.3 The Net Viscoplastic Return Mapping Corrector

To develop an algorithm consistent with the viscoplastic part of the operator split, we first check the loading/unloading conditions.

Step 9: Check for net *yielding*:

The algorithmic counterpart of the Kuhn-Tucker conditions is implemented in terms of the elastic two-parameter damage-self healing trial stress; cf. Simo and Ju (1987b), Ju et al.(2012b). One simply checks:

$$f(\boldsymbol{\sigma}_{n+1}^{trial,net}, \mathbf{q}_{n+1}^{trial}) \begin{cases} \le 0, & \text{elastic - damage - healing} \Rightarrow \text{predictor} = \text{final state} \\ > 0, & \text{viscoplastic} \Rightarrow \text{return mapping} \end{cases} \tag{6.24}$$

Step 10: Net viscoplastic return mapping *corrector*:

In the case of net viscoplastic loading, the predictor stresses and internal variables are "returned back" to the net yield surface along the algorithmic counterpart of the flow generated by Eq. (6.5). The framework of the radial return algorithm is employed in this work.

Step 11: Update the homogenized (nominal) stress $\boldsymbol{\sigma}_{n+1}$:

$$\boldsymbol{\sigma}_{n+1} = \left[\left\{ \mathbf{I} - \mathbf{D}_{n+1}^{net} \right\} : \boldsymbol{\sigma}_{n+1}^{net} \right] \vartheta\left(T_{n+1}\right) \tag{6.25}$$

6.3 Applications and Validations

Firstly, a three-dimensional driver problem based on the developed two-parameter damage-self healing mechanism is conducted by the Matlab codes. Thermo-elastoviscoplastic two parameter damage-self healing models are demonstrated by using a two-invariant Drucker-Prager yield criterion and Perzyna viscoplasticity model. Secondly, for validation of the two-parameter damage-self healing models, experimental data obtained by Texas A&M University (TAMU) and the North Carolina State University (NCSU) for asphalt mixtures is compared with numerical simulations by the proposed thermo-elastoviscoplastic two-parameter damage-healing models.

6.3.1 Three-Dimensional Driver Problem

Based on the proposed two-parameter thermo damage-healing mechanism, the history of homogenized stress, net stress, damage and healing thresholds can be estimated under a specified cycle of strain control such as loading-unlading-reloading (LUR) and one complete cycle. Elastoviscoplastic model case is studied and presented using the *thermo-elastoviscoplastic damage-self healing* model by adjusting temperature conditions, the yield stresses, the initial damage thresholds, and the initial healing thresholds in the Matlab codes. The corresponding computational results are presented and discussed in the following.

Thermo-elastoviscoplastic two-parameter damage-self healing model

Four different scenarios are demonstrated: (1) general LUR, (2) cyclic loading (one cycle), (3) temperature effect for LUR, and (4) rest period effect for LUR. For the general LUR case, the initial volumetric damage and healing thresholds are set as 0.06 and 0.055, respectively, while the initial deviatoric damage and healing thresholds are assumed to be 0.08 and 0.1, respectively. The reason these volumetric and deviatoric values are different to each other is that the volumetric equivalent strain is different from energy norm of deviatoric strain. Drucker-Prager yield function and Perzyan viscoplastic model are chosen for three-dimensional demonstration. Moreover, the axial homogenized and net stresses and axial strain are only employed for figures. Figure 6.1(a) shows that the decrease in stress under the loading condition is observed due to both the evolution of damage and viscoplastic deformation. However, the stress decreases under the loading because of only viscoplastic deformation only considered in net space in Figure 6.1(b). Since we do not consider temperature effect in net space, the net stresses at 10 ℃ and 20 ℃ are the same. On the contrary to the net stresses, the magnitude of the homogenized stresses is different due to the use of *Arrhenius-type temperature term* in physical space. According to the experimental data, the magnitude of the normal stress at low temperature is higher than one at higher temperature presented in Figure 6.1(a). In Figure 6.1(c), strain goes back to certain strain point due to permanent deformation under the unloading condition and the reloading starts again after 300 steps. At 20 ℃ in Figure 6.1(c), the increase in the slope of the stress-strain curve after 300 steps is obviously observed because self-healing lasts for 300 steps, while the slope of the stress-strain curve at 10 ℃ under the reloading steps is not clearly greater than that before 300 steps because the amount of damage at 10 ℃ under the loading condition is greater and the healing at 10 ℃ for 300 steps is smaller than that at 20 ℃. Figure 6.1(d) demonstrates the energy norm of the volumetric and deviatoric strain tensors at 10 ℃ and 20 ℃. Deviatoric equivalent strain is larger than volumetric strain and the energy norm of strain tensors at 10 ℃ is larger than that at 20 ℃. Figure 6.2 shows the shape and magnitude of damage net, damage, and healing variables at each temperature condition. In Figure 6.2(a) and (b), the volumetric and deviatoric damage net variables is shown, respectively, and their shapes are similar to each other, but the magnitude is different due to difference between equivalent volumetric strain and the energy norm of deviatoric strain tensor. Under the loading the damage net variables increase with time and are constant under the unloading conditions. For 300 steps after completion of unloading, healing occurs so that the damage net variables are reduced by the amount of healing. If the energy norm of volumetric strain tensor is greater than healed volumetric damage threshold again, the volumetric damage net variable increases again. Similarly, increase in the deviatoric damage net variable is observed under the condition that equivalent deviatoric strain is greater than healed deviatoric damage threshold. The magnitude of damage net variables at 10 ℃ is larger than that at 20 ℃ due to the temperature effect. On the contrary to volumetric and deviatoric damage net and healing variables, process of volumetric and deviatoric damage is assumed to be irreversible and the damage is a monotonically increasing function of strain energy norm as shown in Figure 6.2(c) and (d). In Figure 6.2(e) and (f), the volumetric and deviatoric healing variables are demonstrated and the amount of healing at 10 ℃ is lower than that at 20 ℃ because of the effect of temperature.

Figure 6.3 shows one cycle loading case from tension to compression. The initial volumetric and deviatoric damage thresholds are the same as LUR case, while the volumetric and deviatoric healing thresholds are assumed to be 0.02 and 0.035, respectively. The magnitude of homogenized stress at 10 ℃ is larger than that at 20 ℃ presented in Figure 6.3(a) due to the temperature effect. Moreover, reduction in homogenized stress under tensile and compressive loading conditions is clearly due to both damage and permanent deformation. Since damage net variable is accumulated with time, tensile stress is obviously larger than compressive stress in physical space. Figure 6.3(b) represents the history of net stress. Decease in the net stress under the tensile and compressive loading is only caused by viscoplastic deformation because the effects of temperature and damage-self healing are not included in net space. In Figure 6.3(c), the shapes of stress-strain curve are similar to each temperature condition whereas the magnitude of homogenized stress at 10 ℃ is clearly larger than that at 20 ℃. Figure 6.3(d) demonstrates the energy norm of volumetric and deviatoric strain tensor and there is no difference between equivalent tensile and compressive strain.

Figure 6.4 represents the histories of two-parameter damage net, damage, and healing variables for one cycle loading. In Figure 6.4(a) and (b), volumetric and deviatoric damage net variables initially increase when the energy norm of volumetric and deviatoric strain tensors exceed their damage thresholds, respectively. Under the tensile reloading condition, two-parameter damage net variables are constant and decrease with increasing healing variables. Increase in volumetric and deviatoric damage net variables is observed again under the compressive reloading condition and these variables are eventually constant when the compressive unloading starts. Volumetric damage variable is only evolved when the volumetric equivalent strain exceeds its threshold under the tensile or compressive loading conditions shown in Figure 6.4(c), while volumetric healing is only initiated when there is no damage evolution and energy norm of volumetric strain tensor is lower than its healing threshold in Figure 6.4(e). The same pattern of deviatoric damage net, damage, and healing variables is observed in Figure 6.4(d) and (f). Both damage and damage net variables at 20 ℃ are lower than those at 10 ℃, whereas healing at 20 ℃ higher because more healing occurs at higher temperature.

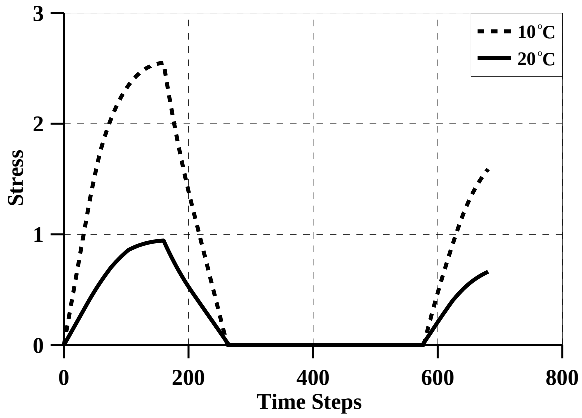

(a) Homogenized Stress

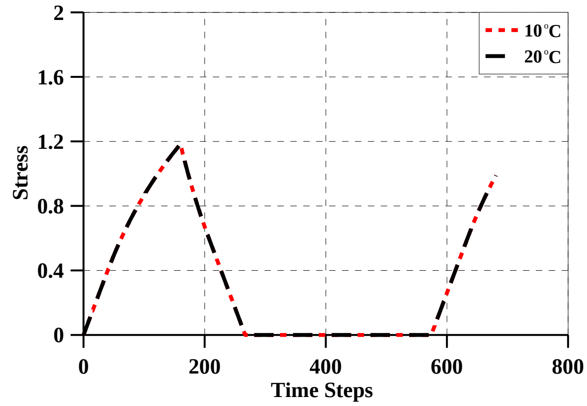

(b) Net Stress

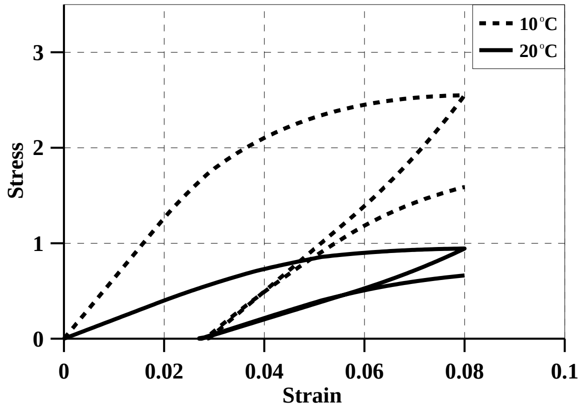

(c) Stress-Strain

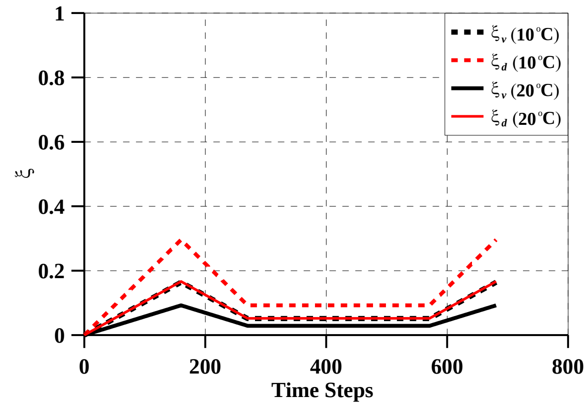

(d) Equivalent Strain

Figure 6.1 Corresponding results of three-dimensional driver problems by thermo-elastoviscoplastic damage-self healing model (10 °C and 20 °C)

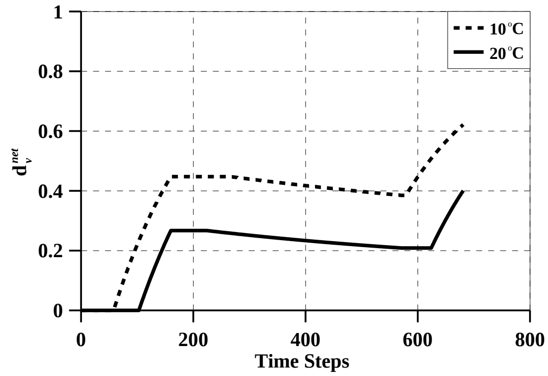

(a) d_v^{net}

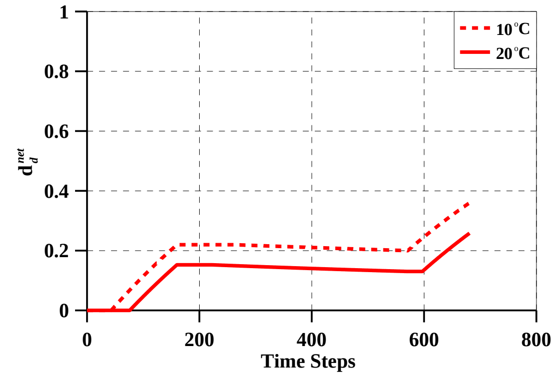

(b) d_d^{net}

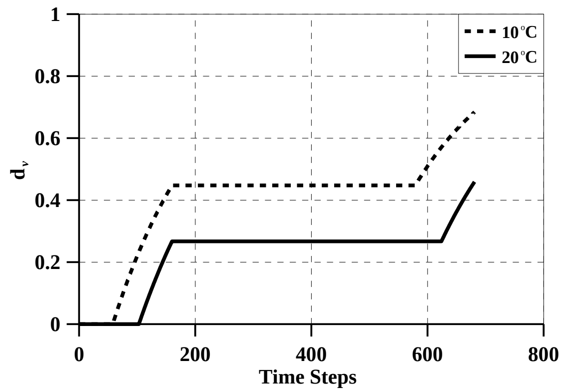

(c) d_v

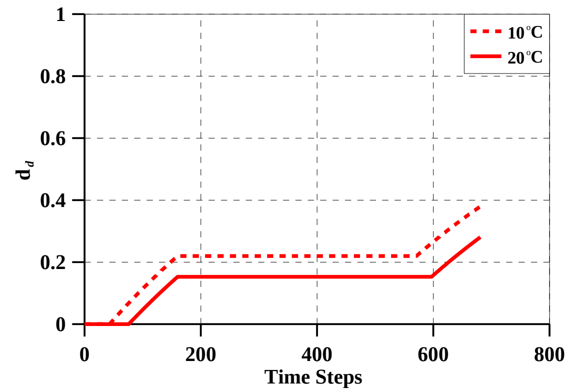

(d) d_d

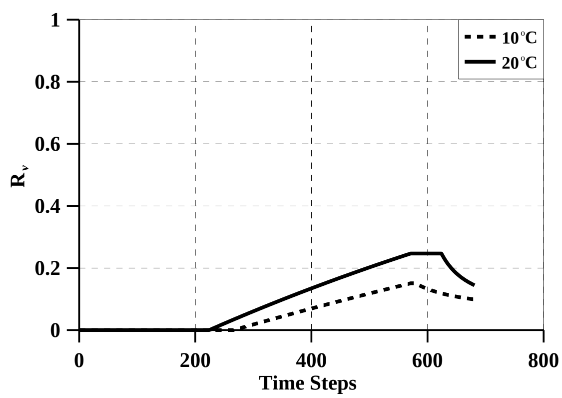

(e) R_v

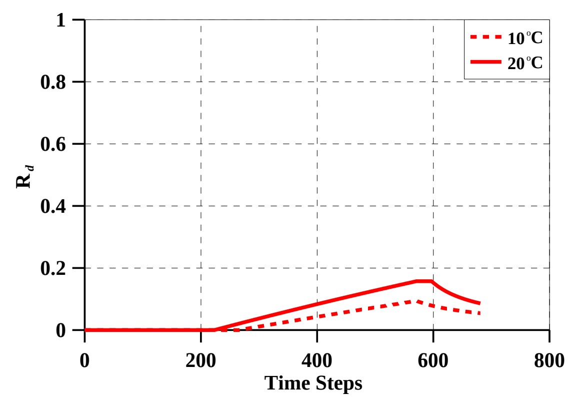

(f) R_d

Figure 6.2 Corresponding damage net variables of three-dimensional driver problems by thermo-elastoviscoplastic damage-self healing model (10 ℃ and 20 ℃)

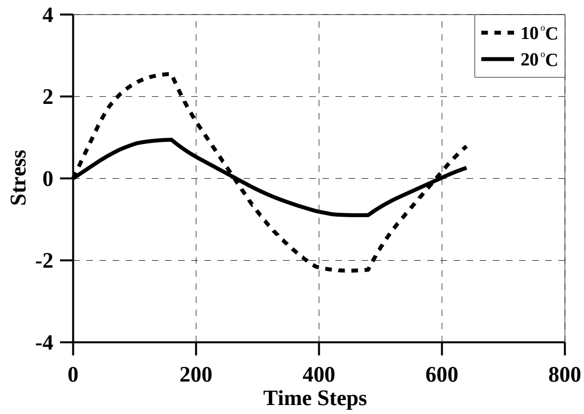

(a) Homogenized Stress

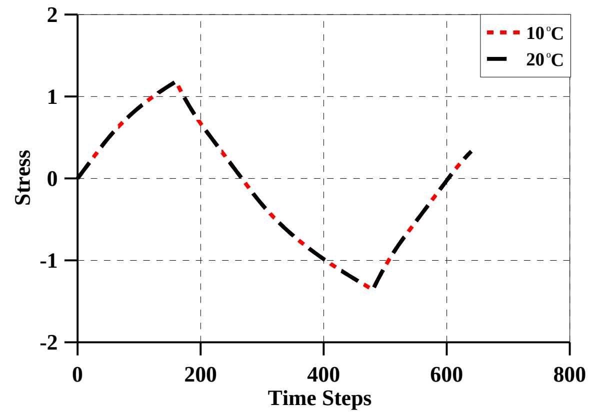

(b) Net Stress

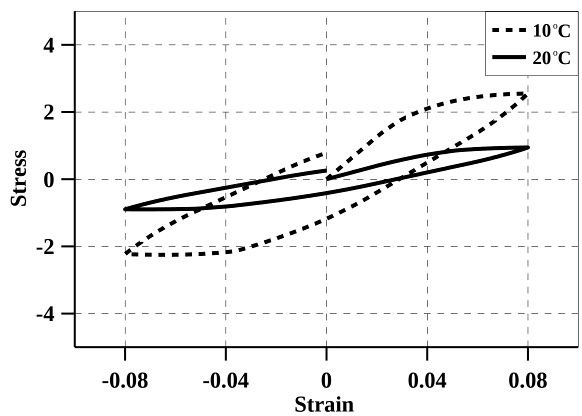

(c) Stress-Strain

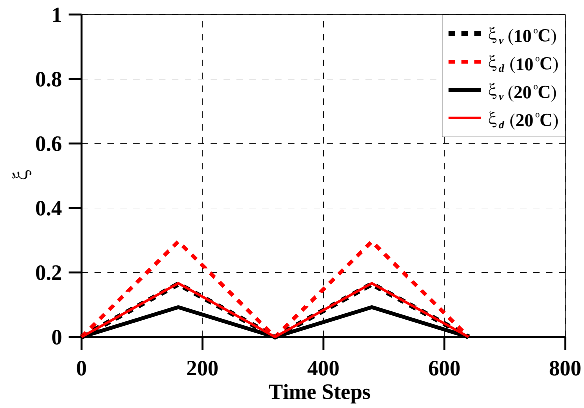

(d) Equivalent Strain

Figure 6.3 Corresponding results of three-dimensional driver problems by thermo-elastoviscoplastic damage-self healing model (10 ℃ and 20 ℃)

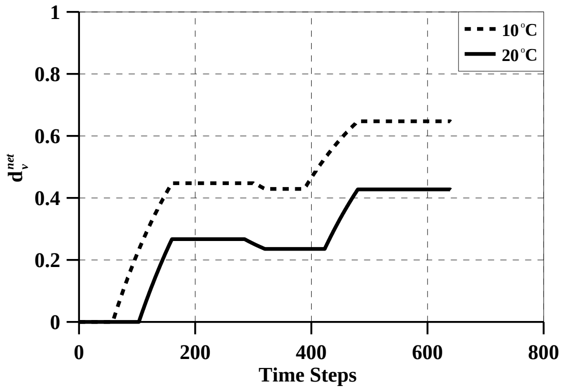

(a) d_v^{net}

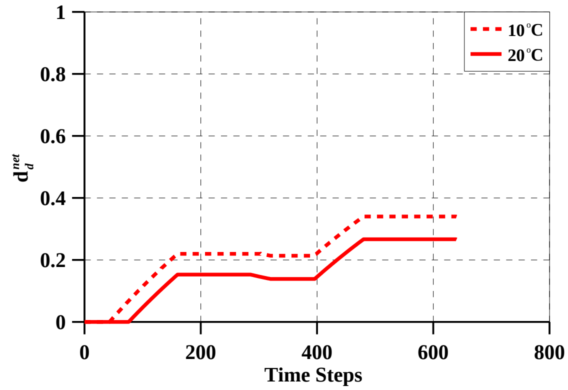

(b) d_d^{net}

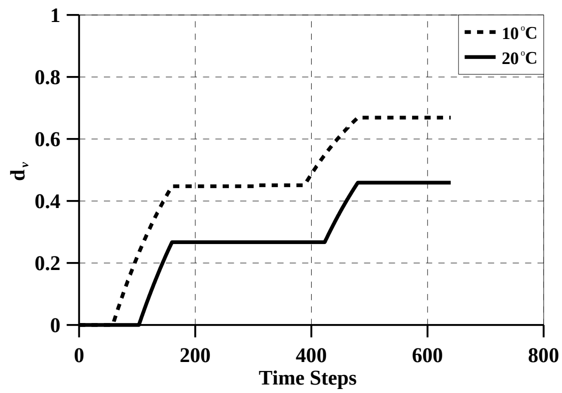

(c) d_v

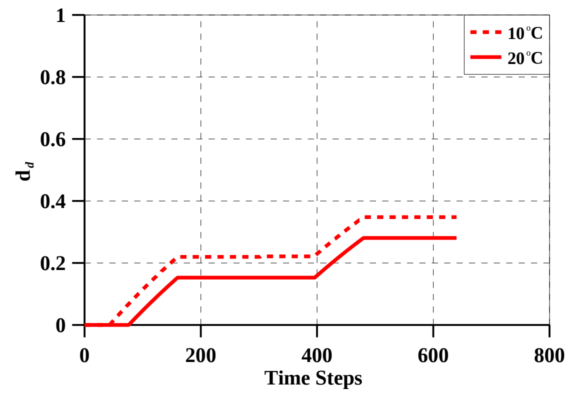

(d) d_d

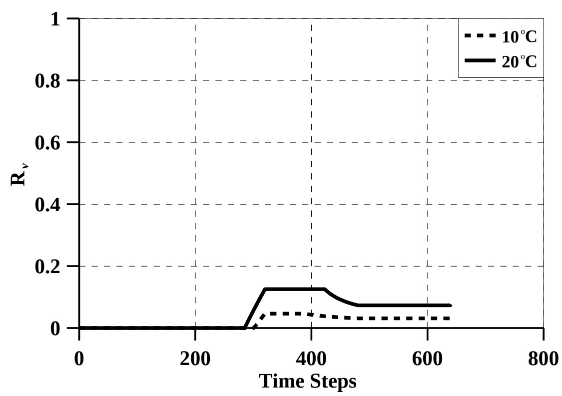

(e) R_v

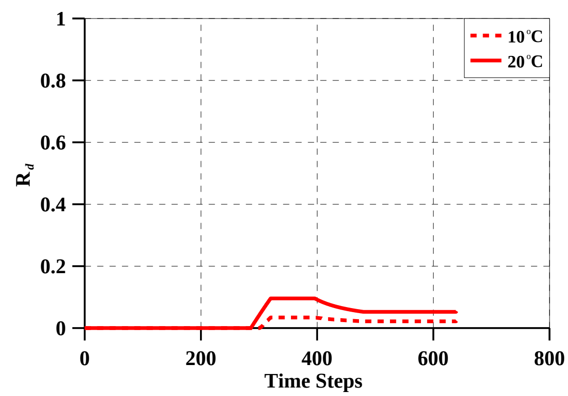

(f) R_d

Figure 6.4 Corresponding damage net variables of three-dimensional driver problems by thermo-elastoviscoplastic damage-self healing model (10 ℃ and 20 ℃)

In Figure 6.5, the effect of healing due to different temperature conditions for 300 steps is demonstrated. It is assumed that the initial volumetric and deviatoric damage threshold and healing threshold are the same as general LUR case. The temperature is set as 20 ℃ until the completion of unloading (point A). One case increase the temperature to 30 ℃ for 300 time steps (from point A and B) and the other case do not change temperature condition. Reloading starts after 300 time steps (point B). In Figure 6.5(a) increase in homogenized stress (dashed line) at 30 ℃ is observed due to the temperature effect. However, there is no difference between net stresses at different temperature because temperature effect, damage, and healing are not included in net space. In Figure 6.5(c), the Elastic Young's modulus at 30 ℃ is definitely greater than that at 20 ℃ after reloading is finished since the bituminous material exposed to 30 ℃ is partially more recovered. The equivalent volumetric and deviatoric strains are the same for two different temperatures shown in Figure 6.5(d) because reference temperature is 20 ℃ for both cases. The same fashion of damage net, damage, and healing variables as general LUR is presented in Figure 6.6. Since the process of damage and healing is completely independent, damage occurs only when healing is not evolved, while healing starts when energy norm is smaller than healing threshold and there is no damage evolution. The amount of healing is different due to temperature difference for the rest period in Figure 6.6 (e) and (f). Therefore, reduction in volumetric and deviatoric damage net variables at 30 ℃ are greater than these at 20 ℃ as presented in Figure 6.6(a) and (b).

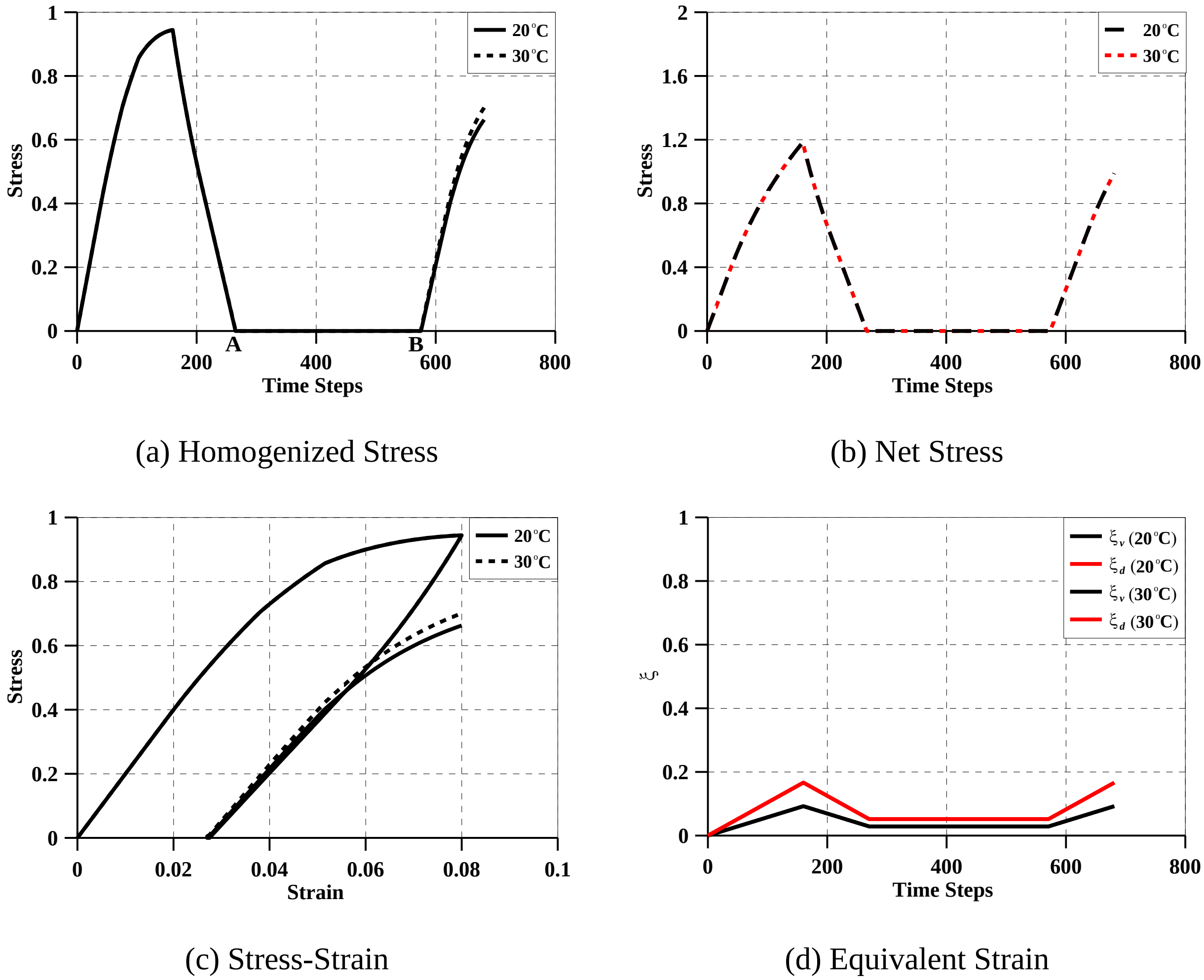

(a) Homogenized Stress (b) Net Stress

(c) Stress-Strain (d) Equivalent Strain

Figure 6.5 Corresponding results of three-dimensional driver problems by thermo-elastoviscoplastic damage-self healing model (30 °C for healing period)

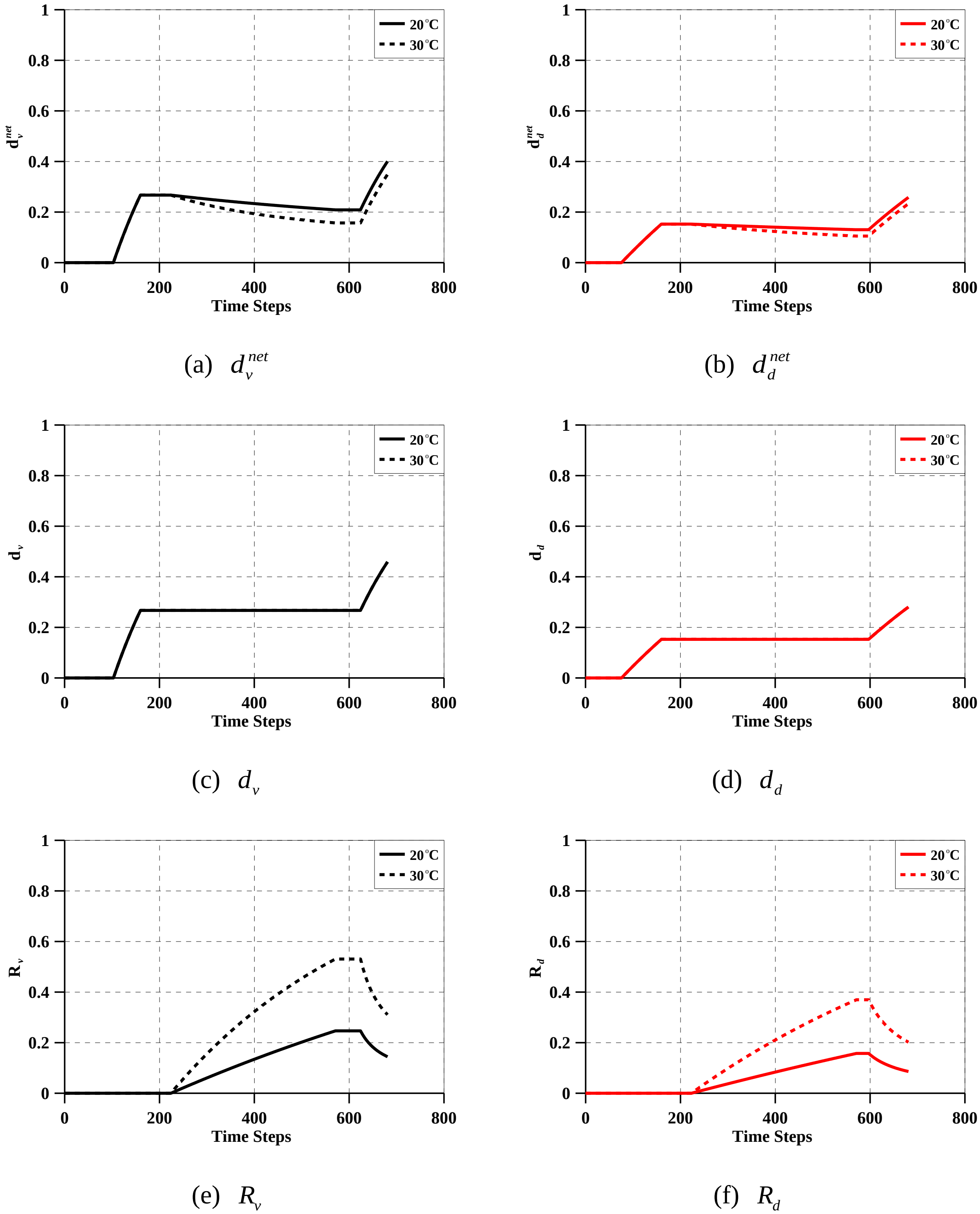

Figure 6.6 Corresponding damage net variables of three-dimensional driver problems by thermo-elastoviscoplastic damage-self healing model (30 ℃ for healing period)

Figure 6.7 and Figure 6.8 provide the healing effect due to the rest period. The initial volumetric and deviatoric damage threshold and healing threshold are assumed to be the same as general LUR case. Temperature keeps constant for entire loading condition, whereas rest periods are different to each other, 100 steps and 300 steps. In Figure 6.7(a), the homogenized stress at the end of reloading for 100 steps is clearly smaller than that for 300 steps. However, the final net stresses at different time steps as shown in Figure 6.7(b) are the same. In Figure 6.7(c), it is observed that the slope of stress-strain curve after 100 steps is slightly small than 300 steps due to the effect of healing. For volumetric and deviatoric damage variables in Figure 6.8(c) and (d), the final volumetric and deviatoric damage variables after 100 steps are smaller than these after 300 steps because more healing makes the damage threshold lower and then more damage can occur. However, when the volumetric damage and healing variables are coupled to make volumetric damage net variables, they become very close to each other as presented in (a), (c), and (e). Similar to the volumetric case, the volumetric damage net variable is the same fashion in (b), (d), and (f). This is the main reason the Young's modulus after 300 steps is slightly higher than that after 100 steps.

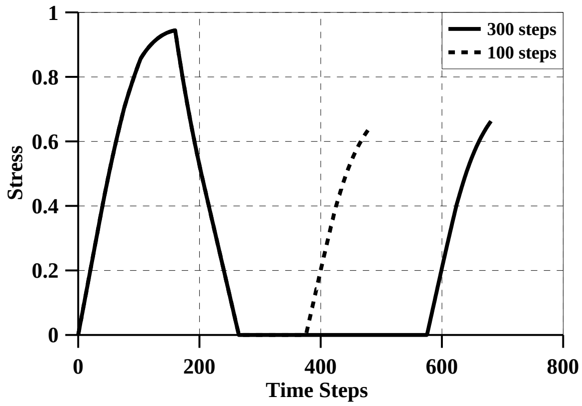

(a) Homogenized Stress

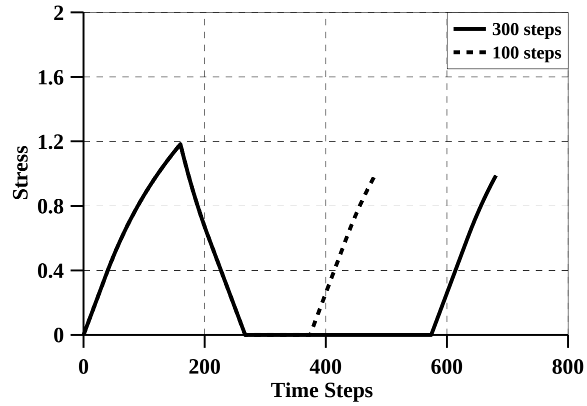

(b) Net Stress

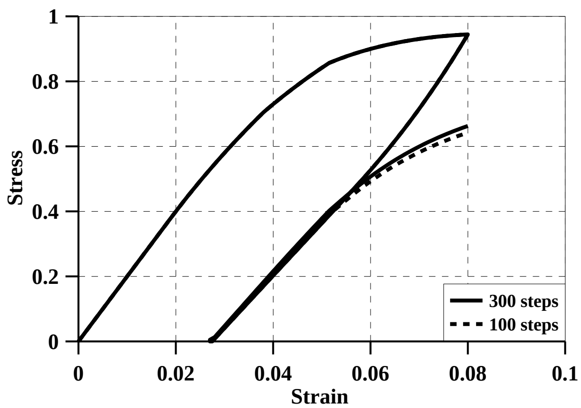

(c) Stress-Strain

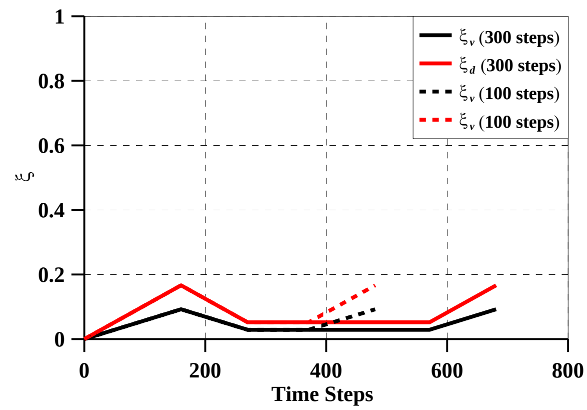

(d) Equivalent Strain

Figure 6.7 Corresponding results of three-dimensional driver problems by thermo-elastoviscoplastic damage-self healing model (100 steps and 300 steps for healing)

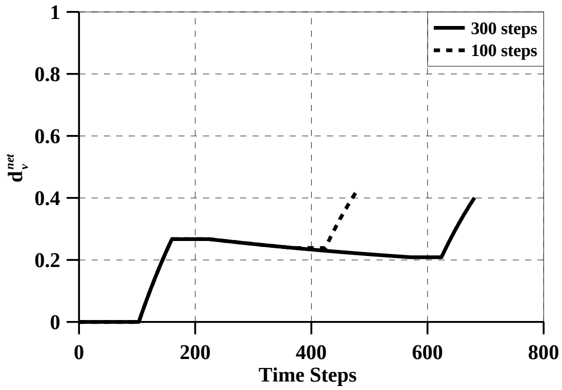

(a) d_v^{net}

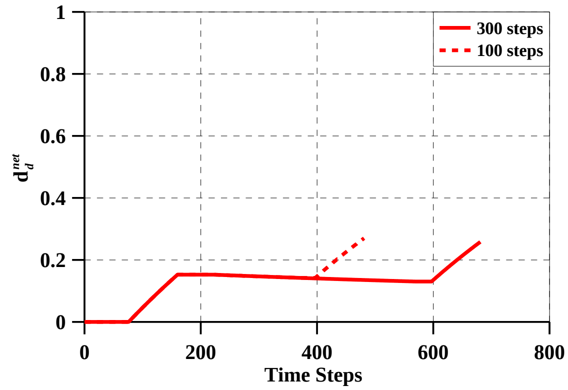

(b) d_d^{net}

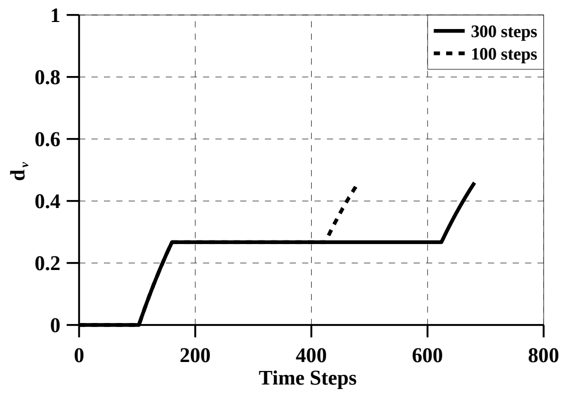

(c) d_v

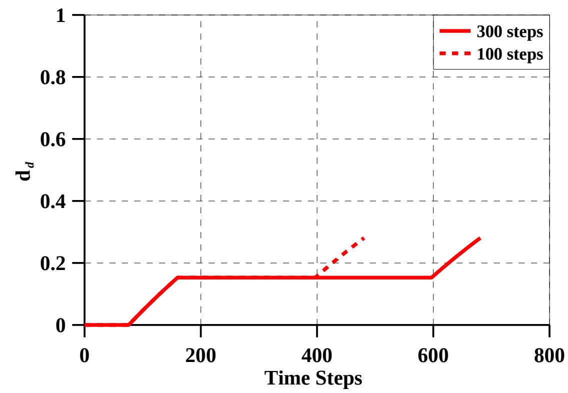

(d) d_d

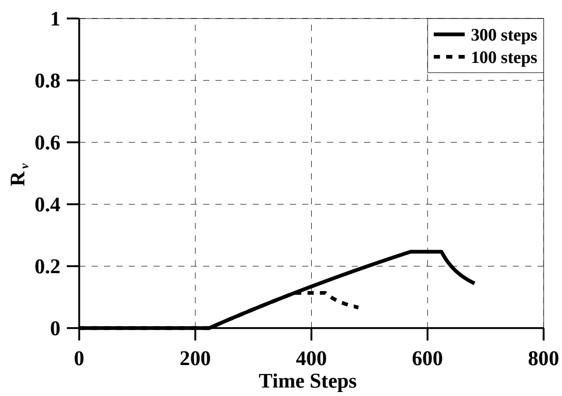

(e) R_v

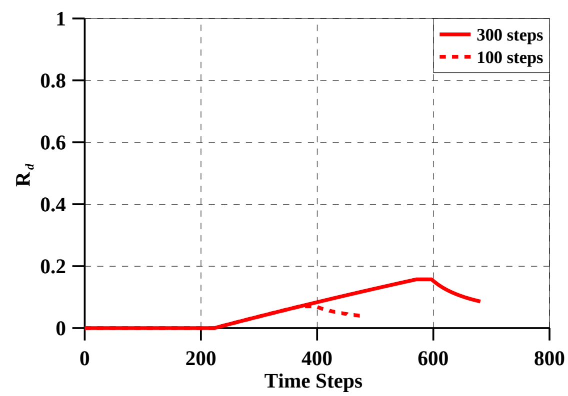

(f) R_d

Figure 6.8 Corresponding damage net variables of three-dimensional driver problems by thermo-elastoviscoplastic damage-self healing model (100 steps and 300 steps for healing)

6.3.2 Comparison between Experimental Results and Model Prediction

The initial energy-based thermo-elastoviscoplastic two-parameter damage-self healing mechanism and computational framework proposed in Chapter 5 and previous section are used in this section for capturing fundamental behavior of bituminous materials within experimental error. In view of the wide scattering in available experimental data for asphalt concrete and the present imperfection of experimental techniques, a precise quantitative evaluation of the predicting capabilities of a given constitutive model with this two-parameter damage-self healing model may not seem to be guaranteed. However, a comprehensive qualitative production of the thermo-mechanical behavior of bituminous composites should play a key role in material modeling.

A two-invariant Drucker-Prager yield criterion with Perzyna viscoplasticity model is mainly selected and used for model prediction in the net space because it is hydrostatic stress dependent and a viscoplastic material. Moreover, non-associative flow rule is employed in the model. According to Lemaitre and Chaboche (1990) and Tan et al. (1994), material constant *A* in Drucker-Pracker yield evolves the permanent deformation while *B* is almost a constant as the materials permanently deforms. Therefore, equivalent viscoplastic strain is employed for the hardening law. Radial return algorithm [4] summarized in Chapter 3 and 4 is used for the model prediction

In order to validate the proposed two-parameter damage-self healing formulation, the experimental data are retrieved from the well-documented experimental program preformed at the Texas A&M University (TAMU) and the North Carolina State University (NCSU) [1][7]. Because of the limitation of available experimental data, the thermo-elastoviscoplastic two-parameter damage model against the monotonic uniaxial compression tests with different strain rates under different temperature conditions is first selected and the elastoviscoplastic two-parameter damage-self healing model against the cyclic strain loading control test at constant temperature for two different asphalt concretes is chosen for the second verification in this section. The proposed thermo-elastoviscoplastic two-parameter damage-self healing model is equivalent to the thermo-elastoviscoplastic two-parameter damage model when the damage is considered only for monotonic uniaxial tests. As a result, the net space is equal to the effective space and volumetric and deviatoric damage net variables are the same as volumetric and deviatoric damage variables, respectively. In the case of the second example, the proposed model becomes the elastoviscoplastic two-parameter damage-self healing model since the experiment was conducted under the only one constant temperature. By comparing these two cases, the proposed models well demonstrate capability in predicting the temperature-dependent mechanical behavior of bituminous composites. Moreover, the two-parameter damage-self healing model better predicts the temperature-dependent mechanical behavior of asphalt concrete pavement and is more versatile than isotropic damage-self healing model in Chapter 3 and 4.

TAMU asphalt concrete data

The experimental data for the following example are taken from the literature paper [1] on monotonic uniaxial compression tests of Hot Mix Asphalt. 10 mm Dense Bitumen Macadam which is a continuously graded mixture with asphalt binder content of 5.5% and Granite aggregates and an asphalt binder with a penetration grade of 70/100 were employed for experiments. The diameter and height of cylindrical specimen were 100 mm and 100 mm, respectively, and the specimen was compacted by the gyrator compactor. The tests were performed at three different temperature conditions, 10 ℃, 20 ℃, and 40 ℃. The three different strain rates were employed from 0.005 s^{-1} to 0.00005 s^{-1} for 10 ℃ and 20 ℃, while for 40 ℃ only two strain rates, 0.005 s^{-1} and 0.0005 s^{-1}, were conducted. The experimental data for 20 ℃ were considered as reference material properties. The optimal material parameters of the asphalt concrete for simulations are obtained from the experimental data by fitting and summarized in Table 6.1.

Table 6.1 The associated bituminous material properties at 20 ℃ in simulations

	$\dot{\varepsilon} = 0.005\ s^{-1}$	$\dot{\varepsilon} = 0.0005\ s^{-1}$	$\dot{\varepsilon} = 0.00005\ s^{-1}$
Young's modulus	290,000 (kPa)	130,000 (kPa)	70,000 (kPa)
Poisson's ratio	0.35		
Viscosity	244 (kPa/sec)		
Lame constants	250,617 (kPa)	112.345 (kPa)	60,493 (kPa)
Shear modulus	107,407 (kPa)	48,148 (kPa)	25,925 (kPa)
Initial volumetric damage threshold	1.8		
Initial deviatoric damage threshold	2.0		
A_0	20 (kPa)		

Figure 6.9 presents comparison between the experimental data and computational results at two or three strain rates under different temperature conditions. In, the stress in y-axis and the strain in x-axis are the stress and the strain in axial direction, respectively. Good qualitative and quantitative agreements between the proposed thermo-elastoviscoplastic two-parameter damage model and the experimental measurements are clearly observed. In particular, softening behaviors are well predicted as shown in. The volumetric and deviatoric damage net variables are equivalent to the volumetric and deviatoric damage variables,

respectively, since the monotonic uniaxial compression experimental results were used for comparisons. As a result, in Figure 6.10 the two-parameter damage net variables were used for the plots. Figure 6.10(a), (c), and (e) represent volumetric damage net variables for each strain rate at different temperature conditions, while the deviatoric variables are demonstrated in Figure 6.10(b), (d), and (f). Since the shapes, magnitudes, and starting points of volumetric variables are different from deviatoric values, the thermo-mechanical responses of bituminous composites at different strain rates under different temperature conditions are well captured by the proposed two-parameter damage-self healing models. For strain rate ($\dot{\varepsilon} = 0.005\ \mathrm{s}^{-1}$) shown in Figure 6.10(a) and (b), the maximum of volumetric and deviatoric damage net variables is slightly above 0.9 at 12% of strain and increase in damage variable is observed with increasing strain. In case of $\dot{\varepsilon} = 0.0005\ \mathrm{s}^{-1}$ in Figure 6.10(c) and (d), the highest volumetric and deviatoric damage net variables at 10 ℃ and 20 ℃ are slightly below 0.9 when the strain approaches 12 %, while the volumetric and deviatoric damage net variables at 40 ℃ are close to 0.7 at 12% of strain. For $\dot{\varepsilon} = 0.00005\ \mathrm{s}^{-1}$ case presented in Figure 6.10(e) and (f), the maximum of volumetric and deviatoric damage net variables are approximately 0.82. At higher temperature, damage for the same strain rate is initiated later because since bituminous composites materials become more viscous and it definitely lowers the damage level. In addition, the volumetric and deviatoric damage at lower temperature start at early stage of strain level. In other words, the asphalt concrete pavements are less susceptible to damage at higher temperature because they become viscous material properties. The damage net variables are redrawn at the same temperature condition as shown in Figure 6.11 for the effect of viscous damage. The damage net clearly increases with increasing strain rate. It means that the fast loading causes more damage on bituminous materials. Figure 6.12 demonstrates comparisons between isotropic damage-self healing model prediction (blue lines) [2][2] and two-parameter damage-self healing model (red line). At 20 ℃, the prediction by two-parameter model is closer to experimental measurements. In particular, softening responses after peak point of stress are well predicted for each strain rate. Although prediction lines from isotropic and two-parameter damage-self healing models are close to experimental results, the latter models slightly well predicts the results of the experiment in terms of small gap between computational and experimental results.

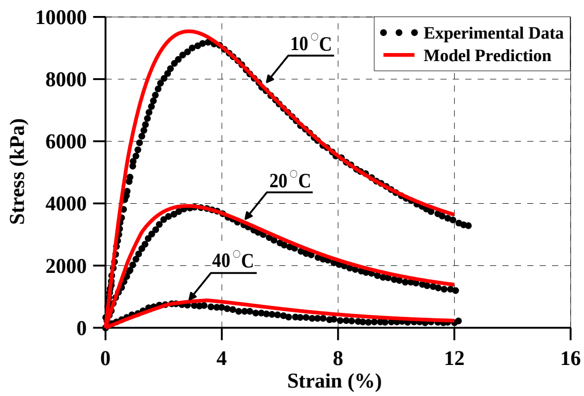

(a) Stress-Strain ($\dot{\varepsilon} = 0.005\ \mathrm{s}^{-1}$)

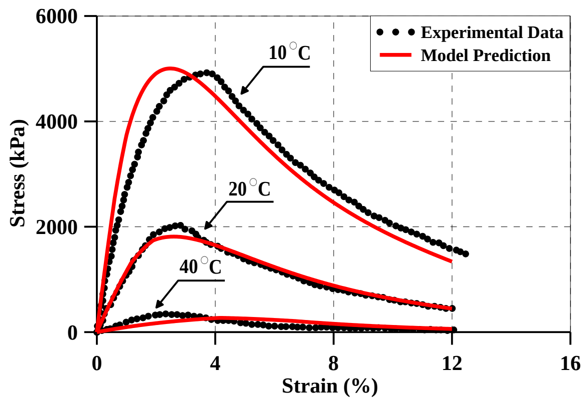

(b) Stress-Strain($\dot{\varepsilon} = 0.0005\ \mathrm{s}^{-1}$)

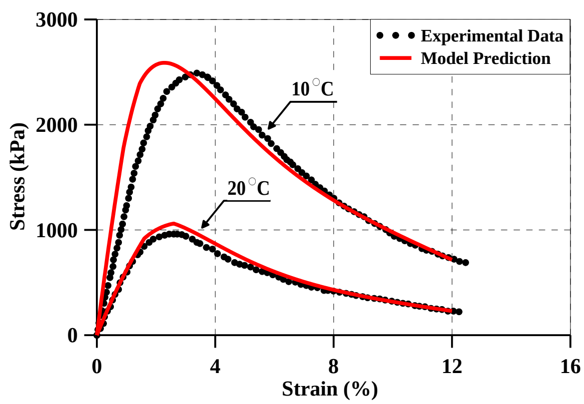

(c) Stress-Strain($\dot{\varepsilon} = 0.00005\ \mathrm{s}^{-1}$)

Figure 6.9 Comparison between experimental data and model prediction for the uniaxial constant strain rate test in compression ($\dot{\varepsilon} = 0.005 \sim 0.00005\ \mathrm{s}^{-1}$)

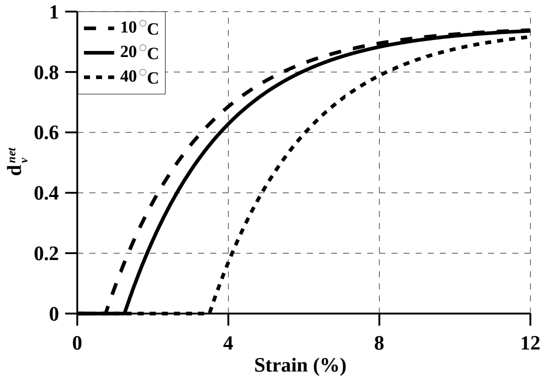

(a) d_v^{net} ($\dot{\varepsilon} = 0.005\ s^{-1}$)

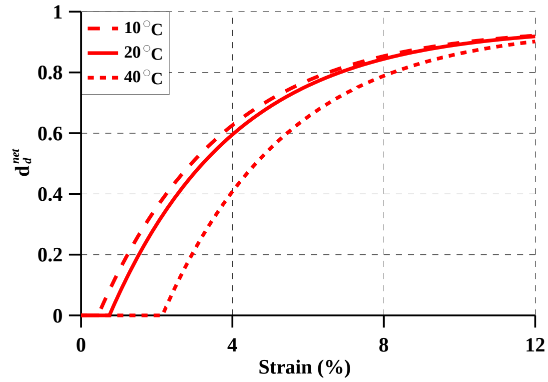

(b) d_d^{net} ($\dot{\varepsilon} = 0.005\ s^{-1}$)

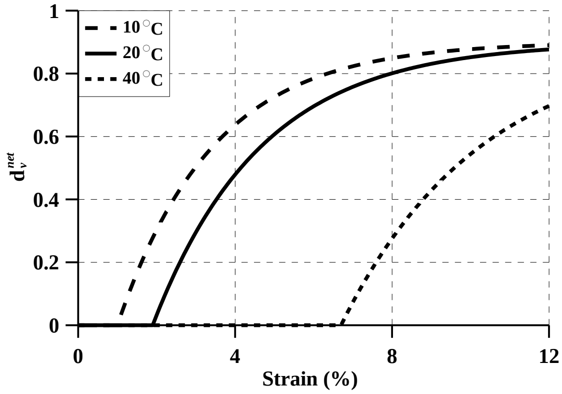

(c) d_v^{net} ($\dot{\varepsilon} = 0.0005\ s^{-1}$)

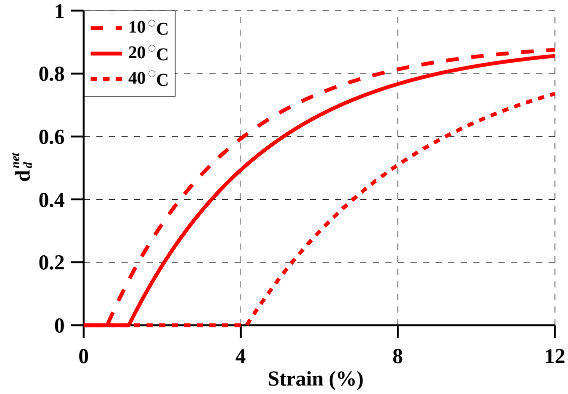

(d) d_d^{net} ($\dot{\varepsilon} = 0.0005\ s^{-1}$)

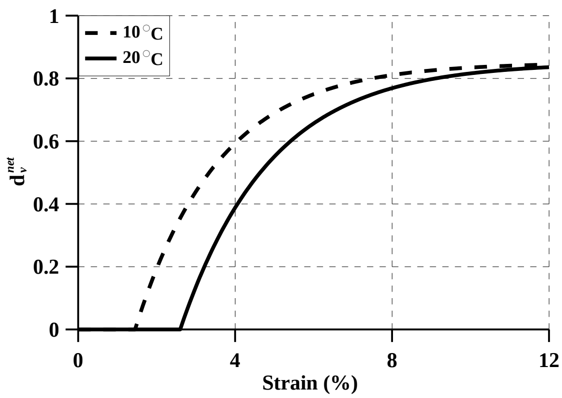

(e) d_v^{net} ($\dot{\varepsilon} = 0.00005\ s^{-1}$)

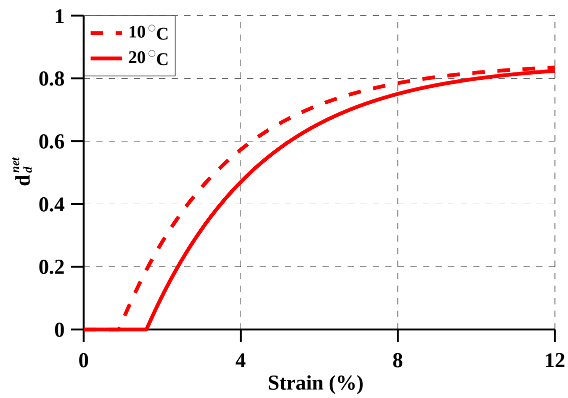

(f) d_d^{net} ($\dot{\varepsilon} = 0.00005\ s^{-1}$)

Figure 6.10 Damage net variables for the uniaxial constant strain rate test in compression ($\dot{\varepsilon} = 0.005 \sim 0.00005\ s^{-1}$)

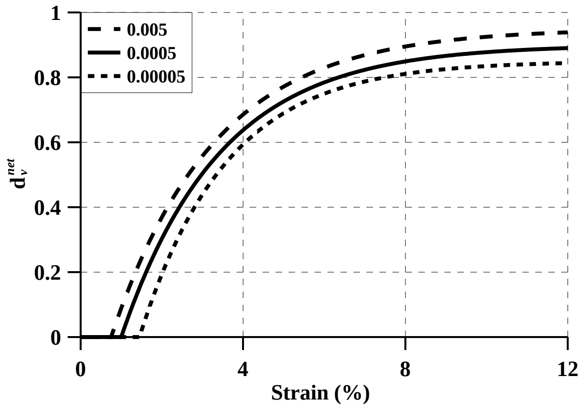

(a) d_v^{net} (10 ℃)

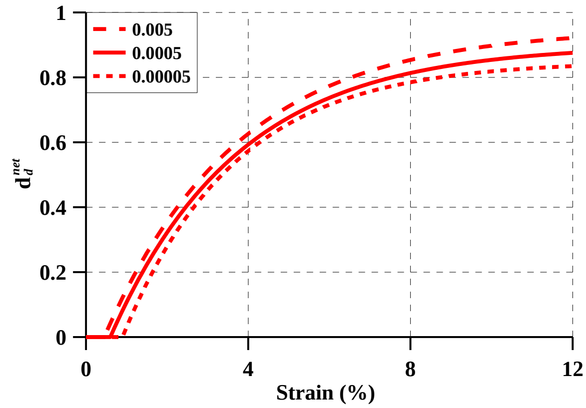

(b) d_d^{net} (10 ℃)

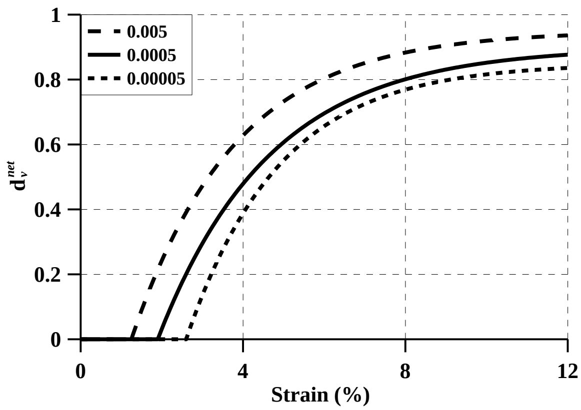

(c) d_v^{net} (20 ℃)

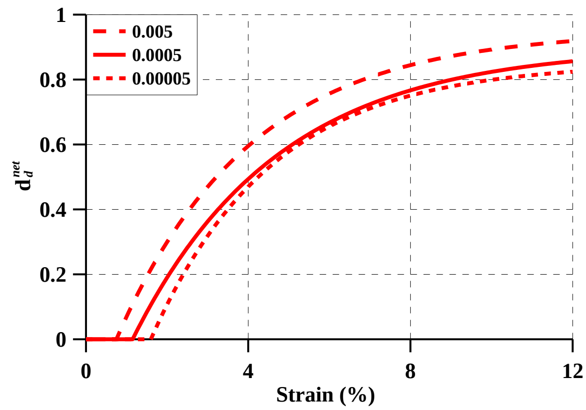

(d) d_d^{net} (20 ℃)

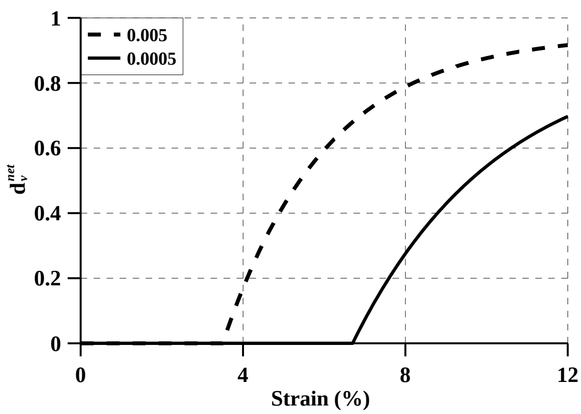

(e) d_v^{net} (40 ℃)

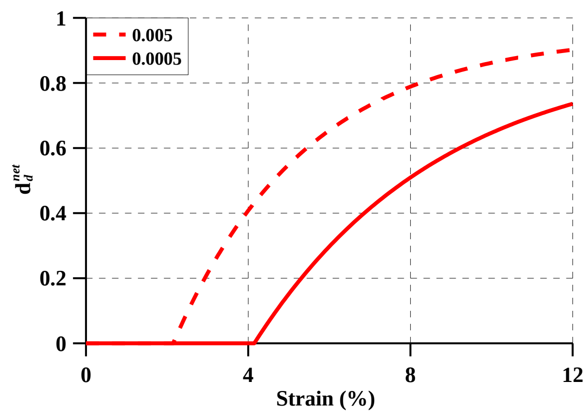

(f) d_d^{net} (40 ℃)

Figure 6.11 Comparison for damage net variables at constant temperature

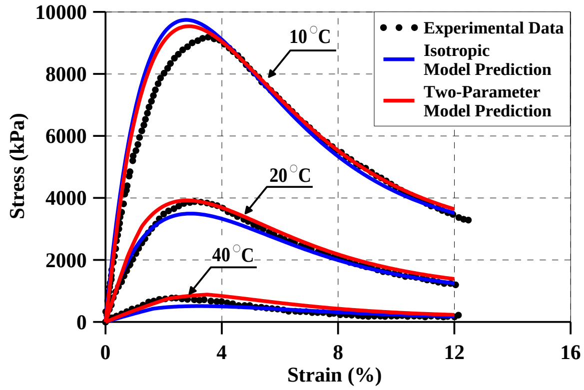

(a) Stress-Strain ($\dot{\varepsilon} = 0.005\ \mathrm{s}^{-1}$)

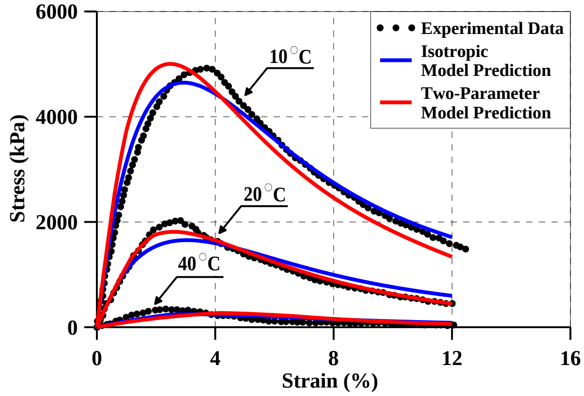

(b) Stress-Strain($\dot{\varepsilon} = 0.0005\ \mathrm{s}^{-1}$)

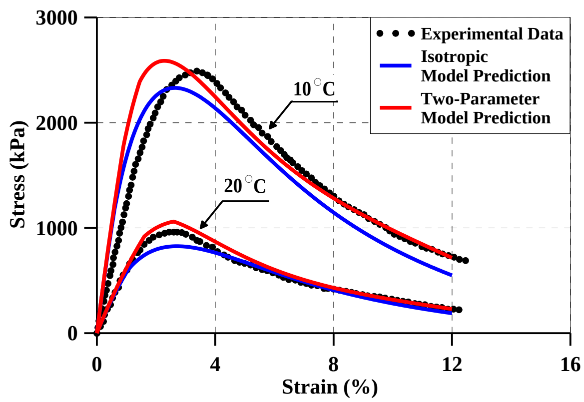

(c) Stress-Strain($\dot{\varepsilon} = 0.00005\ \mathrm{s}^{-1}$)

Figure 6.12 Comparison between isotropic model and two-parameter model prediction for the uniaxial constant strain rate test in compression ($\dot{\varepsilon} = 0.005 \sim 0.00005\ \mathrm{s}^{-1}$)

NCSU asphalt mixture data

The experimental measurements for the following comparisons are retrieved from Lee's dissertation [7] on controlled-strain cyclic tension tests of two different asphalt concretes, AAD, which has a tendency for cracking and age hardening, and AAM, which is described as a good performer with a low temperature susceptibility and potential for a low temperature cracking. The dimension of cylindrical specimen was 10.2 cm in diameter and 25 cm in height. The strain amplitudes of controlled-strain cyclic tests were 0.0009 and 0.001 for AAD and AAM mixtures, respectively, and the frequency of the test was set as 1 Hz. Because of the limitation of experimental tension data at different temperatures, the model and experimental results for the cyclic strain controlled in tension are compared at only one constant temperature, 25 ℃. Although healing theoretically occurs during unloading of the first cycle, it is close to zero because the amount of accumulated volumetric and deviatoric damage is small. As the number of cycles grows, increase in accumulated volumetric and deviatoric damage results in increase in damaged volumetric and deviatoric healing threshold and increase in the amount of volumetric and deviatoric healing. Therefore, more volumetric and deviatoric healing can be observed as the number of cycles increases. The optimal material parameters of AAD and AAM for simulations are also obtained from the experimental data by fitting and summarized in Table 6.2.

Table 6.2 The associated asphalt material properties at 25 ℃ in simulations

	AAD	AAM
Young's modulus	1,300,000 (kPa)	1,200,000 (kPa)
Poisson's ratio	0.3	
Viscosity	244 (kPa/sec)	
Lame constants	750,000 (kPa)	692,307(kPa)
Shear modulus	500,000 (kPa)	461,538 (kPa)
Initial volumetric damage threshold	0.2	0.15
Initial volumetric healing threshold	0.17	0.13
Initial deviatoric damage threshold	0.15	0.15
Initial deviatoric healing threshold	0.13	0.13
A_0	20 (kPa)	

Figure 6.13 demonstrates that the developed elastoviscoplastic two-parameter damage-self healing model can well predicts the experimental measurements of the controlled-strain cyclic loading tests for AAD and AAM. The use of a two-invariant Drucker-Prager yield criterion with Perzyna viscoplasticity model causes that the stress-strain curve moves down as increasing cycles. In other words, stress-strain loops for 287th cycle for AAD and 1188 cycle for AAM move down from the first cycle loop for each type of bituminous materials. In Figure 6.13(c), the computational result (red solid line) well matches the 287th cyclic experimental data for AAD when the damage-self healing model is used, while there are gaps between the model prediction (blue solid line) and experimental results if damage is only considered for simulation. Figure 6.13(d) shows that the numerical result (blue solid line) when the damage model is only chosen does not capture the experimental measurements for 1188th cyclic loading because the healing is not coupled to the model. The histories of volumetric and

deviatoric damage net for AAD and AAM are plotted in Figure 6.13(e) and (f), respectively. The shape of these volumetric and deviatoric damage net variables seems to be similar to the volumetric and deviatoric damage variables as presented in Figure 6.11. However, enlarging volumetric and deviatoric damage net variables shown in Figure 6.14, increase in the volumetric and deviatoric damage net variables is observed with increasing volumetric and deviatoric damage variables, whiles the volumetric and deviatoric damage net variables decrease when equivalent volumetric and deviatoric strains are lower than their volumetric and deviatoric healing thresholds, respectively. Because the volumetric damage net is combination of volumetric damage and healing variables, there exist many different cases for the same volumetric damage net variables so that only volumetric damage net variable is plotted without volumetric damage and healing variables shown in Figure 6.13 and Figure 6.14. For the same reason, deviatoric damage net variable is only drawn in Figure 6.13 and Figure 6.14. When the energy norm of volumetric strain tensor under the reloading exceeds volumetric healed damage threshold (point A) in Figure 6.15(a), volumetric damage and volumetric damage net variables increase until the end of reloading (B). In Figure 6.15(a), the unloading area is between points B and D and the volumetric healing is restarted at point C and damage net variable decreases because volumetric healing causes the reduction in volumetric damage net variable. At point D in Figure 6.15(a), the reloading begins again and volumetric damage and volumetric damage net are constant until it reaches healed damage threshold at point E. We plot volumetric and deviatoric damage net variables for comparison between AAD and AAM in Figure 6.15(b) so that it is concluded that volumetric and deviatoric damage net variables definitely depend on material properties. Figure 6.16 demonstrates comparison between isotropic and two-parameter damage-self healing models. From the comparison, it is noted that there are noticeable differences between isotropic model and two-parameter model. In addition, model prediction by isotropic model is entirely inside of that by two-parameter model, which is more general and realistic, because isotropic model is a special case of two-parameter and volumetric damage is not the same as deviatoric damage. For simplification purpose, isotropic model prediction may be acceptable under certain circumstance.

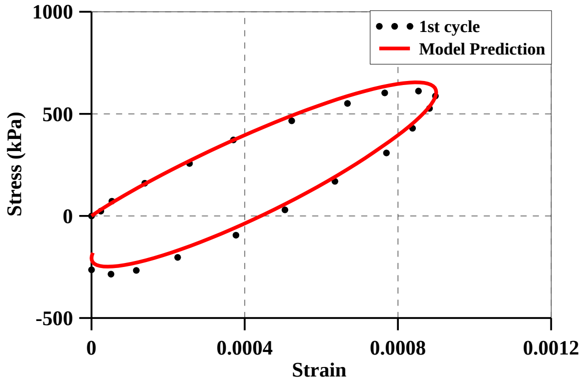

(a) 1st Cycle (AAD)

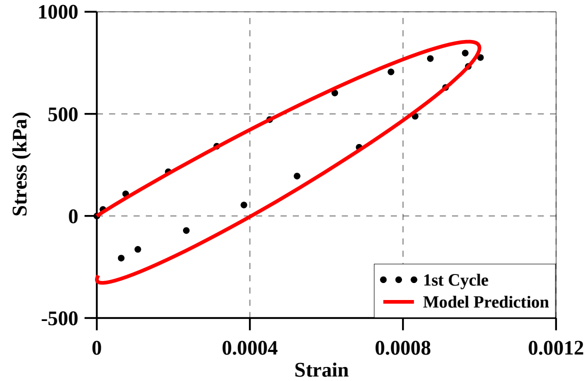

(b) 1st Cycle (AAM)

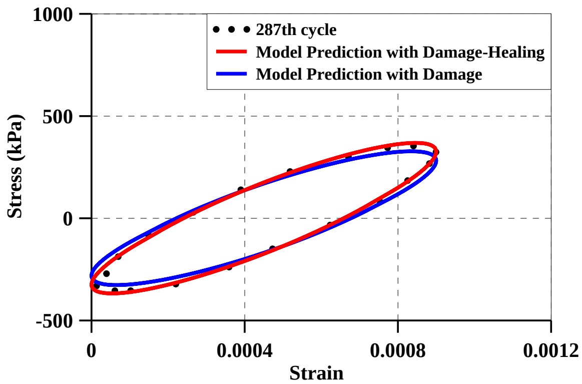

(c) 287th Cycle (AAD)

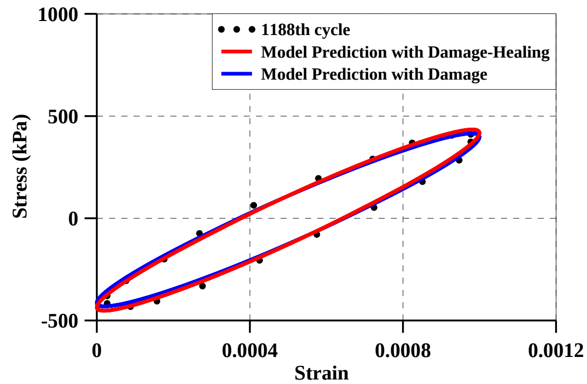

(d) 1188th Cycle (AAM)

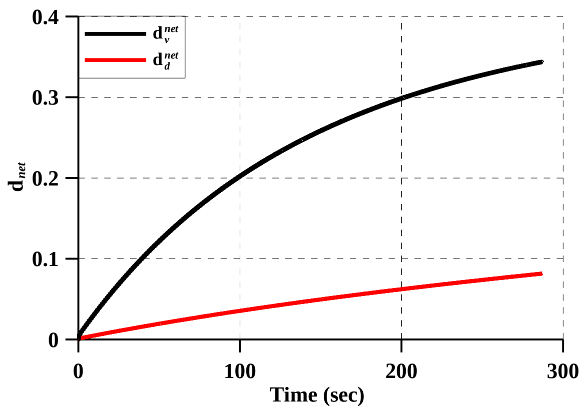

(e) Damage Net Variable (AAD)

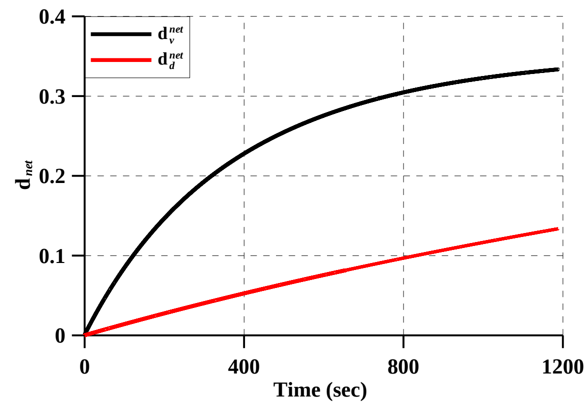

(f) Damage Net Variable (AAM)

Figure 6.13 Comparison between experimental data and model prediction for the cyclic loading in tension

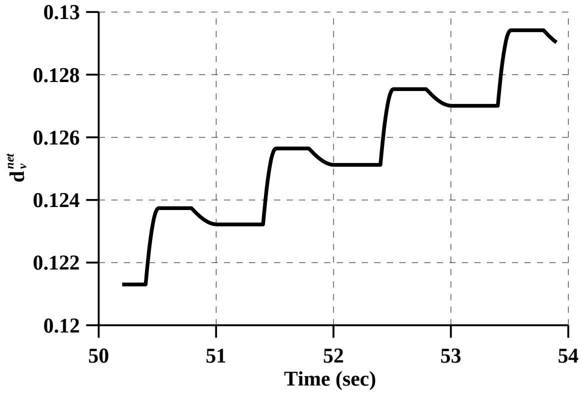

(a) d_v^{net} (AAD)

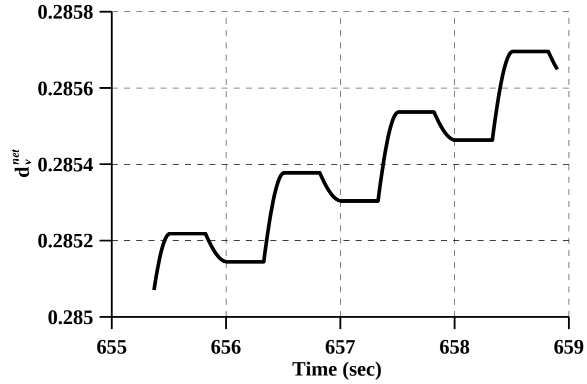

(b) d_v^{net} (AAM)

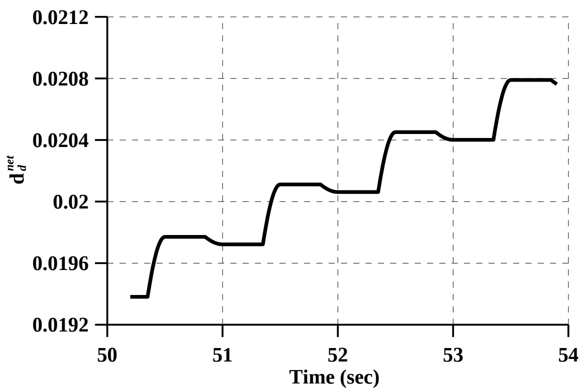

(c) d_d^{net} (AAD)

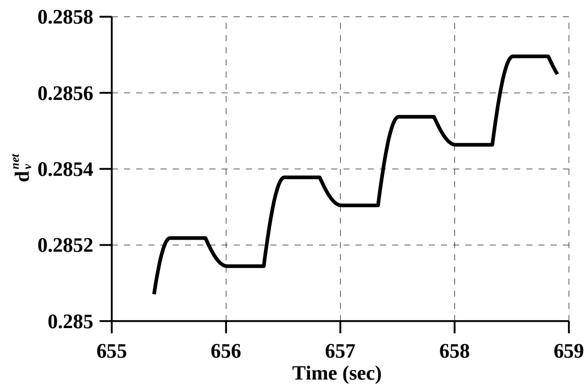

(d) d_d^{net} (AAM)

Figure 6.14 Enlarged damage net variables

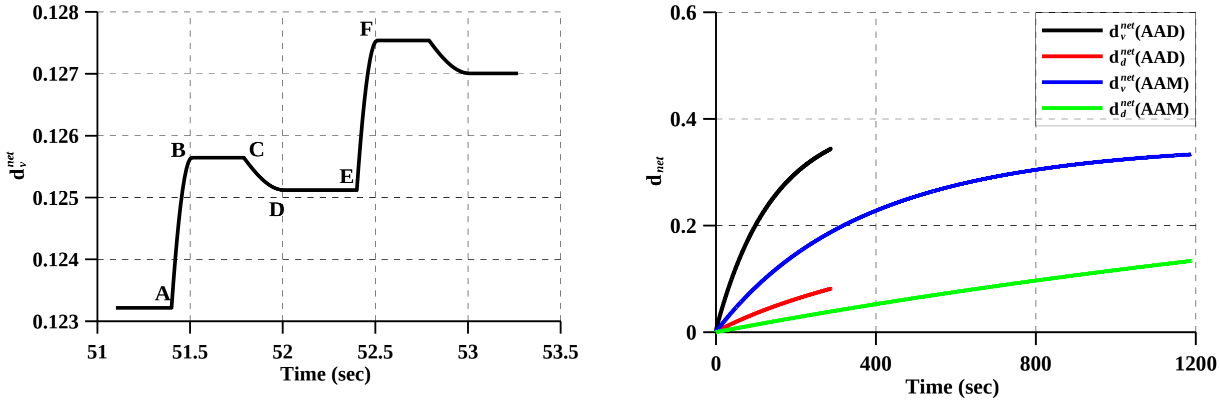

(a) Loading Cycle (AAD) (b) Damage Net Variables

Figure 6.15 Loading cycle for AAD and comparison of damage net variables between AAD and AAM

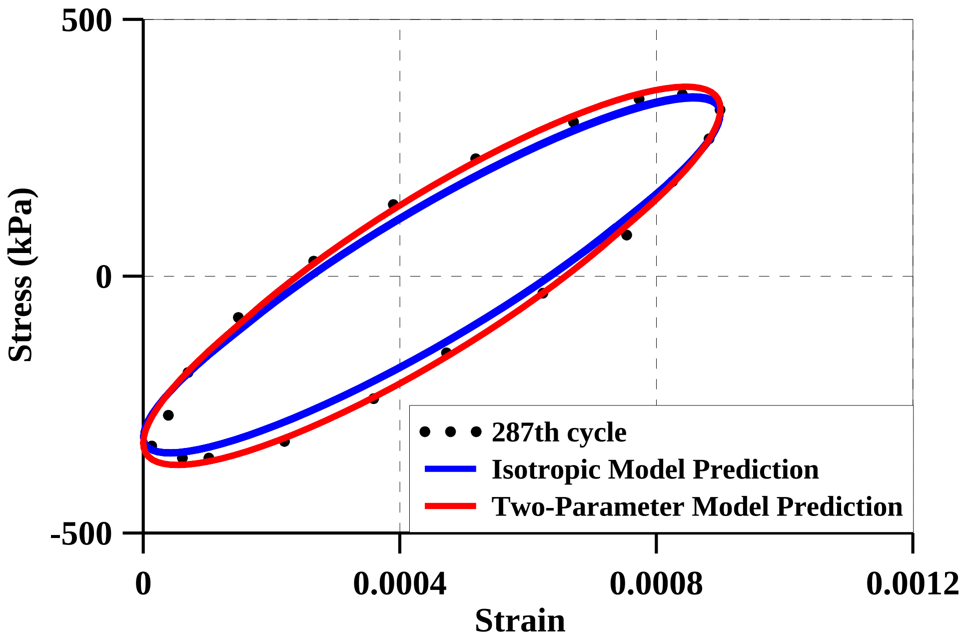

(a) 287th Cycle (AAD)

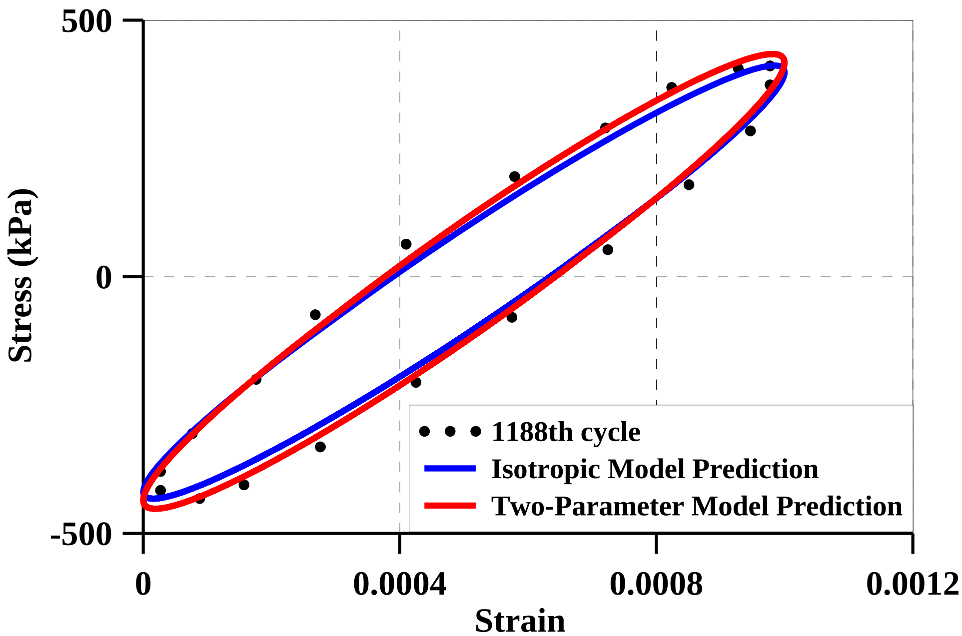

(b) 1188th Cycle (AAM)

Figure 6.16 Comparison between isotropic model and two-parameter model prediction

6.4 Reference

[1] Darabi, M. K., Abu Al-Rub, R.K., Masad, E.A., and Little, D.N. (2011). "Thermodynamic-based model for coupling temperature-dependent viscoelastic, viscoplastic, and viscodamage constitutive behavior of asphalt mixtures." Int. J. Numer. Anal. Meth. Geomech. DOI: 10.1002/nag.1030

[2] Hong, S., Yuan, K.Y., and Ju, J.W. (2014a). "Innovative Strain Energy Based Thermo-Elastoviscoplastic Isotropic Damage-Self Healing Model for Bituminous Composites– Part I: Formulations." International Journal of Damage Mechanics. (Submitted)

[3] Hong, S., Yuan, K.Y., and Ju, J.W. (2014b). "Innovative Strain Energy Based Thermo-Elastoviscoplastic Isotropic Damage-Self Healing Model for Bituminous Composites– Part II: Computational Aspects." International Journal of Damage Mechanics. (Submitted)

[4] Ju, J. W. (1989). On Energy-Based Coupled Elastoplastic Damage Theories-Constitutive Modeling and Computational Aspects, *International Journal of Solids and Structures*, **25**: pp. 803-833.

[5] Ju, J. W., Yuan, K.Y. Kuo, W., Chen, J.S. (2012b). Novel Strain Energy Based Coupled Elastoplastic Damage and Healing Models for Geomaterials - Part II: Computational Aspects, *International Journal of Damage Mechanics*, **21** (4): pp. 551-576.

[6] Ju, J. W., Yuan, K.Y., and Kuo, W. (2012a). Novel Strain Energy Based Coupled Elastoplastic Damage and Healing Models for Geomaterials - Part I: Formulations, *International Journal of Damage Mechanics,* **21** (4): pp. 525-549.

[7] Lee, H. J. (1996). Uniaxial Constitutive Modleing of Asphalt Concrete Using Viscoelasticity and Continuum Damage Theory, Department of Civil Engineering, North Carolina State University, Ph.D. Dissertation.

[8] Lemaitre, J. and Chaboche, J.-L. (1990). Mechanics of solid materials. Cambridge University Press, Cambridge, UK

[9] Oda, M., and Nakayama, H. (1989). Yield function for soil with anisotropic fabric, *Journal of Engineering Mechanics, ASCE*, **15**(1), 89-105.

[10] Simo, J. C., and Ju, J.W. (1987a). Strain-Based and Stress-Based Continuum Damage Models, Part I: Formulation, *International Journal of Solids and Structures*, **23**: pp. 821-840.

[11] Simo, J. C., and Ju, J.W. (1987b). Strain-Based and Stress-Based Continuum Damage Models, Part II: Computational Aspects, *International Journal of Solids and Structures*, **23**: pp. 841-869.

[12] Tan, S. A., Low, B.H., and Fwa, T.F. (1994). Behavior of asphalt concrete mixtures in triaxial compression, *Journal of Testing and Evaluation*, **22**: pp. 195-203. .

7. CONCLUSIONS AND FUTURE WORK

7.1 Conclusions

In this research, new ***initial elastic strain energy*** based thermo-elastoviscoplastic ***isotropic*** and ***two-parameter*** damage-healing models accounting, based on a continuum thermodynamic framework, have been developed and implemented for comparisons between model predictions and experimental measurements. New initial strain energy based thermo-elastoviscoplastic ***isotropic*** damage-self healing models and the ***net stress*** in conjunction with the ***hypothesis of strain equivalence*** are introduced in Chapter 3. Chapter 4 presents two-step computational algorithms based on the proposed damage-self healing model, as shown in Chapter 3 and present several numerical examples of one-dimensional problems and experimental validation. new initial strain energy based thermo-elastoviscoplastic ***two-parameter*** damage-self healing formulations are proposed in Chapter 5. In Chapter 6, the algorithmic frameworks by using the proposed two-parameter damage-self healing models are employed for predicting the temperature-dependent mechanical behavior of bituminous materials under complex loading conditions with different temperatures. The conclusions of this dissertation are summarized below:

1. An ***Arrhenius-type temperature term*** is proposed and uncoupled with Helmholtz free energy potential to account for the effect of temperature for bituminous composites.
2. The concept of ***net space*** is defined for healing effect because the effective space only considers the damage. Moreover, the effective stress and the net stress are equal to each other only if either damage variable or healing variable is zero. Otherwise, the effective stress is

always greater than the net stress since damage net variable is smaller than the damage variable due to the healing effect.

3. The governing ***incremental damage and healing evolutions*** are coupled and characterized through the net stress concept in conjunction with the hypothesis of strain equivalence.

4. New methodology for two-step ***operator split*** algorithms is proposed and employed, involving the elastic damage-self healing predictor and the net viscoplastic return mapping corrector with Arrhenius-type temperature term.

5. From the comparisons of two sets of experiments and model predictions, it is observed that the proposed constitutive models can qualitatively and quantitatively capture the nonlinear behavior of bituminous composites under the different loading conditions with the different temperatures. In particular, ***softening responses*** of the bituminous composites for monotonic constant strain tests are reasonably predicted.

6. From the comparisons between isotropic and two-parameter models, it is noted that there are noticeable differences between isotropic model and two-parameter model. In addition, model prediction by isotropic model is entirely inside of that by two-parameter model, which is more ***general*** and ***realistic***, because isotropic model is a special case of two-parameter and volumetric damage is not the same as deviatoric damage. For simplification purpose, isotropic model prediction may be acceptable under certain circumstance. It is noted that the two-parameter model can *better predict* the thermo-mechanical behavior of asphalt and is more ***versatile*** than isotropic damage-self healing model.

7.2 Future Work

In this section, we present a plan and lay out a foundation for future research as extension of this doctoral dissertation:

1. **More Validation of the Proposed Damage-Self Healing Models**: Due to the limitation of associated experimental data from the literature, our proposed damage-self healing formulations and algorithms have compared with two experimental data sets: (1) the monotonic uniaxial compression tests with different strain rates at different temperatures and (2) the cyclic strain loading control test at constant temperature for two different asphalt materials. In order to enhance the prediction and reliability of the proposed damage-self healing models, more validations to the parameters, i.e., damage and healing thresholds, in damage and healing evolutions must be performed once the experiment data is available. All possible experiments, such as uniaxial test, can be done in environmental chamber to control temperature.
2. **Relationship between Poisson's Ratio and Two-Parameter Parts**: For the isotropic model, the apparent Poisson's ratio never changes because the volumetric and deviatoric parts must be degraded or healed together and at the same rate. Typically, the Poisson's ratio changes as the number of cycle increases, such that the relationship between the Poisson's ratio and the two-parameter parts must be considered to develop the two-parameter damage-self healing model for bituminous materials. The existing data in Chapters 4 and 6 are what we can find at this time in this dissertation; we will perform more comparisons in the future when we can find more experimental data from the University of California Pavement Research Center or other sources.

3. **Anisotropic Damage-Self Healing Models**: Isotropic damage-self healing models can extend anisotropic damage-self healing model by using the fourth-order transformation tensor because damage and healing can be initiated in an anisotropic manner and propagated inside the composite materials. Through the reliable experiments, the parameters in the anisotropic model must be identified and the validations have to be performed.
4. **Development of Moisture-Damage (Freeze and Thaw)-Self Healing Model**: One of the environmental conditions is moisture condition, which must be considered to develop reliable constitutive models of mechanical behavior of bituminous composite. Therefore, a series of fundamental interlinked investigations have to be studied through experiments and the physical theories and their computational frameworks must be proposed for engineers and designers.
5. **Application to Self-Healing Composites**: In Chapter 2, the self-healing materials describe the ability of composite materials with a polymeric-matrix or cementitious matrix to heal automatically. Such materials can reduce material degradation with the aid of a healing agent by means of chemical interactions. The system can be rehabilitated and the integrity of the materials is healed to a certain extent or even their original condition. The proposed energy-based thermo-elastoviscoplastic damage-healing models can be modified and applied to predict damage-healing and irreversible deformation processes for self-healing composite materials.
6. **Continuous Change of Temperature**: We are not modeling continuous changes of temperatures because the existing experimental data were conducted at constant temperatures. However, in order to better predict the thermo-mechanical behavior of asphalt under changes

of temperatures, we must consider continuous changes of temperatures and the corresponding thermo-elastic strain ($\varepsilon_e = \alpha \Delta T$) and thermo-viscoplastic strain (thermo-creep) should be included in the improved model in the future work.